PB 203 469

Comprehensive Report

FIELD STUDY FOR INITIAL EVALUATION OF AN URBAN DIFFUSION MODEL FOR CARBON MONOXIDE

Prepared for:

COORDINATING RESEARCH COUNCIL
30 ROCKEFELLER PLAZA
NEW YORK, NEW YORK 10020

ENVIRONMENTAL PROTECTION AGENCY
DIVISION OF METEOROLOGY
RESEARCH TRIANGLE PARK, NORTH CAROLINA 27711

CONTRACT CAPA-3-68 (1-69)

Reproduced by
NATIONAL TECHNICAL
INFORMATION SERVICE
Springfield, Va. 22151

STANFORD RESEARCH INSTITUTE
Menlo Park, California 94025 · U.S.A.

254

STANFORD RESEARCH INSTITUTE
Menlo Park, California 94025 · U.S.A.

Comprehensive Report

June 1971

FIELD STUDY FOR INITIAL EVALUATION OF AN URBAN DIFFUSION MODEL FOR CARBON MONOXIDE

By: W. B. JOHNSON
W. F. DABBERDT
F. L. LUDWIG
R. J. ALLEN

Prepared for:

COORDINATING RESEARCH COUNCIL
30 ROCKEFELLER PLAZA
NEW YORK, NEW YORK 10020

ENVIRONMENTAL PROTECTION AGENCY
DIVISION OF METEOROLOGY
RESEARCH TRIANGLE PARK, NORTH CAROLINA 27711

CONTRACT CAPA-3-68 (1-69)

SRI Project 8563

Approved by:

R. T. H. COLLIS, *Director*
Atmospheric Sciences Laboratory

RAY L. LEADABRAND, *Executive Director*
Electronics and Radio Sciences Division

Copy No. 296

ABSTRACT

A measurement program in San Jose, California, during November and December 1970, provided data to evaluate and improve our existing receptor-oriented Gaussian diffusion model for calculating urban carbon monoxide (CO) concentrations. Seven stations were operated in a two-block downtown area to measure CO at five heights, winds, and temperature gradients. CO concentrations and temperatures were also measured by helicopter and two vans. San Jose's automated downtown network provided traffic data.

A helical air circulation in the street canyon was observed when roof level winds were within 45° of the cross-street direction. In these cases, CO concentrations were proportional to vehicle emissions in the canyon and to the reciprocal of wind speed. In front of buildings that face the roof-level wind, observed concentrations from street emissions are inversely proportional to the street width and nearly constant with height; on the other side of the street they are inversely proportional to the slant distance from the nearest traffic lane and hence decrease with height. These relationships are incorporated in a new street effects submodel. For winds parallel to the street, the expressions for the two cross-wind cases are averaged, giving concentrations that are the same on both sides of the street.

Transport of CO into and out of the downtown area was determined from vertical profiles of wind and horizontal profiles of CO concentrations at various heights up to 300 m along the perimeter of the central area. The computed CO input at the surface deduced on this basis was compared with our emissions submodel calculations. On the average, the two methods gave values within a factor of about 1.5. Mixing depths from helicopter measurements of temperature and CO profiles were compared with those from our mixing depth submodel; six of the nine cases agreed within 15 percent, and eight within 41 percent. On the basis of helicopter observations, the stability submodel was modified to account for more stable conditions during immediate post-sunrise and pre-sunset hours. The revised model also uses an increased diffusion rate appropriate to urban areas. The changes were based on reevaluation of earlier urban diffusion studies. The Gaussian nature of the model is retained.

Evaluation of the revised model has shown that significant improvements have been made. The model reproduces the observed frequency distributions very well for street-canyon sites. At these sites, hourly predictions are well correlated (correlation efficient of about 0.6 to 0.7) with observations, and about 80 percent of the calculated values are within 3 ppm of the observed, which ranged as high as 16 ppm. This level of uncertainty is about half that found in earlier work before the model was revised.

CONTENTS

ABSTRACT iii

LIST OF ILLUSTRATIONS ix

LIST OF TABLES xvii

SUMMARY AND CONCLUSIONS xix

I INTRODUCTION 1

  A. General Program Objectives 1

  B. Review of the First-Stage Model Development 2

    1. Description of the Basic Model 2
    2. Capabilities of the Basic Model 8

  C. Scope of the Current Project 10

II DESCRIPTION OF THE SAN JOSE FIELD PROGRAM 19

  A. Background 19

  B. Experimental Area 19

    1. Selection of San Jose 19
    2. Downtown San Jose 20

  C. Instrumentation and Operations 24

    1. Fixed-Station Measurements 24
    2. Mobile Measurements 33

  D. Supplementary Data Available from Other Agencies 39

    1. Traffic Data 39
    2. Meteorological Data 41
    3. Air Pollutant Monitoring Data 42

CONTENTS (Concluded)

D. Vertical Diffusion Rates 99

E. Mixing Depth 107

F. Local (Street) Effects 107

VI EVALUATION OF THE PERFORMANCE OF THE REVISED MODEL 109

A. Introduction 109

B. Tests of the Subcomponents 109

1. Emissions Submodel 109
2. Mixing Depth Submodel 114
3. Stability Class Submodel 115
4. Street Effects Submodel 116

C. Evaluation of the Composite Model 116

D. Frequency Distribution of Concentrations 137

VII RECOMMENDATIONS 141

ACKNOWLEDGMENTS 143

Appendix A--FIXED-STATION INSTRUMENTATION SYSTEM

Appendix B--VAN INSTRUMENTATION SYSTEM

Appendix C--HELICOPTER INSTRUMENTATION SYSTEM

Appendix D--DATA PROCESSING

Appendix E--PILOT-BALLOON DATA SUMMARY

REFERENCES

ILLUSTRATIONS

Figure 1 Computer Display of Traffic Links for Chicago 3

Figure 2 Hourly Distribution of Traffic for Two Facility Types in St. Louis 4

Figure 3 Vertical Diffusion According to Gaussian Formulation 5

Figure 4 Diagram of Segments Used for Spatial Partitioning of Emissions 6

Figure 5 Meteorological Input Parameters Required for the Diffusion Model--Chicago Data (19-25 October 1964) .. 8

Figure 6 Calculated Carbon Monoxide Concentrations (ppm) for Chicago 9

Figure 7 Calculated St. Louis Concentration Patterns for Two Grid Sizes 11

Figure 8 Calculated Concentration Patterns Based on Forecast of 1990 St. Louis Traffic 12

Figure 9 Calculated St. Louis CAMP Station CO Concentration Frequency Distribution for 1965 Traffic Conditions; 0800, 1200, and 1800 Hours 13

Figure 10 Calculated St. Louis CAMP Station CO Concentration Frequency Distribution for 1965 Traffic Conditions; 1-Hour, 8-Hour, and 24-Hour Averages 14

Figure 11 Comparison of Calculated and Observed Hourly CO Concentrations at the Denver CAMP Station for a One-Week Period 15

Figure 12 Chicago CAMP Station 17

ILLUSTRATIONS (Continued)

Figure 13 Aerial Photograph of San Jose Showing Intersection Studied and Helicopter and Van Routes 21

Figure 14 Map of Area around Intersection of First and San Antonio Streets 22

Figure 15 Looking Toward First and San Antonio from First and San Fernando 23

Figure 16 Installation of Instrumentation and CO Inlet Tubing 26

Figure 17 Three-Component Wind Sensor 28

Figure 18 Radiation Shield and Ventilation System for Temperature Sensor 29

Figure 19 Instrumented Van 34

Figure 20 Helicopter and Van Routes (with check points) around the Central Business District, San Jose, California 37

Figure 21 Instrumented Helicopter 38

Figure 22 Area Coverage of San Jose Traffic Sensing System ... 40

Figure 23 Indicated Typical Helical Air Flow over a Street (adapted from Georgii, 1967) 50

Figure 24 Specification for Leeward and Windward Cases on the Basis of Receptor Location, Street Orientation, and Wind Direction 52

Figure 25 CO Patterns in San Jose for Three Heights for Early Morning on 11 December 1970 55

Figure 26 CO Patterns in San Jose for Three Heights at Noon on 11 December 1970 56

Figure 27 CO Patterns in San Jose for Three Heights during Late Afternoon on 11 December 1970 57

Figure 28 CO Patterns in San Jose for Three Heights during Late Evening on 11 December 1970 58

ILLUSTRATIONS (Continued)

Figure 29 CO Patterns in San Jose for Three Heights During the Night of 12 December 1970 59

Figure 30 Average of Horizontal CO Distribution at 3 m (above) and Vertical CO Profiles (below), for Mean Rooftop Wind from 045° (±22.5°) 63

Figure 31 Average of Horizontal CO Distribution at 3 m (above) and Vertical CO Profiles (below), for Mean Rooftop Wind from 090° (±22.5°) 64

Figure 32 Average of Horizontal CO Distribution at 3 m (above) and Vertical CO Profiles (below), for Mean Rooftop Wind from 135° (±22.5°) 65

Figure 33 Average of Horizontal CO Distribution at 3 m (above) and Vertical CO Profiles (below), for Mean Rooftop Wind from 180° (±22.5°) 66

Figure 34 Average of Horizontal CO Distribution at 3 m (above) and Vertical CO Profiles (below), for Mean Rooftop Wind from 225° (±22.5°) 67

Figure 35 Average of Horizontal CO Distribution at 3 m (above) and Vertical CO Profiles (below), for Mean Rooftop Wind from 270° (±22.5°) 68

Figure 36 Average of Horizontal CO Distribution at 3 m (above) and Vertical CO Profiles (below), for Mean Rooftop Wind from 315° (±22.5°) 69

Figure 37 Average of Horizontal CO Distribution at 3 m (above) and Vertical CO Profiles (below), for Mean Rooftop Wind from 360° (±22.5°) 70

Figure 38 Schematic of Cross-Street Circulation between Buildings 73

Figure 39 Vertical Profiles of Carbon Monoxide and Temperature at Spartan Stadium, San Jose, California 80

Figure 40 Horizontal Traverses of Carbon Monoxide at Indicated Heights for Box Pattern over Downtown San Jose, California 83

ILLUSTRATIONS (Continued)

Figure 41 Lidar-Observed Time-Height Cross Sections of the Urban Haze Layer over San Jose, California, on 11 December 1970 92

Figure 42 Dependence of the Vertical Diffusion Parameter σ_z upon Travel Distance for Selected St. Louis Tracer Tests Conducted by Leighton and Dittmar (1953) 102

Figure 43 Comparison of Results from Tracer Tests Conducted in St. Louis over Short Ranges (Leighton and Dittmar, 1953--"L&D") with those for Intermediate Ranges (McElroy and Pooler, 1968--"M&P") 103

Figure 44 Comparison of Urban Vertical Dispersion Data with the Pasquill-Gifford Curves (Adapted from McElroy and Pooler, 1968) 104

Figure 45 Vertical Diffusion as a Function of Travel Distance and Stability Category, as Revised for Urban Conditions 106

Figure 46 Diurnal Emission Patterns for St. Louis 111

Figure 47 Total Number of Traffic Counts for All Detectors in Downtown San Jose 112

Figure 48 Calculated and Observed CO Concentrations for Station 4 at Two Heights for 19 and 20 November and 7 December 1970 117

Figure 49 Calculated and Observed CO Concentrations for Station 4 at Two Heights for 9, 10, and 11 December 1970 118

Figure 50 Calculated and Observed CO Concentrations for Station 4 at Two Heights for 14 and 15 December 1970 119

Figure 51 Calculated and Observed CO Concentrations for Station 5 at Two Heights for 19 and 20 November and 7 December 1970 120

ILLUSTRATIONS (Continued)

Figure 52 Calculated and Observed CO Concentrations for Station 5 at Two Heights for 9, 10, and 11 December 1970 121

Figure 53 Calculated and Observed CO Concentrations for Station 5 at Two Heights for 14 and 15 December 1970 122

Figure 54 Calculated and Observed CO Concentrations for Station 6 at Two Heights for 19 and 20 November and 7 December 1970 123

Figure 55 Calculated and Observed CO Concentrations for Station 6 at Two Heights for 9, 10, and 11 December 1970 124

Figure 56 Calculated and Observed CO Concentrations for Station 6 at Two Heights for 14 and 15 December 1970 125

Figure 57 Calculated and Observed CO Concentrations for Station 7 at Two Heights for 19 and 20 November and 7 December 1970 126

Figure 58 Calculated and Observed CO Concentrations for Station 7 at Two Heights for 9, 10, and 11 December 1970 127

Figure 59 Calculated and Observed CO Concentrations for Station 7 at Two Heights for 14 and 15 December 1970 128

Figure 60 Calculated and Observed CO Concentrations for Station 8 at Two Heights for 19 and 20 November and 7 December 1970 129

Figure 61 Calculated and Observed CO Concentrations for Station 8 at Two Heights for 9, 10, and 11 December 1970 130

ILLUSTRATIONS (Continued)

Figure 62 Calculated and Observed CO Concentrations for Station 8 at Two Heights for 14 and 15 December 1970 131

Figure 63 Scatter Diagram of Calculated Versus Observed CO Concentrations for all Five Levels at Stations 7 and 8 138

Figure 64 Calculated and Observed Frequencies of One-Hour Average CO Concentration 139

Figure A-1 Block Diagram of Fixed-Station Instrumentation System A-5

Figure A-2 Type A Terminal Sensors and Support System A-8

Figure A-3 Dual Roof Boom--Part of Sensor Support System A-9

Figure A-4 Beckman Carbon Monoxide Analyzer with Remote Line Coupler A-11

Figure A-5 Block Diagram of CO Measuring System Using Beckman Analyzer A-13

Figure A-6 Block Diagram of Temperature System A-17

Figure A-7 Temperature and UVW Electronics A-22

Figure A-8 Block Diagram of Remote Line Couplers A-29

Figure A-9 Mini-Computer and Peripheral Devices at Central Station A-34

Figure A-10 Block Diagram of NOVA Computer A-36

Figure B-1 Electronic Console in Van B-4

Figure B-2 Block Diagram of Van Instrumentation System B-5

Figure B-3 Functional Diagram, Van and Helicopter Carbon Monoxide Measuring System B-7

ILLUSTRATIONS (Concluded)

Figure C-1 Helicopter Instrumentation C-4

Figure D-1 Example of Real-Time Summary Printout D-5

Figure D-2 Example of Partially Corrected Data Contained in One Record of the Tape Generated by Initial CDC 6400 Processing D-7

Figure D-3 Example of Information Contained in One Record of the Basic Data Summary Tape D-9

Figure D-4 Simplified Flow Chart of Data-Averaging Program D-10

Figure D-5 Example of Averaged Data D-11

Figure D-6 Computer Output Format for Helicopter Temperature and Carbon Monoxide Profile Data D-16

Figure D-7 Computer Output Format for Helicopter Temperature and Carbon Monoxide Traverse Data D-17

Figure D-8 Example of Raw Traffic Data Summary D-18

Figure D-9 Magnetic Tape Format for Traffic Data D-20

Figure D-10 Average Link Volumes, 1100-1130 .... D-25

BLANK PAGE

TABLES

Table 1 Resolution Limitations Imposed by the Analog-to-Digital Converter 30

Table 2 Master Data Summary--San Jose Field Program, 5 November-15 December 1970 45

Table 3 Wind Direction Sectors for San Jose Street Stations 77

Table 4 Corresponding Helicopter and Van Legs, Indicating Weighting Factors for Determination of Average CO along Van Route Segments 82

Table 5 Values of p in Eq. 22 After Frost (1947) 86

Table 6 Transport Rates of Carbon Monoxide through the Sides, Top, and Bottom of the Sublayers of the San Jose Budget Box 88

Table 7 Average Vehicle Speeds in the Downtown Sector of San Jose for Specified Times During the Period 9-11 December 1970 89

Table 8 Carbon Monoxide Emission Rates (Q) for the Budget Area Determined from the Mass Budget Analysis and Traffic Data [with Eq. 27] 90

Table 9 Comparison of Mixing Depth Estimates Obtained from the Mixing Depth Submodel and the Subjective Analysis of the Helicopter Profile Data, with the Lidar-Observed Haze-Layer Structure at San Jose, California 93

Table 10 Modified Pasquill-Turner Stability Categories Used with the Diffusion Model (Ludwig et al., 1970) as a Function of Insolation, Wind Speed, and Cloud Cover 95

TABLES (Concluded)

Table 11 Comparison of Bulk Stability Coefficients Computed from Eq. (28) with Stability Categories Determined from the Diffusion Model for the Period 20 November to 11 December 1970, at San Jose, California 96

Table 12 Revised Stability Categories 99

Table 13 Test Conditions for Analyzed Leighton and Dittmar (1953c) St. Louis Data 101

Table 14 Values of Constants in Eq. (34) as a Function of Atmospheric Stability Category 105

Table 15 Ambient Carbon Monoxide Background Concentrations ... 134

Table 16 Correlation Coefficients (r) between Observed and Predicted Carbon Monoxide Concentrations 136

Table A-1 Manufacturer's Stated Performance Specifications for the Nondispersing Infrared CO Analyzer A-12

Table A-2 Mode Codes for Indicated Remote Coupling Units A-27

Table A-3 Remote Line Coupler Assigned Scanning Sequence A-31

Table A-4 Characteristics of NOVA Computer A-37

Table B-1 Manufacturer's Stated Performance Specifications for the Mercuric Oxide Reduction CO Analyzer B-9

Table D-1 Traffic at Intersection of First and San Antonio Streets for Monday, 2 November 1970 .... D-22

Table D-2 Total Traffic Counts from 291 Sensors in Downtown San Jose for Tuesday, 24 November 1970 .... D-23

Table E-1 Pilot Balloon Data Summary--San Jose State College (1970) E-4

SUMMARY AND CONCLUSIONS

Background--The measurements and original research described in this report have been used to test and improve the diffusion model developed during earlier phases of the program (Johnson et al., 1969; Ludwig et al., 1970). That model, based on existing experimental data and previous research results, was designed to calculate carbon monoxide (CO) concentrations from available traffic and meteorological data. It calculates CO concentrations from the emissions in the city, vertical diffusion rate, mixing depth, and the wind.

Predictions based on this model in its initial form were compared with measured data from Continuous Air Monitoring Program (CAMP) stations; the calculated and observed values often differed significantly in magnitude, although they tended to have similar trends. The studies described in this report show that there were several reasons for this. Foremost is the fact that local effects in street canyons and around buildings can sometimes cause CO concentrations to vary by as much as a factor of 3, or 10 ppm from one side of the street to the other. It is obvious that any model that did not account for these effects could be expected to have large errors. One of the principal accomplishments of the research reported here is a new submodel that does describe these street-canyon effects and substantially improves the model.

The program has also uncovered and corrected some other shortcomings of the earlier model. These corrections further improve the model's performance. The nature of the new street effects submodel and the other changes are discussed below.

Except for wind, none of the inputs to the model are regularly measured, so submodels have been developed to derive the emissions, atmospheric stabilities, and mixing depths from measured quantities. The program reported here has checked the performance of these submodels using special measurements made in San Jose, California, during November and December 1970.

Emissions Submodel Evaluation--San Jose has an extensive computer-based traffic-monitoring system that provides detailed information on the traffic in the central business district. This detailed traffic information allowed the emissions submodel to be applied in this area with good confidence. The emissions submodel describes the amount of CO emitted per vehicle-mile as a function of the average vehicle speed. The traffic flow is known from the monitoring network; the average vehicle speed was determined from the movements of a project van around the downtown perimeter. Emissions calculated from the submodel were compared to independent estimates made from a CO mass budget analysis that was based on upper level wind measurements and CO concentrations measured around the central business district with helicopter- and van-borne instruments. The difficulties with this method include uncertainties in the wind field and possible significant changes of CO emission rate during the measurement periods, but the results are sufficiently reliable to uncover serious inaccuracies in the emissions submodel. The averages of the four cases studied show that the two types of CO emission estimates agree within a factor of 1.5. There seems to be no justification for changing the submodel at this time.

Mixing Depth Submodel Evaluation--Vertical profile measurements of CO concentration and temperature obtained during helicopter flights up to 1000 m were used to determine mixing depths, and these values were compared with submodel calculations. Abrupt decreases of CO or increases in temperature with height usually marked the top of the mixing layer. On several days the mixing depth was also estimated from measurements made with a laser radar (lidar) that can detect a sharp reduction in aerosol concentration at the top of the mixing layer. The submodel mixing depth was within ±15 percent of the mixing depth* obtained from helicopter CO and temperature soundings in six of nine cases studied, and within 41 percent in eight. The submodel used to determine the mixing depth is adequate if representative low-level morning temperature soundings are available.

Vertical Diffusion Revisions--The basic model is receptor-oriented and treats the vertical distribution of CO concentration from a continuous source as Gaussian, where the standard deviation, σ_z, changes with distance downwind of the source and with atmospheric stability. The dependence of σ_z on downwind distance and stability has been revised to reflect the vertical diffusion observed during urban fluorescent particle tracer tests in St. Louis, Minneapolis, and Winnipeg (Leighton and Dittmar, 1952-1953; Pooler, 1966; McElroy and Pooler, 1968). The dependence of σ_z on downwind distance, x, is of the form

$$\sigma_z = a\, x^b \quad ,$$

where a ranges from 1.35 for slightly stable to 0.07 for very unstable conditions and b from 0.51 to 1.28. The a and b values are such that σ_z equals 10 m at x equal to 50 m, regardless of stability category. This value of σ_z, 10 m, represents initial mechanical mixing caused by roughness elements near the source.

---

* Sometimes there was evidence of two upper bounds to the mixing layer. In our comparisons we have used the values that are most consistent with the calculations.

Stability Submodel Revisions--The methods used to determine stability category have also been revised to reflect the more stable conditions observed during the immediate post-sunrise and pre-sunset hours. The revisions were based on estimates of stability derived from surface wind speeds and the helicopter-measured vertical temperature gradient in the lower layers.

Development of the Street-Canyon Effects Submodel--The diffusion model as constituted at the beginning of the research described in this report had no provision for effectively describing the behavior of pollutants in street canyons and around buildings near sources. Street effects strongly influence concentrations to which pedestrians are exposed. If the model is to be tested properly against observed concentrations, the calculated values must account for the small-scale effects that can cause large variations in the concentrations around streets and busy intersections, where most air monitors are located.

An intersection in downtown San Jose was instrumented to obtain the data necessary to describe and model the street effects. We measured CO concentrations (at five levels between 3 m and rooftop) and 3-m winds at seven sites; roof-level winds and vertical temperature gradients were measured at two of the locations. Data were automatically collected and recorded on magnetic tape. Fifteen days' data were used to determine the air circulations and the distributions of CO in the street canyon. The data analysis showed that rooftop wind direction is the most important meteorological factor in determining the distribution of CO in the street. When the roof-level wind blows within about ±45° of the cross-street direction, a helical circulation develops in the street. At street level the cross-street component is opposite the roof-level wind direction, causing a downflow of relatively clean air in front of the "downwind" buildings that face the roof-level wind, and an upflow across the street.

The resulting low-level CO concentrations in front of the downwind buildings are often only half those observed across the street. Cross-street gradients of CO are quite small for winds approximately parallel to the street.

A simple model based on physical principles has been developed that describes the observed distribution of CO in the street canyon. First, the model presumes that the emissions from the local street traffic are added to the CO already present in the air that enters from roof level. These additive concentrations are proportional to the local street emissions, Q (g m^{-1} s^{-1}), and inversely proportional to the roof-level wind speed (u), which is augmented by a small amount to account for the mechanically induced air movement caused by traffic; 0.5 m s^{-1} gives good results.

In front of the downwind buildings the downward air flow produces relatively little vertical variation of concentration. "Box model" reasoning indicates that the CO concentration is inversely proportional to street width, w, and uniform with height. Thus, on the side of the street where the buildings face the roof-level wind, the CO concentration added by street sources, ΔC, is given by:

$$\Delta C + k \frac{Q}{w(u + 0.5)} \quad .$$

On the upwind side of the street the model is also based on box model reasoning, but the volume into which the emissions can be mixed is limited by the helical circulation that transports street emissions toward the buildings and upward. As the air moves from the source, the volume into which the pollutants are mixed increases, so the concentration is taken to be inversely proportional to the slant distance, r, between the receptor and the nearest traffic lane. For concentrations in front of the upwind buildings, the equation is height dependent:

$$\Delta C = k \frac{Q}{r(u + 0.5)} \quad .$$

The constant, k, is the same for both equations. When the wind blows nearly parallel to the street, the additive concentration, ΔC, is described by the average of the values from the two equations and is the same on both sides of the street.

Overall Performance of the Model--The performance of the total model, including all its subunits, has been checked against the data obtained at the fixed CO-measuring sites in downtown San Jose. Since traffic data are available only for a limited area, the concentrations arising from emissions at the greater distances, beyond about 2 km, have been simulated using concentrations measured during helicopter flights or estimated on the basis of values measured at a height of 34 m at one of the fixed stations. Data suitable for the evaluations were available for 70 hours during eight separate days.

The total model was evaluated in two ways. First, the values predicted by the model were compared with observations on an hour-by-hour basis; second, the histograms of observed concentration were compared with those for calculated concentration.

For the hour-by-hour comparisons, we found that the calculated values (at heights from 3 m to rooftop) were within ±3 ppm of the observed for nearly 80 percent of the hours at two midblock street-canyon stations. Observed values ranged from about 1 to 16 ppm. For two stations near the intersection, the results were not quite so good; about 75 percent of the calculated cases were within 3 ppm of the observed.

In general, hour-by-hour calculated values followed the observed trends of CO concentration. This was particularly true of the midblock street-canyon stations as evidenced by their correlation. For concentrations at a height of 3 m the correlation coefficients were 0.55 and 0.68. Somewhat poorer results were obtained near the intersection, where correlation coefficients ranged from 0.47 to 0.58. Qualitatively, there appears to be some lag between the calculated and observed values. Observed concentration changes lag behind changes of wind or stability, but calculated values, based on current observations, respond immediately.

As noted earlier, the model was used to calculate frequency distributions of CO concentrations. It is quite important that the model perform well in this application, because this type of output is important in planning applications. The frequency of occurrence of CO concentrations was determined for five geometrically spaced class intervals (1 to 2 ppm, 2 to 4 ppm, etc.) The frequency distribution of 70 observed and 70 calculated 3-m CO concentrations were compared for each station. For the two midblock sites the two frequency distributions differed by no more than four cases (i.e., less than 6 percent of the sample) in any class interval. On the other hand, there was considerable difference (as many as 21, i.e., 31 percent) between the frequency distributions for stations near the intersection.

In conclusion, the results have shown that the combined model is capable of estimating CO concentrations within about ±3 ppm of those experienced in the downtown streets of a moderate-size city. This level of uncertainty is about half that found in our earlier work (Ludwig et al., 1970), indicating that this research has resulted in significant improvements in the model.

BLANK PAGE

I INTRODUCTION

A. General Program Objectives

The long-term objective of this research program is the development of a methodology for predicting the concentrations of motor-vehicle-generated air pollutants throughout an urban area as a function of local meteorology and the distribution of traffic. The results of this work are intended primarily to be used as a tool in planning activities to predict the pollution patterns in any urban region resulting from planned traffic changes or predicted growth. In addition, the model can be used in an operational mode for short-term predictions.

Our first goal has been the development of such a methodology for a quasi-inert pollutant such as carbon monoxide (CO). For the initial development we used available data from five cities having CAMP* air monitoring stations: Chicago, St. Louis, Denver, Cincinnati, and Washington, D.C. The current status of this program is as follows:

- A working model for CO has been developed.
- A field program, designed to fill gaps in the available data, has been carried out in San Jose, California.
- On the basis of these data, the initial refinement and evaluation of the model have been completed.

---

*Continuous Air Monitoring Program stations, run by the Federal Air Pollution Control Office, Environmental Protection Agency.

In this and following sections, the structure and capabilities of the basic model are reviewed, the results of the field program are reported, and the progress in the refinement and evaluation of the model is discussed in detail.

B. Review of the First-Stage Model Development

1. Description of the Basic Model

Instead of an emissions inventory, which is the basic information on sources used by diffusion models for other pollutants, the CO model uses a traffic inventory. An example of a network of traffic "links," in this case for Chicago, is shown in Figure 1. Each straight road segment, or link, is assigned an average daily traffic volume, based upon historical or forecast data furnished by traffic agencies. Each link is also identified in the computer memory by its length and the geographical locations of its endpoints and is designated as a particular road type.

To calculate emissions at a given time, a temporal adjustment factor such as is illustrated in Figure 2 is first applied to the daily traffic volumes to obtain traffic volumes for that particular hour. Then the emission rate, E (g-CO vehicle-mi^{-1}), is estimated from the mean vehicle speed, S (mi h^{-1}), by an empirical equation of the form

$$E = \alpha S^{-\beta} \quad . \tag{1}$$

Here α and β are constants that depend on the characteristics of the emission control devices installed. These can be parameterized reasonably well by vehicle model year. Estimated values of S are used that depend upon the type of road and the time of day (whether during peak or off-peak traffic conditions). The total CO emission for a given traffic

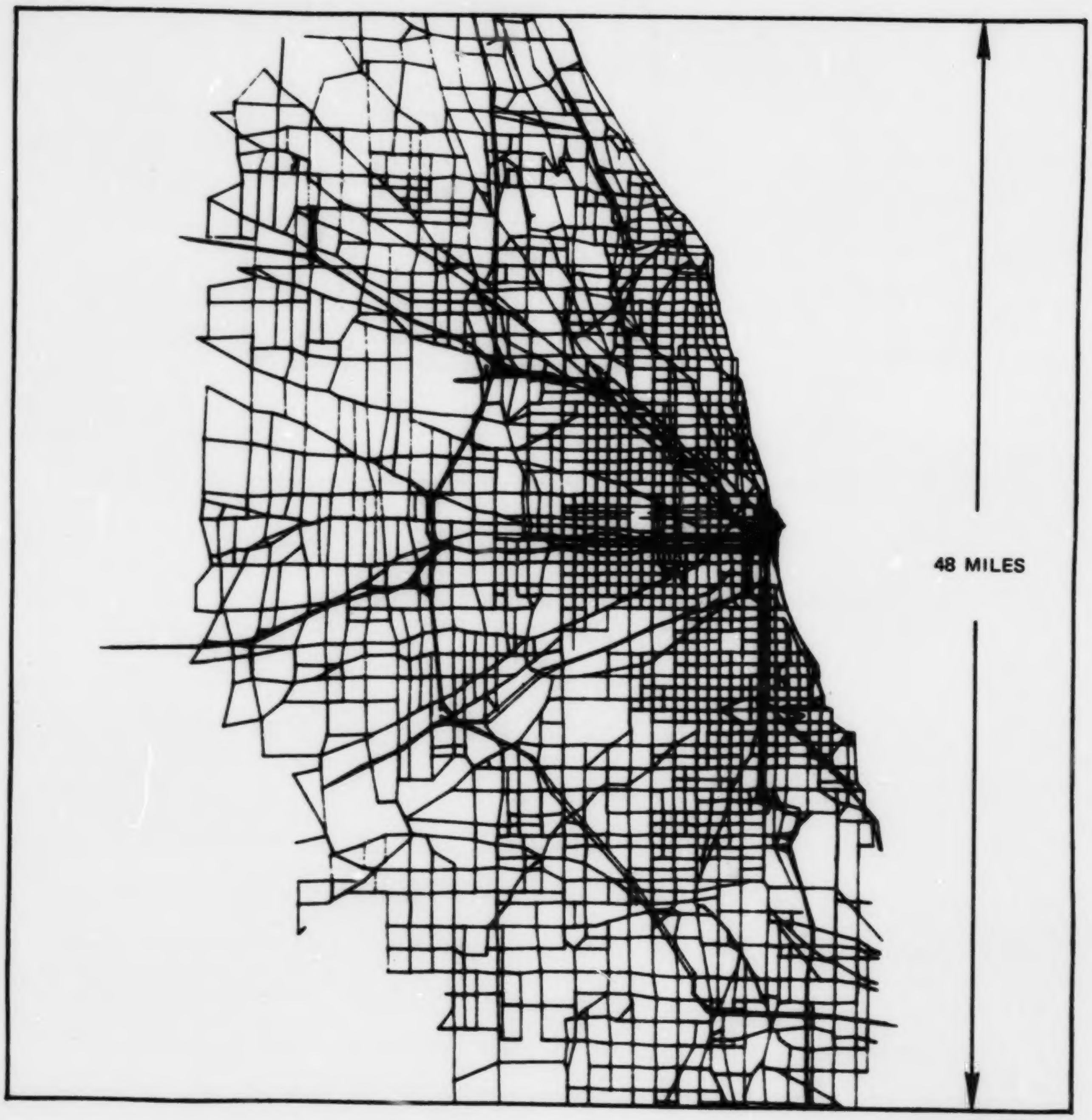
48 MILES

TA-7874-78

FIGURE 1 COMPUTER DISPLAY OF TRAFFIC LINKS FOR CHICAGO

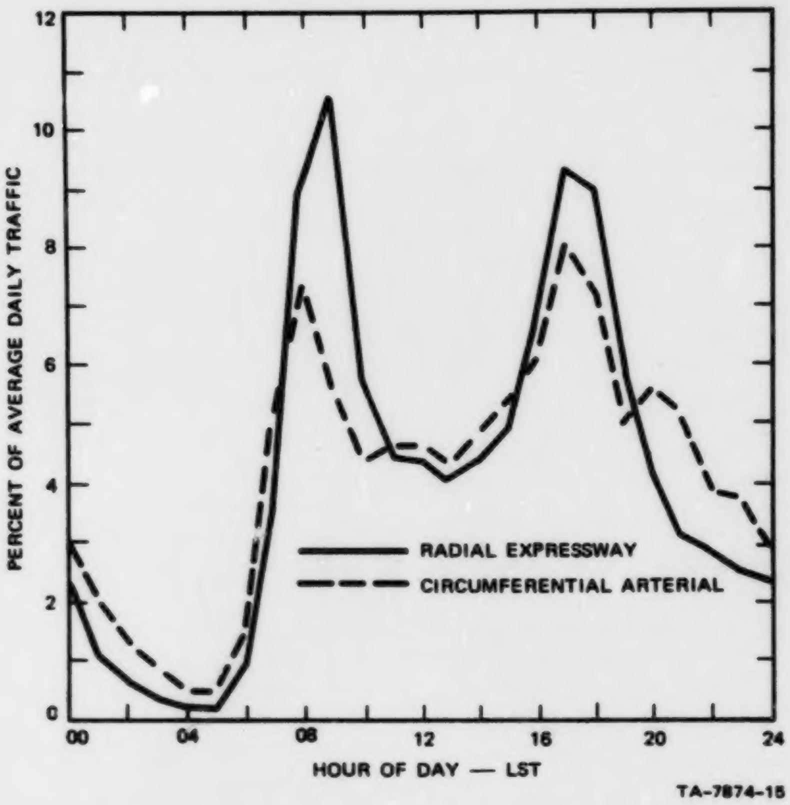

FIGURE 2 HOURLY DISTRIBUTION OF TRAFFIC FOR TWO FACILITY TYPES IN ST. LOUIS

link is found by multiplying E by the length of the link and by the hourly traffic volume.

Given the network of emissions, the diffusion model is applied on an area-source basis. The model uses a "Gaussian plume" diffusion formulation, in which the vertical concentration profile from a crosswind line source (such as a road) is assumed to be Gaussian in shape, as shown schematically in Figure 3. The spread of this vertical concentration distribution is characterized by its standard deviation, σ_z. On the basis of experimental data, σ_z, which represents the extent of the vertical diffusion, is taken to have the form

$$\sigma_z = ax^b \quad , \tag{2}$$

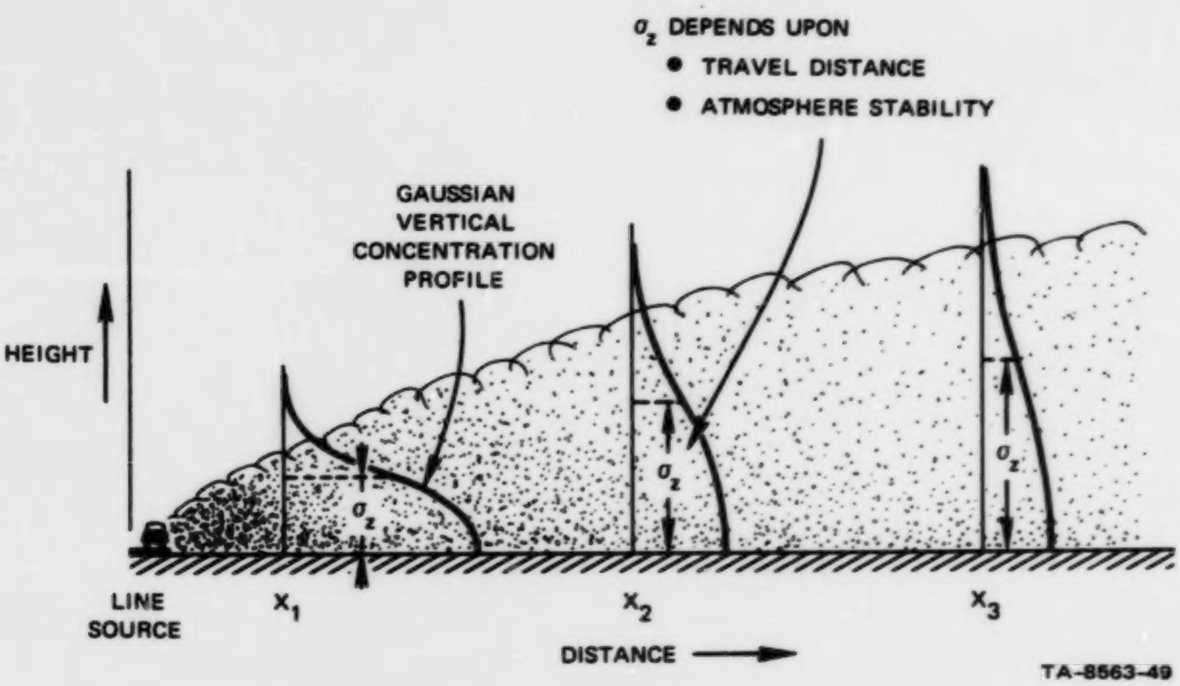
σ_z DEPENDS UPON
● TRAVEL DISTANCE
● ATMOSPHERE STABILITY
GAUSSIAN VERTICAL CONCENTRATION PROFILE
HEIGHT
σ_z
σ_z
σ_z
LINE SOURCE
x_1
x_2
x_3
DISTANCE
TA-8563-49

FIGURE 3 VERTICAL DIFFUSION ACCORDING TO GAUSSIAN FORMULATION

where x is the downwind distance and the parameters a and b depend upon atmospheric stability.

So that nearby sources can be more precisely located, the model uses a number of area segments spaced at logarithmic upwind range intervals, as shown in Figure 4. These area segments are oriented in the direction of the transport wind, and they overlay the emissions (traffic) network. The traffic links and portions of links falling within each area segment are identified, the emissions from the individual links accumulated, and the total emission then assumed to be released uniformly over the area segment.* The contributions from each of

---

*To save computer time, the emissions within the four segments farthest from the receptor are calculated by a different technique than that used for the closer segments. The outermost segments are larger than those nearby, and it was felt that the spatial resolution achieved by the link assignment technique was not necessary when the emissions were to be averaged over the entire large area of each outer segment.

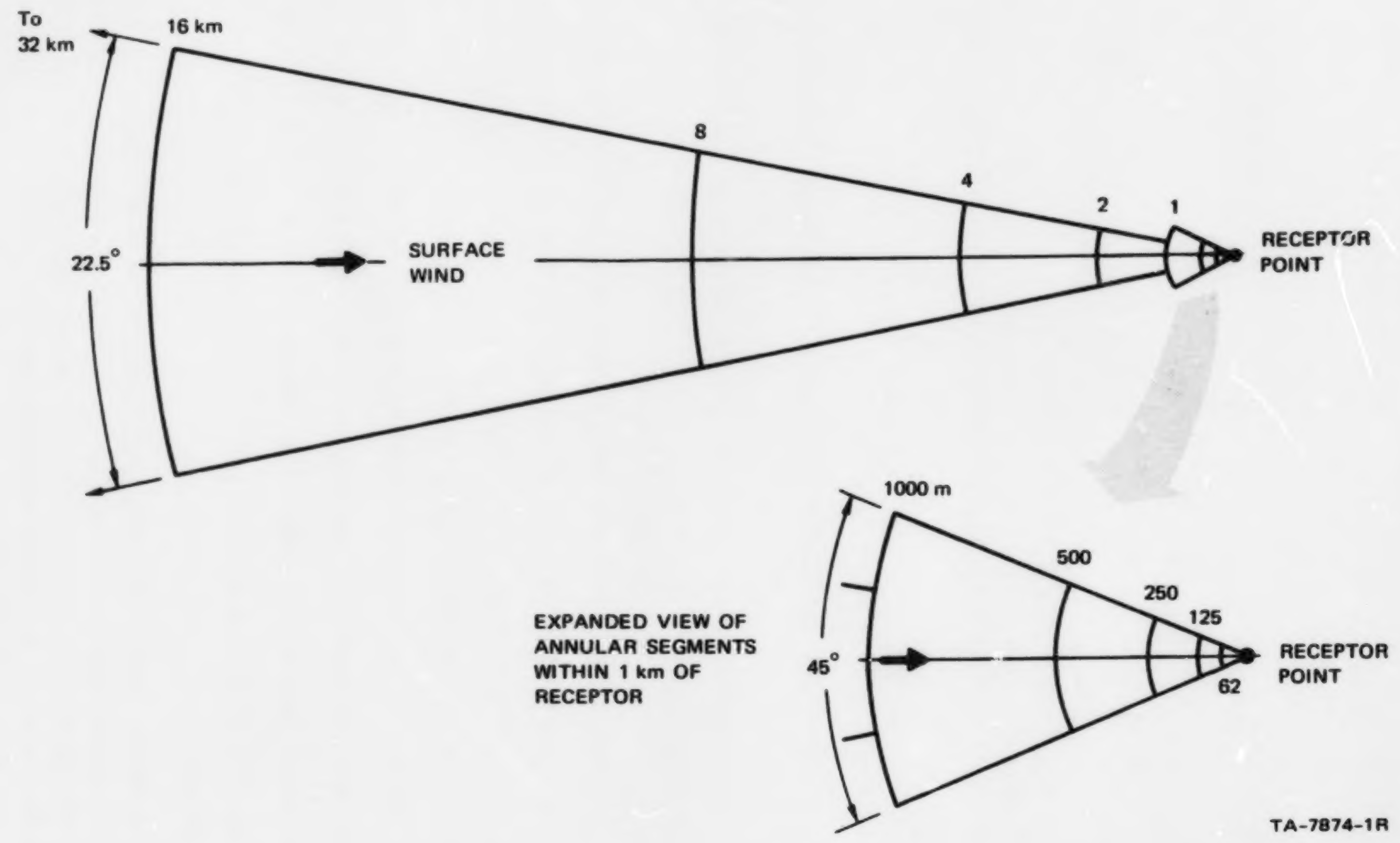
To
32 km
16 km
22.5°
SURFACE
WIND
8
4
2
1
RECEPTOR
POINT
1000 m
500
250
125
62
RECEPTOR
POINT
45°
EXPANDED VIEW OF
ANNULAR SEGMENTS
WITHIN 1 km OF
RECEPTOR
TA-7874-1R

FIGURE 4 DIAGRAM OF SEGMENTS USED FOR SPATIAL PARTITIONING OF EMISSIONS

the ten area sources to the CO concentration at the receptor are computed individually using the simple formulation given below, and then added to find the total concentration (C):

$$\left(\frac{C}{Q_A}\right)_{ij} = \frac{0.8}{u\,a_{ij}}\left(1 - b_{ij}\right)^{-1}\left(x_{i+1}^{1-b_{ij}} - x_i^{1-b_{ij}}\right) \quad , \qquad (3)$$

where Q_A is the average area emission rate (g m^{-2} s^{-1}) from a particular segment, u is the transport wind speed, and the subscripts denote different segments (i) and stability classes (j).

A simple "box" model,

$$\left(\frac{C}{Q_A}\right)_i = \frac{r_{i+1} - r_i}{uh} \quad , \qquad (4)$$

is applied for distant segments when there is a limited mixing depth (h) determined by the vertical temperature stratification. Under these conditions, pollutants tend to become uniformly distributed in the vertical after sufficient travel has taken place. We change from the Gaussian model to the box model at the distance where the two (in their respective line source formulations) give equal concentration values.

Besides the traffic data, the input variables required for the model are (1) transport wind direction, (2) transport wind speed, (3) mixing depth, and (4) atmospheric stability type, as exemplified in Figure 5 by a week's data for Chicago. The model is designed to be generally applicable to any city, where conventional (airport) weather observations might be the only observations available. None of the required input variables are directly observed. The airport surface wind speed and direction have been applied as a first approximation to the transport wind, but suitable adjustments need to be made to account for urban effects. Separate submodels had to be developed to estimate

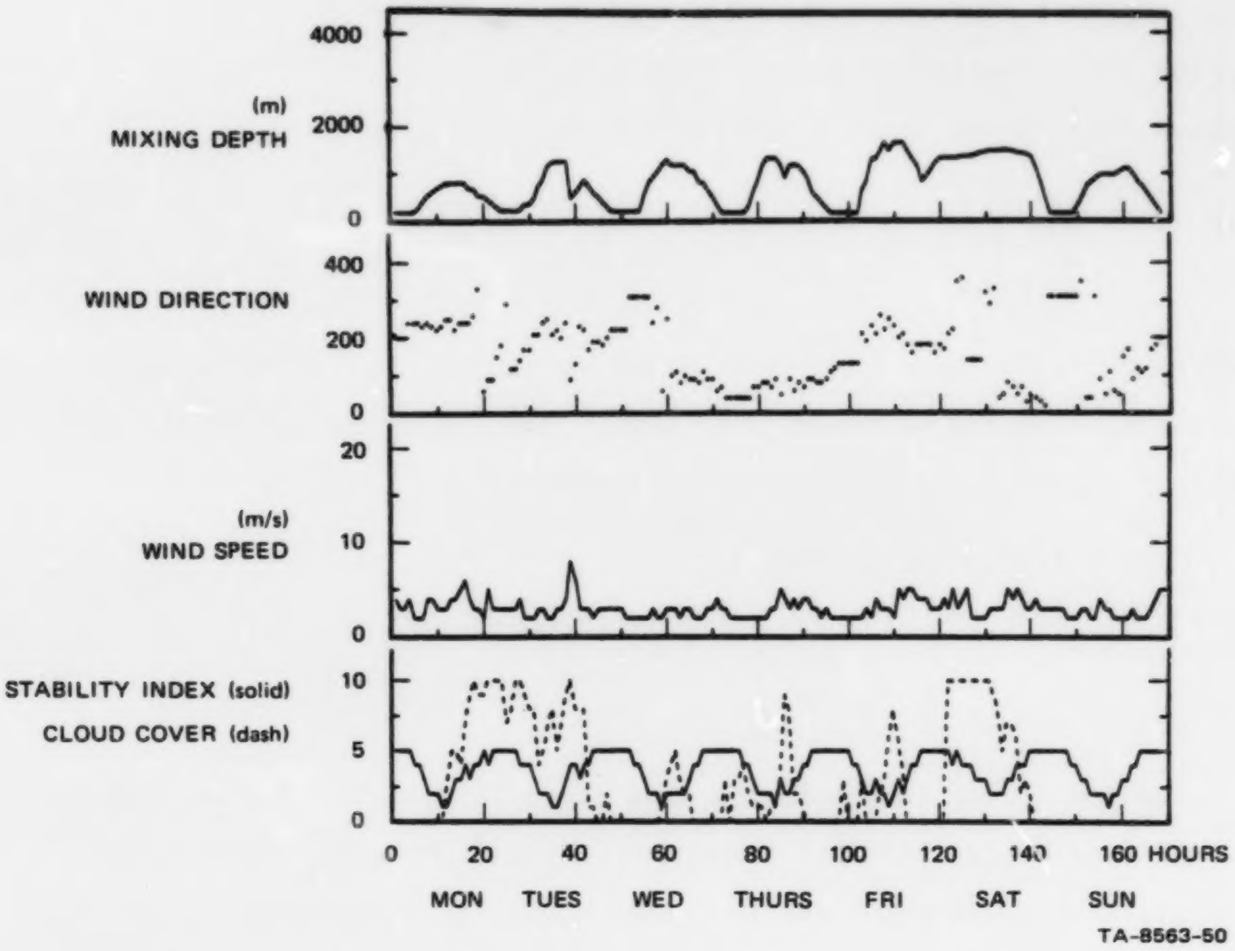

FIGURE 5 METEOROLOGICAL INPUT PARAMETERS REQUIRED BY THE DIFFUSION MODEL—CHICAGO DATA (19-25 October 1964)

mixing depths and stability categories from the available airport observations.

2. Capabilities of the Basic Model

There are two configurations of the basic model: (1) synoptic and (2) climatological. The former is useful in an operational sense; the latter is designed as a tool for planning activities. The synoptic model uses hour-by-hour values of meteorological and traffic data and calculates hour-average CO concentrations at a point or for a grid of points. An example of the latter is presented in Figure 6, where the

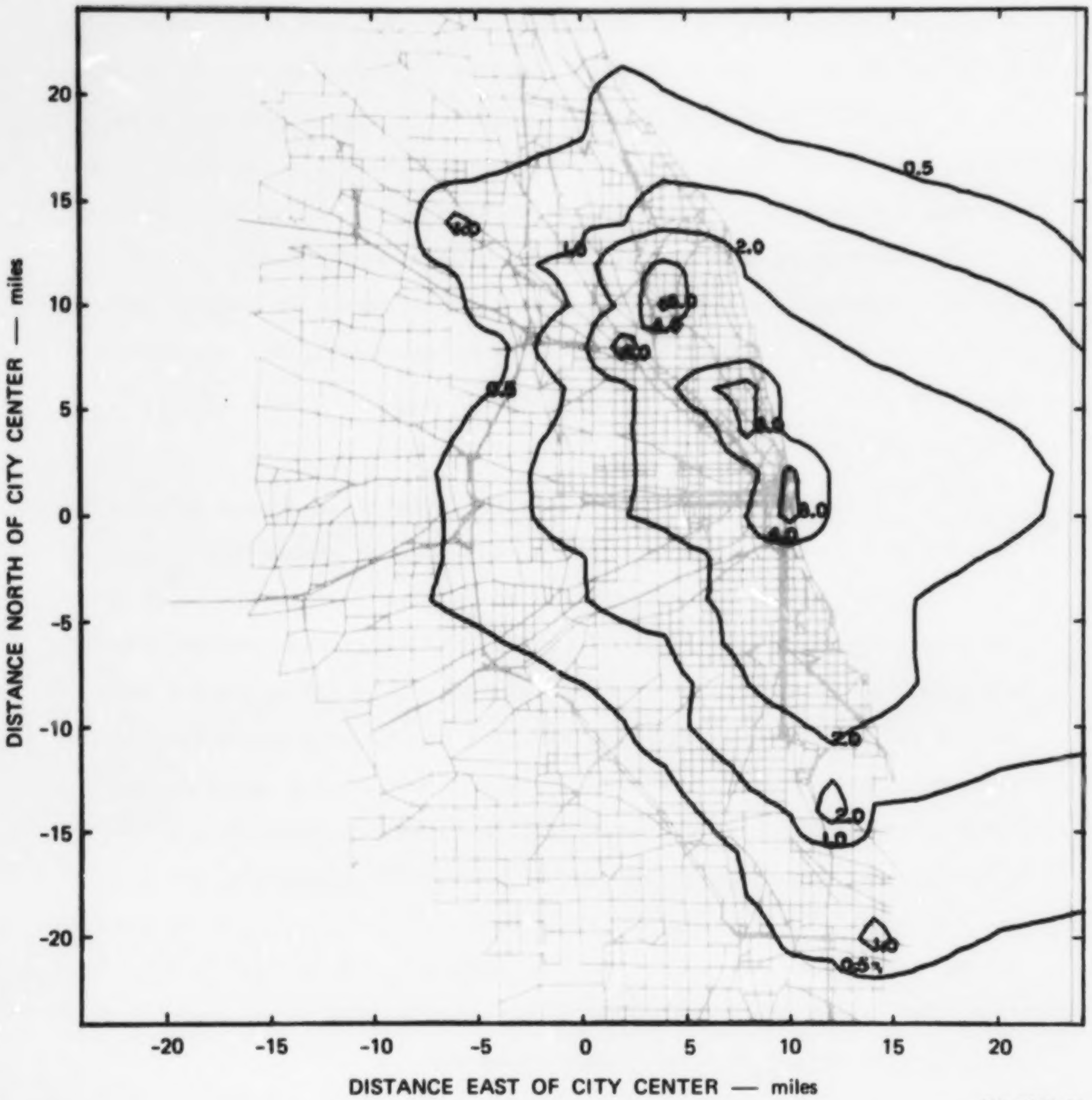
0.5
2.0
1.0
0.5
2.0
2.0
1.0
1.0
0.5
20
15
10
5
0
-5
-10
-15
-20
DISTANCE NORTH OF CITY CENTER — miles
-20
-15
-10
-5
0
5
10
15
20
DISTANCE EAST OF CITY CENTER — miles

TA-7874-62

FIGURE 6 CALCULATED CARBON MONOXIDE CONCENTRATIONS (PPM) FOR CHICAGO. (0700-0800 LST; wind 4 ms^{-1}, 270°; mixing depth 200 m; neutral stability)

concentration calculations, objective contouring, and graphical display were all controlled by a CDC 6400 computer.* The road network is shown as an underlay. Figure 7 illustrates the telescoping grid or "zoom" capability of the model. In the bottom section of the figure, the grid spacing was reduced by a factor of ten to depict the detailed concentration pattern in downtown St. Louis. The synoptic model can use either historical, current, or forecast input data. An example of a projection of CO concentration patterns in St. Louis, for specified meteorological conditions, is presented in Figure 8; here forecast traffic data for the year 1990 were used.

The climatological model is really a trimmed-down version of the synoptic model, which has been streamlined to reduce the computing time required for each concentration calculation. This was necessary because the climatological model is designed to furnish probability or frequency distributions of CO concentrations at a point, rather than only a single value, as with the synoptic model. The concentration frequency distributions are built up from hour-by-hour calculations using a long series (five years) of climatological data for a given city. Using this large number of concentration values, one can obtain various types of frequency distributions, such as for different times of the day (Figure 9), or for various averaging times (Figure 10). Thus, for example, the 90-percentile concentrations to be expected for a variety of situations can readily be found.

C. Scope of the Current Project

In evaluating the performance of the model after the first-stage development, we made extensive comparisons (including regression analyses)

---

*Typical computer costs for a 625-point calculation, analysis, and display, as shown in Figure 6, are about $40.

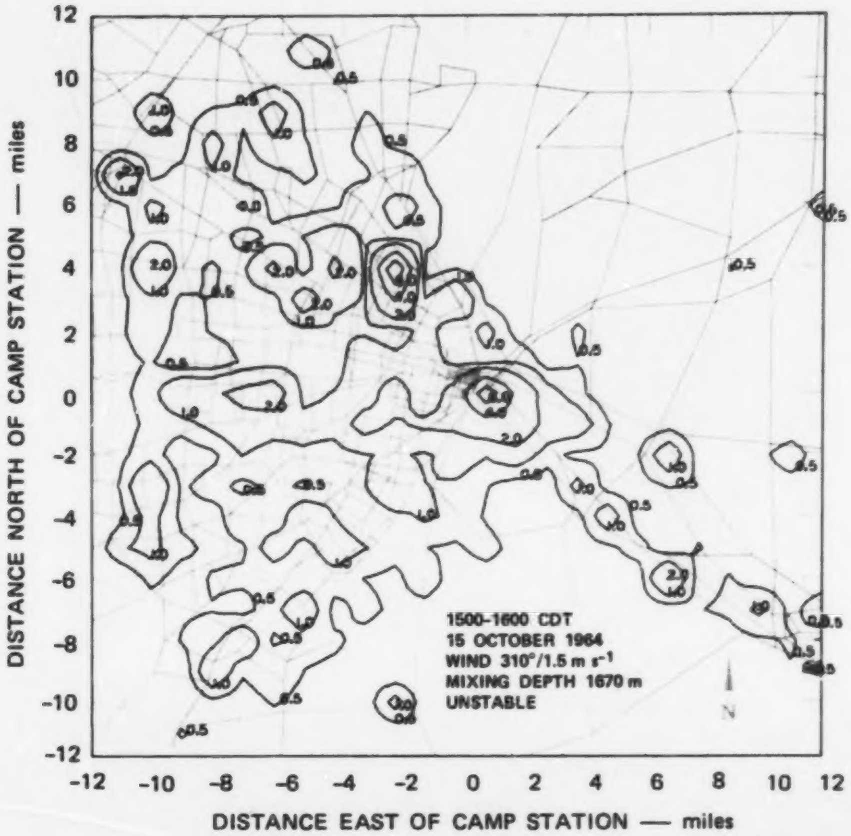

TA-7874-26

(a) 1-MILE (1.6 km) GRID SPACING

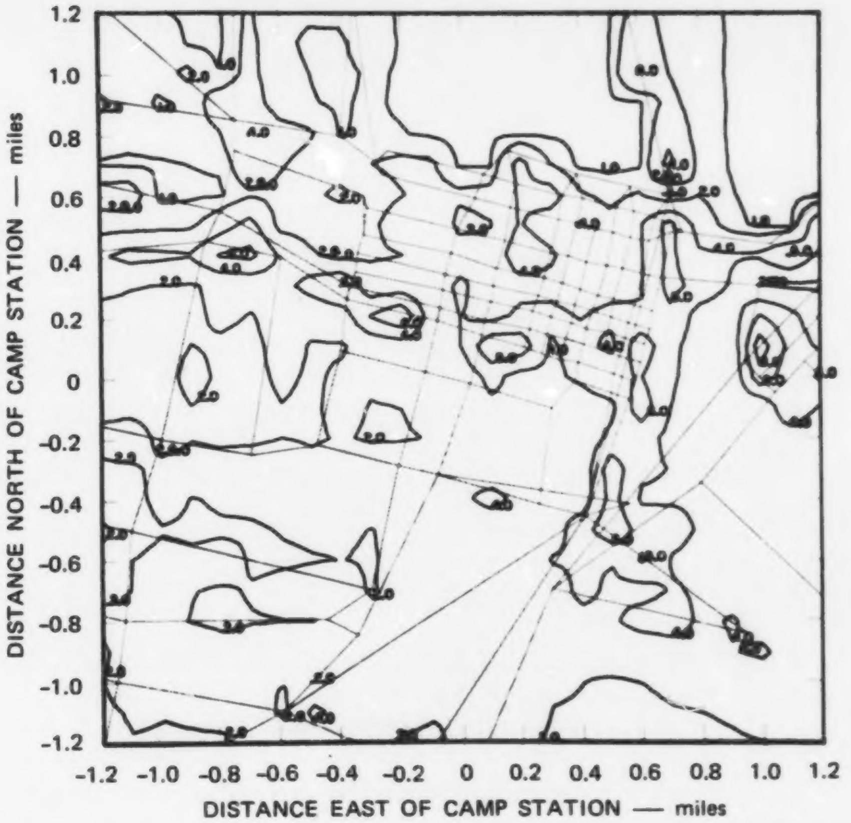

TA-7874-24

(b) 0.1-MILE (0.16 km) GRID SPACING

FIGURE 7 CALCULATED ST. LOUIS CONCENTRATION PATTERNS FOR TWO GRID SIZES

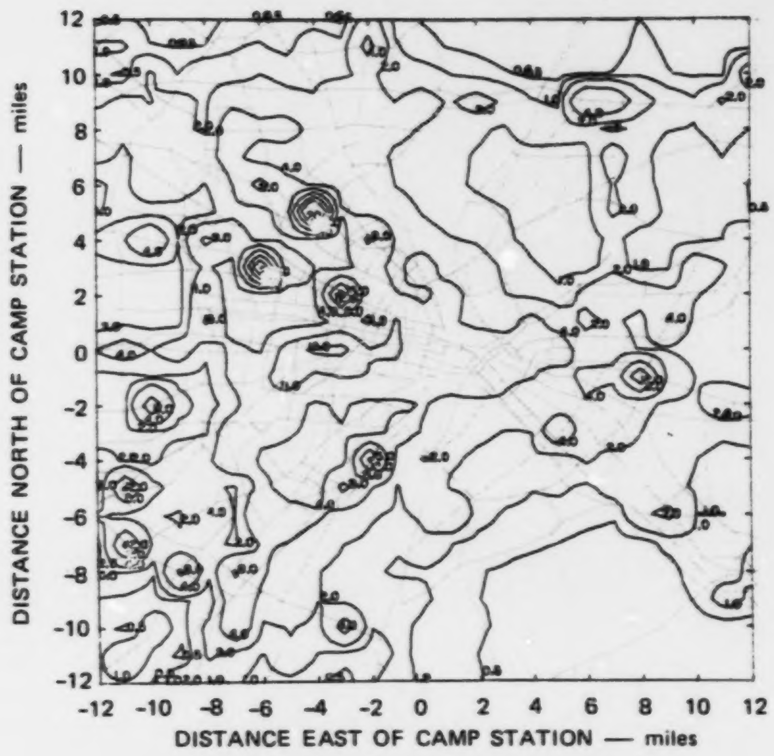

(a) WITHOUT EXHAUST EMISSION CONTROLS

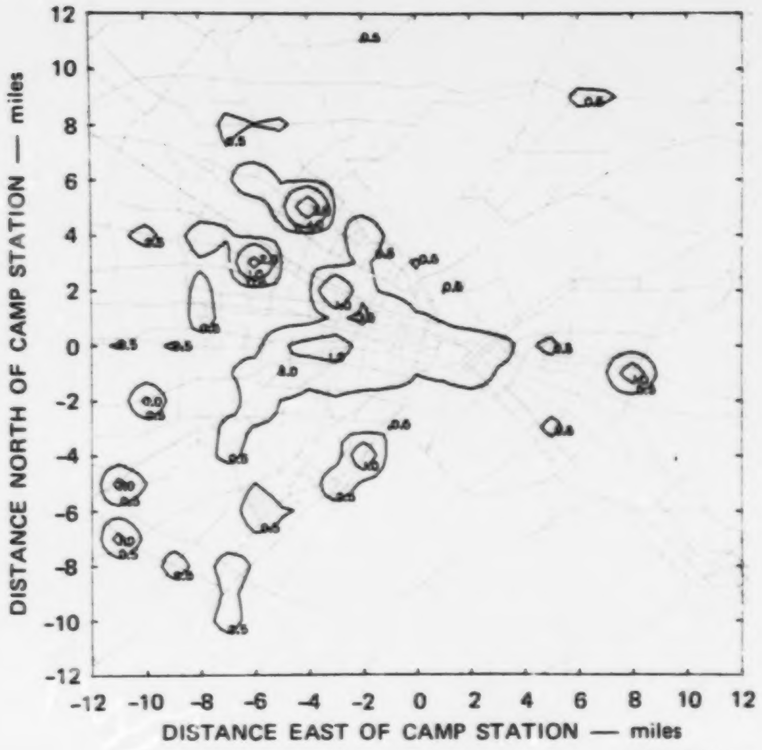

TA-7874-61

(b) WITH EXHAUST EMISSION CONTROLS

FIGURE 8 CALCULATED CONCENTRATION PATTERNS BASED ON FORECAST OF 1990 ST. LOUIS TRAFFIC

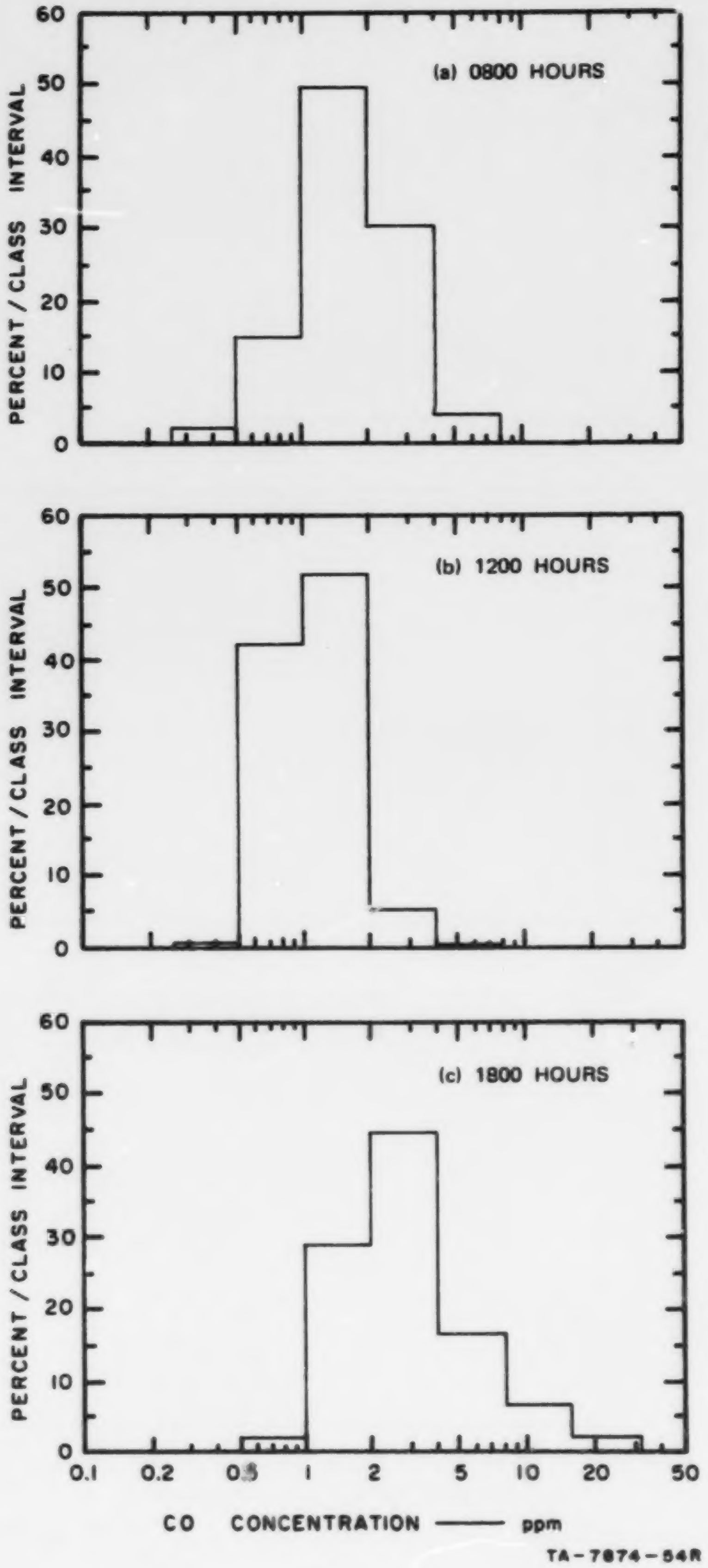

FIGURE 9 CALCULATED ST. LOUIS CAMP STATION CO CONCENTRATION FREQUENCY DISTRIBUTION FOR 1965 TRAFFIC CONDITIONS; 0800, 1200, AND 1800 HOURS

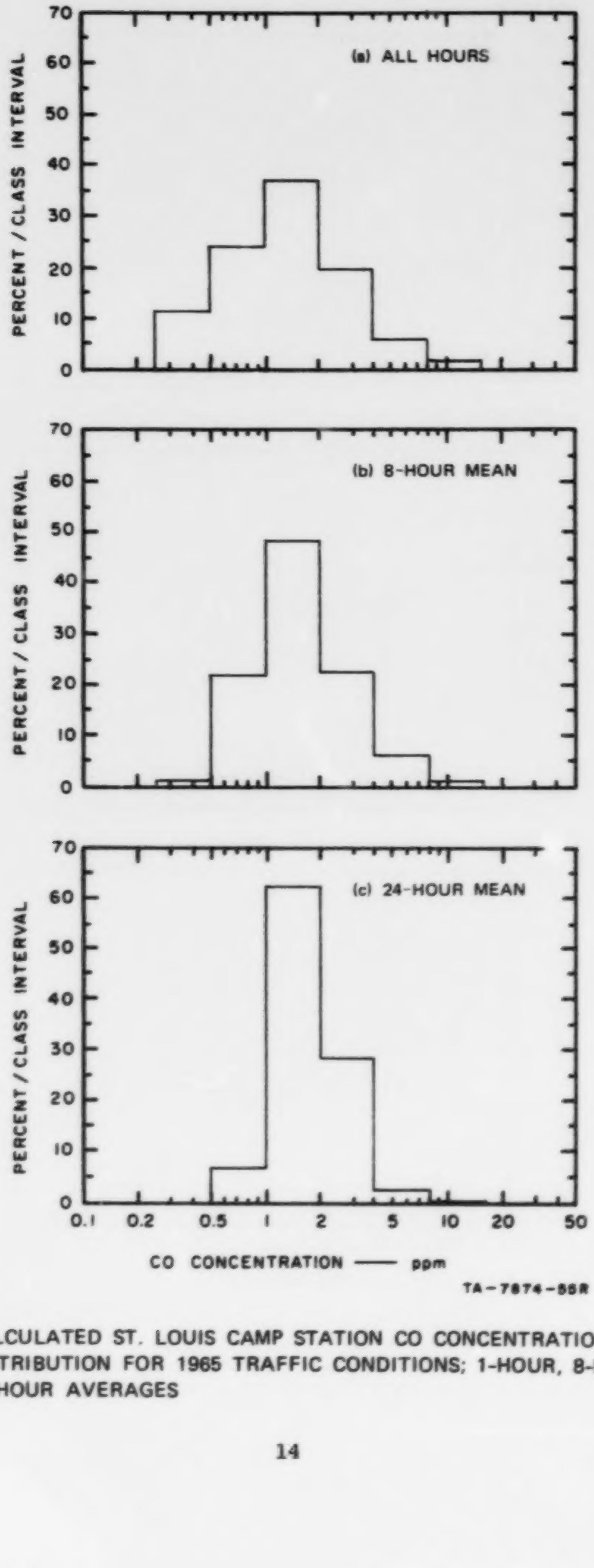

FIGURE 10 CALCULATED ST. LOUIS CAMP STATION CO CONCENTRATION FREQUENCY DISTRIBUTION FOR 1965 TRAFFIC CONDITIONS; 1-HOUR, 8-HOUR, AND 24-HOUR AVERAGES

of calculated concentrations and those observed at the CAMP stations in Chicago, St. Louis, Denver, Cincinnati, and Washington, D.C. An example of such a comparison for hourly concentrations is presented in Figure 11. Generally, the agreement is fair to good, at least in terms of trends, although there are some instances of poor agreement.

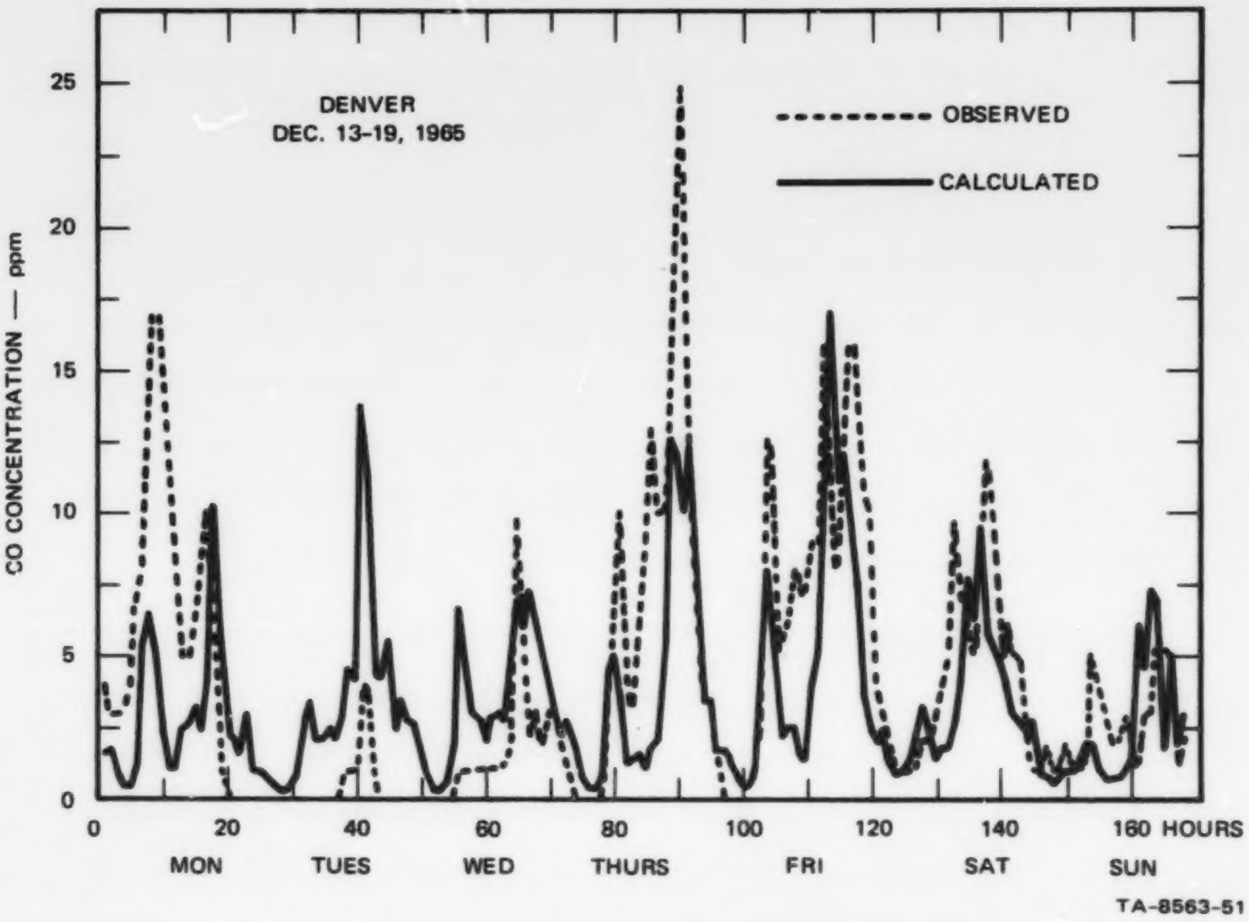

FIGURE 11 COMPARISON OF CALCULATED AND OBSERVED HOURLY CO CONCENTRATIONS AT THE DENVER CAMP STATION FOR A ONE-WEEK PERIOD

The weaknesses in the model performance were ascribed to three main factors:

(1) Deficiencies in the input data, particularly the traffic data.

(2) Weaknesses in the basic model formulation itself and in the submodels used to estimate some of the input parameters from conventional meteorological data.

(3) The lack of a suitable street-effects submodel to handle the problem of local diffusion within street canyons and to compensate for the influences of buildings on concentrations measured at nearby receptor sites.

The last factor is perhaps the most important in terms of achieving better agreement between calculated concentrations and CAMP-measured values. This is apparent when one considers that the CAMP stations were deliberately located to make measurements in areas where concentrations were expected to be high, as in the case of the Chicago station shown in Figure 12. This station is near a heavily traveled street and immediately adjacent to a tall building.

The second phase of this research effort, then, has been concerned with improving and evaluating the model in the areas discussed above. To do this, we have conducted a field study in San Jose, California, which has excellent traffic data. In this comprehensive measurement program, we have collected the special data needed for the following tasks: (1) improve the submodels for estimation of input parameters, (2) develop a street-effects submodel, and (3) evaluate the performance of the basic model and its subunits. The structure of this experimental program, and its results, will be described in subsequent sections.

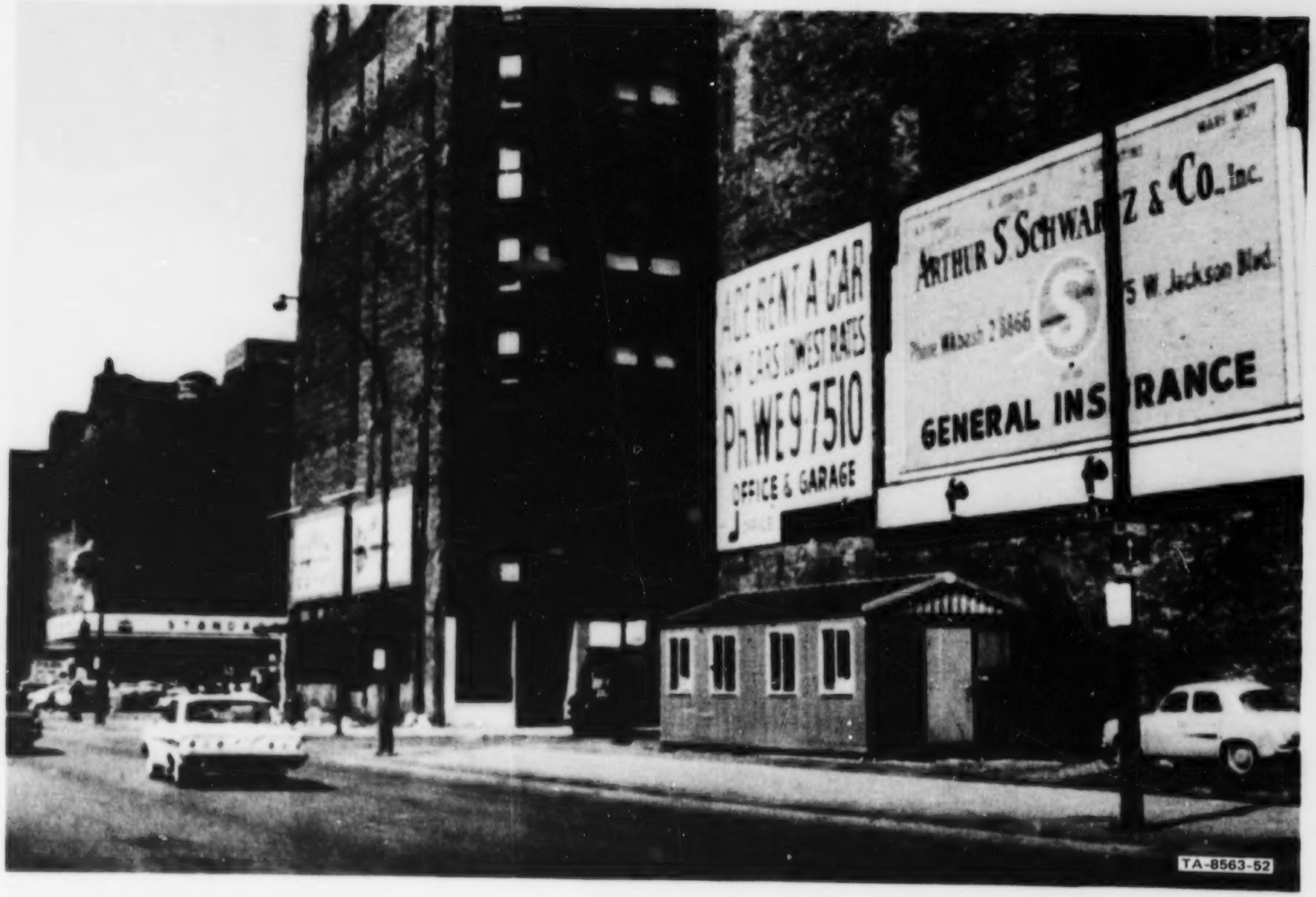
ACE RENT A CAR
NEW CARS LOWEST RATES
Ph WE 9 7510
OFFICE & GARAGE
ARTHUR S. SCHWAR Z & Co. Inc.
Phone WAbash 2 3866
S W. Jackson Blvd.
GENERAL INS RANCE
TA-8563-52

FIGURE 12 CHICAGO CAMP STATION

BLANK PAGE

II DESCRIPTION OF THE SAN JOSE FIELD PROGRAM

A. Background

As has already been noted, the field program described in this report had been designed to check the operation of the diffusion model developed earlier (Ludwig et al., 1970). In particular, we were concerned about the ability of the model to cope with small-scale effects such as occur around buildings and in street canyons. We also wanted to check some of the fundamental aspects of the model design as they related to describing the behavior of the emission and dispersion of pollutants on a scale of a few kilometers. To study all these factors, we heavily instrumented an intersection in a downtown area and organized a program for making airborne and street-level measurements around the perimeter of that downtown area. This section of the report describes the experimental program only in sufficient detail so that the reader can understand the results that follow in later sections. Instrumentation, data processing, and other aspects of the program are described in greater detail in the appendices to this report.

B. Experimental Area

1. Seclection of San Jose

Two factors entered most heavily into the selection of San Jose as the location for our initial experiments. San Jose has some advantages that make it a valuable experimental site. Most important of these is the City's traffic monitoring network. This network provides computer-compatible information about traffic in the downtown area. This information is available with high resolution in both space and

PRECEDING PAGE BLANK

time. We considered the availability of these traffic data to be very important. The nature of these traffic data and of other corollary information available in San Jose will be discussed further on subsequent pages. San Jose is also a desirable location with regard to the practical matters of program management. The experiment we planned was quite complicated; much of the equipment was newly designed or had been assembled into unique combinations. The siting arrangements were somewhat unusual and required considerable contacts with building owners and public officials. All these facts dictated that the experiments be conducted nearby, so that the resources of the Institute would be available when we encountered the inevitable difficulties of complex field experiments.

2. Downtown San Jose

The city of San Jose has a population of about 435,000 (Rand McNally, 1970). Because of its proximity to San Francisco and Oakland and because of the plethora of large neighborhood shopping centers, downtown San Jose is not as developed as many cities of its size. However, it does have a number of multistory buildings, as can be seen in the aerial view shown in Figure 13. The location of the streetside experiment at the intersection of First and San Antonio Streets is marked by the circle on this photograph.

This particular location was selected because it is an area of relatively uniform building height, compared to most other downtown intersections. When originally selected, the buildings at all four corners of the intersection were available to be used for the experiment. Subsequently, the building at the south corner of the intersection was extensively remodeled, which prevented us from making measurements there. Figure 14 shows a map of the area surrounding the intersection, the

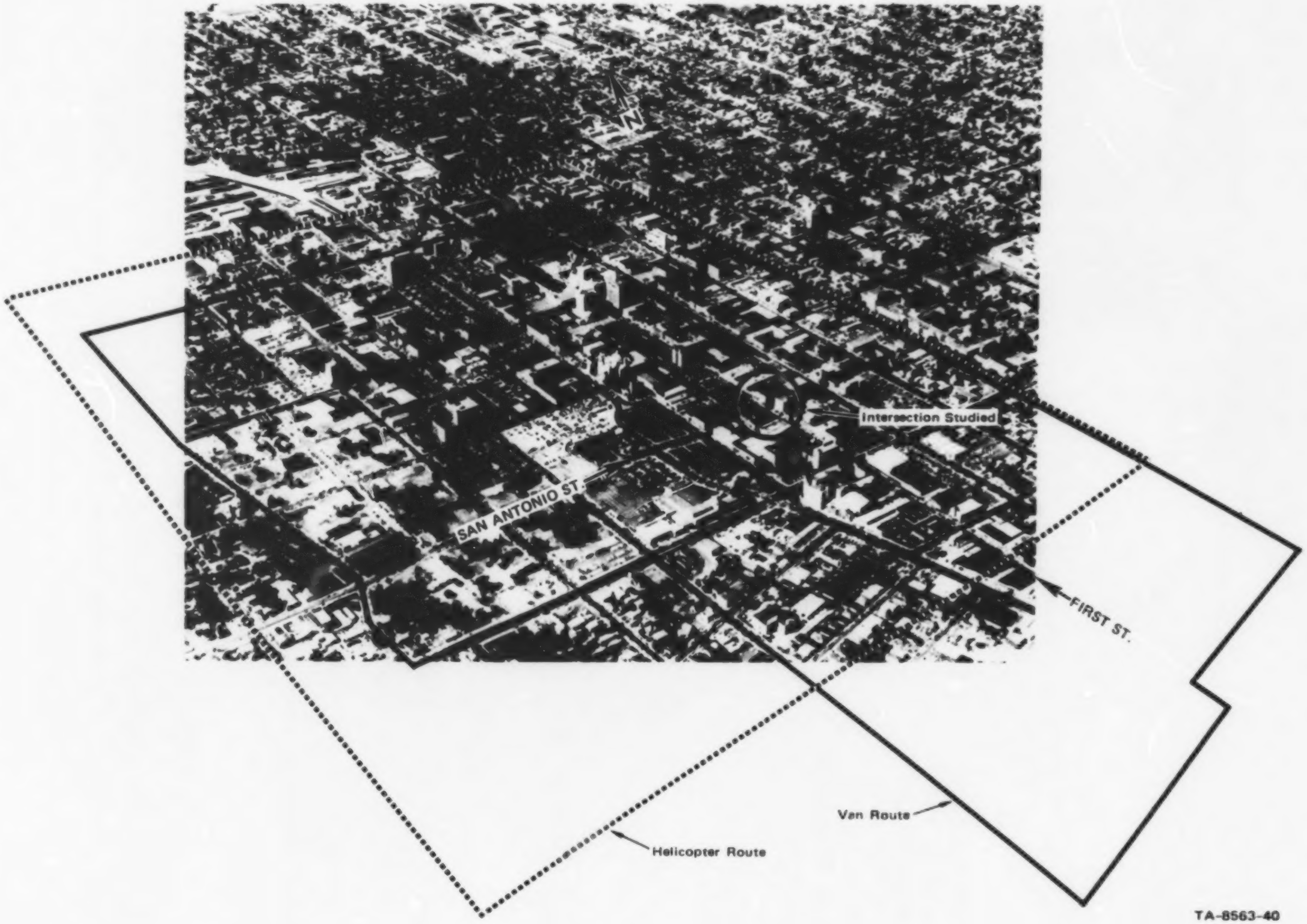
N
Intersection Studied
SAN ANTONIO ST.
FIRST ST.
Van Route
Helicopter Route
TA-8563-40

FIGURE 13 AERIAL PHOTOGRAPH OF SAN JOSE SHOWING INTERSECTION STUDIED AND HELICOPTER AND VAN ROUTES

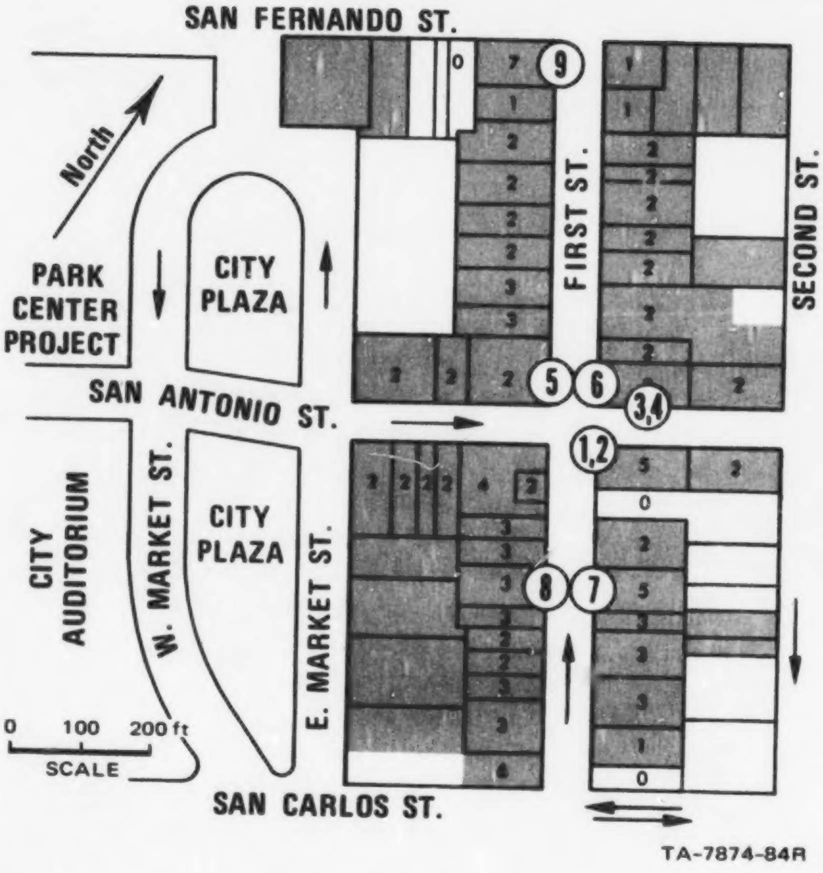
SAN FERNANDO ST.
North
PARK CENTER PROJECT
CITY PLAZA
CITY PLAZA
SAN ANTONIO ST.
CITY AUDITORIUM
W. MARKET ST.
E. MARKET ST.
FIRST ST.
SECOND ST.
SAN CARLOS ST.
0 100 200 ft
SCALE
9
5
6
3,4
1,2
8
7

(BUILDINGS ARE SHADED AND NUMBERS OF FLOORS ARE INDICATED BY SMALL NUMERALS)

TA-7874-84R

FIGURE 14 MAP OF AREA AROUND INTERSECTION OF FIRST AND SAN ANTONIO STREETS

locations of our experimental sites, the building heights, and traffic flow directions. Figure 15 is a picture taken toward the intersection of First an San Antonio Streets from the top of the seven-story building at First and San Fernando Streets, Site 9. As can be seen in this photograph, the area is typical of the downtown regions of many middle-sized cities.

In addition to the streetside experiment conducted around the one downtown intersection, large-scale experiments were undertaken to define the effects from the entire downtown area. These involved helicopter- and truck-borne instrumentation traveling about the downtown area. The routes taken by these vehicles around the central downtown area are marked in Figure 13.

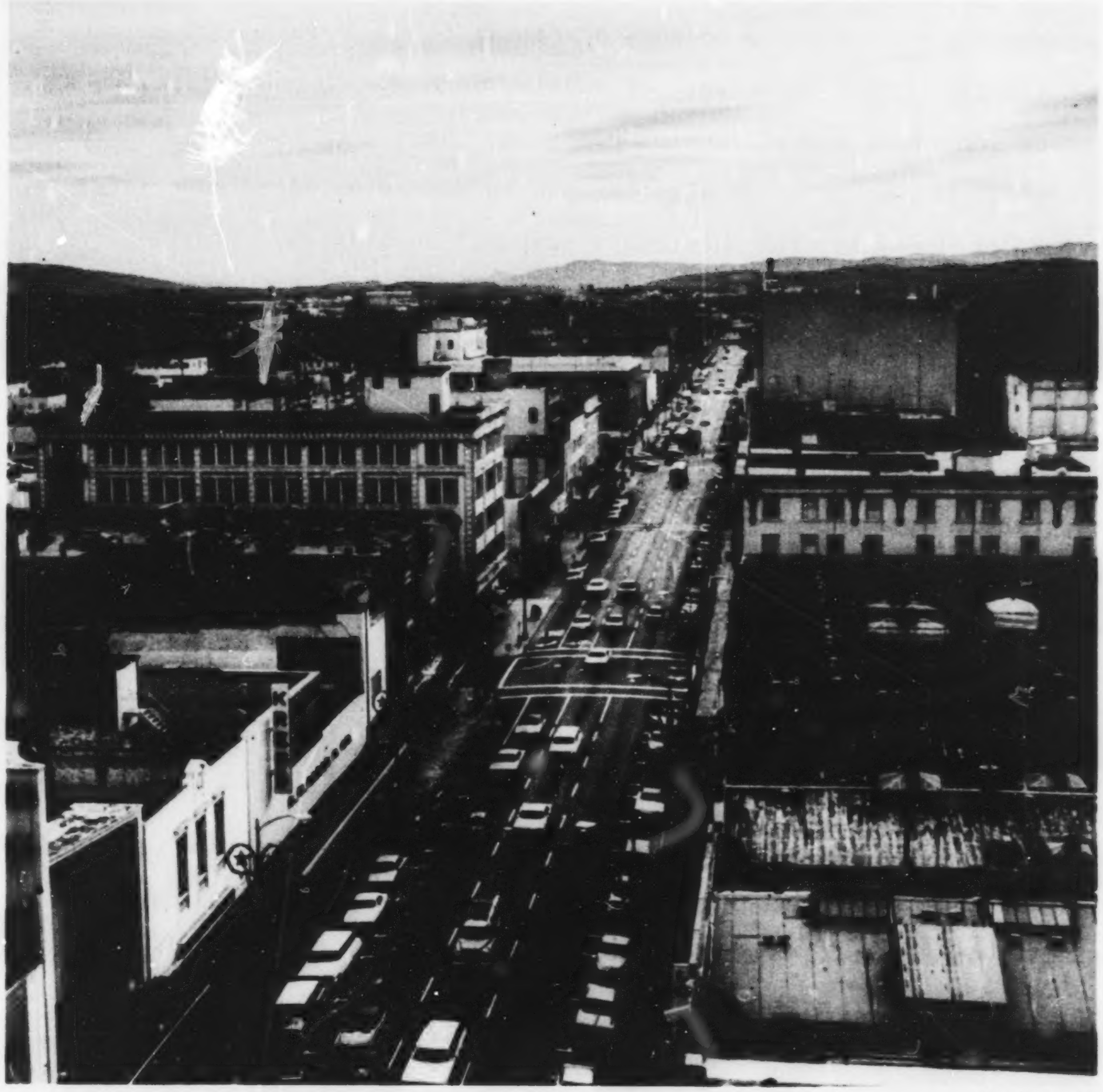

TA-8563-41

FIGURE 15 LOOKING TOWARD FIRST AND SAN ANTONIO FROM FIRST AND SAN FERNANDO

C. Instrumentation and Operations

1. Fixed-Station Measurements

Three types of measurements were considered useful for determining the street-scale processes operating to disperse the CO emitted from traffic. Most important, of course, were the CO concentrations at various locations around the intersection. Next were the winds in the vicinity. The winds could also be used to determine turbulence intensities, if measured with sufficient temporal resolution. Finally, the vertical temperature gradients were of some importance in determining the thermal stability of the air in the street canyons.

In addition to data that we would obtain from measurements, there were other data that we got from other sources. These included the traffic data already mentioned, meteorological observations in the area, and pollutant concentrations at a location outside downtown San Jose.

a. Instrumentation

The instrumentation is described in detail in Appendices A through C. In this section we only outline the basic nature of the equipment and its principles of operation. Two types of measuring stations or terminals were employed (see Figure A-1 in Appendix A). At the Type A terminals (Remote Units 1-2 and 3-4), CO was measured at five different levels; the three wind components were measured at roof level and at a height of 3 m, and the temperature difference in the vertical was determined from sensors at five different heights. The second type of station (Type B terminals) was installed at the other five locations. At these, CO was also measured, but not temperature gradients, and only two-component winds at the 3-m level were determined.

1) Carbon Monoxide

Nondispersive infrared analyzers were used to measure the CO concentrations. These devices were manufactured by Beckman Instruments. They have a 40-inch-long absorption cell and use an optical filter to remove the effects of water vapor interference. They have a sensitivity of about 0.5 ppm, and during our operations we found that they generally maintained their calibration within about this same limit.

Inasmuch as it would have been prohibitively expensive to have provided a CO analyzer for each of the levels sampled, we used a single analyzer at each site and a manifold system with five inlets. This manifold system used solenoid-actuated valves to switch the CO analyzer from one inlet to another. The four levels that were not being sampled at any given time were continually purged with an auxiliary pump. Thus, the CO analyzer pump did not need to exhaust dead air from the tubing when air from a new level was switched to the instrument. The 1/4-inch-ID polyethylene tubes used to bring air from the five levels to the instrumentation were about 200 feet long; the CO analyzer samples at a rate of 2 liters min^{-1}, which exhausts the tube volume in about one minute. The purge-pump flow rate was about three times the CO sampler's flow rate. Checks of the polyethylene tubing indicate that there was no interference from this relatively inert material.

Figure 16 shows the CO inlet tubing as it appeared when installed on the building at the two types of stations. At the end of each tube was a filter to remove particulates that would interfere with the proper operation of the CO analyzer. Over these filters, facing downward, we placed polyethylene bottles to prevent rain from entering the system.

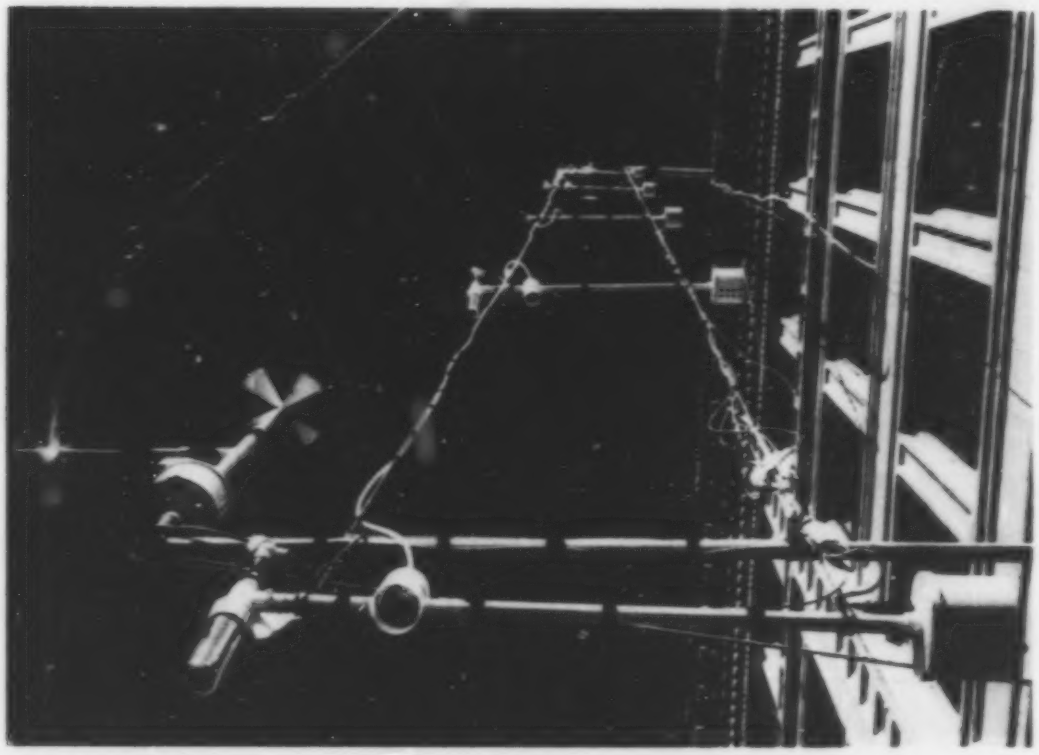

(a) SITE MEASURING CO, TEMPERATURE GRADIENT, AND THREE-COMPONENT WINDS

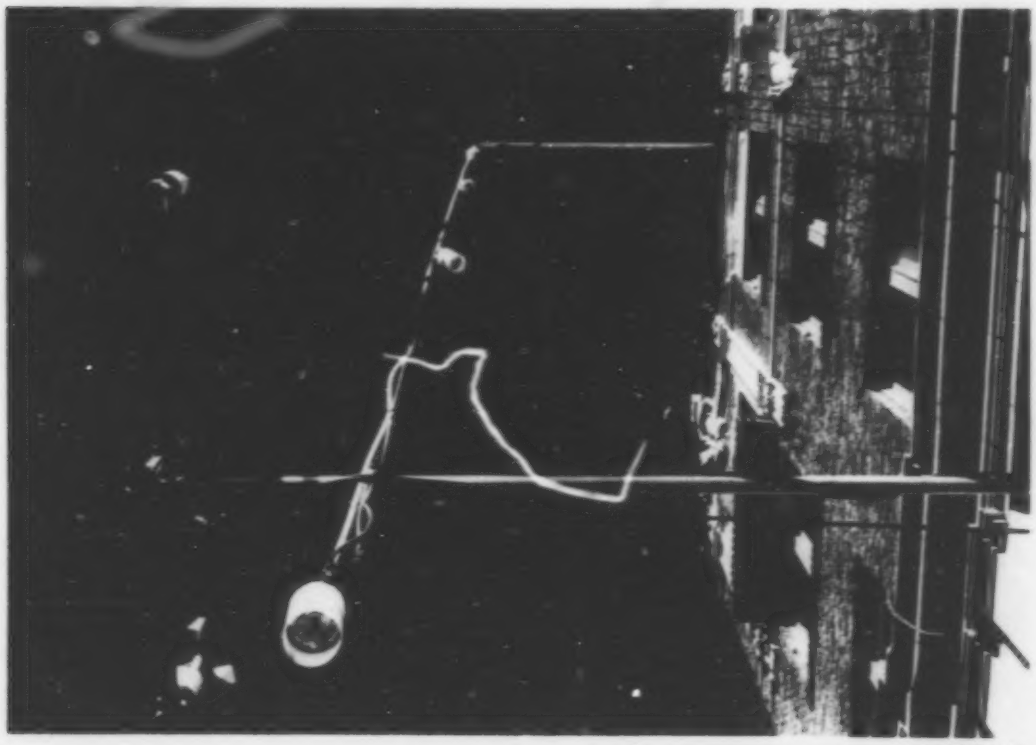

(b) SITE MEASURING CO AND TWO-COMPONENT WINDS

TA-8563-42

FIGURE 16 INSTALLATION OF INSTRUMENTATION AND CO INLET TUBING

2) Winds

Two basic types of wind sensor were used on this project. At the stations where the winds were measured at only the 3-m level, we used conventional low-inertia cup and vane sensors. These have a starting speed of less than 1 mi h^{-1}. They were located on booms extending about 3 m from the building, as shown in Figure 16.

Three-dimensional winds were measured at the sites of Remote Units 1 and 3, at both rooftop and 3-m levels. The units chosen for these measurements use three low-inertia propeller sensors whose axes of rotation are orthogonal. The starting speed of these instruments is about 0.5 mi h^{-1}. They were placed about 3 m from the building. The roof-level sensors were above the parapet top; one is shown in Figure 17. All the wind direction measurements were made relative to the street direction rather than to north. For those sites on First Street, a wind along the street, from approximately southeast, was taken to be a 180° wind.

3) Vertical Temperature Gradients

Platinum wire resistance elements were used to measure vertical temperature gradients. The actual elements were mounted in stainless steel tubes 0.125 inch in diameter, which were placed in silvered, double-walled glass cylinders similar to a Dewar flask. The inside diameter of these radiation shields is 3.2 cm. Ventilation was provided at a rate of about 15 ft s^{-1} by a blower located in a housing 1.1 m from the sensor. The time constant of the aspirated, steel-housed sensor is about 40 seconds. The whole assembly is shown in Figure 18.

The sensors were suspended at five equally spaced heights from 3 m to rooftop. The temperature differences between adjacent levels

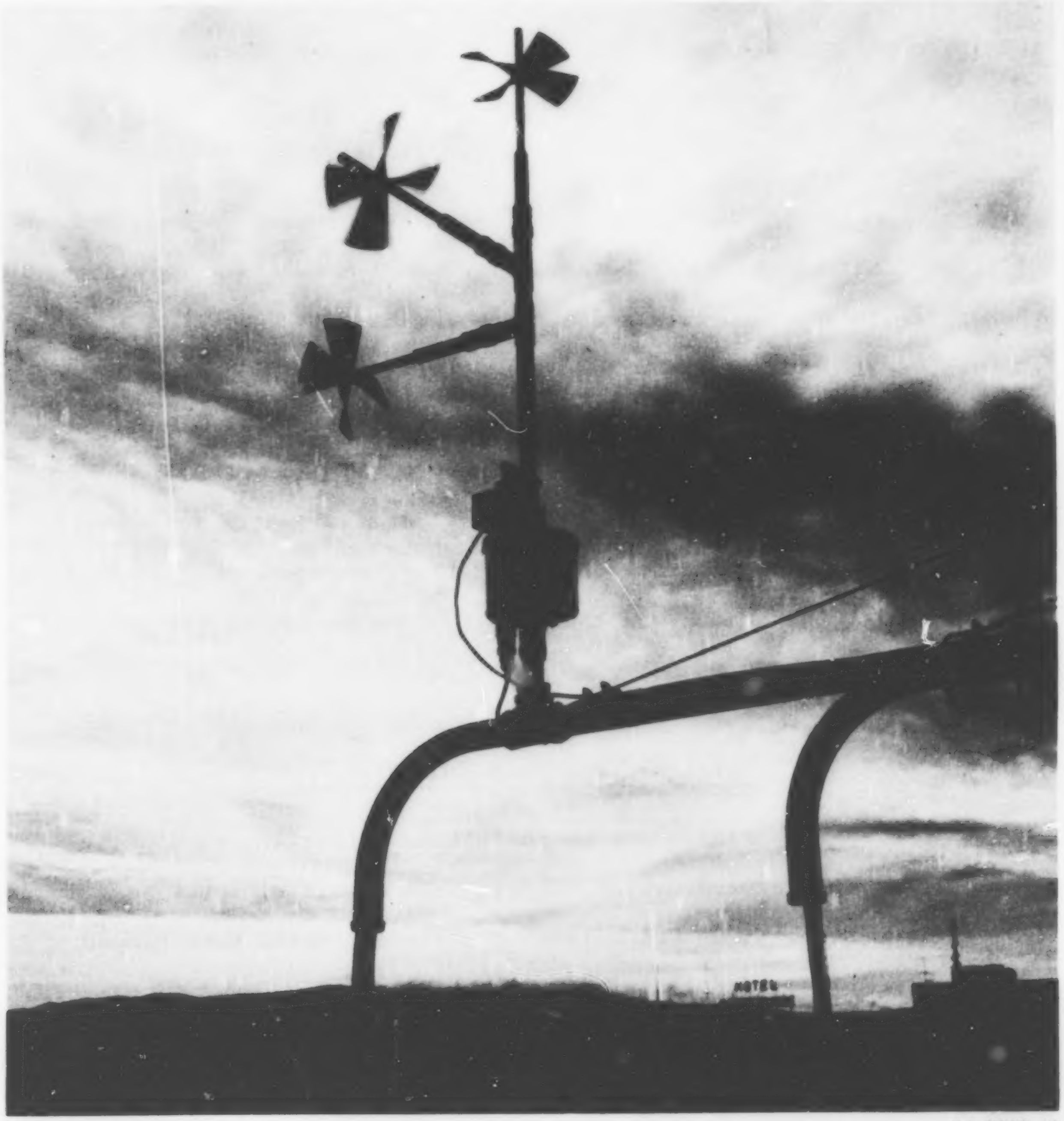

TA-8563-43

FIGURE 17 THREE-COMPONENT WIND SENSOR

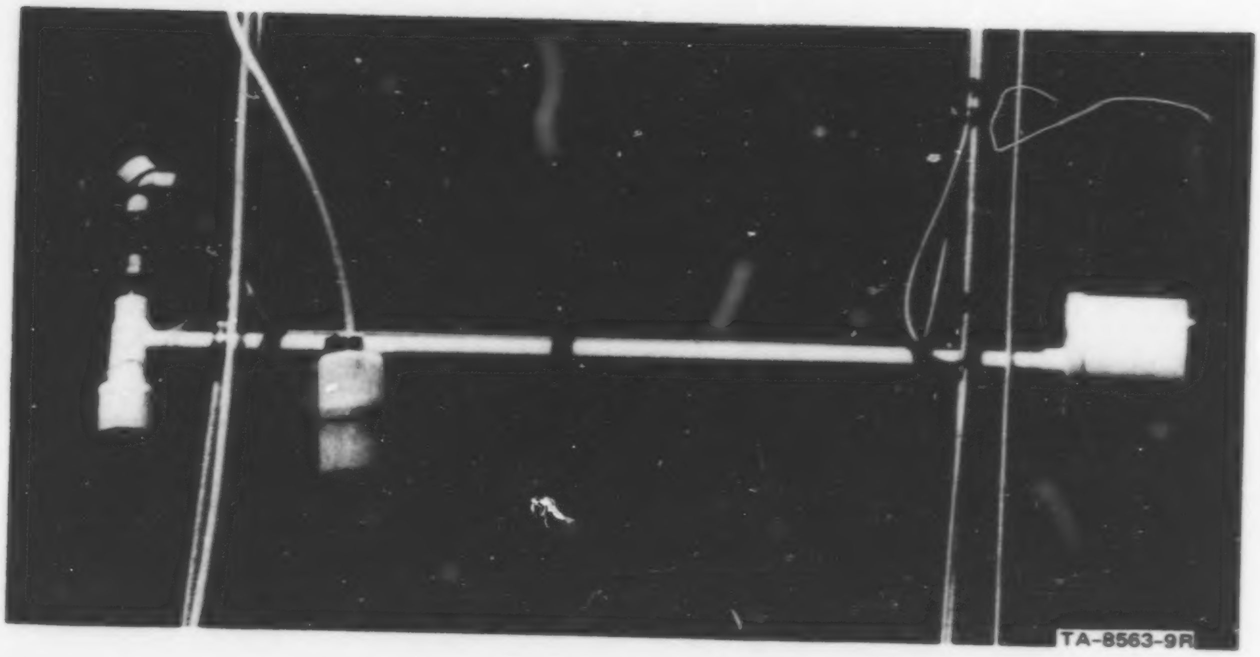

FIGURE 18 RADIATION SHIELD AND VENTILATION SYSTEM FOR TEMPERATURE SENSOR

were sensed and the voltage signal was electronically amplified. In this system the temperature difference could be detected to about ±0.01°C. Three ranges of ΔT were available: 0° to 1°C, 0° to 2°C, and 0° to 5°C.

b. Control and Data Acquisition System

The block diagram shown in Figure A-1 in Appendix A indicates the nine remote units used at the seven different sites. Inputs 1 and 2, and Inputs 3 and 4 were paired at two different sites. The first-named input of each pair transmitted the three-component winds, and the second the temperature and CO concentration information. Each remote unit had several sensors connected to it. The signal voltages from these sensors are selected by a reed relay multiplexer that connects one signal at a time to the input of an analog-to-digital (AD) converter. The AD converter has a resolution of 1/128 volt from -1 volt to +1 volt. Table 1 shows how this relates to the resolution available for each of the measured parameters. In this table the most commonly used range settings are marked by asterisks.

Table 1

RESOLUTION LIMITATIONS IMPOSED BY THE ANALOG-TO-DIGITAL CONVERTER

Parameter	Range	Resolution
Wind speed, components	-20.3 to +20.3 m s^{-1}	0.16 m s^{-1}
Wind speed, cup and vane	0 to 6.7 m s^{-1}	0.05 m s^{-1}
	*0 to 13.4 m s^{-1}	0.1 m s^{-1}
	0 to 26.8 m s^{-1}	0.2 m s^{-1}
Wind direction	0 to 360°	2.8°
Temperature difference	*-1 to +1° C	0.008° C
	-2 to +2° C	0.016° C
	-5 to +5° C	0.039° C
Carbon monoxide concentration	0 to 50 ppm	0.4 ppm

*Most commonly used range settings.

A small general-purpose computer with a magnetic tape recorder was located at one of the stations, marked "1, 2" in Figure 14. Each remote unit was connected to the computer and to the other remote units through two dc (20-mA) teletype circuits installed by the telephone company. The computer's transmitter contacts and the remote-unit receiver terminals were connected in series in one circuit, the command line. The other circuit, the data line, connected all the remote units' transmitter contacts and the computer's receiver terminals in series. Thus, the computer transmitted to all remote units simultaneously, and a single remote unit transmitted to the computer at any one time. The computer terminals were in a line-coupler unit that converted the low-voltage (~20 V) operation of the computer's second teletype interface to the higher voltage (~100 V) needed to drive the lines.

The sequence of operations was as follows. The computer sent a command message, consisting of two characters, to all the remote units. The first character was an address code, which would be recognized by one remote unit. On recognition of the address code, the activated remote unit began to send its data message to the computer. The second character of the command message was a sampling-height (level) code that the remote unit stored temporarily and then decoded to set the appropriate intake level for the CO analyzer.

The data message returned to the computer from the remote unit consisted of the level code stored at the time of the preceding command, followed by the CO measurement and the other measurements that the unit was programmed to make. The data message ended with its address code. Each measurement was transmitted as a 7-bit binary number plus even parity.

After the computer received the complete message, it checked the address code to verify that it corresponded to the address that was transmitted. Then another unit was commanded to report. The timing of command messages was derived from the computer's real-time clock in a programmed sequence. The sequence was as follows. It started by interrogating the seven remote units that had CO concentration inputs. At the time of interrogation, these units were switched to sample another level. This process took about one second per station. While the CO instruments were equilibrating to the inputs from the new levels, the three-component wind stations were interrogated. For 52 seconds the interrogation alternated between the two stations at which these measurements were made. Then the CO measuring stations were again interrogated in sequence and the complete cycle started once more.

In addition to interrogating the remote units and receiving their data, the computer had two other functions. It arranged the data for recording, and it did some averaging and preprocessing. When sufficient data had been accumulated, it wrote them on the magnetic tape. After each of the CO levels had been sampled and the data recorded on magnetic tape, the computer prepared and printed a summary for the 5-minute period necessary to accumulate those data. This summary was printed out on a teletype attached to the computer, taking about one minute to type the summarized information. No data were recorded during the printout period. An example of this material is shown in Figure D-1 of Appendix D. It proved quite useful for monitoring system performance in the field.

c. Operations

In general, the equipment was operated only during the daytime for this test, usually from about 0700 to 1800 PST. The electronic systems of the carbon monoxide analyzers were left running continually to maintain their stability. The computer was turned on and its control and recording functions were started at the beginning of the day. Each of the sites was then visited and the instruments put on line. This usually took about 15 minutes. During this time, data were only being recorded from those instruments that had been turned on. At the end of the operating period a similar situation arises as the instruments are taken off line and put on "standby" one by one.

After the instruments were all operating in the morning, the CO analyzers were calibrated. We used one source of zero gas and one of span gas to calibrate all the instruments. A high-purity helium was used to zero the instruments. A mixture of 19 ppm (certified analysis) CO in nitrogen was used to set the span on the equipment. The calibration results were recorded so that they could be used later in the data processing to correct the CO readings when the instruments had drifted significantly. It took about 5 to 10 minutes to calibrate an individual analyzer. It usually took one to two hours to make the rounds of the sites and complete the calibration of all the instruments.

The summarized data were monitored periodically, and if the operator detected any possible equipment malfunctions, they were checked and corrected where necessary. Of course, if there were equipment problems, they were noted in the station log and accounted for in subsequent data processing.

The station log was also used to record other significant events, e.g., street blockage by maintenance crews, idling vehicles near sampling sites (if noticed), and unusual events such as parades.

2. Mobile Measurements

a. Van

The streetside measurements were supplemented by data collected using instrumentation in a compact van. Two identically instrumented vans were used; one of these is shown in Figure 19. Temperature, wind, and CO concentrations were measured when the vans were stationary, and temperature and CO concentrations during traverses around the downtown area.

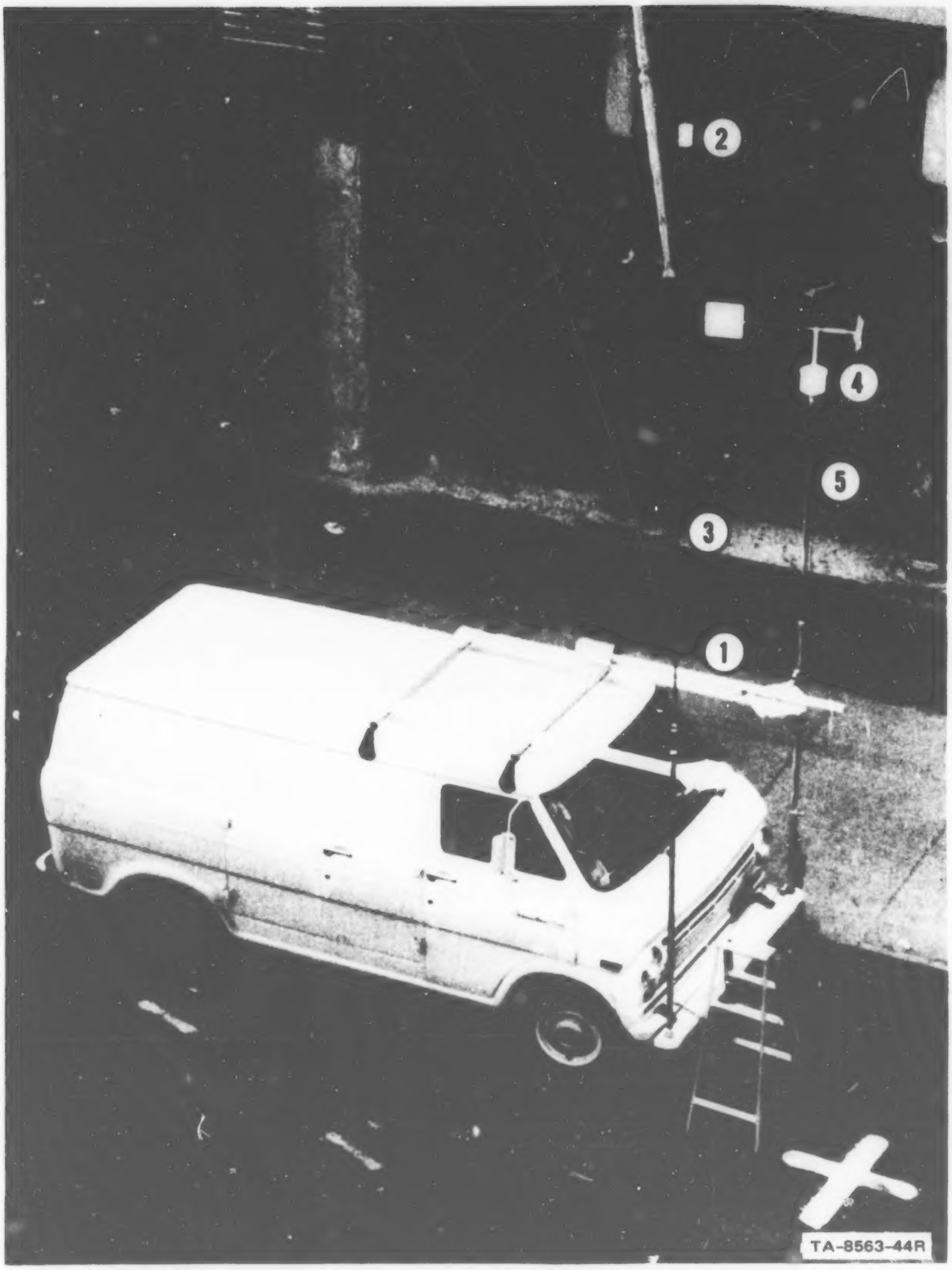

1. Aspirated Radiation Shield for Temperature Sensor
2. Inlet for CO Analyzer with Rain Shield
3. Telescoping CO Intake Mast (10 m Max. Height)
4. Wind Sensor
5. Telescoping Wind Mast with Plumb Adjustment (5 m Max. Height)

FIGURE 19 INSTRUMENTED VAN

The CO analyzers used in the vans employed a different principle of measurement than those used at the streetside sites. In this instrument, heated mercuric oxide is chemically reduced by carbon monoxide in the atmosphere. This reaction releases mercury vapor, which is quantitatively detected by its absorption of ultraviolet radiation from a mercury vapor lamp. The details of this instrument are described in Appendix B.

The inlet to the CO analyzer was through a length of polyethylene tubing supported inside a telescoping antenna mounted on the right side of the front bumper. The inlet could be quickly located at heights ranging from about 2 to 10 m by extending the supporting antenna to the desired length.

The temperature sensor was a radiation-shielded, ventilated thermistor. It was mounted on the left side at the roof level of the van, about 2 m high. The readings of both the CO analyzer and the temperature sensor were recorded on a strip chart recorder. They were also recorded as analog signals on magnetic tape.

The wind measurements on the van were made at a height of about 4 m with a propeller and vane device. The wind direction sensor was oriented consistently with the streetside wind direction sensors. The low-inertia anemometer had a starting speed of about 0.25 m s^{-1}. It's signals were recorded in analog form on the same magnetic tape as the temperature and CO data.

All the equipment was powered from a large bank of storage batteries. The battery voltage was converted by an inverter to the 117-volt ac required by the instrumentation. The batteries could power the instrumentation for about 8 hours without recharging, and could be completely recharged overnight for the next day's operation.

During stationary operation the van could be left unattended, but usually the opertor raised and lowered the inlet to different levels at intervals of 10 to 15 minutes. Each change of inlet height was noted in the log. The chart record was also marked and the change was noted on the voice channel of the magnetic tape recorder.

The CO analyzer was turned on about an hour before sampling began. This allowed the temperature of the mercuric oxide cell to stabilize and also ensured stable operation of the electronics. The CO instrument was calibrated at the beginning of each day's operations.

The CO inlet was kept at a height of about 3.5 m during mobile operation when the van traversed the perimeter of the downtown area. The route shown in Figures 13 and 20 was used and the chart records were marked whenever the van passed one of the numbered points. A voice record of the traverses was kept on the magnetic tape.

b. Helicopter

The instrumentation used on the helicopter was similar to that used on the van (except of course that there was no wind sensor) with the addition of a pressure transducer. The CO analyzer on the helicopter was identical to those in the vans. The inlet to the instrument was located on the port skid ahead of the helicopter cab.

Temperature was monitored with a thermistor element mounted forward on the starboard skid. Having the sensors located ahead of the cab and maintaining a forward speed with the helicopter made it possible to avoid the effects of the main rotor downwash. The pressure transducer, of the aneroid potentiometer type, was located in the cockpit. The outputs of the CO, temperature, and pressure instruments were recorded on a chart recorder.

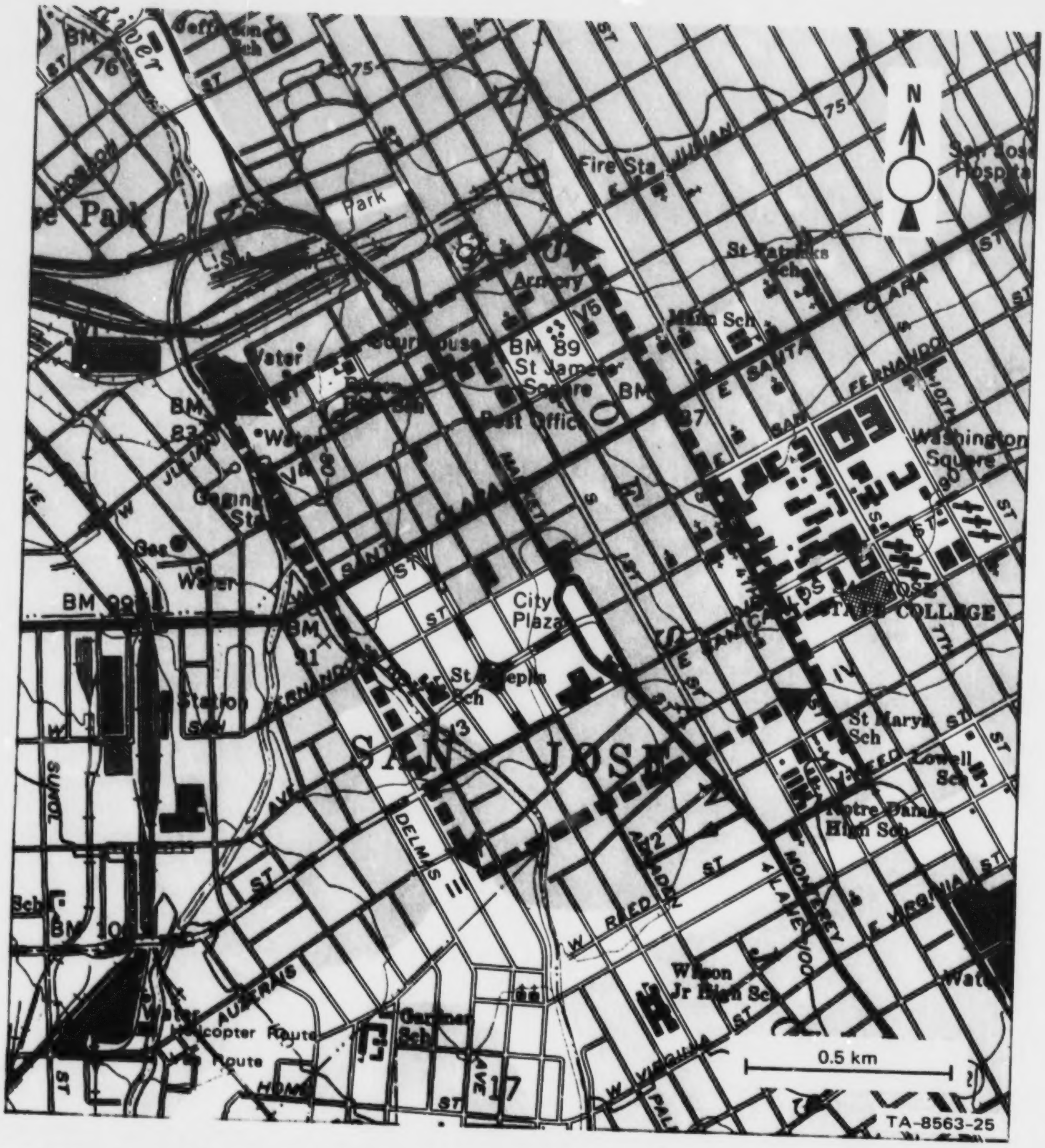
N
Helicopter Route
Van Route
0.5 km
TA-8563-25
SAN JOSE
City Plaza
St James Square
Post Office
Court House
Armory
Fire Sta
Station
Washington Square
SAN JOSE STATE COLLEGE
St Marys Sch
Lowell Sch
Notre Dame High Sch
Wilson Jr High Sch
Gardner Sch
San Jose Hospital
Park

FIGURE 20 HELICOPTER AND VAN ROUTES (with check points) AROUND THE CENTRAL BUSINESS DISTRICT, SAN JOSE, CALIFORNIA

All the equipment was designed so that it could be installed or removed quickly from the Hughes 300 helicopter that was chartered for this program. The helicopter with the equipment installed is shown in Figures 21 and C-1 (Appendix C).

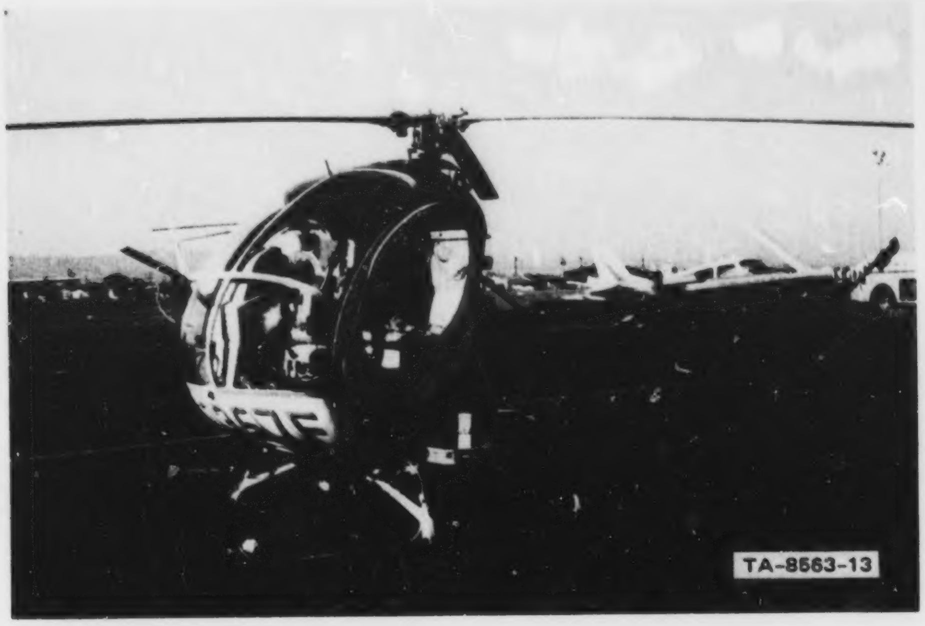

FIGURE 21 INSTRUMENTED HELICOPTER

Operations of the mercuric oxide CO analyzer in the helicopter impose some special problems, because this instrument is sensitive to the mass flow rate of the sampled air through the device. The flow rate was sensitive to changes in altitude, so it was necessary for the operator to make frequent flow rate adjustments. As with the van, it was necessary to prewarm the CO analyzer for about an hour before use. The CO analyzer was calibrated at the beginning of each flight. The calibration technique was much the same as that used with the analyzers in the vans.

Two basic kinds of measurements were made with the instrumented helicopter: vertical profiles, and horizontal traverses around the downtown area. The vertical profiles were usually obtained at a site near Spartan Stadium, about 3 km southeast of the downtown center, from heights of about 15 to 1000 m, although on several occasions profiles were obtained over the intersection of First and San Antonio Streets. Restrictions imposed by the presence of the city buildings and the approach pattern for the San Jose airport limited the downtown observations to the height range between 60 and 300 m.

The horizontal traverses around the downtown perimeter were made along the track shown in Figures 13 and 20. The first traverse was at a height of about 60 m. Subsequent traverses were made at heights of 90 m, 150 m, and also at 300 m, if the top of the mixing layer had not been penetrated below 150 m. The top of the mixing layer was usually identified by an abrupt decline in CO concentration. During all the flights the operator annotated the chart records and kept a position log.

D. Supplementary Data Available from Other Agencies

1. Traffic Data

As noted earlier, the detailed traffic data available for San Jose played a very important part in the selection of San Jose as the location for our experiments. The area covered by the computer-controlled signal network in San Jose has two main parts: (1) a four-by-six-block rectangular grid, covering the "heart" of the downtown area, and (2) a 3.5-mile "panhandle," along one of the major streets which connects to the grid. Figure 22 is a schematic representation of the area covered by the network. Within the grid area, 100-percent coverage of the traffic movement is provided by approximately 225 magnetic vehicle detectors, located in every lane of all street links.

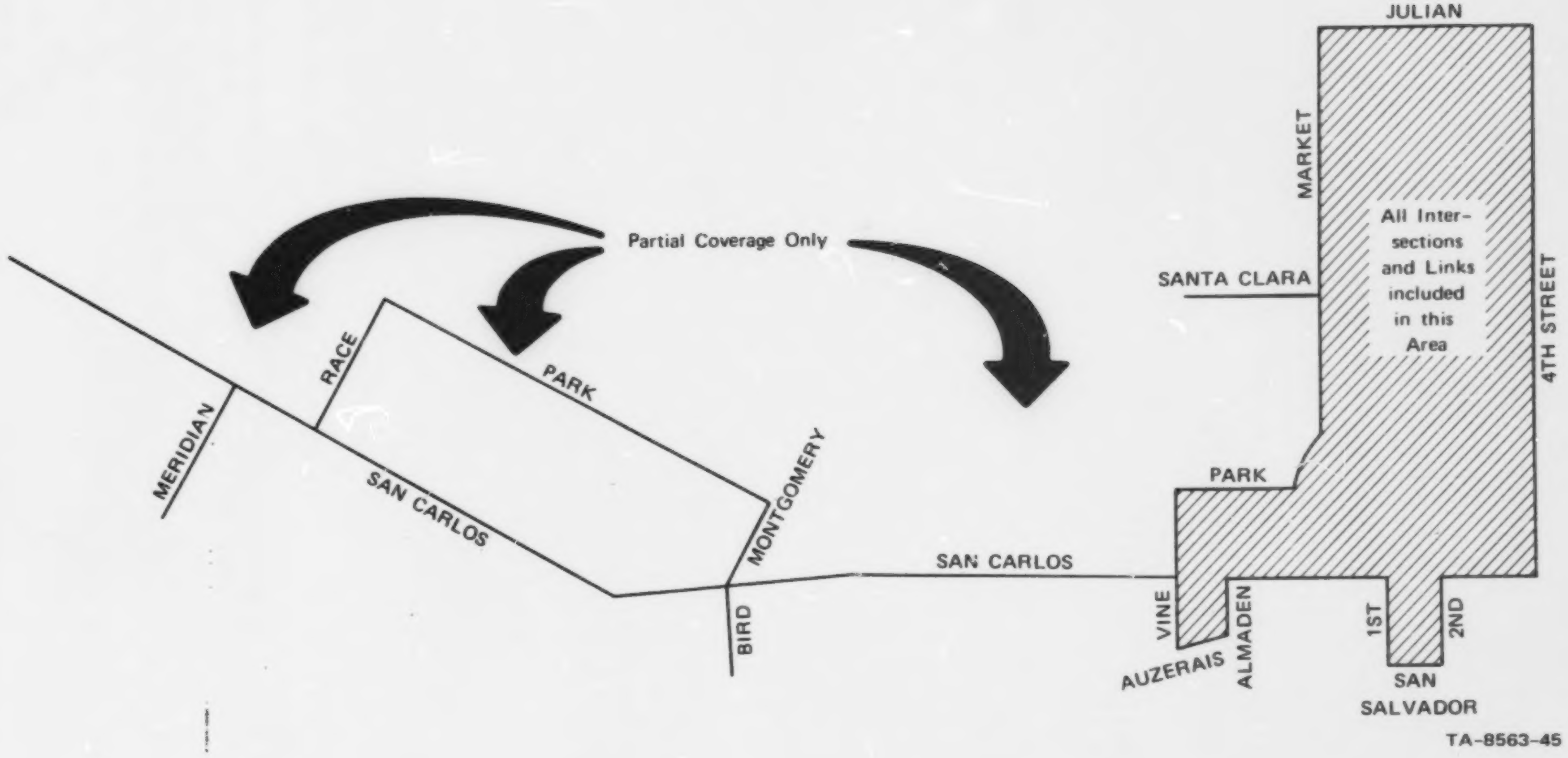
Partial Coverage Only
MERIDIAN
RACE
PARK
SAN CARLOS
MONTGOMERY
BIRD
SAN CARLOS
VINE
AUZERAIS
ALMADEN
PARK
SANTA CLARA
MARKET
JULIAN
All Inter-
sections
and Links
included
in this
Area
4TH STREET
1ST
2ND
SAN
SALVADOR
TA-8563-45

FIGURE 22 AREA COVERAGE OF SAN JOSE TRAFFIC SENSING SYSTEM

Each detector is connected through an interface to a computer (IBM 1800) operated by the city of San Jose. Pulses generated by a vehicle passing over any detector are monitored by the computer and stored in terms of a sensor identification number and pulse time tag. Program options permit summarizing these raw data as total vehicle counts obtained for each sensor during selected time intervals. For this project, 5-minute intervals were selected. Although longer periods might have been sufficient, the 5-minute raw summaries were possible at very little extra cost (all data were generated and processed by machine), and the more conservative interval was chosen. The 5-minute volume histories were generated by the traffic control computer as both printed listing and punched card output.

The punched cards became the input for further processing on an SRI computer (CDC 6400). The description of this processing appears in Appendix D (Data Processing) of this report.

Traffic data were collected in three phases. During the first, from 2 to 23 November 1970, traffic volumes were obtained only from the links adjacent to the intersection of San Antonio and First Streets. Ten sensors were monitored in all. The second phase, from 23 November to 11 December 1970, was directed toward monitoring all operational detectors in the system (291). In both phases, data were collected on weekdays during rush hours (0645-0830, 1100-1300, 1600-1800 PST) only.

The final phase was a two-day effort, 14 and 15 December. Data were collected from all sensors during the entire period of 0645 to 1800 PST.

2. Meteorological Data

Conventional meteorological surface observations are available from San Jose Municipal Airport, about 5 km northwest of downtown

San Jose. The Navy also makes regular meteorological observations at Moffett Field, 17 km to the northwest. Radiosondes are released twice daily from the Oakland Airport, about 50 km northwest of San Jose. In general we used only the observations from the San Jose Airport.

The San Jose State College Meteorology Department has several recording instruments, including wind speed and direction, located on top of a seven-story building about 0.7 km east of the intersection of First and San Antonio. On several occasions, College personnel made pilot-balloon measurements of the upper level winds (see Appendix E).

3. Air Pollutant Monitoring Data

The Bay Area Air Pollution Control District maintains a pollution monitoring station about 2.3 km south-southeast of the downtown area. A variety of pollutants, among them carbon monoxide, are monitored. The carbon monoxide analyzer is of the nondispersive infrared type, as are those used at our streetside sites.

E. Preparation of the Data for Analysis

The details of the data processing for analysis are given in Appendix D, and later sections of the body of the report deal with some of the analyses that have been prepared from the data. In this section, some of the corrections that were made on the data will be enumerated and the preprocessing briefly described.

1. Streetside Data

The streetside data were quite extensive, and it was necessary to perform some editing and condensation. The data handling began by translating the binary data as originally recorded to the binary-coded decimal used in subsequent processing. At the time of translation, those measurements made during periods of calibration (determined from equipment status codes) were eliminated from the records. The recorded voltages were converted to engineering units at the same time. The conversion factors used were also based on recorded equipment status codes.

The next step involved further corrections based on records kept by operators during the experiment. These corrections included those made on the basis of CO analyzer calibrations, or to convert wind components to a common frame of reference.

The corrections were followed by a consolidation of the data onto a new magnetic tape. Each record contained information for a 5-minute period. All the CO concentration and temperature data appeared in this record, as did all the cup-and-vane wind data. The three-component wind measurements were also consolidated by summarizing these data for each period. The reduced wind information was recorded as: (1) the number of observations of each component during the period, (2) the algebraic sums of each observed component magnitude during the period, and (3) the sums of the squares of the observed component magnitudes during the period. This information can be used to calculate mean values and their standard deviations for the individual periods and for combinations of individual periods.

2. Mobile Data

The mobile data were generally recorded on charts and transferred to computer-compatible form by hand. Much of the editing and correcting was done by hand during this part of the processing.

The CO data from the stationary vans were recorded on magnetic tape. The tape contains CO concentrations at 1-minute intervals, van locations, inlet height, date and time. The data collected during the mobile traverses were punched on cards that give locations on the city perimeter, average CO concentrations over the specified route segments, date, and time. Similar records of the helicopter data are available; these include heights in addition to the other information.

3. Data Available for Analysis

All of the times that data were collected are shown in Table 2. Only those data collected after 18 November 1970 were processed and analyzed for this report. Prior to 19 November, the magnetic tape recorder was not working, so the data are available only as paper copy summaries or punched paper tape. Because data in these forms are not readily suitable for electronic data-processing techniques and because we had sufficient data for analysis recorded on magnetic tape, we chose to exclude the earlier period from our studies.

Table 2

MASTER DATA SUMMARY--SAN JOSE FIELD PROGRAM, 5 NOVEMBER-15 DECEMBER 1970

Date (1970)	Traffic	Street Stations	Van A	Van B	Helicopter	Lidar	Time	Clouds	Visibility* (mi)	Temp/dewpoint (°F)	Wind (deg/kt)
5 November (Thursday)	0645-0830† 1600-1800	1220-1300	--	--	1408-1530 (V)‡	1337-1552 (F)§	0700	23⊕	8R--	63/62	190/11
							1000	25⦷	15	68/60	170/11
							1200	25⦷	15	72/62	190/11
							1400	40⦷	20	67/59	290/13
							1700	40⦶ 100⦷	35	65/57	340/04
6 November (Friday)	0645-0830 1100-1300 1600-1800	0901-1035	--	--	--	--	0700	15⦶ 30⦷	12	59/57	160/10
							1000	5⦶ 20⦷	5R-	60/58	140/12
							1200	5⦶ 20	5RW	61/60	140/10
							1400	5⦶ 40⦷	10R--	62/60	150/04
							1700	23⦶ 80⦷	15	63/59	140/03
9 November (Monday)	0645-0830 1100-1300 1600-1800	0805-1208 1430- ?	--	--	1435-1445 (V) 1448-1507 (H)	--	0700	60⦶ 90⦷	10	59/59	030/04
							1000	60⦶ 100⦷	5HK	65/60	180/03
							1200	40⦷	6HK	69/61	010/08
							1400	35⦷	5R-	68/64	320/09
							1700	35⦷	7	67/63	340/08
10 November (Tuesday)	0645-0830 1100-1300 1600-1800	--	--	--	1000-1025 (H)	--	0700	6⦶ 14⦷	5FK	60/60	320/07
							1000	8⦶ 19⊕	5FK	61/59	310/06
							1200	25⊕	7	64/57	040/04
							1400	20⦶	7	67/57	090/04
							1700	○	7	68/58	350/07
11 November (Wednesday)	0645-0830	0745-0937 0948-1124 1240-1650	--	--	--	--	0700	30⦷	3HK	58/58	120/04
							1000	60⦶ 120⦷	6HK	65/57	130/15
							1200	30⦶ 60⦷	10	70/58	160/13
							1400	20⦶ 32⊕	15	69/59	200/10
							1700	28⦷	12	67/60	220/10
12 November (Thursday)	1600-1800	0625-1030	--	--	1713-1720 (V) 1720-1750 (H) 1750-1800 (V)	--	0700	20⦶	15	54/52	300/10
							1000	○	15	60/52	320/12
							1200	○	15	64/51	320/14
							1400	⊙	50	68/48	320/15
							1700	○	50	63/40	320/11

---

[*] The alphabetical symbols indicate weather conditions as follows: R--rain, RW--rain shower, H--haze, K--smoke, F--fog. The minus and double minus signs following the symbols indicate light and very light weather conditions, respectively.

[†] Periods of data collection are given in PST throughout.

[‡] Suffixes (V) and (H) denote vertical and horizontal helicopter profiles.

[§] Suffixes (F) and (M) denote fixed and mobile operational modes.

Table 2 (Continued)

Date (1970)	Traffic	Street Stations	Van A	Van B	Helicopter	Lidar	Time	Clouds	Visibility (mi)	Temp/dewpoint (°F)	Wind (deg/kt)
13 November (Friday)	1100-1300 1600-1800	0730-1113 1128-1410	--	--	--	--	0700	○	50	52/40	320/06
							1000	○	50	64/36	120/04
							1200	○	50	68/37	240/07
							1400	○	50	70/36	300/12
							1700	○	50	63/39	270/06
16 November (Monday)	0645-0830 1100-1300 1600-1800	0730-1439	--	--	--	1625-1632 (F)	0700	16⦷	10	47/42	120/04
							1000	○	10	60/46	360/06
							1200	○	6HK	64/55	340/07
							1400	○	6HK	66/56	330/09
							1700	○	10	63/57	330/10
17 November (Tuesday)	0645-0830 1100-1300 1600-1800	0850-1434	0725-1453 (F)	--	0827-0837 (V)	1540-1627 (F)	0700	○	4HK	46/46	120/03
							1000	4⦷	1F	55/55	340/04
							1200	○	2F	59/55	100/04
							1400	○	5HK	66/55	350/06
							1700	○	6HK	63/55	340/08
18 November (Wednesday)	1100-1300 1600-1800	0740-1211	0815-1223 (F) 1230-1315 (M)	--	--	--	0700	WOX	1/4F	52/52	350/04
							1000	WIX	3/8F	54/54	310/06
							1200	○	3F	57/56	320/06
							1400	○	6HK	65/51	340/09
							1700	○	15	63/55	350/08
19 November (Thursday)	0645-0830 1100-1300 1600-1800	0725-1208*	--	--	0854-0903 (V) 0903-0934 (H) 0938-0948 (V)	--	0700	○	20	47/46	140/04
							1000	○	30	64/13	230/07
							1200	○	50	68/42	320/08
							1400	○	30	69/43	300/11
							1700	○	30	62/47	330/08
20 November (Friday)	0645-0830 1600-1800	0735-0755 0850-1045 1105-1800	0822-1240 (F)	--	1654-1713 (V) 1719-1744 (H) 1751-1801 (V)	1540-1815 (M)	0700	○	10	44/43	180/04
							1000	○	5HK	57/46	150/05
							1200	○	5HK	66/46	130/04
							1400	○	5HK	--	330/08
							1700	150⦶	5HK	61/45	320/08
23 November (Monday)	0645-0830 1100-1300† 1600-1800	0735-0800 0831-1245	0718-1530 (F)	--	0807-0825 (V) 0825-0901 (H) 0903-0921 (V)	--	0700	40-⦷	7	47/43	000/00
							1000	250⦶	5HK	58/45	090/04
							1200	250⦶	5HK	64/45	320/04
							1400	250⦶	5HK	68/48	340/04
							1700	100⦶	5HK	63/47	320/08

*Start of data recording on digital magnetic tape.

†Start of data collection from all traffic detectors in downtown area; previous data are for First and San Antonio Streets only.

Table 2 (Continued)

Date (1970)	Traffic	Street Stations	Van A	Van B	Helicopter	Lidar	Time	Clouds	Visibility (mi)	Temp/dewpoint (°F)	Wind (deg/kt)
24 November	0645-0845	0850-1325	0819-1142 (F)	--	1217-1233 (V)	1430-1507 (M)	0700	25⦷	4HK	48/44	080/04
(Tuesday)	1100-1300		1142-1310 (M)		1233-1243 (H)		1000	17⦶ 150⦶	5HK	62/50	130/05
	1600-1800						1200	40⦶ 150⦷	12	70/51	030/05
							1400	45⦷	15	70/51	260/05
							1700	50⦷	15	69/52	320/05
25 November	0645-0845	0745-0955	0819-1630 (F)	--	--	--	0700	23⦷	7R-	61/57	130/10
(Wednesday)	1600-1800	1020-1226					1000	25⦷	15	62/56	140/07
							1200	25⦷	10RW-	64/57	140/06
							1400	25⦷	15	65/57	210/08
							1700	25⦷	10	62/56	320/08
30 November	1100-1300	0725-1045	0735-1620 (F)	--	0824-0849 (H)	--	0700	23⦶ 38⊕	12RW-	51/46	150/13
(Monday)	1600-1800	1058-1329			0855-0905 (V)		1000	30⦶ 45⊕	12	54/47	160/12
							1200	30⦶ 45⊕	12	59/47	160/16
							1400	30⦷	7	58/49	190/16
							1700	10⊕	7	51/50	150/05
1 December	0645-0845	--	--	--	--	--	0700	30⦶ 100⦷	10	53/47	140/09
(Tuesday)	1100-1300						1000	30⦶ 45⦷	10RW-	56/47	160/13
	1600-1800						1200	20⦶ 45⦷	20	57/50	170/12
							1400	20⦶ 45⦷	15	59/48	180/13
							1700	25⦷	7RW-	57/49	160/09
2 December	1100-1300	--	--	--	--	--	0700	40⊕	10RW	51/44	180/04
(Wednesday)	1600-1800						1000	40⦷	15	55/41	250/10
							1200	38⦷	15RW	54/39	290/18
							1400	40⦷	15	55/42	240/15
							1700	40⦶	30	52/37	210/04
3 December	0645-0845	0753-0830	0731-0824 (M)	--	0753-0813 (V)	--	0700	45⦷	20	47/37	140/13
(Thursday)	1100-1300	0942-1332	0827-1514 (F)		0817-0856 (H)		1000	60⦷	20	51/36	160/14
	1600-1800						1200	40⦷	15	55/36	150/12
							1400	40⦷	15	57/39	140/15
							1700	28⦷	10	58/43	150/13
4 December	0645-0845	--	--	--	--	--	0700	30⊕	7R-	56/51	130/10
(Friday)	1100-1300						1000	35⦷	10	58/51	160/10
	1600-1800						1200	35⦶ 50⊕	12	61/53	140/11
							1400	35⦷	12RWN	64/54	160/10
							1700	25⦷	15	63/52	160/08
7 December	0645-0845	0741-1200	0803-1245 (F)	0849-1426 (F)	1226-1246 (V)	1240-1410 (F)*	0700	6⊕	3F	57/52	320/07
(Monday)	1100-1300	1230-1800	1254-1410 (M)	1448-1703 (F)	1247-1308 (H)		1000	7⦷	3HK	59/52	180/03
	1600-1800		1449-1630 (F)		1652-1652 (V)		1200	200⊕	5HK	65/52	140/13
			1636-1740 (M)		1701-1728 (H)		1400	100⦷	15	68/46	160/10
							1700	45⦶ 55⦷	15	62/50	040/06

*Start of 90° lidar observations for height-time displays; previous data are RHI elevation scans.

Table 2 (Concluded)

Date (1970)	Traffic	Street Stations	Van A	Van B	Helicopter	Lidar	Time	Clouds	Visibility (mi)	Temp/dewpoint (°F)	Wind (deg/kt)
8 December (Tuesday)	0645-0845 1100-1300 1600-1800	0721-1320	0750-0906 (M)	--	0758-0817 (V) 0819-0841 (H)	--	0700	20⦶ 50⊕	15	59/53	160/07
							1000	20⦶ 45⊕	10	61/54	140/13
							1200	10⦶ 23⦷	20	62/55	140/15
							1400	32⦷	20	62/52	190/12
							1700	25⦷	15	56/50	340/09
9 December (Wednesday)	0645-0845 1100-1300 1600-1800	0715-1059 1105-1800	0701-0740 (F) 0740-0853 (M) 1005-1115 (F) 1132-1252 (M) 1313-1341 (F) 1627-1805 (M)	0700-1357 (F) 1700-1748 (F)	0747-0806 (V) 0806-0832 (H) 1145-1206 (V) 1206-1223 (H) 1642-1702 (V) 1707-1731 (H)	0746-1733 (F)	0700	40⦶	15	45/39	120/03
							1000	40⦶	20	55/45	320/07
							1200	40⦶	20	57/43	330/11
							1400	40⦶	20	58/41	350/10
							1700	200⦶	20	53/42	340/08
10 December (Thursday)	0645-0845 1100-1300 1600-1800	0745-0840 0845-1800	0746-0858 (M) 0900-1140 (F) 1145-1247 (M) 1317-1420 (F) 1610-1749 (M)	0720-1422 (F) 1640-1802 (F)	0758-0808 (V) 0811-0843 (H) 1150-1210 (V) 1211-1239 (H) 1650-1710 (V) 1711-1740 (H)	0730-0825 (F) 1433-1539 (F) 1632-1746 (F)	0700	⦶	15	40/36	200/03
							1000	⦶	6HK	50/41	330/03
							1200	250⦶	10	56/40	320/05
							1400	⦶	15	59/41	350/07
							1700	⦶	15	56/41	300/08
11 December (Friday)	0645-0845 1100-1300 1600-1800	0800-2400	0814-1400	0742-0851 (M) 0909-1130 (F) 1137-1255 (M) 1409-1628 (F) 1631-1851 (M)	0802-0820 (V) 0826-0837 (H) 1156-1215 (V) 1222-1239 (H) 1641-1702 (V) 1702-1725 (H)	0725-1800 (F)	0700	8⦶ 250⦷	15	44/39	140/04
							1000	5⦶ 250⦷	5HK	52/46	020/03
							1200	10⦶ 250⦷	7	56/45	330/10
							1400	⦶	10	60/42	340/09
							1700	⦶	15	56/38	280/09
12 December (Saturday)	--	0000-1000	--	--	--	--	0700	⦶	15	36/31	310/05
							1000	200⦶	10	49/37	020/03
							1200	200⦶	7	53/39	320/04
							1400	⦶	7	56/42	320/08
							1700	⦶	7	51/42	320/07
14 December (Monday)	0645-1800	1120-1225 1231-1800	1255-1320 (F) 1400-1800 (F)	--	--	--	0700	40⦶ 60⊕	10	42/38	160/04
							1000	30⦶ 140⦷	12	48/40	160/08
							1200	25⦷ 140⊕	12	54/42	150/06
							1400	25⦶ 40⦷	12	51/45	060/04
							1700	35⦶ 70⊕	12	57/45	110/04
15 December (Tuesday)	0645-1800	0740-1800	0742-1800 (F)	--	--	--	0700	200⦶	20	43/39	210/04
							1000	120⦶ 250⊕	20	52/44	130/08
							1200	90⦷	20	59/44	140/14
							1400	30⦶ 250⊕	20	63/46	150/15
							1700	35⦷ 150⊕	20	58/45	140/16

III STREETSIDE DATA ANALYSIS AND RESULTS

A. Background

Because of the finite spacing of sources within a city, area-source simulation such as is used in the intraurban model is best applied at scales above a certain lower limit. This minimum spatial scale can be considered to be on the order of a city block, hence the choice of 62 m as the finest resolution in the intraurban model. For shorter source-receptor distances, an alternative technique is needed.

Additional complications arise because, contrary to the usual situation in nonurban diffusion studies, the scale of the largest urban roughness elements (buildings and so on) is very large compared to the local scales of emission and reception. This means that the aerodynamic effects of structures become important.

Models that do not include the effects of microscale diffusion will normally undercalculate concentrations in comparison with those measured at CAMP Stations, which are often located near streets. For example, the model used by Ott et al. (1967) gave average concentrations that amounted to 36 percent of the CAMP average.

The street effects have great importance for two reasons. First, they must be considered if we are to use existing data to verify the performance of our model. Most available observations are taken near streets in downtown areas where local effects are likely to be significant. The second reason for the importance of the street effects is that they contribute substantially to those concentrations to which large parts of the population are exposed.

Current knowledge about street effects on CO concentrations is based largely upon the extensive measurements of Georgii et al. (1967) in Frankfurt/Main, Germany; McCormick and Xintaras (1962), Schnelle et al. (1969), and Rouse (1951) have also made experimental contributions in this area.

Georgii's experiment involved extensive measurements of CO concentrations and wind speeds at different levels above three different streets in built-up areas, along with occasional traffic counts. A major finding was that the CO concentrations on the leeward sides of buildings were considerably higher than those on the windward sides, implying a helical cross-street circulation component near the surface in the opposite direction from the roof-level wind (see Figure 23). In addition, the averaged data showed that (1) the vertical concentration profiles on either side of the street assume an exponential form, (2) the

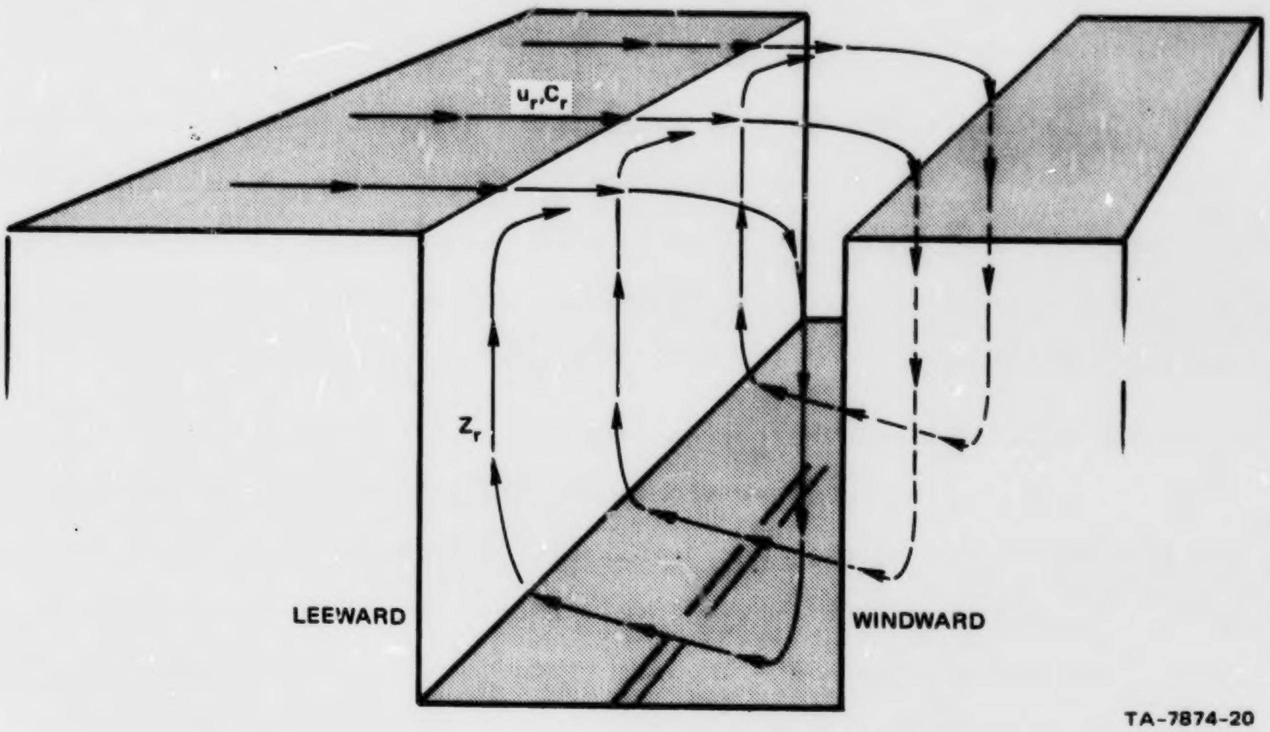

FIGURE 23 INDICATED TYPICAL HELICAL AIR FLOW OVER A STREET (adapted from Georgii, 1967)

mode of air circulation above the street apparently changes when the rooftop wind speed exceeds about 2 m s^{-1}, and (3) the concentrations are exponentially related to traffic density. Examination of the measurements reported by Schnelle et al. (1969) also indicates general agreement with (1) and (2) above; their data are insufficient for verifying (3).

During the first year's effort (Johnson et al., 1969), an attempt was made to develop a street submodel, based largely upon Georgii's findings. The final equations, applicable to a street canyon, were

$$C_W = C_b \exp\left[29(Q)\left(1 - z/z_r\right)\right] \tag{5}$$

$$C_L = C_b \exp\left[(45.6 + 4.68\ U)(Q)\left(1 - z/z_r\right)\right] \quad , \tag{6}$$

where

C_W = streetside concentration on the windward side of the building

C_L = streetside concentration on the leeward side of the building

C_b = background urban concentration

Q = line source emission rate (g m^{-1} s^{-1})

U = rooftop wind speed (m s^{-1})

z/z_r = ratio of receptor height to building height.

The specification of leeward and windward cases was carried out according to the quadrant including the observed wind direction, as illustrated in Figure 24. For intermediate wind directions, the concentration profile was taken to be the average of that given by Eqs. (5) and (6).

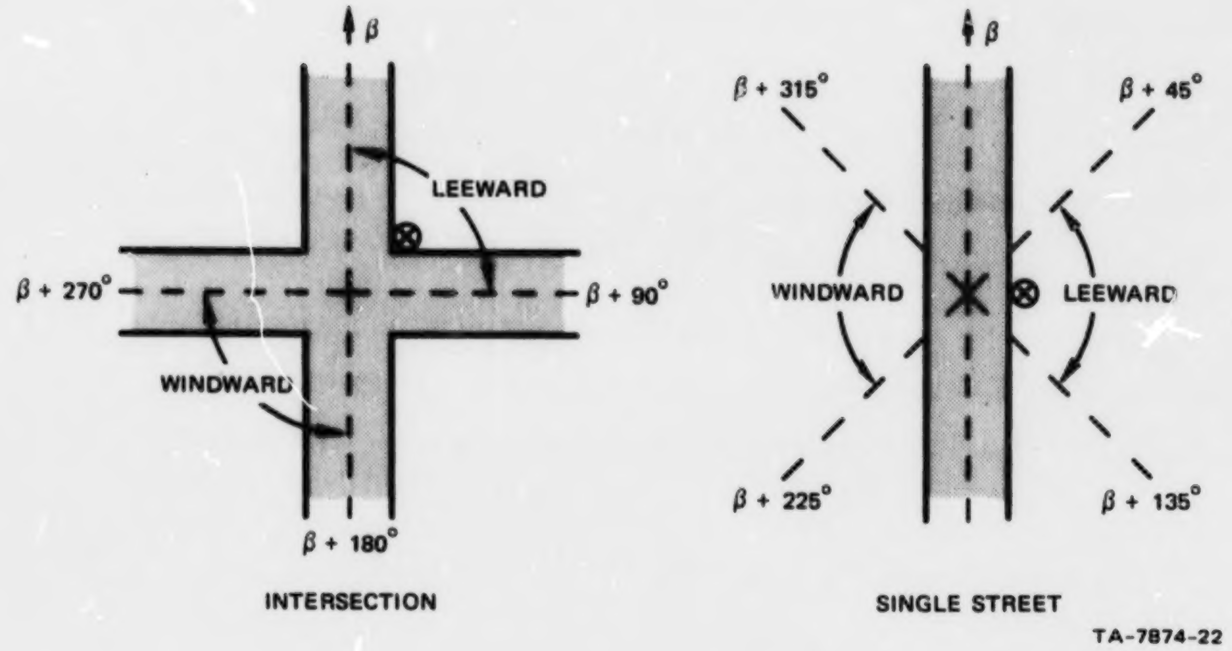

FIGURE 24 SPECIFICATION FOR LEEWARD AND WINDWARD CASES ON THE BASIS OF RECEPTOR LOCATION, STREET ORIENTATION, AND WIND DIRECTION

Although these formulas give CO profiles that fit Georgii's averaged data reasonably well, the results were not satisfactory when the submodel was applied to the CAMP data. There are several shortcomings to this methodology that may be to blame: (1) the equations are strictly empirical, rather than physical; (2) the concentration component due to locally generated emissions should be additive to the background concentration, rather than proportional to it; (3) there is no provision for a variable distance from the roadway; and (4) the concentration at the receptor level $z = z_r$ may not be equal to the background concentration. Because of a number of problems encountered in applying the empirical model on a general basis, it has not been incorporated into the diffusion model. A new technique has been developed with the aid of the data from the San Jose street experiment. The data analysis, the results, and the development of the new methodology are described in the next sections.

B. Data Analysis

The basic processing of the data has been discussed in a preceding section of this report, and is described in detail in Appendix D. Most of this processing was directed toward simplifying the stratification and class-averaging of the data. The first step was to calculate hour averages and standard deviations of all measured and derived variables (CO concentrations, wind speeds, wind directions, turbulence intensities, and vertical temperature differences) for all time periods when the data were available on magnetic tape. These averages were reduced to a format similar to that shown in Figure D-5 of Appendix D. CO concentrations for the 7.5-m and 12-m levels were obtained by interpolation.

Contour analyses were prepared for these hour-averaged data for the levels of 3, 7.5, and 12 m for each hour for which there were a sufficient number of cases to constitute a representative average. This basic set of analyses has been helpful in determining the general types of concentration and circulation patterns, in establishing the criteria for stratifying the data into classes, and in judging the representativeness of patterns subsequently shown by the analyses of the stratified data.

In selecting bases for stratification of the data, we were also guided by the work of Georgii et al. (1967). Their studies, as well as our hour-averaged data, suggested that wind direction, wind speed, and CO emission rates in the street were the most significant variables influencing the distribution of CO within a street canyon. Accordingly, the data were stratified in three forms:

(1) By wind direction (±22.5° sectors) only

(2) By wind direction and hour of the day

(3) By wind direction, wind speed, and traffic volume in the downtown area.

As with the hour-averaged data, these three sets of stratified data were plotted and analyzed for three different heights. In addition, CO profiles for all seven stations were graphed for the first two sets of data.

C. Results

To illustrate the basic nature of the wind circulations and CO patterns observed within the street canyon during the San Jose experiment, we have selected two sets of data to be presented as examples from among the many analyses that have been prepared and studied. The first set is a case study of hour-averaged data for selected hours throughout a 24-hour period on 11-12 December 1970. The second set consists of the total body of data stratified into eight wind-direction classes. When viewing these analyses, one should keep in mind that they are based on only a few widely separated data points, and that in some cases there is little justification for drawing the concentration contours in the region of the intersection itself. Nevertheless, this was done to aid in the interpretation.

1. Case Study of Hourly Averaged Data for 11-12 December 1970

The weather during the period of 11-12 December (see Table 2) was characterized by scattered low clouds during the morning hours of 11 December, becoming clear after noon and for the rest of the period. Winds were relatively light throughout the period; the wind direction was quite variable.

Horizontal CO distributions for three heights (3, 7.5, and 12 m) for the periods 0800-0900, 1200-1300, 1700-1800, 2300-2400, and 0300-0400 PST are presented in Figures 25 to 29. The first three periods were selected to coincide with the peak traffic periods. Vehicle

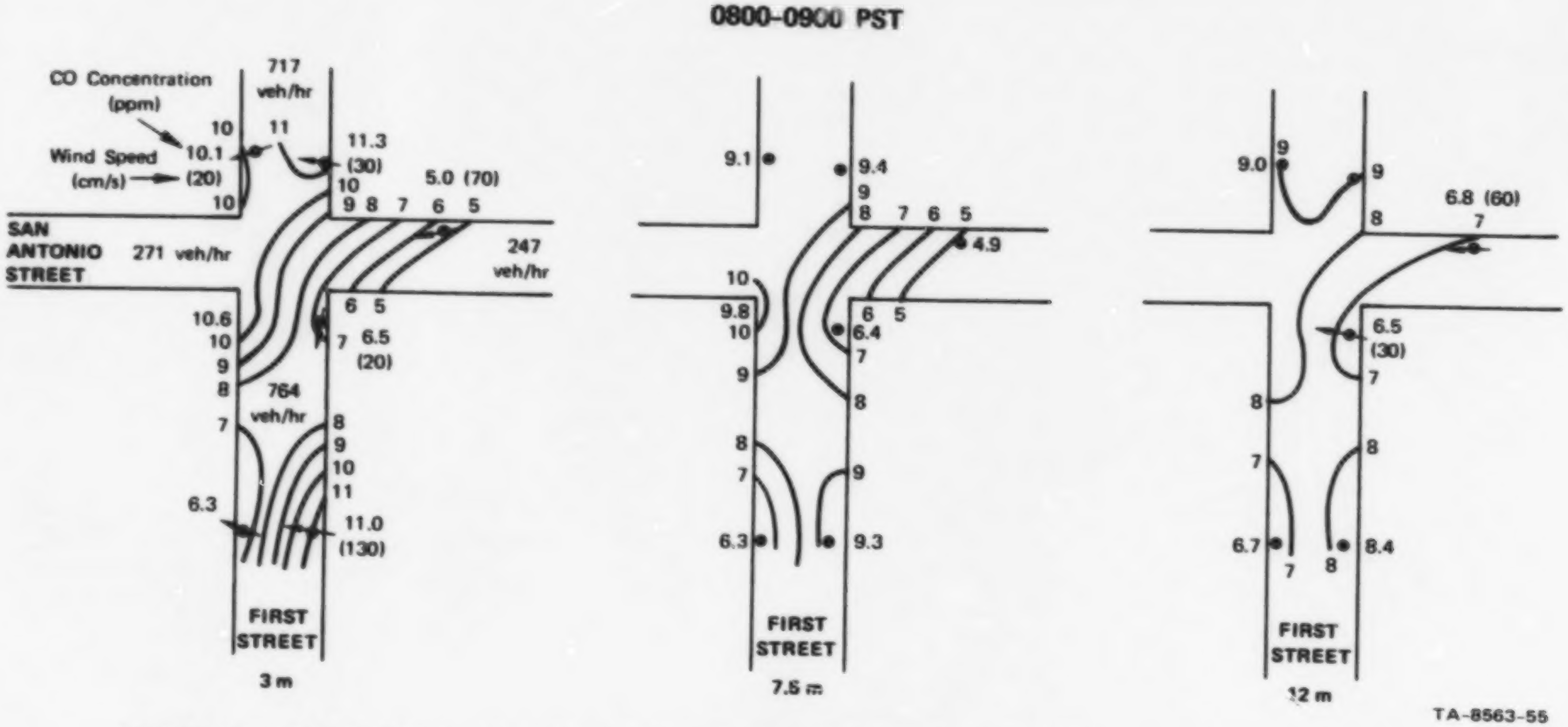
0800-0900 PST
CO Concentration (ppm)
Wind Speed (cm/s)
10.1
(20)
717 veh/hr
11.3
(30)
5.0 (70)
SAN ANTONIO STREET
271 veh/hr
247 veh/hr
10.6
6.5
(20)
764 veh/hr
6.3
11.0
(130)
FIRST STREET
3 m
9.1
9.4
4.9
10
9.8
6.4
6.3
9.3
FIRST STREET
7.5 m
9.0
6.8 (60)
6.5
(30)
6.7
8.4
FIRST STREET
12 m
TA-8563-55

FIGURE 25 CO PATTERNS IN SAN JOSE FOR THREE HEIGHTS FOR EARLY MORNING ON 11 DECEMBER 1970

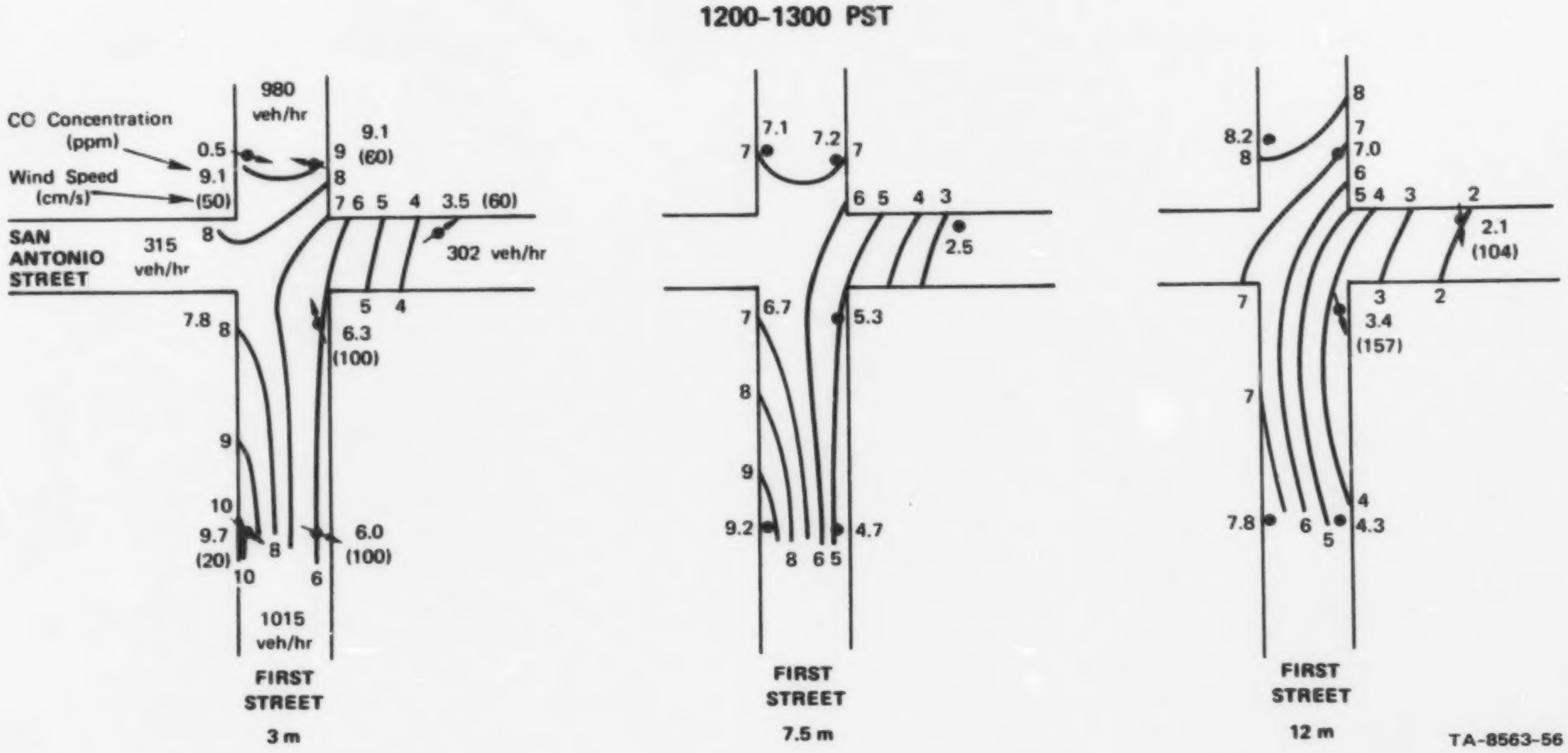
1200-1300 PST
CO Concentration (ppm)
Wind Speed (cm/s)
0.5
9.1
(50)
980 veh/hr
9.1
(60)
3.5 (60)
302 veh/hr
SAN ANTONIO STREET
315 veh/hr
7.8
6.3
(100)
9.7
(20)
6.0
(100)
1015 veh/hr
FIRST STREET
3 m
7.1
7.2
2.5
6.7
5.3
9.2
4.7
FIRST STREET
7.5 m
8.2
7.0
2.1
(104)
3.4
(157)
7.8
4.3
FIRST STREET
12 m
TA-8563-56

FIGURE 26 CO PATTERNS IN SAN JOSE FOR THREE HEIGHTS AT NOON ON 11 DECEMBER 1970

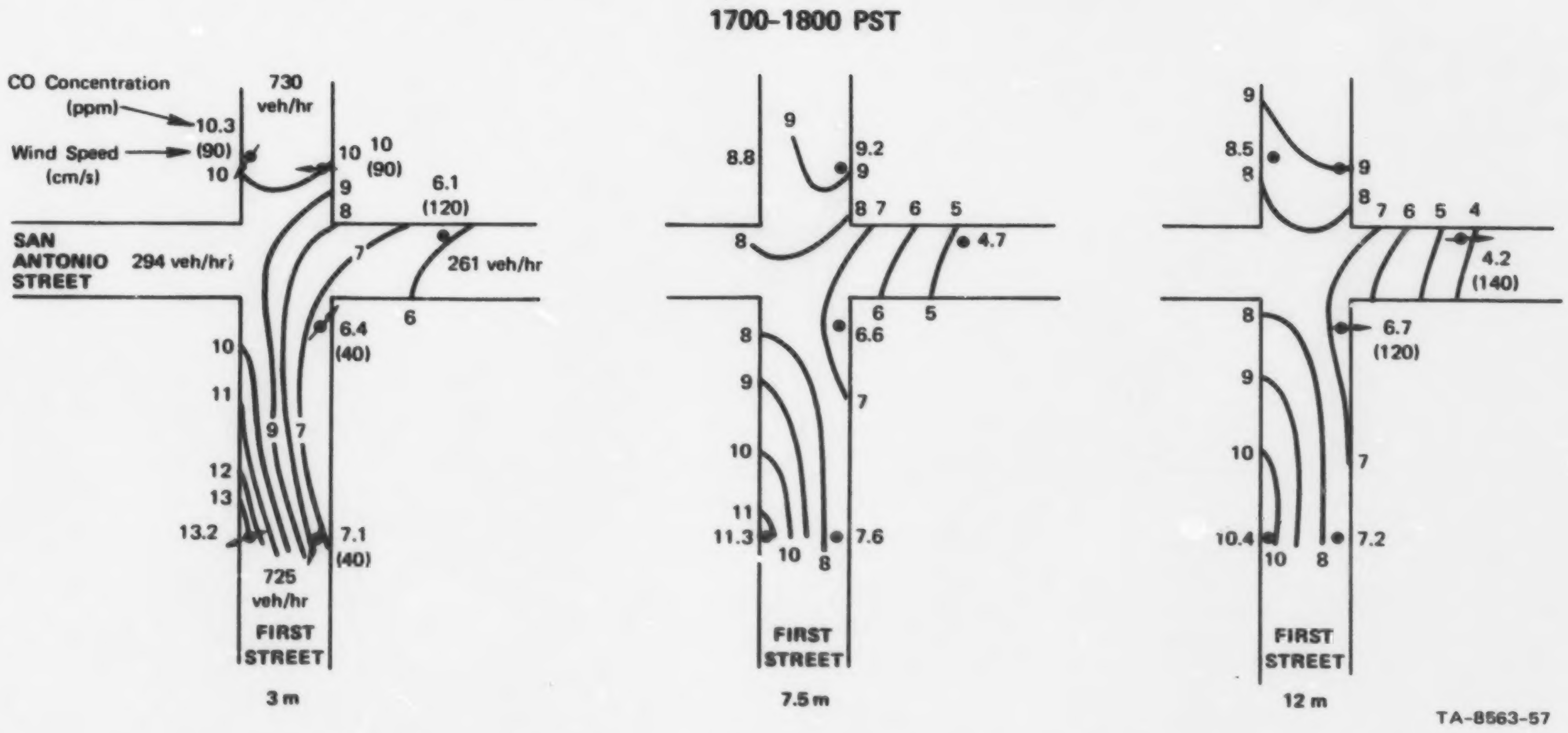
1700-1800 PST

CO Concentration (ppm)
Wind Speed (cm/s)
10.3
(90)
10
730 veh/hr
10
10
(90)
9
8
6.1
(120)
SAN ANTONIO STREET
294 veh/hr
7
261 veh/hr
6
6.4
(40)
10
11
9
7
12
13
13.2
7.1
(40)
725 veh/hr
FIRST STREET
3 m
9
8.8
9.2
9
8 7 6 5
8
4.7
6
6.6
5
8
9
7
10
11
11.3
10
8
7.6
FIRST STREET
7.5 m
9
8.5
8
9
8
7 6 5 4
4.2
(140)
8
6.7
(120)
9
10
7
10.4
10
8
7.2
FIRST STREET
12 m
TA-8563-57

FIGURE 27 CO PATTERNS IN SAN JOSE FOR THREE HEIGHTS DURING LATE AFTERNOON ON 11 DECEMBER 1970

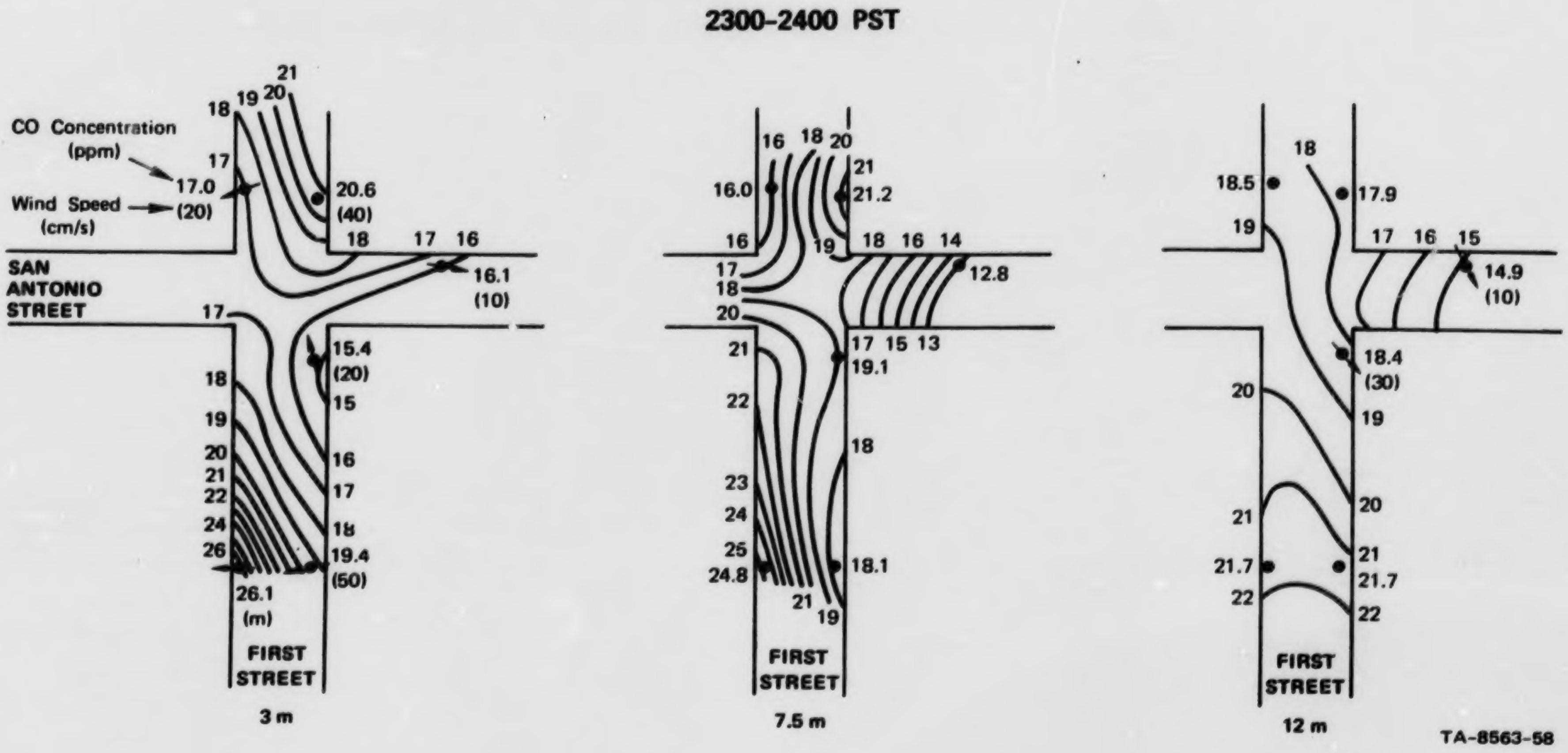
2300-2400 PST
CO Concentration (ppm)
Wind Speed (cm/s)
17.0
(20)
SAN ANTONIO STREET
18
19
20
21
17
20.6
(40)
18
17
16
16.1
(10)
17
15.4
(20)
15
18
19
20
21
22
24
26
16
17
18
19.4
(50)
26.1
(m)
FIRST STREET
3 m
16
18
20
16.0
21
21.2
16
19
18
16
14
12.8
17
18
20
17
15
13
21
19.1
22
18
23
24
25
24.8
18.1
21
19
FIRST STREET
7.5 m
18
18.5
17.9
19
17
16
15
14.9
(10)
18.4
(30)
20
19
21
20
21.7
21
21.7
22
22
FIRST STREET
12 m
TA-8563-58

FIGURE 28 CO PATTERNS IN SAN JOSE FOR THREE HEIGHTS DURING LATE EVENING ON 11 DECEMBER 1970

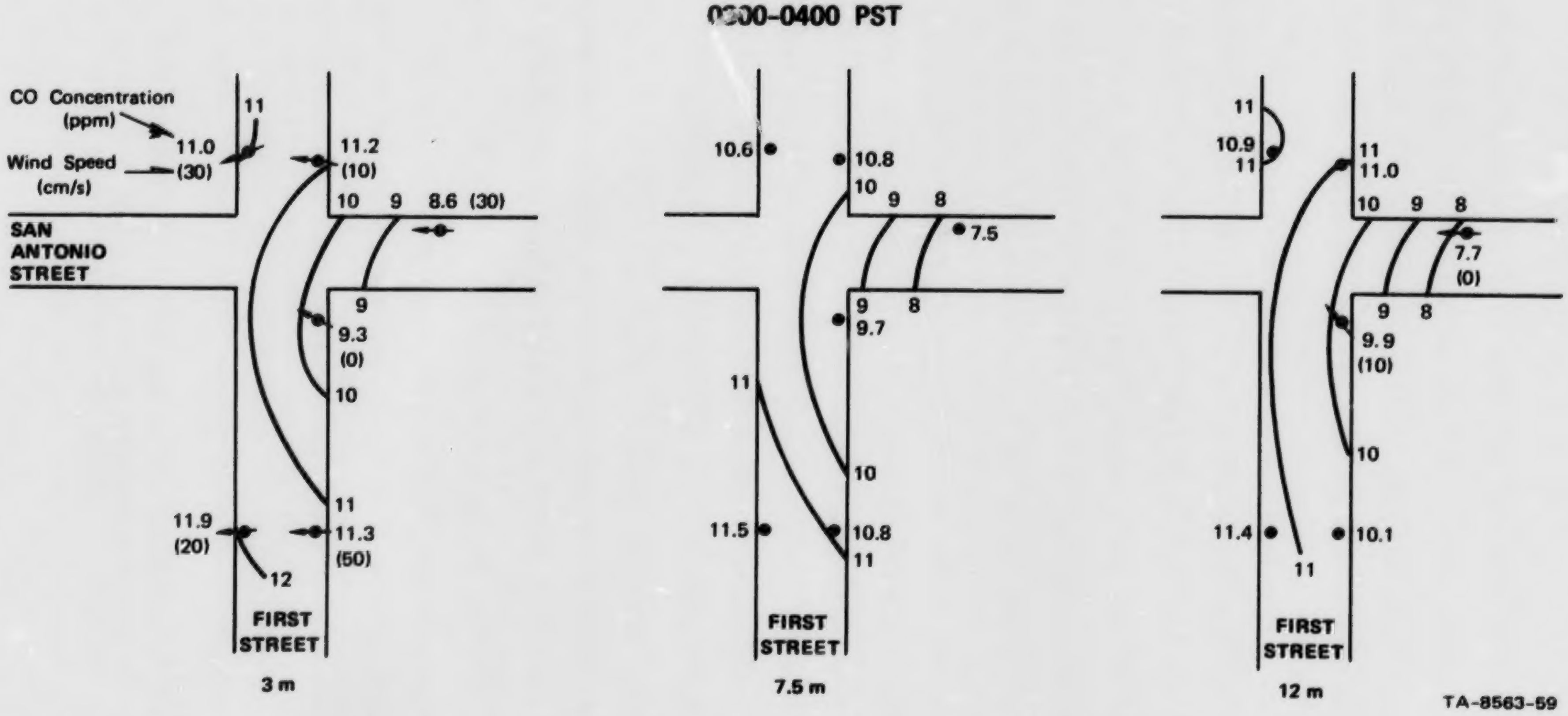

0300-0400 PST
CO Concentration (ppm)
Wind Speed (cm/s)
11.0
(30)
11
SAN ANTONIO STREET
11.2
(10)
10
9
8.6 (30)
9
9.3
(0)
10
11
11.9
(20)
11.3
(50)
12
FIRST STREET
3 m
10.6
10.8
10
9
8
7.5
9
8
9.7
11
10
11.5
10.8
11
FIRST STREET
7.5 m
11
10.9
11
11
11.0
10
9
8
7.7
(0)
9
8
9.9
(10)
10
11.4
10.1
11
FIRST STREET
12 m
TA-8563-59

FIGURE 29 CO PATTERNS IN SAN JOSE FOR THREE HEIGHTS DURING THE NIGHT OF 12 DECEMBER 1970

counts as obtained from the San Jose traffic monitoring network are indicated for First Street and San Antonio Street on the first three analyses. Unfortunately, no traffic data were available after 1800 PST, since the monitoring network was not in operation after that time.

Wind directions and speeds are plotted for six[*] stations for the 3-m levels, and for Stations 2 and 4 (the only stations having upper-level winds) on the 12-m analyses. These winds were actually observed at heights of 22 and 15 m, respectively. It turns out that the rooftop wind, as characterized by that at Station 2, furnishes the best indicator of the type of street-level CO pattern observed at any given time.

For the first period, there is a light easterly[†] rooftop wind, which sets up a leeward-windward circulation for Stations 7 and 8. The observed CO concentration at Station 7 at 3 m is almost double that at Station 8. However, the 3-m wind directions at these two stations are opposite to what would be expected from the primary vortex circulation. This occurred frequently; the most likely explanation for this apparent anomaly is that the wind sensors, which are located 3 m away from the buildings as well as 3 m above the street, are influenced by the secondary corner vortices, which are depicted in Figure 38 (presented later in this section).

---

[*] The data from Station 9 were not included in these analyses because of its separated location, at the intersection of First and San Fernando (see Figure 14). This station was mainly used as a control to ensure that the First and San Antonio data were representative of other intersections, and to furnish data up to higher levels (35 m) for comparison with the helicopter data.

[†] First Street is oriented at an azimuth direction of 330°-150°. All observed winds and discussions of these winds are relative to the First Street direction, which for convenience is taken to be N-S.

Another feature worth noting is the difference between the First Street concentrations and that at Station 4 on San Antonio Street, which has only about one-third the traffic present on First Street. Also, the concentrations at most stations decrease with height, as would be expected, with much less horizontal variation at the 12-m level.

The traffic volumes for the second period, 1200-1300 PST (Figure 26), are about 30 percent higher than for the morning period, but the observed concentrations are about the same in magnitude. This probably reflects the increase in observed wind speed rather than any changes in atmospheric stability. The rooftop wind direction has shifted to NNW, and the concentration gradient at First Street between Stations 7 and 8 has reversed from the earlier case.

This CO pattern stays approximately the same for the late afternoon case, 1700-1800 PST (Figure 27). The rooftop wind has shifted slightly to a westerly direction, and the leeward situation at Station 8 is still apparent. The traffic volumes are about the same as for the early morning case, but concentrations are slightly higher.

Figure 28 depicts an unusual situation of high CO concentrations during what is normally an off-peak traffic period, at 2300-2400 PST. However, at this time on Friday nights, a local custom of "cruising" of the downtown business district by the young people of the area produces traffic volumes estimated to be roughly double that of the late afternoon period, or about 1500 vehicles/hour on First Street. (Unfortunately, no traffic data are available for this period.) This heavy traffic, combined with light winds, caused the observed high concentrations. There is an indication of some leeward-windward effects at street level, as well as a general down-street gradient at 12 m, in accordance with the northwesterly rooftop wind direction.

The last period, 0300-0400 PST (Figure 29), is interesting in that it shows the result when the traffic is essentially "turned off." The traffic volume at this time was probably only about 10 percent of the daytime values, or roughly 100 vehicles/hour on First Street. However, the winds are very light over the city, and the general urban background concentration, much of which is probably due to traffic during earlier hours, remains high. The analysis shows that there is almost no vertical variation in the observed CO concentrations, as would be expected for a weak street-level emissions source, and very little horizontal variation.

2. Data Stratified by Wind Direction Classes

As previously discussed and as noted in the analyses just presented, the roof-level wind direction is apparently a controlling factor of the street-level CO patterns. Accordingly, we used the rooftop wind direction at Station 2 as the primary classification parameter. Other multiparameter stratifications were carried out, using in one case wind direction and time of day, and in the other case, wind direction, wind speed, and traffic volume. However, the simple classification by wind direction alone turned out to be the most revealing and the easiest to use. The CO patterns varied only slightly with time of day, except as influenced by traffic changes; the consistency of the concentration distributions from hour to hour was quite striking. In general, the stratification that included wind speed showed that there was a form of inverse dependence of concentration upon wind speed, as was to be expected.

Figures 30 to 37 depict the total CO and wind data classed and averaged by eight 45° wind direction sectors. Horizontal 3-m concentration distributions as well as vertical concentration

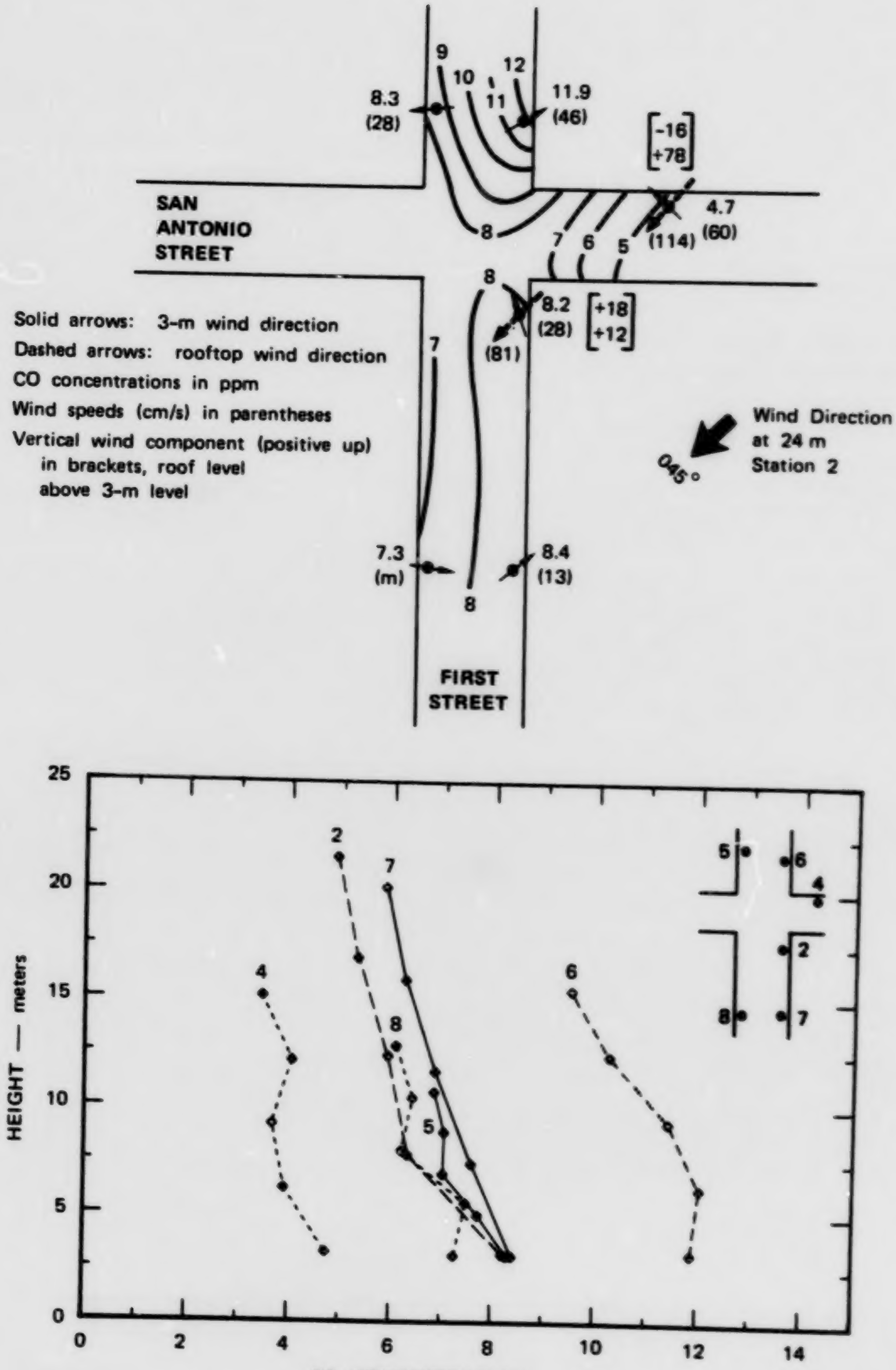

TA-8563-60

FIGURE 30 AVERAGE OF HORIZONTAL CO DISTRIBUTION AT 3 m (ABOVE) AND VERTICAL CO PROFILES (BELOW), FOR MEAN ROOFTOP WIND FROM 045° (±22.5°)

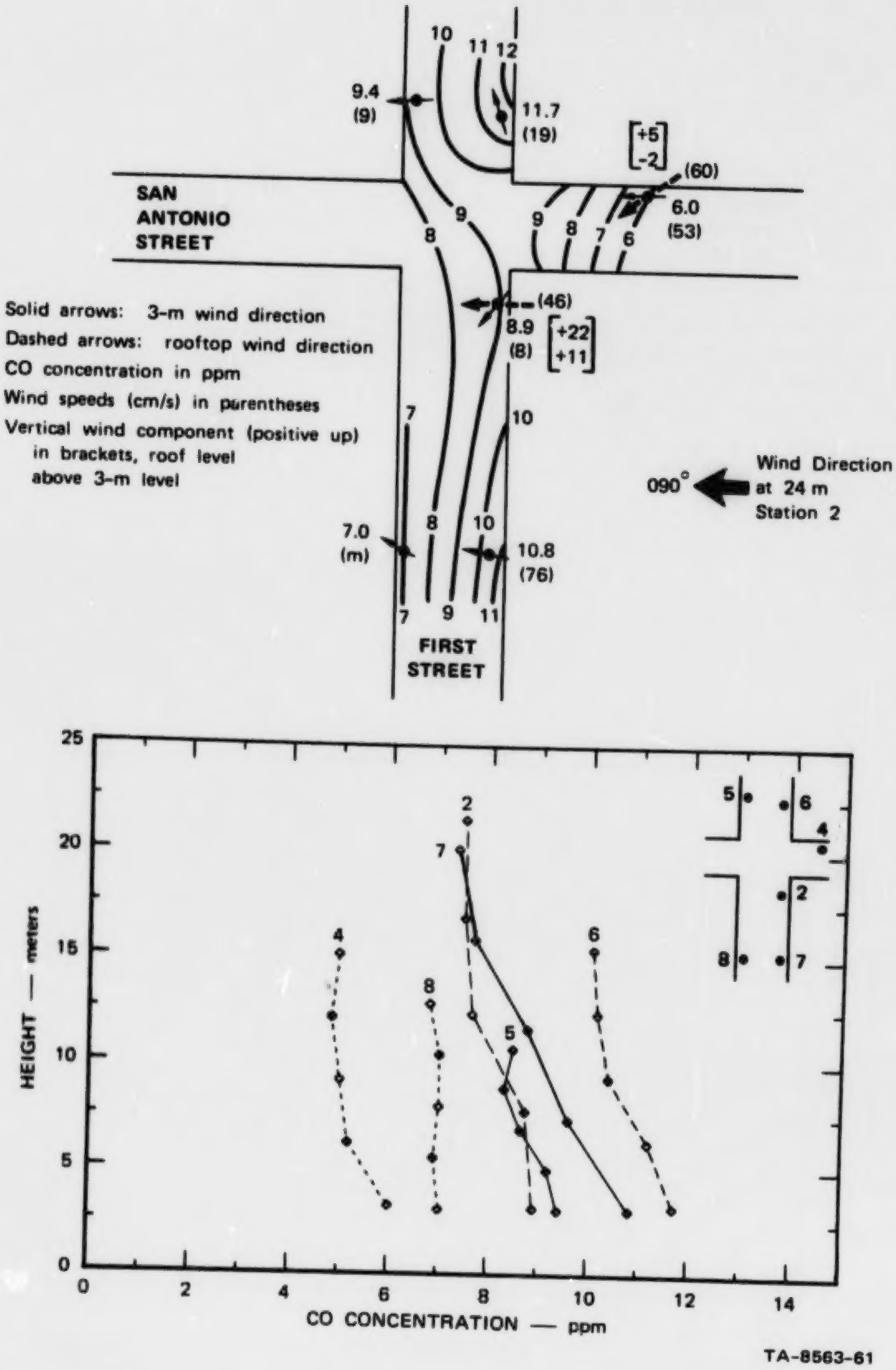

FIGURE 31 AVERAGE OF HORIZONTAL CO DISTRIBUTION AT 3 m (ABOVE) AND VERTICAL CO PROFILES (BELOW), FOR MEAN ROOFTOP WIND FROM 090° (±22.5°)

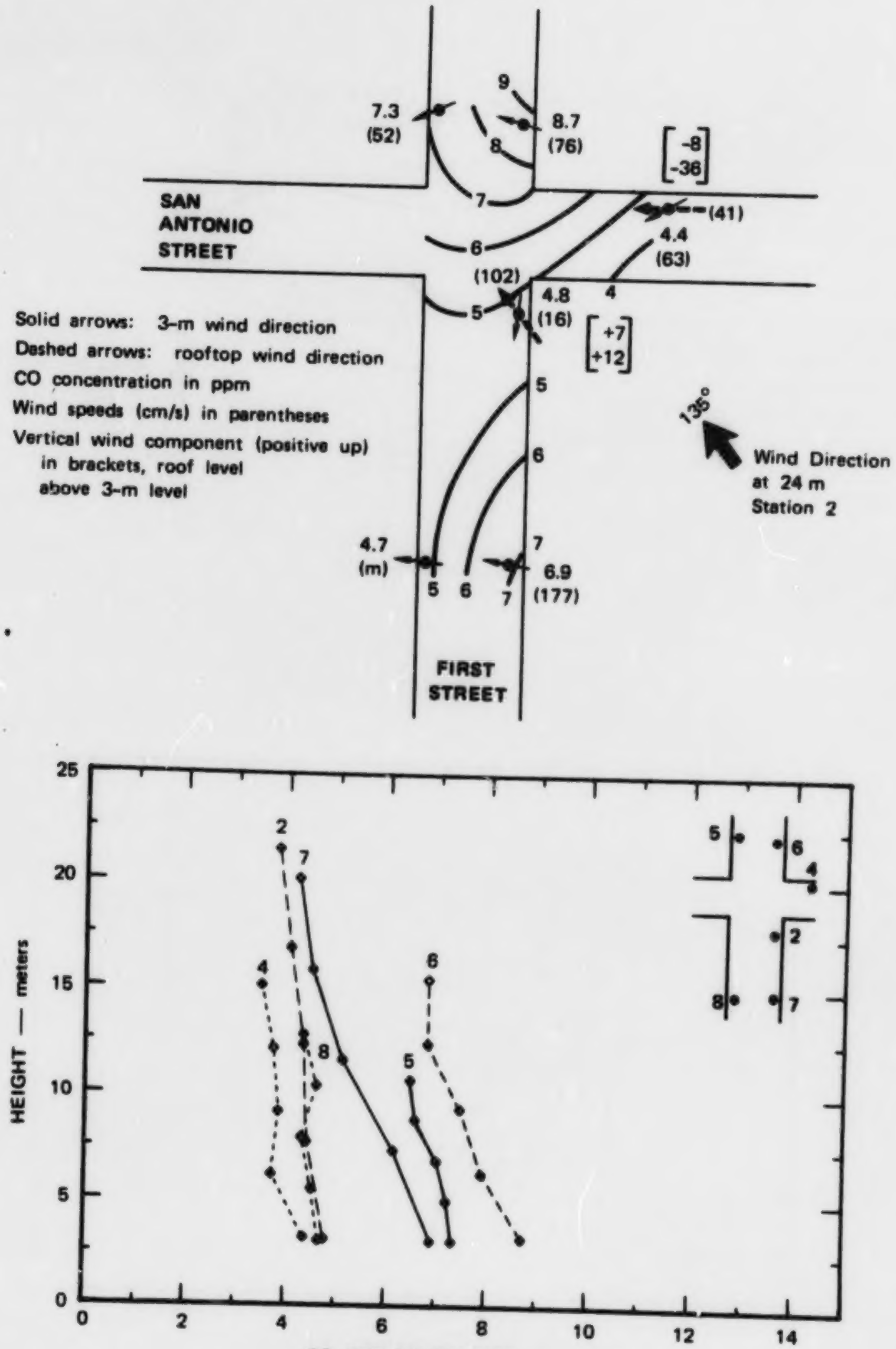

TA-8563-62

FIGURE 32 AVERAGE OF HORIZONTAL CO DISTRIBUTION AT 3 m (ABOVE) AND VERTICAL CO PROFILES (BELOW), FOR MEAN ROOFTOP WIND FROM 135° (±22.5°)

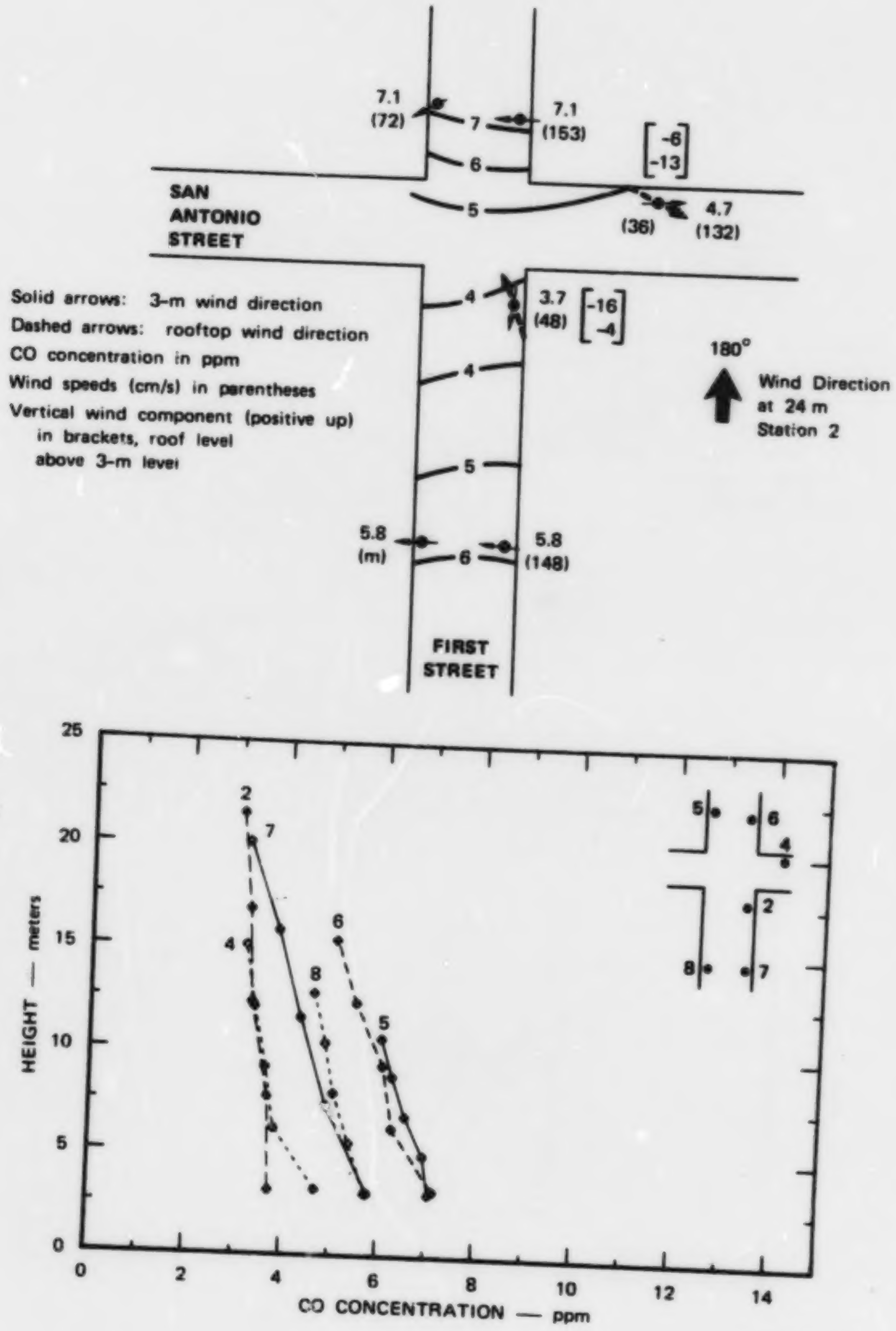

TA-8563-63

FIGURE 33 AVERAGE OF HORIZONTAL CO DISTRIBUTION AT 3 m (ABOVE) AND VERTICAL CO PROFILES (BELOW), FOR MEAN ROOFTOP WIND FROM 180° (±22.5°)

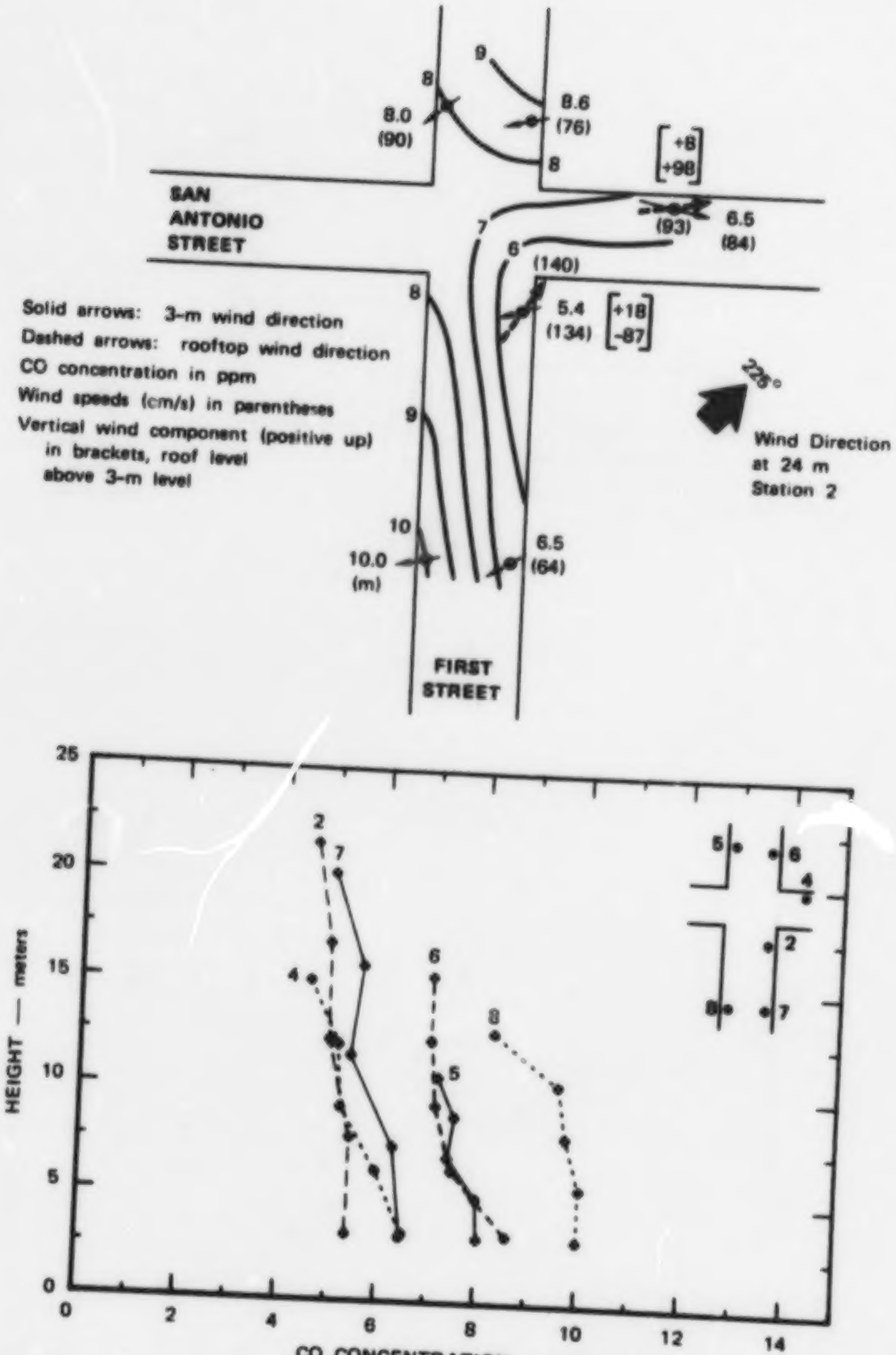

TA-8563-64

FIGURE 34 AVERAGE OF HORIZONTAL CO DISTRIBUTION AT 3 m (ABOVE) AND VERTICAL CO PROFILES (BELOW), FOR MEAN ROOFTOP WIND FROM 225° (±22.5°)

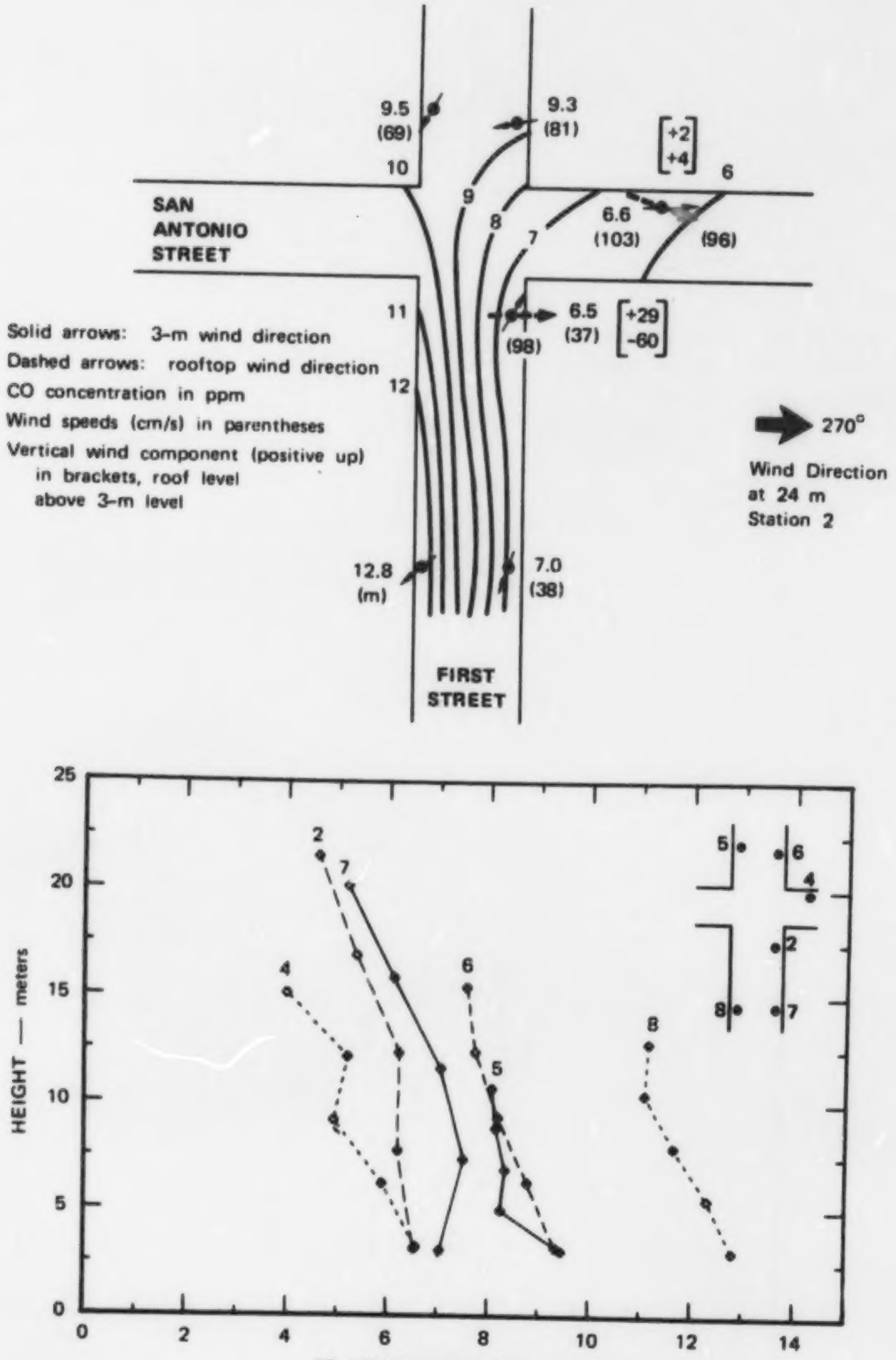

TA-8563-65

FIGURE 35 AVERAGE OF HORIZONTAL CO DISTRIBUTION AT 3 m (ABOVE) AND VERTICAL CO PROFILES (BELOW), FOR MEAN ROOFTOP WIND FROM 270° (±22.5°)

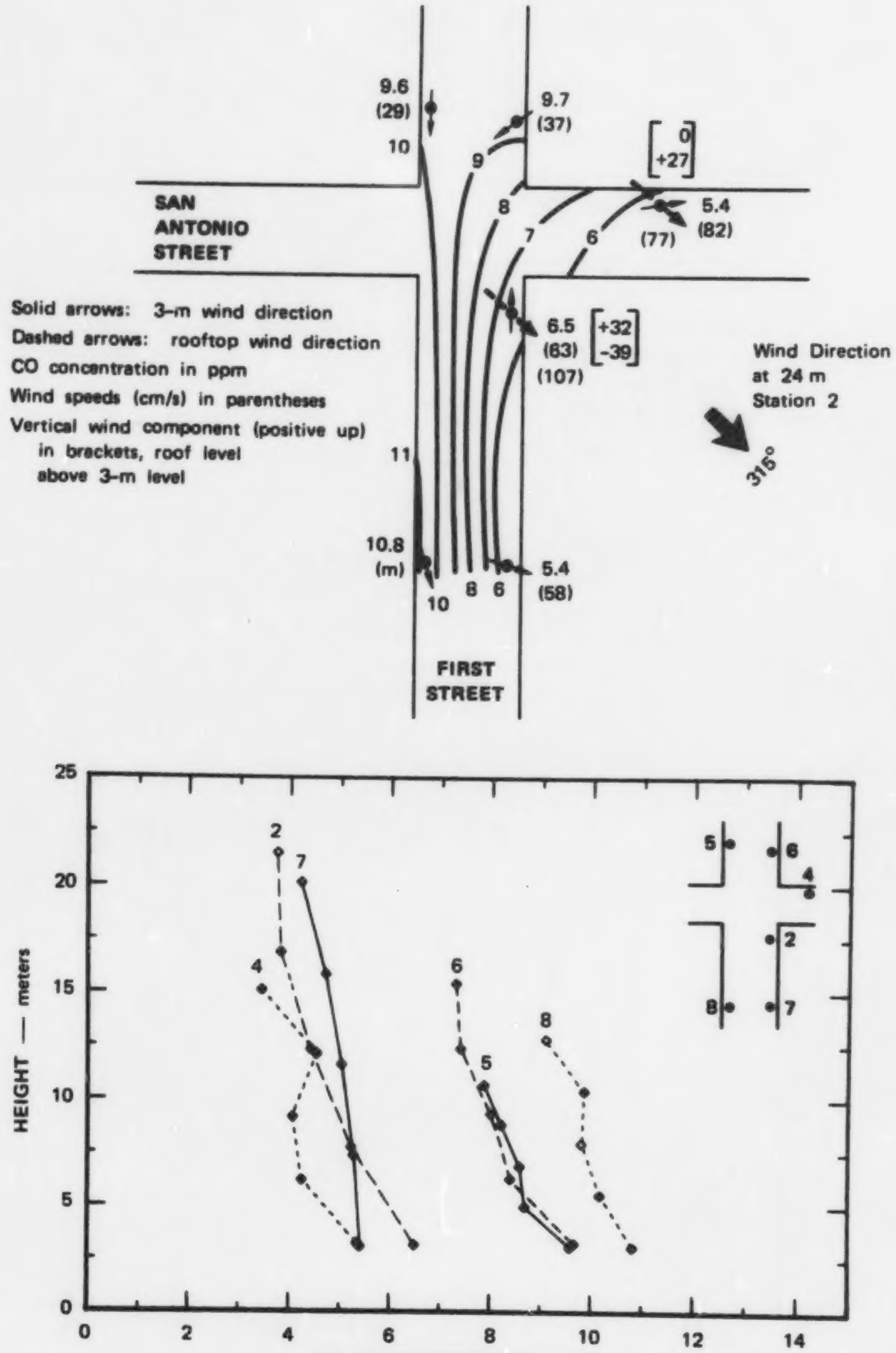

TA-8563-66

FIGURE 36 AVERAGE OF HORIZONTAL CO DISTRIBUTION AT 3 m (ABOVE) AND VERTICAL CO PROFILES (BELOW), FOR MEAN ROOFTOP WIND FROM 315° (±22.5°)

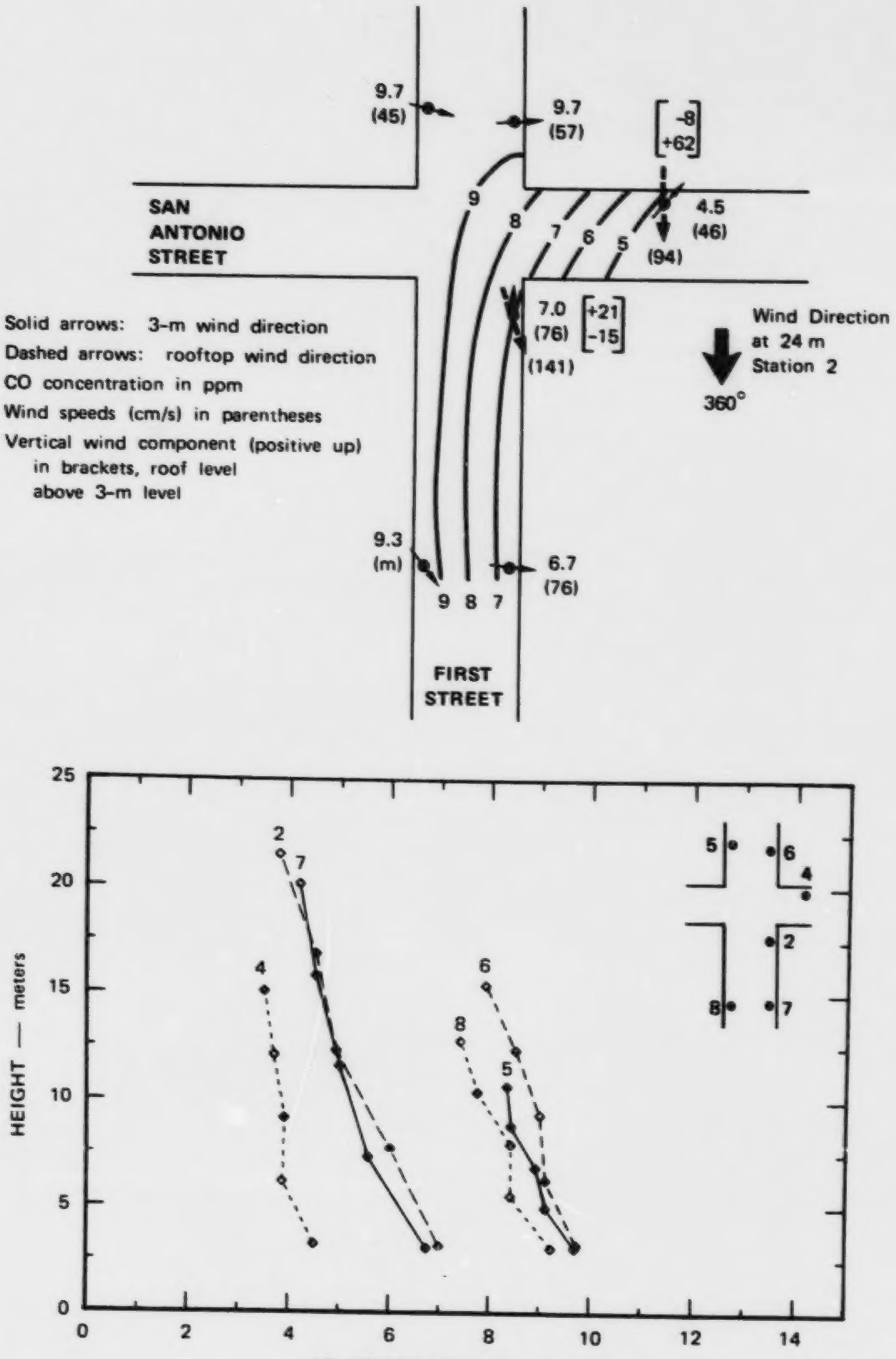

TA-8563-67

FIGURE 37 AVERAGE OF HORIZONTAL CO DISTRIBUTION AT 3 m (ABOVE) AND VERTICAL CO PROFILES (BELOW), FOR MEAN ROOFTOP WIND FROM 360° (±22.5°)

profiles for each station are shown. In addition, the vertical wind components at Stations 2 and 4 are included. These analyses are fairly self-descriptive, but a few comments are in order.

Generally, for rooftop winds from the eastern sectors, Stations 6 and 7 show a significant leeward effect, while those across First Street, Stations 5 and 8, indicate a windward case. This situation reverses for rooftop winds from the western sectors. Station 4 shows little variation for north and south winds, possibly because of the much lighter traffic on San Antonio Street.

For rooftop winds up First Street from the south (Figure 33), there is no cross-street gradient, and the concentrations increase north of the intersection. For the opposite case of north winds (Figure 37), the concentrations at Stations 5 and 6 are uniform, but Stations 7 and 8 still indicate a cross-street gradient. For slightly more easterly winds, from 045° (Figure 30), the cross-street gradient for these stations reverses, with Station 7 becoming slightly higher. This indicates that the concentrations at the two stations become uniform (analogous to the 180° case) for a wind direction of about 020° to 030°. The reason for this asymmetry in the CO patterns is unknown, but the substantial difference in building heights at Stations 7 and 8 may be involved. In addition, the proximity of Stations 2, 5, and 6 to the intersection complicates the circulation patterns compared to that characteristic of a typical street canyon, which is basically a two-dimensional situation. The latter is best represented in our data by that from Stations 7 and 8.

As expected, the CO profiles generally indicate a decrease with height. However, it is worthy of note that this slope is larger for stations in the lee of buildings, while more uniform concentrations with height are apparent for those stations on the windward side. A good example of this is found in the profiles for Stations 7 and 8 in Figure 31.

Little relation was found between the observed CO concentrations and the atmospheric thermal stratification, as characterized by the observed temperature profiles between 3 and 20 m. This probably reflects the dominance of mechanical mixing effected by the air flow around the buildings and the motion of the vehicles, as compared with mixing caused by convective processes.

D. Street Effects Submodel

In the development of this submodel, we have sought to find a simple technique that has a sound physical basis and, of course, that gives good results. In view of the importance of the upper-level wind direction relative to the street orientation, as found by Georgii et al. (1967) and confirmed by the San Jose data, we have retained the principle of separation into leeward and windward cases, as used before.

Figure 38 illustrates the basic rationale behind the street submodel. Given a general helical air circulation of the type shown, the receptors on the leeward side of the building (on the right in the figure) are exposed to substantially higher concentrations than those on the windward (left) side, because of the reverse flow component across the street near the surface. It is assumed that the concentration (C) at a receptor consists of two components that are superimposed. One component is the background concentration (C_b) in the air entering the street canyon from above, and the other concentration component (ΔC) arises from the locally generated CO emissions in the street,

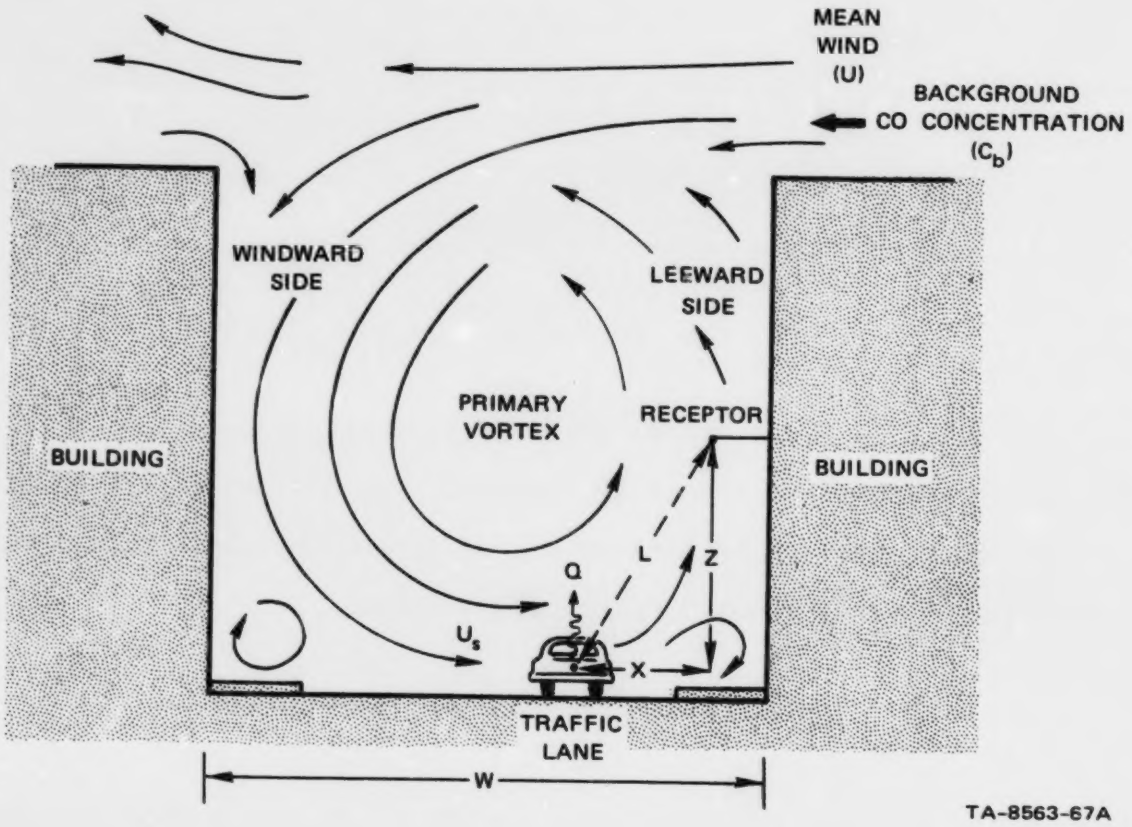
MEAN
WIND
(U)
BACKGROUND
CO CONCENTRATION
(C_b)
WINDWARD
SIDE
LEEWARD
SIDE
PRIMARY
VORTEX
RECEPTOR
BUILDING
BUILDING
Q
L
Z
U_s
X
TRAFFIC
LANE
W
TA-8563-67A

FIGURE 38 SCHEMATIC OF CROSS-STREET CIRCULATION BETWEEN BUILDINGS

Q (mg m^{-1} s^{-1}). Hence, we have

$$C = C_b + \Delta C \quad . \tag{7}$$

It is reasonable to assume that the concentration value computed by the basic intraurban diffusion model represents C_b. On the leeward side, the diffusion can be represented by a simple box model of the form

$$\Delta C_L = Q/U_s Y \quad , \tag{8}$$

where Y is the depth of the mixing volume, and U_s is the mean wind speed near the street. For short distances, Y is likely to be proportional to the travel distance (L):

$$Y = k_1 L \quad . \tag{9}$$

Also U_s may be taken to be linearly related to the roof-level wind, U (m s^{-1}):

$$U_s = k_2 \, (U + 0.5) \quad , \tag{10}$$

where the additive 0.5 m s^{-1} is an estimate that accounts for the mechanical air movement caused by traffic. The motions of the cars also mix the CO into an initial volume of dimensions (L_o) comparable to the vehicle size, about 2 m; Eq. (9) becomes

$$Y = k_1 \left(L + L_o \right) = k_1 \, (L + 2) \quad . \tag{11}$$

Now L is the diagonal distance from the center of the nearest traffic lane to the receptor. From Figure 38, we have,

$$L = \left(x^2 + z^2 \right)^{1/2} \quad , \tag{12}$$

where x and z are the horizontal distance and the height of the receptor relative to the center of the traffic lane. Combining Eqs. (8), (10), (11), and (12), we have

$$\Delta C_L = \frac{Q}{k_1 \, k_2 \, (U + 0.5) \left[\left(x^2 + z^2 \right)^{1/2} + 2 \right]} \quad . \tag{13}$$

We can represent a 50/50 mix of pre- and post-1965 model cars by the emission formula (Ludwig et al., 1970):

$$E = 0.5\left(245\ S^{-0.48} + 1120\ S^{-0.85}\right)\left(\frac{g}{\text{veh-mile}}\right) \qquad (14)$$

or approximately,

$$E \cong 700\ S^{-0.75}\left(\frac{g}{\text{veh-mile}}\right)\ , \qquad (15)$$

where S is the average vehicle speed (miles per hour). If E is multiplied by the traffic flow, N (vehicles per hour), we obtain the line source strength, Q in units of g mi^{-1} h^{-1}. If we change the units of Q to mg m^{-1} s^{-1}, we get

$$Q = 0.12\ N\ S^{-0.75}\ . \qquad (16)$$

Combining Eqs. (13) and (16), and introducing a factor of 0.87 to convert units of mg m^{-3} to ppm, we have

$$\Delta C_L = \frac{(0.1)\ K\ N\ S^{-0.75}}{(U + 0.5)\left[\left(x^2 + z^2\right)^{1/2} + 2\right]}\ , \qquad (17)$$

where $K = 1/k_1 k_2$. A reasonable value of the dimensionless constant k was found from our data to be about 7. In downtown San Jose, we measured S as approximately 14 mi h^{-1}. Substituting these values into Eq. (17) gives

$$\Delta C_L = \frac{0.07\ N}{(U + 0.5)\left[\left(x^2 + z^2\right)^{1/2} + 2\right]}\ . \qquad (18)$$

This equation and Eq. (7) were used to calculate leeward concentration profiles for comparison with the San Jose data, using x = 8 m for First Street and x = 7 m for San Antonio Street.

On the windward side, the air flow is mostly downward. Hence the air should be fairly well mixed, since it has traveled a considerable distance from the source, and there should be little vertical concentration variation. We have again used the box model, assumed the mixing volume to be constrained only by the width of the street (W), and have considered that the vertical concentration is uniform, giving

$$\Delta C_W = \frac{0.1\ K\ N\ S^{-0.75}}{W\ (U + 0.5)} \quad , \qquad (19)$$

or

$$\Delta C_W = \frac{0.07\ N}{W\ (U + 0.5)} \quad , \qquad (20)$$

when the previously used values of K and S are incorporated.

When the wind direction is such that neither a leeward nor a windward case is appropriate, an intermediate concentration (ΔC_I) is found by averaging the results of Eqs. (18) and (20):

$$\Delta C_I = 1/2 \left(\Delta C_L + \Delta C_W\right)$$

$$\Delta C_I = \frac{0.035\ N}{(U + 0.5)} \left\{ \frac{1}{\left[\left(x^2 + z^2\right)^{1/2} + 2\right]} + \frac{1}{W} \right\} \quad . \qquad (21)$$

There remains only the specification of wind direction sectors for the three different cases. This is carried out basically as set out in Figure 24. However, for a few of the stations in San Jose, these sectors had to be shifted by 15° to 45°, presumably because of the complexities in the flow caused by the differing building heights and the proximity to the intersection of several stations. The wind direction sectors used for the various stations are given in Table 3.

Table 3

WIND DIRECTION SECTORS FOR SAN JOSE STREET STATIONS

Station No.	Wind Direction Ranges for Various Cases		
	Leeward	Windward	Intermediate
2 (B)	060°-150°	210°-360°	000°-060°, 150°-210°
4 (D)	315°-045°	135°-225°	045°-135°, 225°-315°
5 (E)	225°-315°	045°-135°	315°-045°, 135°-225°
6 (F)	045°-135°	225°-315°	315°-045°, 135°-225°
7 (G)	060°-150°	210°-360°	000°-060°, 150°-210°
8 (H)	210°-360°	060°-150°	000°-060°, 150°-210°
9 (I)	225°-315°	045°-135°	315°-045°, 135°-225°

Equations (18), (20), and (21), along with Table 3 constitute the methodology developed to handle street effects for San Jose. The results of the verification tests using this simple street submodel are described in Section VI.

BLANK PAGE

IV ANALYSIS OF HELICOPTER AND MOBILE VAN DATA

A. Introduction

The helicopter and mobile van measurements of carbon monoxide concentration and temperature provide a unique set of data for use in the refinement and validation of the urban diffusion model. The vertical profiles provide detailed information on the structure of the lower atmosphere and have been used for the determination of background CO concentrations, mixing depth, and stability. Additionally, they provide a qualitative "feel" for the experimental conditions in terms of the meteorology and traffic. The aerial and surface traverses were made about the perimeter of the central business district (see Figures 13 and 20); analysis of these data provides an independent estimate of the rate of vehicular emission of CO over the area, while the data also permit us to compute the vertical diffusion of CO. Vertical profiles of wind structure over the city during selected periods were obtained from pilot balloon (pibal) ascents at nearby San Jose State College; the pibal data are summarized in Appendix E.

B. Data Reduction Techniques

The vertical profiles of temperature and CO were determined at intervals of about 15 m to a height of 152 m and then at 30.5-m intervals to the top of the profile (nominally 1000 m). As examples, four sets of CO and temperature profiles are given in Figure 39, corresponding to periods for which pibal data are available.

The traverse data obtained by the helicopter comprise 19 point values around the circuit shown in Figure 20 for each level. Values

PRECEDING PAGE BLANK

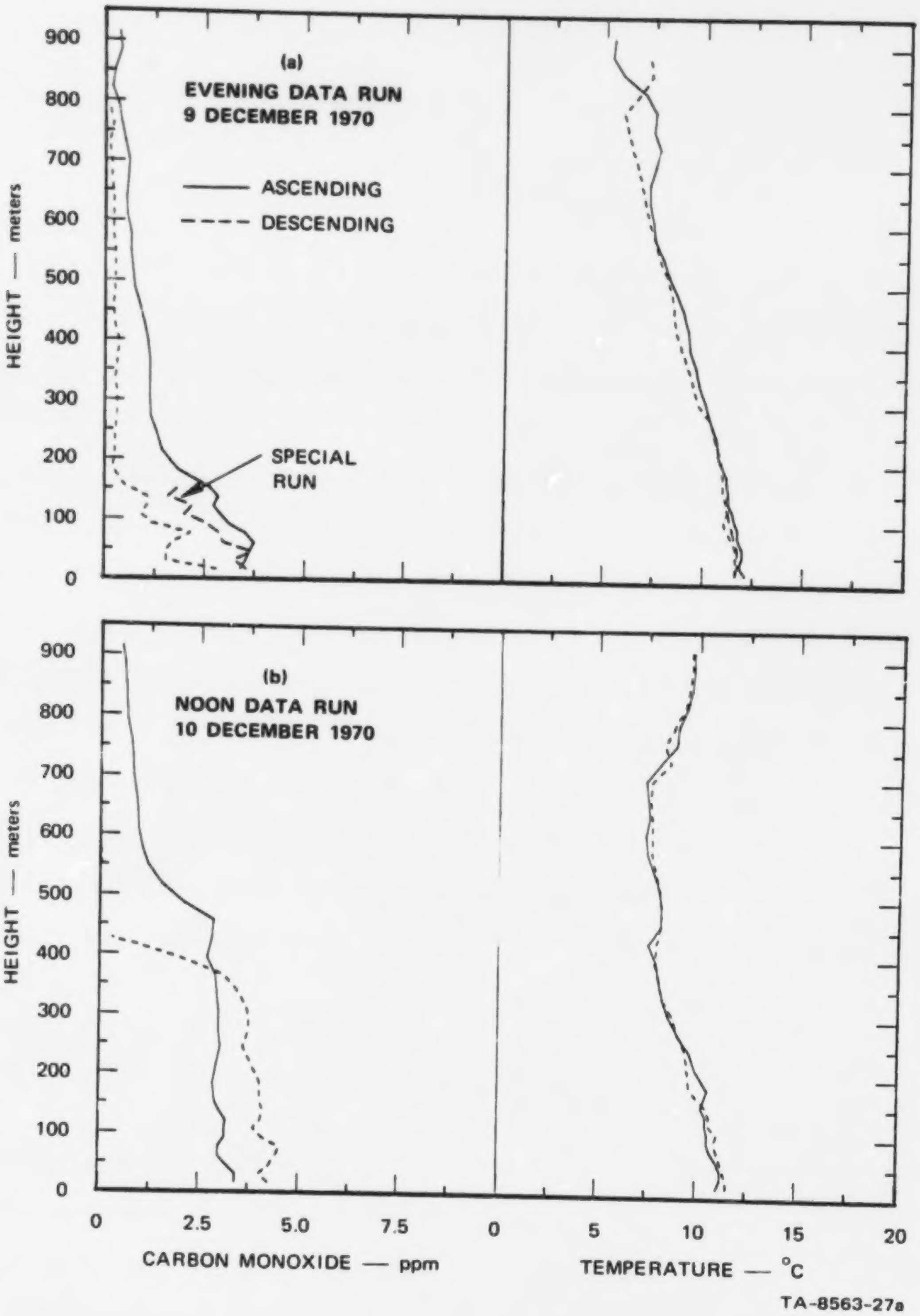

FIGURE 39 VERTICAL PROFILES OF CARBON MONOXIDE AND TEMPERATURE AT SPARTAN STADIUM, SAN JOSE, CALIFORNIA

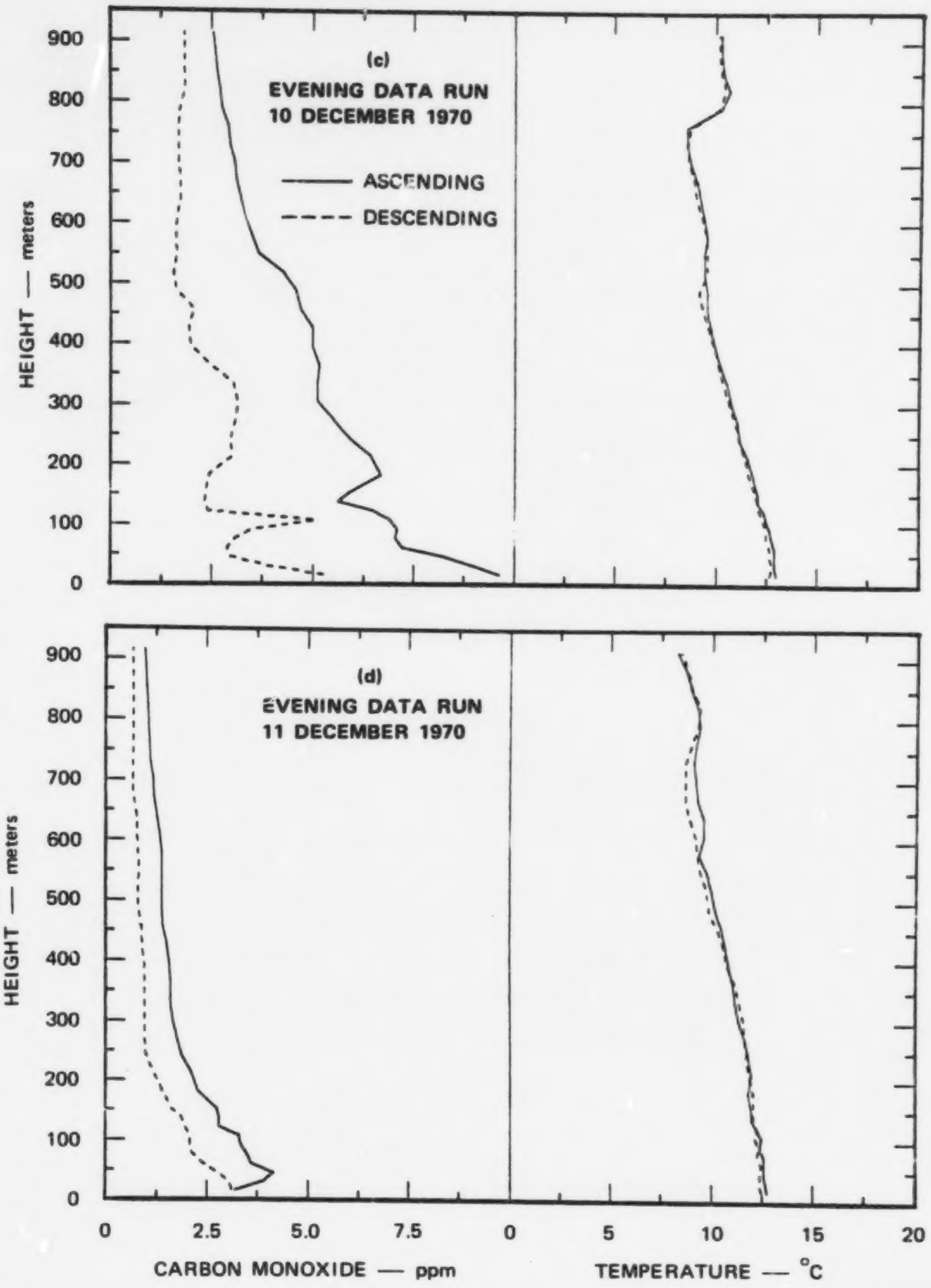

TA-8563-27b

FIGURE 39 VERTICAL PROFILES OF CARBON MONOXIDE AND TEMPERATURE AT SPARTAN STADIUM, SAN JOSE, CALIFORNIA (Concluded)

are given at each corner of the pattern (the first corner is repeated at the end of the flight) and for three intermediate points on the two short legs and four on each of the two long legs. Examples of the CO traverse data for four periods are given in Figure 40. For the mobile van measurements, averages over the route segments shown in Figure 20 were used rather than point values, owing to the highly variable nature of the street level concentrations. An average of five van traverses were made during each data period. Because of street patterns, the route of the van differs slightly from that of the helicopter, particularly along the southern leg (see Figure 20). The effect of these differences is minimized when leg averages are determined corresponding to the helicopter pattern. The weighting procedure is straightforward and is summarized in Table 4.

Table 4

CORRESPONDING HELICOPTER AND VAN LEGS, INDICATING WEIGHTING FACTORS FOR DETERMINATION OF AVERAGE CO ALONG VAN ROUTE SEGMENTS

Helicopter Leg	Corresponding Van Leg			
	Segment	Weight	Segment	Weight
I-II	V5-V4	1.00		
II-III	V4-V3	0.75	V3-V2	0.25
III-IV	V3-V2	0.33	V2-V1	0.67
IV-I	V1-V6	0.40	V6-V5	0.60

C. Results

1. Determination of Vehicular Emissions and Vertical Diffusion of Carbon Monoxide

The vehicular emissions and the vertical diffusion of carbon monoxide within the downtown area have been determined through mass budget analysis. The horizontal perimeter of the budget box is described by the near-coincident routes of the helicopter and van traverses; the top is defined by the vertical extent of the aerial measurements. The volume is divided into various sublayers by the heights of the helicopter traverses (61, 92, 152, 213, and 305 m).

The mean transport of CO into or out of the four sides of the sublayers is given by the area integral of the product of the component of the wind speed normal to the sides and the mean CO concentration along the sides. In the absence of detailed wind measurements in the sublayer nearest the surface, it was assumed that the wind profile could reasonably be approximated by a simple power law,

$$S = S_*\left(z/z_*\right)^p \quad , \qquad (22)$$

where S is the wind speed normal to the side at height z, and S_* is the normal component of the measured wind speed at z_*, the lowest level resolved from the pibal ascents (nominally 72 m). Values of the exponent p are given in Table 5 as a function of atmospheric stability (represented by the difference between the 122-m and 2-m temperatures). Carbon monoxide concentration was assumed to change linearly with height within each sublayer. Therefore, the mean transport through each of the sides of the lowest layer is given as

$$\int_0^h \int_{L_1}^{L_2} S\,\bar{X}\,dz\,dL = \frac{S_* L}{z_*^p}\left[\frac{X_o h^{p+1}}{p+2} + \frac{a h^{p+2}}{p+2}\right] \quad , \qquad (23)$$

where $\bar{X}$ is mean CO concentration along the side, h is the layer thickness, L is the length of the side, the subscript zero denotes a surface value, and the parameter a is the bulk CO gradient over the layer,

$$a = \frac{\bar{X}_h - \bar{X}_o}{h} \quad . \qquad (24)$$

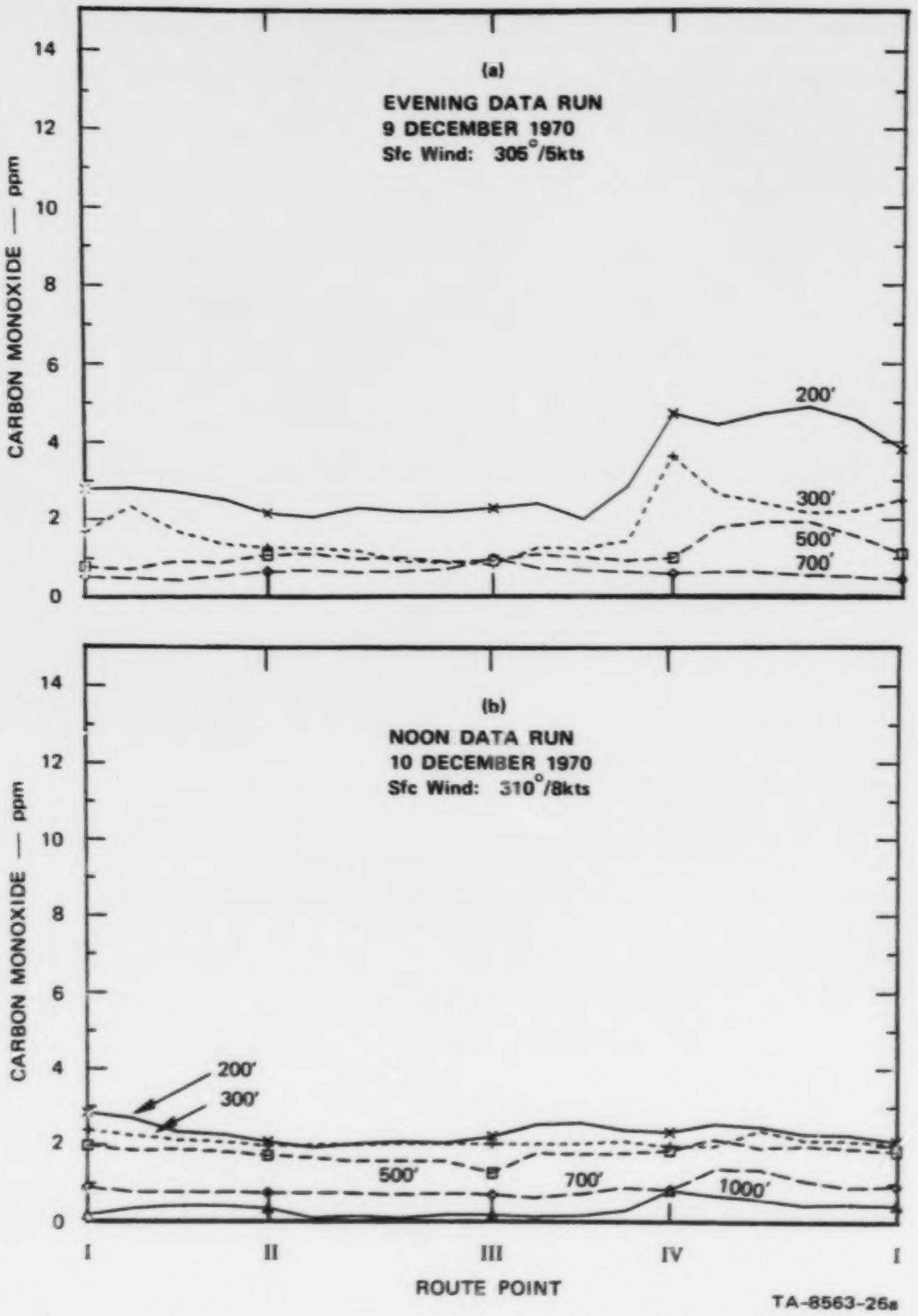

FIGURE 40 HORIZONTAL TRAVERSES OF CARBON MONOXIDE AT INDICATED HEIGHTS FOR BOX PATTERN OVER DOWNTOWN SAN JOSE, CALIFORNIA

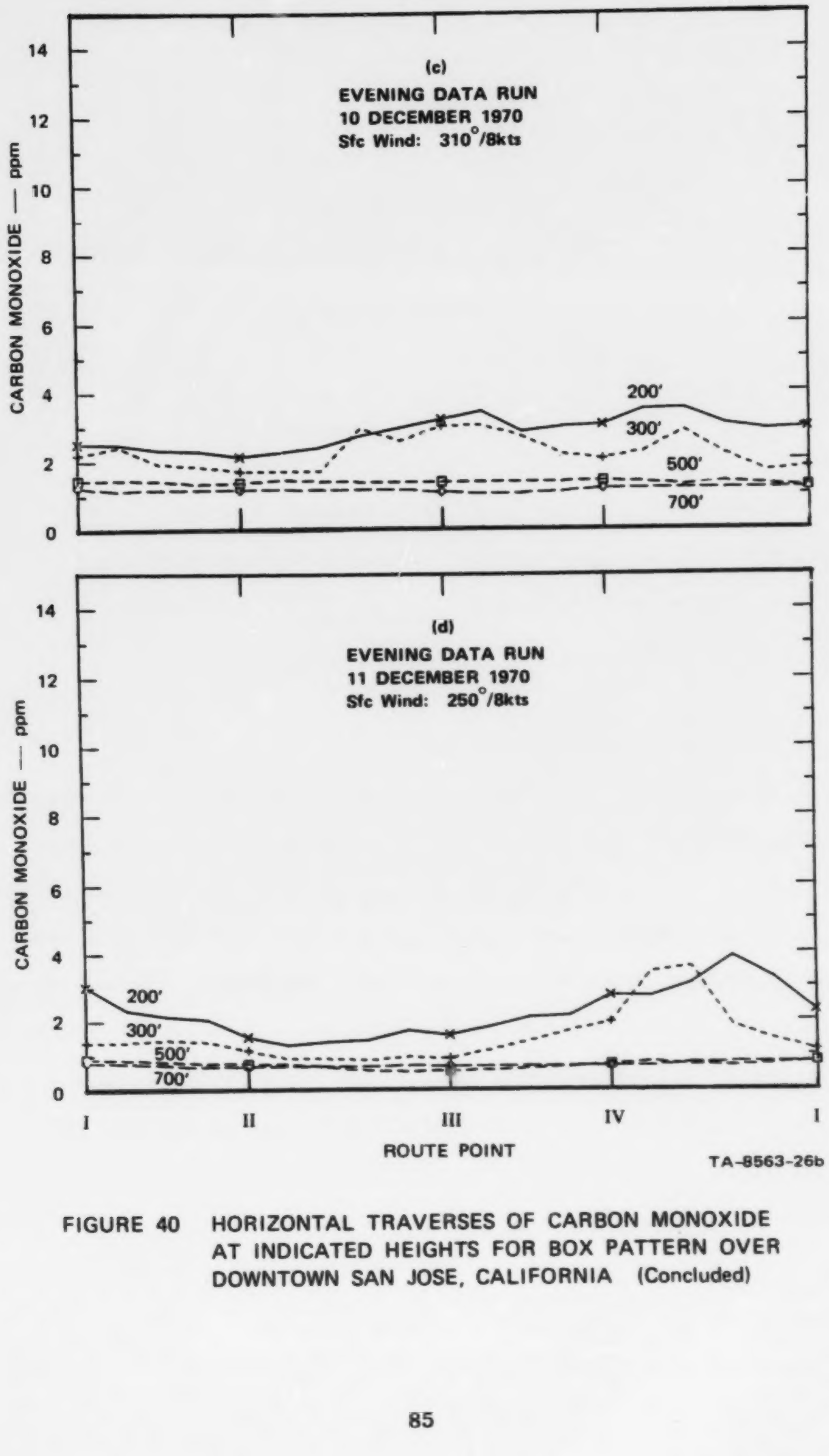

FIGURE 40 HORIZONTAL TRAVERSES OF CARBON MONOXIDE AT INDICATED HEIGHTS FOR BOX PATTERN OVER DOWNTOWN SAN JOSE, CALIFORNIA (Concluded)

Table 5

VALUES OF p IN EQ. (22) AFTER FROST (1947)

$T_{122m}-T_{2m}$ (°C)	p
-2.2 to -1.1	0.145
-1.1 to 0	0.25
0 to 1.1	0.32
1.1 to 2.2	0.44
2.2 to 3.3	0.59
3.3 to 4.4	0.63

Computation of the mean CO transport through the upper layers incorporated the additional assumption of linear wind changes with height between.pibal data levels, where

$$\int_{z}^{z+\Delta z} \int_{L_1}^{L_2} S \overline{X} \, dz \, dL = {}^{z}\overline{S\ X}^{z+\Delta z} \, L\Delta z \quad . \qquad (25)$$

Implicit in the budget analysis is the assumption that the net horizontal turbulent flux of CO for each layer is negligibly small compared to the net transport by the mean wind. This condition is satisfied by a horizontally homogeneous emission source and wind field over the area. Furthermore, when the mean vertical component of the wind is taken as zero, the net horizontal transport for any given layer is then balanced by the net vertical (turbulent) flux of CO through the bottom and top. The uppermost traverse was made sufficiently high such that the vertical diffusion through that level is essentially zero. Working down toward the surface, the vertical CO fluxes through the various levels can be determined as the residue in the budget, where the near-surface (3-m) flux corresponds to the vehicular CO emission rate. The vertical separation of approximately 3 meters between the emission source (automobile exhausts) and the receptor height of the van may be considered negligible for the majority of atmospheric conditions although it may lead to slight underestimates of the emission rate during near-stagnation episodes.

Results of the budget analysis are given in Table 6. The analysis for the 1211-1238 PST period on 10 December 1970 was done twice with two different assumed shapes for the wind profile. The only pibal sounding available on that date was made approximately 4 hours later. However, because of the constancy of the surface winds during the afternoon (obtained from the hourly observations at the nearby San Jose Municipal Airport), it was felt that the sounding would be representative of the midday vertical wind field, and the first analysis for the noted period follows from this assumption. The second analysis uses an assumed power profile [Eq. (22)] for the wind based on the airport surface wind observation and the vertical temperature gradient obtained from the helicopter measurements. This second approach is essentially one which a researcher might be forced to employ in the absence of low-level wind profile data. The two methods differ by a factor of 2.4. This relatively large difference emphasizes the importance of the low-level wind field for pollution transport computations in general, and for mass budget analysis in particular.

Vehicular carbon monoxide emissions were also determined with the empirical emissions model presented by Ludwig et al. (1970), and slightly modified for this study, where

$$E = 0.5 \left(245 \ S^{-0.48} + 1120 \ S^{-0.85}\right) \quad . \qquad (26)$$

E is the emission rate in g-CO per vehicle-mile, and S is the average vehicle speed in miles per hour. The first term in the parentheses represents emissions from post-1968 vehicles; the second term is for

Table 6

TRANSPORT RATES OF CARBON MONOXIDE THROUGH THE SIDES, TOP, AND BOTTOM OF THE SUBLAYERS OF THE SAN JOSE BUDGET BOX

Date/Time	Height of Layer (m)		Horizontal Transport ($g\text{-}CO\ s^{-1}$)		Vertical Flux ($g\text{-}CO\ s^{-1}$)	
	Top	Bottom	Total In	Total Out	In through Bottom	Out through Top
9 December 1970 1707-1729 PST	213	152	678	779	101	0
	152	92	624	870	347	101
	92	61	474	642	515	347
	61	3	2875	3184	823	515
10 December 1970 1211-1238 PST*	305	213	139	167	29	0
	213	152	280	306	55	29
	152	92	478	490	67	55
	92	61	274	278	72	67
	61	3	1270	1507	310	72
10 December 1970 1211-1238 PST†	305	213	722	870	148	0
	213	152	1105	1211	253	148
	152	92	1590	1628	292	253
	92	61	846	859	305	292
	61	3	2324	2759	739	305
10 December 1970 1711-1743 PST	213	152	287	275	-12	0
	152	92	442	464	23	~ 0
	92	61	278	338	83	23
	61	3	1428	1632	287	83
11 December 1970 1702-1724 PST	213	152	301	276	-25	0
	152	92	562	821	259	~ 0
	92	61	446	749	562	259
	61	3	3626	4253	1189	562

*With 1700 PST pibal data.

†With assumed "power law" wind profile.

earlier-model vehicles. The average vehicle speed was taken as 13.7 mi h^{-1} for all periods as determined from an analysis of the mobile van movement through the downtown sector. Table 7 gives a synopsis of the van speeds for the period 9-11 December 1970.

Table 7

AVERAGE VEHICLE SPEEDS IN THE DOWNTOWN SECTOR OF SAN JOSE
FOR SPECIFIED TIMES DURING THE PERIOD 9-11 DECEMBER 1970

Time Period	Number of Van Circuits	Average Speed (mi h^{-1})	Standard Deviation (mi h^{-1})
0740-0900	15	14.3	1.5
1137-1245	13	14.3	1.1
1616-1757	17	12.7	3.4

The traffic monitoring network comprises approximately 44 percent of the surface area of the budget box. Therefore, it was necessary to estimate the traffic volume outside the network, but within the box. Since daily, routine data are not available for this outer area, it was assumed that the traffic volume for this region is proportional to that within the monitoring network. To determine the proportionality constant, we used a selective traffic count conducted by the City of San Jose (Turturici, 1970) where traffic volumes obtained during August 1969 are presented by street segments for a region encompassing all of the budget area. The ratio of traffic in the budget area to that within the monitoring network was found to be 1.64. Furthermore, it was assumed that the mean vehicular speed was constant over the entire area. Using the results of the emissions model [Eq. (26)], the total emission rate (Q, gm-CO s^{-1}) over the budget area is obtained from the equation

$$Q = 1.64\ E\ L\ N \quad , \qquad (27)$$

where L is the mean link length (0.1 mile) and N is the total number of vehicle counts registered in the monitoring network per second (averaged over a 90-minute period). The results of this computation are given in Table 8, together with those obtained from the mass budget analysis.

Table 8

CARBON MONOXIDE EMISSION RATES (Q) FOR THE BUDGET AREA DETERMINED FROM THE MASS BUDGET ANALYSIS AND TRAFFIC DATA [WITH EQ. (27)]

Date (1970)	Time (PST)	N^* (cts s^{-1})	Q, Traffic Data (g-CO s^{-1})	Q, Budget Analysis (g-CO s^{-1})
9 December	1707-1729	25.76	408	823
10 December	1211-1238	22.43	355	310
10 December	1711-1743	26.24	416	287
11 December	1702-1724	28.15	446	1189
Average		25.64	406	652

* N is the number of traffic counts per second within the traffic monitoring network.

The mean area emission rate determined from the traffic data differs from the mean of the budget values by 38 percent. The differences in the individual cases probably arise because of the following factors: (1) inhomogeneities in the horizontal wind field, (2) nonzero vertical wind components, (3) changes of the CO field during the observation period, and (4) inaccurate representation of the total traffic flow by assuming it to be a constant factor of that within the monitoring network. It is encouraging that these two totally independent methods agree to the extent indicated. At this time there does not appear to be any justification for changing the emissions model.

2. Mixing Depth Estimates

The helicopter profiles of temperature and carbon monoxide concentration have been used to estimate the depth of the San Jose urban mixing layer for the period 7, 9, 10, and 11 December 1970. These estimates are compared with values from the mixing depth submodel (Ludwig et al., 1970) and, additionally, with values obtained from the SRI/APCO Mark VIII lidar system, which was operated coincident with this program under another project.

The Mark VIII lidar is composed basically of a laser transmitter, which emits a very brief, high-intensity pulse of coherent monochromatic light, and a receiver, which detects the energy at that wavelength backscattered from atmospheric aerosols, as a function of range. Some of the features of this ruby-lidar system are: (1) coaxial transmitter-receiver alignment, (2) high pulse rate (20/minute), (3) range compensation, and (4) automatic programmed elevation scanning and firing. The data are recorded on a magnetic disk in a format that permits an intensity-modulated range-height indicator (RHI) display on an oscilloscope. The resulting vertical cross sections through the haze can be analyzed to determine time-average composites through multiple displays and photographic exposures.

The lidar was used to monitor the mixing layer depth as represented by the lower haze layer(s). The displays in Figure 41 represent a series of time-height cross sections obtained by vertical observations 12 seconds apart on 11 December at the Spartan Stadium area. The time variation in the haze layer heights is striking. The mean heights, however, correspond reasonably well with significant levels on the

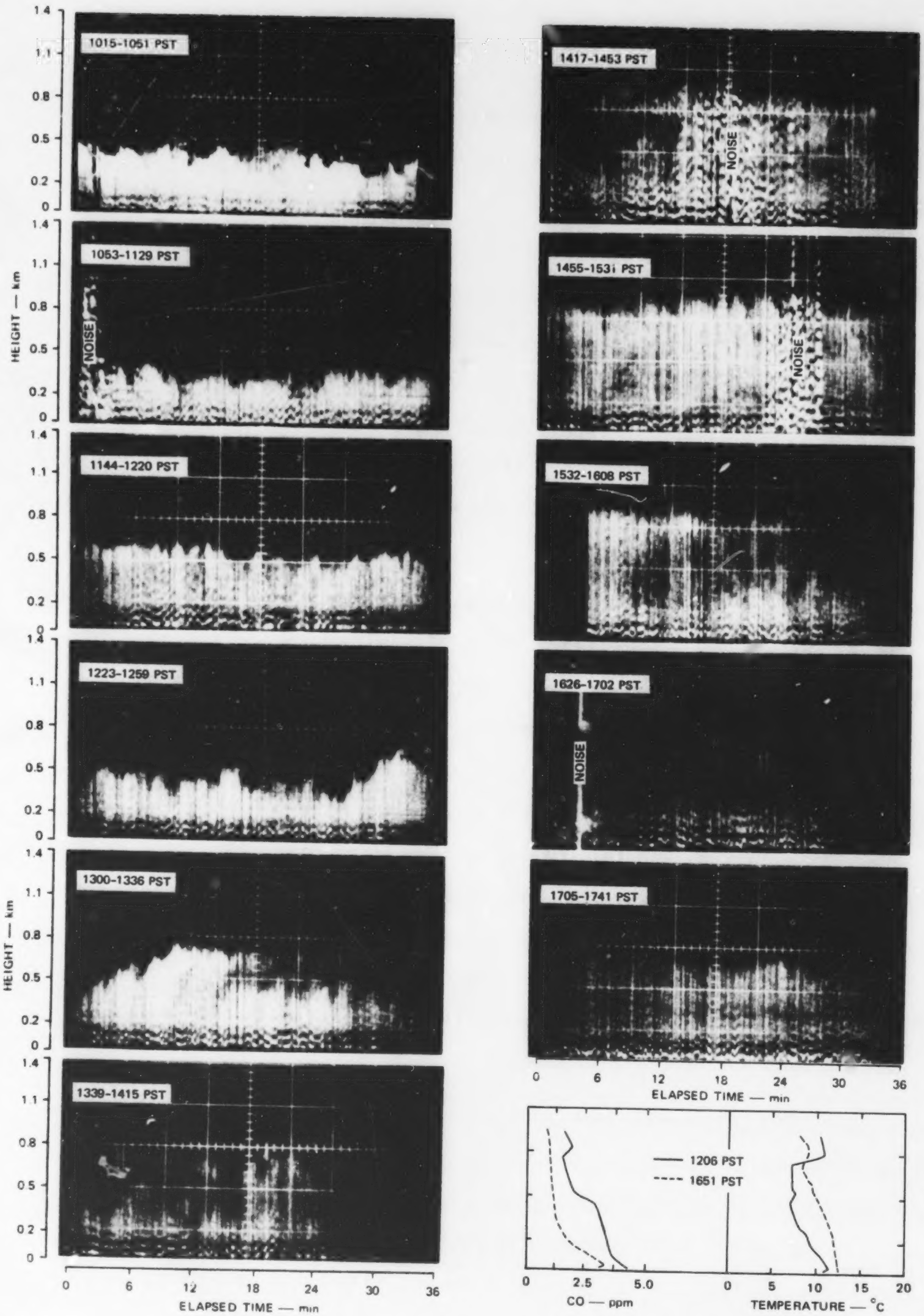

FIGURE 41 LIDAR-OBSERVED TIME-HEIGHT CROSS SECTIONS OF THE URBAN HAZE LAYER OVER SAN JOSE, CALIFORNIA, ON 11 DECEMBER 1970. Concurrent helicopter profiles of carbon monoxide (CO) and air temperature are shown at the bottom right.

corresponding helicopter profiles; these values are summarized in Table 9. Mixing depths computed for the same time periods during the morning helicopter temperature soundings and the submodel used with the diffusion model are also given in the table. The agreement among the three methods is generally good.

Table 9

COMPARISON OF MIXING DEPTH ESTIMATES OBTAINED FROM THE MIXING DEPTH SUBMODEL AND THE SUBJECTIVE ANALYSIS OF THE HELICOPTER PROFILE DATA, WITH THE LIDAR-OBSERVED HAZE-LAYER STRUCTURE AT SAN JOSE, CALIFORNIA

Date (1973)	Time (PST)	Mixing Depth (m)		Lidar-Observed Haze Layers[*] (m)
		Model	Helicopter	
7 December	1240	--	215	450, 850[†]
9 December	0800	115	100	300-500 (variable)
	1200	950	125, 675[†]	450-600 (variable)
	1700	672	200, 725	750
10 December	0800	143	125	300
	1200	567	425	450[‡]
	1700	567	500, 750	250
11 December	0800	148	60, 550	Low Clouds
	1200	539	500, 725	350-700 (variable)
	1700	539	600	600-750 (variable)

[*] Indicating the height variation over a one-half hour period.

[†] Multiple values for the helicopter and lidar data represent the tops of the surface and elevated mixing layers.

[‡] Lidar observation made at 1430 PST.

The helicopter and lidar data often indicate the presence of multiple stable layers in the lowest 1000 m above the surface. The CO profiles on these occasions show that there is some penetration of CO through the near-surface mixing layer. This occurs when the lid is not particularly strong (as indicated by the temperature profile) while the concurrent lidar observations frequently indicate intermittancy in the occurrence and/or height of the lid. This intermittancy may be the result of local (convective) or advective effects and seems to represent a transitional stage in the lower atmospheric structure.

3. Stability Estimates

The helicopter temperature profiles were used in conjunction with the airport wind speeds to compute a bulk stability coefficient (B),

$$B = \frac{T_{90} - T_{15}}{U_3^2} \quad , \tag{28}$$

where T is temperature (°C), U is the wind speed (knots), and the subscripts are the heights (m) of the various measurements.[*] The bulk stability coefficients were compared with modified Pasquill-Turner stability categories determined from the diffusion model (Ludwig et al., 1970) as a function of insolation strength, wind speed, and cloud cover as summarized in Table 10.

---

[*] The coefficient B provides an estimate of the ratio of the production of energy by buoyant forces to the dissipation of mechanical energy by turbulence. Neutral atmospheric conditions are indicated by values of B near zero; unstable conditions result in $B < 0$ and stable conditions in $B > 0$.

Table 10

MODIFIED PASQUILL-TURNER STABILITY CATEGORIES* USED WITH THE DIFFUSION MODEL (Ludwig et al., 1970) AS A FUNCTION OF INSOLATION, WIND SPEED, AND CLOUD COVER

Surface Winds (knots)	Daytime Insolation			Night Clouds	
	Strong	Moderate	Slight	≥5/10	≤4/10
≤3	1	2	2	5	5
3-6	1	2	3	4	5
6-10	2	3	3	4	4
10-12	3	3	4	4	4
≥13	3	4	4	4	4

*1 = extremely unstable, 2 = moderately unstable,
3 = slightly unstable, 4 = neutral, 5 = slightly stable.

The stability estimates from the diffusion model agree very well with the observed thermal stability (given by B) for neutral and slightly unstable conditions as shown in Table 11. However, the model often appears to break down by predicting moderately unstable conditions during the morning hours when, in fact, stable conditions are observed. The presence of a morning, surface-based inversion with corresponding low wind speeds is, in essence, indicative of "night" conditions, despite the slight insolation. With reference to Table 10, employing the nighttime hypothesis leads to the prediction of neutral or slightly stable conditions in agreement with observed conditions.

In summary, the model predicts atmospheric stability reasonably well except for the few morning hours shortly after sunrise during light wind conditions. On these occasions, reasonable stability estimates are obtained by considering the situation to be better simulated by the nighttime case in the stability estimation methodology.

Table 11

COMPARISON OF BULK STABILITY COEFFICIENTS COMPUTED FROM EQ. (28) WITH STABILITY CATEGORIES DETERMINED FROM THE DIFFUSION MODEL FOR THE PERIOD 20 NOVEMBER TO 11 DECEMBER 1970, AT SAN JOSE, CALIFORNIA

Time (PST)	Stability Categories		
	Moderately Unstable (Category 2)	Slightly Unstable (Category 3)	Neutral (Category 4)
0800-0900	0.0440	-0.0468	0.0041
	0.1300	-0.0040	-0.0023
	0.0035		
1200-1300	-0.0140	-0.0035	
	-0.0074	-0.0531	
1700-1800			-0.0062
			-0.0039
			-0.0030
			-0.0054
			-0.0097
Average	0.0312	-0.0269	-0.0039

V INCORPORATION OF THE RESULTS INTO THE URBAN DIFFUSION MODEL

A. Introduction

In this section we summarize the actual refinements that have been made to the basic urban diffusion model as a result of the San Jose field program and of further analyses of data from experiments by other groups. Our rationale in determining the necessary revisions has been to measure the input variables and CO concentrations as completely and as accurately as possible. In this way, (1) the performance of the submodels that estimate certain of the input parameters for the model can be assessed, and (2) the accuracy of the basic diffusion model in predicting CO concentrations may be determined by using accurately measured input parameters, rather than indirect estimates. However, the fundamental design specification that, in practice, the model will use available conventional meteorological data has remained as a guiding principle.

B. Emissions Submodel

In past work we have assumed that CO emissions (E, g $\text{veh}^{-1}\text{mi}^{-1}$) can be estimated from the mean vehicle speed (S, mi h^{-1}) on the basis of empirical relationships of the type proposed by Rose et al. (1964):

$$E = cS^{-\beta} \quad , \qquad (29)$$

where c and β are constants. We used the formulas

$$E = 1120\ S^{-0.85} \qquad (30)$$

for pre-1965 vehicles without exhaust control systems, and

$$E = 245\ S^{-0.48} \tag{31}$$

for post-1968 model year automobiles.

As shown in the preceding section, equations of the form of Eq. (29) can give results that agree well with independent measurements of emissions if some accounting is made of the mix of exhaust-controlled and uncontrolled vehicles. On this basis, there appears to be no reason to change the emissions model substantively. Of course, some account must be taken of the vehicle mix. For instance, if p is the fraction of the cars newer than 1965 (and 1 - p, the fraction older) then an equation of the following form would be used in the model:

$$E = 1120\ (1 - p)S^{-0.85} + 245\ p\ S^{-0.45} \quad . \tag{32}$$

When the mix is 50/50, i.e., p = 0.5, Eq. (32) reduces to

$$E = \frac{1}{2}\left(1120\ S^{-0.85} + 245\ S^{-0.48}\right) \quad . \tag{33}$$

Over a reasonable range of speeds the two terms of Eq. (33) can be well approximated by a single exponential, as was done in Eq. (15).

C. Estimation of Atmospheric Stability

The helicopter temperature profiles were used to drive a bulk stability parameter with which to check the stability category estimation procedure, as described in Section IV. The results of this analysis showed that the original model underestimated atmospheric stability when it was applied to early-morning, light wind situations. Accordingly, the table based upon modified Pasquill-Turner categories has been further revised to the form shown in Table 12. The changes consist of adding an additional time classification for early morning and late afternoon cases, and of adjusting the times for the daytime classification accordingly.

Table 12

REVISED STABILITY CATEGORIES

Surface Winds (knots)	Daytime (SR* + 4 hours to SS - 3 hours) Strong Insolation	Daytime (SR* + 4 hours to SS - 3 hours) Moderate Insolation	Daytime (SR* + 4 hours to SS - 3 hours) Slight Insolation	Early AM and Late PM (SR + 1 to SR + 3 and SS - 2 to SS - 1)	Nighttime (SS to SR) ≥ 5/10 Clouds	Nighttime (SS to SR) ≤ 4/10 Clouds
≤ 3	1	2	2	4	5	5
3-6	1	2	3	4	4	5
6-10	2	3	3	4	4	4
10-12	3	3	4	4	4	4
≥ 13	3	4	4	4	4	4

*SR = Sunrise, SS = Sunset.

D. Vertical Diffusion Rates

The Pasquill-Gifford curves that have been used to find values of the vertical dispersion parameter (σ_z) as a function of travel distance and stability have been a subject of discussion in the meteorological community for some time. These curves are based upon measurements taken in England over rolling, wooded countryside containing small towns, and hence the applicability of the data to urban areas has been questionable.

In an effort to develop more representative σ_z curves for urban areas, we have examined available data from the few urban experiments carried out by other groups. There are two comprehensive field programs that are the most help in this regard. The data that are best known are those of Pooler (1966) and McElroy and Pooler (1968) ("M & P"), who conducted tracer tests with florescent particles (FP) in St. Louis during the period 1963-1965. An additional data source that has been largely neglected because of its originally classified nature is the extensive series of tracer (FP) experiments carried out in St. Louis, Minneapolis, and Winnipeg by Leighton and Dittmar (1952, 1953a-e) ("L and D") during the period 1952-1953.

We have carried out further analyses of certain of the test results from the latter study. The line-source releases are of special interest because the FP was released from a dispenser mounted on a moving automobile, which closely simulates the typical emission conditions for automobile exhaust. The automobile was driven approximately cross-wind for a route of about 2 miles across the city, and a network of samplers downwind gave ground-level dosage values. If the release rate, release time, transport wind speed, and the cross-wind integrated dosage as a function of distance downwind are known, the variation of σ_z with travel distance can be computed from the requirement for mass balance, if the assumption of a Gaussian-shaped vertical concentration distribution is made. A similar procedure was used by McElroy and Pooler (1968).

Table 13 summarizes the test conditions for the five cases analyzed, which included three line-source tests (all that were carried out), and two point-source releases that were conducted close in time to the line-source tests. The objectives of the analysis were to determine σ_z versus distance for the five tests and to see whether this depended significantly upon the type of release.

Table 13

TEST CONDITIONS FOR ANALYZED LEIGHTON AND DITTMER (1953c) ST. LOUIS DATA

Test No.	Release Type	Date (1953)	Time (CST)	Wind ($m\ s^{-1}$)	ΔT Lapse (SFC-100m)	Mixing Depth (m)	Sky
1012 A	Point	6/15	2045	135°/2.3	1.7°C	125*	HI ⦷
1012 B	Line	6/15	2227	135°/2.0	1.2°C	125*	MID ⦷
1006 A	Line	5/29	2335	200°/1.8	1.0°C	130	CLEAR
1006 B	Point	5/30	0126	220°/1.6	0.9°C	120	CLEAR
1006 C	Line	5/30	0335	220°/1.5	0.8°C	120	CLEAR

*Weak inversion at top of mixing layer.

As indicated in Table 13, these tests were all conducted in the early summer at night, with light winds and a neutral to slightly unstable lapse rate. The wiresonde temperature data for the 15 June tests showed a weak inversion at 125 m, whereas those for the 29-30 May experiments revealed a strong inversion at about the same height.

The results of the analysis are presented in Figure 42. Test numbers 1006 A and 1006 C gave essentially identical results, so they are plotted as the same line to reduce clutter on the graph. No consistent differences between the diffusion from the point and line sources are indicated. It is interesting that the σ_z values for the 29-30 May tests show a leveling-off between about 130 and 200 m in magnitude. This is probably a reflection of the vertical trapping due to the strong inversion lid present on that occasion.

Since the L and D data are mostly for short ranges between 0.1 km and 1.5 km, while the M and P data generally cover the intermediate ranges from 0.7 km to 10 km, it is appropriate to compare the results from both

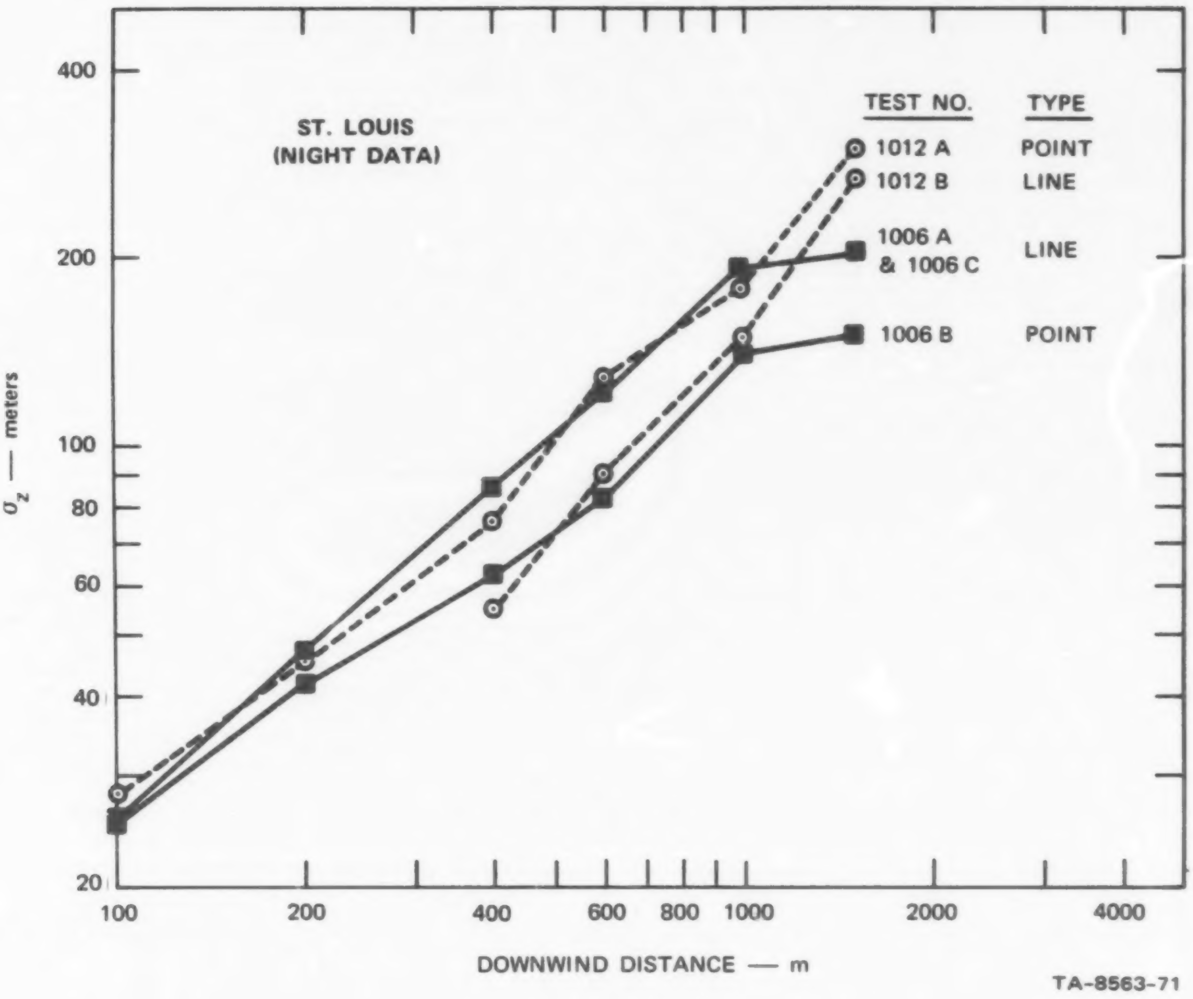

FIGURE 42 DEPENDENCE OF THE VERTICAL DIFFUSION PARAMETER σ_z UPON TRAVEL DISTANCE FOR SELECTED ST. LOUIS TRACER TESTS CONDUCTED BY LEIGHTON AND DITTMAR (1953c)

studies on one graph (Figure 43). Here the L and D data have been added to a figure taken from the report by McElroy and Pooler (1968). The stability classification for the L and D tests is best described as neutral, or in the "C" category. The results from the two experiments match reasonably well; the L and D results line up approximately as an extrapolation of the M and P "C" line.

In Figure 44, we have added the L and D results to a figure from McElroy and Pooler (1968) comparing the derived St. Louis σ_z curves, plus data from other experiments, with the original Pasquill-Gifford

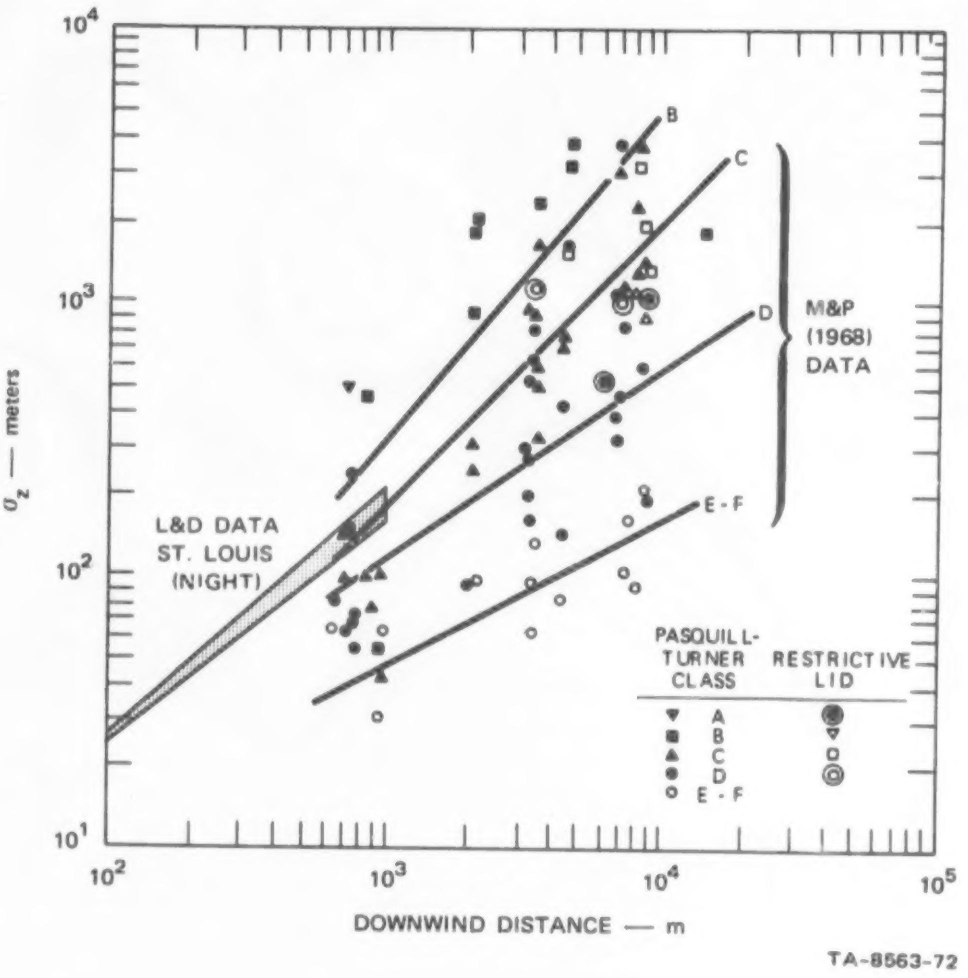

FIGURE 43 COMPARISON OF RESULTS FROM TRACER TESTS CONDUCTED IN ST. LOUIS OVER SHORT RANGES (LEIGHTON AND DITTMAR, 1953—"L&D") WITH THOSE FOR INTERMEDIATE RANGES (McELROY AND POOLER, 1968—"M&P")

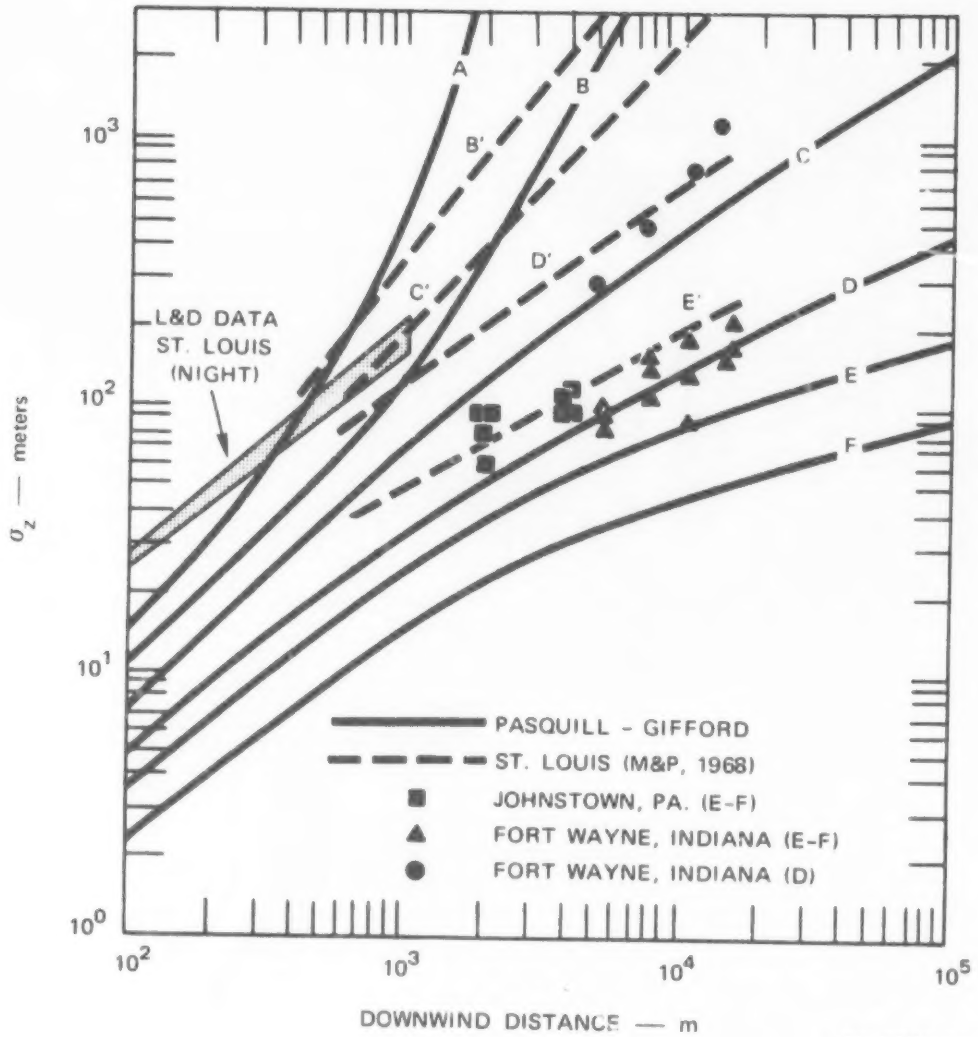

TA-8563-73

FIGURE 44 COMPARISON OF URBAN VERTICAL DISPERSION DATA WITH THE PASQUILL-GIFFORD CURVES (ADAPTED FROM McELROY AND POOLER, 1968)

curves (Pasquill, 1961; Gifford, 1961). It is apparent that the latter give underestimates of vertical diffusion in urban areas. We have revised the model to incorporate better vertical diffusion estimates based on the M and P data and the limited L and D results. As shown in Figure 45, we have approximated and extrapolated the σ_z curves of Figure 43 by expressions of the form

$$\sigma_z = a\,x^b \quad , \tag{34}$$

where x is downwind distance. The values of the constants a and b for the various stability categories are given in Table 14. These new values replace those previously used with the model, which were taken from the Pasquill-Gifford curves. Figure 45 shows a unique feature of the new curves; they all intersect at $\sigma_z = 10$ m for $x = 50$ m. This represents a reasonable value for the initial mechanical mixing due to roughness elements near the source. Accordingly, for the model we have assumed that $\sigma_z = 10$ m for $x \leq 50$ m.

Table 14

VALUES OF CONSTANTS IN EQ. (34)
AS A FUNCTION OF ATMOSPHERIC STABILITY CATEGORY

Stability Category	Stability Type	a	b
1 (A)	Very unstable	0.07*	1.28*
2 (B)	Unstable	0.12	1.14
3 (C)	Slightly unstable	0.23	0.97
4 (D)	Neutral	0.50	0.77
5 (E)	Slightly stable	1.35	0.51

*Estimated from extrapolation of a's and b's for other categories (no data available).

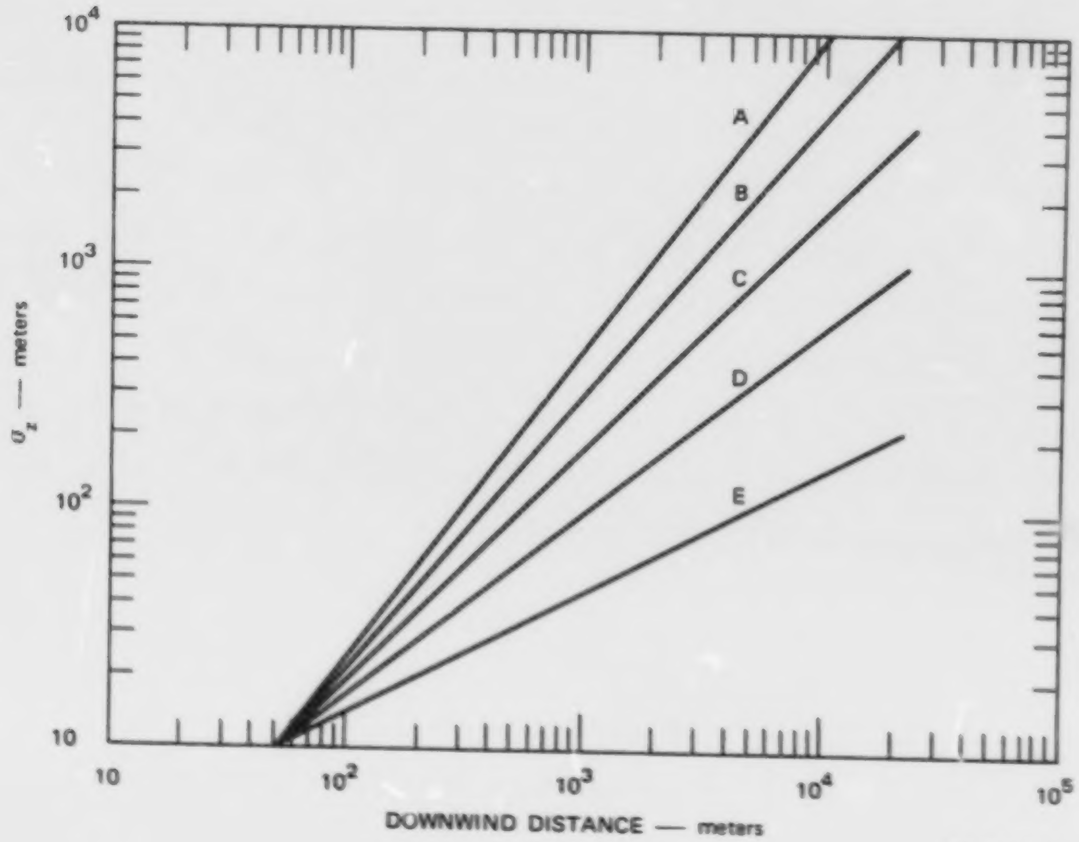

TA-8563-98

FIGURE 45 VERTICAL DIFFUSION AS A FUNCTION OF TRAVEL DISTANCE AND STABILITY CATEGORY, AS REVISED FOR URBAN CONDITIONS

E. Mixing Depth

Table 9 in the preceding section shows that the methods used in the model to define the mixing depth give values that are comparable to those determined from the helicopter profiles of CO and temperature. There do not seem to be any systematic differences that would warrant changing the mixing depth submodel at this time.

F. Local (Street) Effects

This new submodel, used to compensate for effects of the street canyon on CO concentration at streetside receptors, is thoroughly described in Section III by Equations (7), (15), (17), and (19), plus Table 3. In effect, a concentration increment (ΔC) is computed from this procedure and added to the urban concentration (C_b) calculated from the basic urban diffusion model. Since the traffic on the street passing directly by the receptor is included in the calculation of ΔC, this same traffic is neglected in calculating C_b. The concentration increment, ΔC, depends upon rooftop wind direction and wind speed, local traffic volume and average vehicle speed, width of the street, height of the receptor above the street, and horizontal distance of the receptor from the center of the nearest traffic lane. The results of verification tests using this new procedure and the other model revisions are described in the next section.

A final word is in order regarding the appropriate wind speed to use as an input to the street effects submodel. Rooftop winds above the street will not generally be available, and airport wind speeds will have to be used. In this case an appropriate relation to apply, derived from the San Jose data, is

$$U = 0.47\,U_a - 0.60\ \mathrm{m\ s^{-1}} \quad , \qquad (35)$$

where

U = rooftop wind speed and

U_a = airport wind speed.

This does not differ substantially from the relationship that Schnelle et al. (1969) found for Nashville, Tennessee.

VI EVALUATION OF THE PERFORMANCE OF THE REVISED MODEL

A. Introduction

From the beginning, the diffusion model has been developed as a composite of separate modules (Johnson et al., 1969; Ludwig et al., 1970). The reasons for this are simple: it allows changes in various parts of the model without a complete disruption of the entire structure. It also allows us to check the performance of each of the modules and thereby diagnose the model's weaknesses. We have exploited this feature in designing different parts of the San Jose field project to test different subunits of the model.

In this section, the performance of the various modules will be reviewed. We will also present the results of our attempts to check the overall performance of the composite model. It is this overall performance that is of greatest interest to the potential user. Finally, the results of the tests are discussed in terms of those conditions under which the model performs well and those under which it performs poorly. This aspect of the validation study was undertaken partly to help the designers of the model decide where to concentrate the future efforts at improvement and partly to help users avoid conditions for which the model may give unreliable results.

B. Tests of the Subcomponents

1. Emissions Submodel

a. General

The emissions submodel requires traffic data as inputs. Hourly traffic volumes and average vehicular speeds are needed for the different highway segments in the area. In practice the model uses measurements of total 24-hour volumes and distributes the total traffic among the hours of the day according to a temporal function based on a limited number of observations of diurnal traffic patterns. To obtain the speeds to be used in the model, each road segment is assigned to one of several classifications (e.g., suburban freeway, local or feeder street). Each street classification has two "typical" speeds, which are used for emission calculations. The slower speeds are used for the peak traffic hour calculations. As with the diurnal traffic cycle, these typical speeds are based on very limited data.

b. Traffic Data

It is clear from the preceding discussion that there are at least three potential sources of error in calculating the emissions: the nature of the equation relating emissions to traffic parameters (discussed in the next section), traffic volumes, and average speed. Traffic volumes can be misestimated because we have inaccurate total 24-hour counts or because we have an inaccurate diurnal assignment function.

The detailed traffic data from San Jose indicate that the traffic on any given street link, for a given hour of the day, does not vary much from one weekday to another. The standard deviations of day-to-day values of half-hour traffic volumes in downtown San Jose at a given time of day are generally in the range of 5 to 15 percent of the average volume. This implies that the standard deviation of the 24-hour traffic volume totals is probably less than 15 percent. Since emissions are directly proportional to traffic volumes, the emission errors would be similar in relative magnitude to the traffic volume errors that cause them.

It appears that uncertainties in the diurnal traffic patterns may be more serious than uncertainties in 24-hour total traffic volumes. Some evidence of this was presented in an earlier report (Ludwig et al., 1970). The solid line in Figure 46, taken from that report, shows the daily emission cycle used for the model. The dashed line shows a daily emission cycle derived from a statistical analysis of five years of St. Louis CO observations. This derived emission cycle

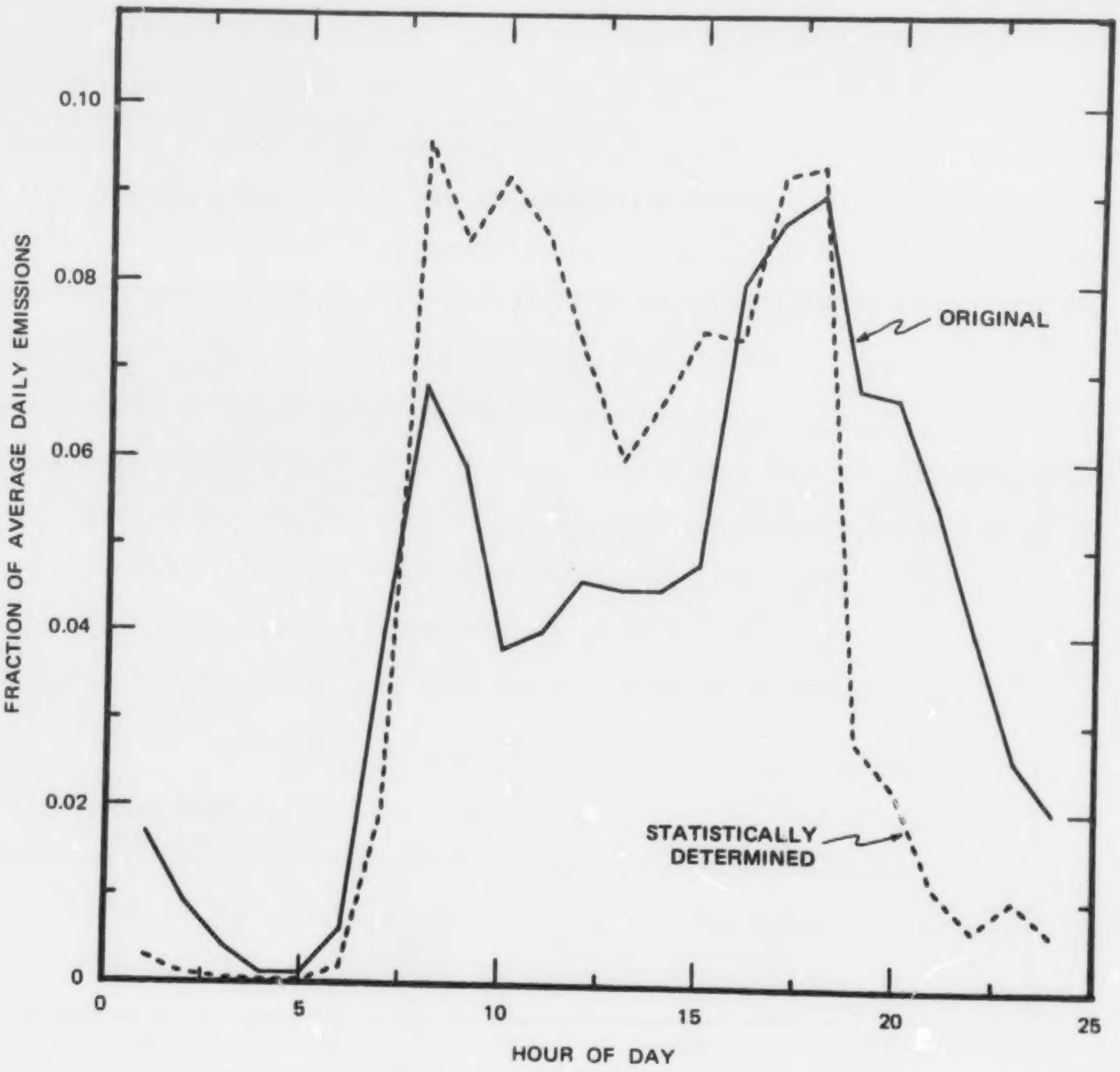

TA-7874-70

FIGURE 46 DIURNAL EMISSION PATTERNS FOR ST. LOUIS

gives the best agreement between calculated and observed CO concentration values. The emission cycle is very closely related to the traffic cycle, differing only in that it includes the effects of reduced rush-hour speeds. It is evident from Figure 46 that there are considerable differences between the statistically determined values and those originally hypothesized for the model. The dashed curve is less peaked at the morning and evening rush hours than hypothesized. Figure 47 shows the total traffic in the downtown San Jose area on two successive days, for the hours between 0630 and 1730. These curves are different from either of those in Figure 46 but are closer to the statistically determined case in that they show little decrease in traffic at midday. The fact that the two curves in Figure 47 are nearly superimposed

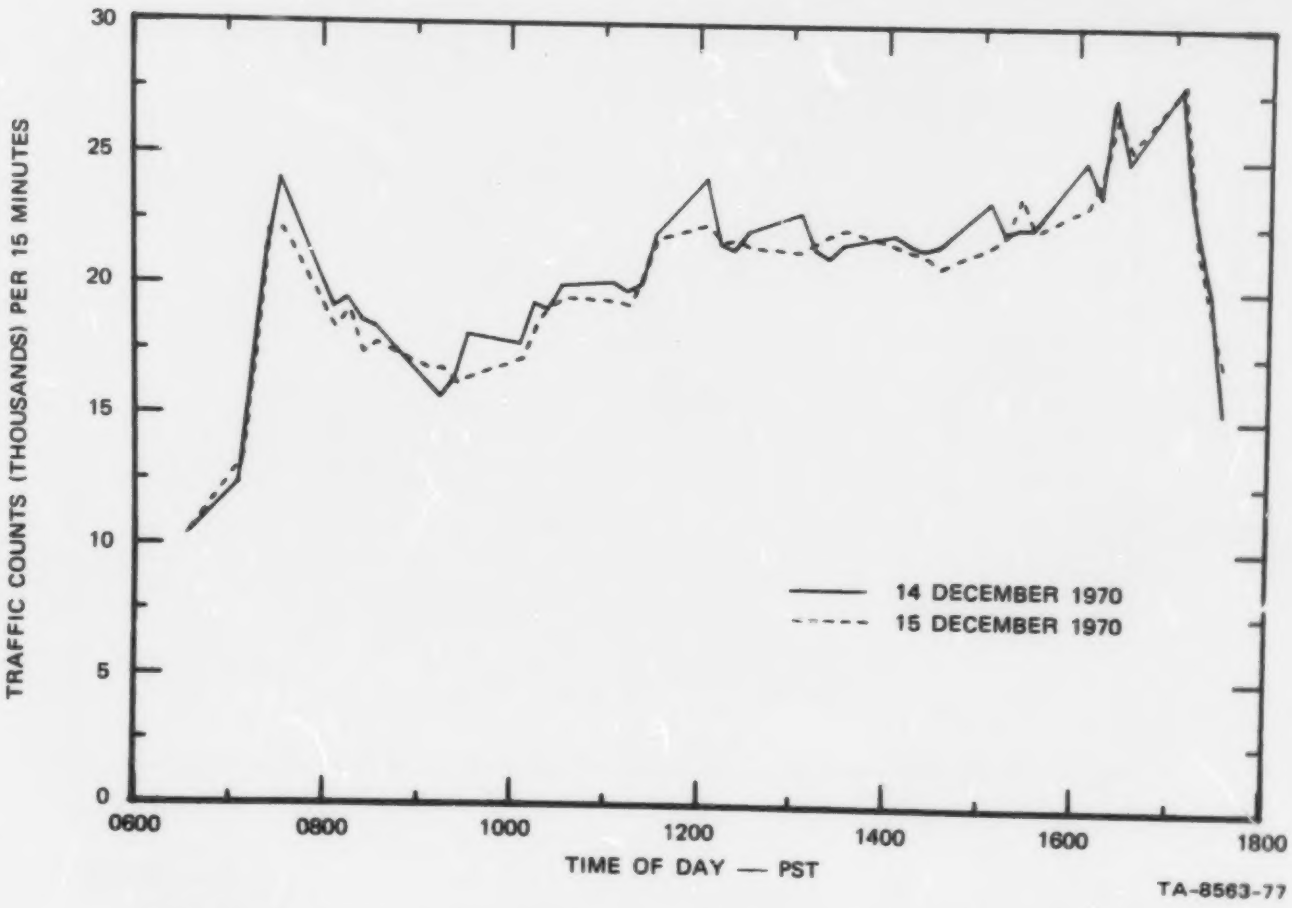

FIGURE 47 TOTAL NUMBER OF TRAFFIC COUNTS FOR ALL DETECTORS IN DOWNTOWN SAN JOSE

suggests that there is very little day-to-day variability and that it would not take very many observations in a given area of a city to obtain reliable diurnal traffic cycles for that area.

Not enough data were collected on this program to determine the accuracy of our estimates of speed. Our three-day sample of 95 total circuits around the downtown area indicates an average speed of about 14 mi h^{-1}, but there is considerable variation in speed among route segments and from circuit to circuit, particularly at certain times, such as 1700. The variability of speed is substantially greater in the morning and evening than at midday.

Spot speeds can be estimated from the time required for a vehicle to pass over a magnetic sensor in the traffic network. Limited data of this type were collected on First Street during morning and evening rush hours on 6 May 1971. These data indicate that the afternoon traffic at this location tended to travel more slowly, about 70 percent of the morning speeds, for all comparable traffic volumes. Data from all sources suggest that there may be considerable variability in average speeds, even among streets that appear, in other respects, to be similar. The speed variability is evident, also, on the same street for equal volumes, when measured at different times of the day.

The model assumes that traffic on downtown arterials travels at a rate of 24 mi h^{-1} during peak traffic and 30 mi h^{-1} at other times. This is substantially different from the 14 mi h^{-1} that we measured in the downtown area. Speed uncertainties of this magnitude could cause significant changes in calculated emissions; for instance, according to Eq. (26), the emissions per vehicle-mile at 14 mi h^{-1} are 1.7 times those at 30 mi h^{-1}. Thus, better estimates of vehicle speed on the various road types and at the different times of day would substantially improve the performance of the emissions submodel.

c. The CO Emission Equation

The special traffic data in San Jose allowed us to check the validity of Eq. (26) in a situation where the input parameters, traffic volume, and vehicle speed were accurately known. The results of the comparison of emission rates determined from the equation with those determined independently have been presented in Section IV. Since the independent measurements have substantial uncertainty, they cannot serve as a precise check on the emissions submodel, but they do lead us to believe that the equation is probably at least as accurate as the traffic data that are usually available. We hope that future work can improve our assessment of the performance of the emissions submodel.

2. Mixing Depth Submodel

The mixing depth submodel proved to be reasonably accurate, as shown by the comparison presented in Table 9. The calculated mixing depths, with one exception, were all within 150 m of observed values based on helicopter profiles of temperature and carbon monoxide. The model makes use of the early morning vertical temperature gradient in the lowest few hundred meters to determine the early morning mixing depth. It is important that these soundings come from an open area that is geographically similar to that for which we wish to calculate the mixing depth. This was the case for the soundings used to calculate the model values shown in Table 9, and as a result the morning values were quite accurate. However, when the values were recalculated using radiosonde data from Oakland, 50 km distant, the calculated depths were found to be considerably greater, which might be expected.

Afternoon mixing depths, as determined by the submodel, are also based on the morning sounding, but in this case, the higher levels of the sounding are generally more important than the lower layers. The

Oakland sounding yields overestimates of afternoon mixing depths as well as of morning mixing depths, but the afternoon values are more nearly correct, probably because of the smaller effect of the Bay at higher levels.

The above discussion indicates that some care should be exercised in selecting a source of upper air data for use with the model. The closest radiosonde station may not give the best results if it is characterized by substantially different geographical surroundings than the city of interest. If, however, a representative sounding is available, the mixing depth submodel appears to perform well.

3. Stability Class Submodel

The performance of the submodel that was originally used to determine stability was discussed in Section IV. As noted there, and in Section V, that submodel gives good results except in the hours just after sunrise and just before sunset. The changes described in Section V make the submodel more consistent with the observed values of the bulk stability parameter. However, we have only a limited number of measurements of the bulk stability parameter, so a full evaluation of the revised stability index submodel will have to await the availability of more data. Such data should be available from the field program that we have recommended be undertaken in St. Louis.

Although we have not collected data suitable for checking the variations of σ_z with distance from the source, other studies (Leighton and Dittmar, 1952, 1953; McElroy and Pooler, 1968) indicate that the changes described in Section V will give results more appropriate to urban conditions.

4. Street Effects Submodel

The street effects submodel presumes that the emissions from traffic on the local street are added to the concentrations from emissions outside the immediate area that enter the street canyon from above. We assume that the basic diffusion model calculates the concentrations of CO entering the street canyon and adds to those the concentration component from the street effects submodel. To evaluate the performance of the street effects submodel separately requires some measure of CO concentrations free of the effects of emissions in the immediate area. Unfortunately, such measurements are not available, since even the top sampling levels at our streetside stations are exposed to considerable CO from the adjacent street. Thus, it has been necessary to evaluate the street effects submodel indirectly, and by inference from the results of the composite model evaluation.

The street effects submodel is designed for application in a street canyon, i.e., away from an intersection, near the center of the block. We would therefore expect it to perform best at sites 7 and 8, not quite so well at site 4, and poorly at the other intersection sites. The data collected during the experiments confirm this. It is apparent that the modeling of intersection effects will require further study, perhaps including wind tunnel work. Nevertheless, the data collected in San Jose can be valuable in confirming the applicability of any future theoretical or laboratory work.

C. Evaluation of the Composite Model

The composite model has been evaluated through comparison of observed and predicted hourly concentrations (Figures 48 to 62) of CO for eight days at two levels at each of five stations (Nos. 4, 5, 6, 7, and 8). The predicted concentrations may be resolved into the

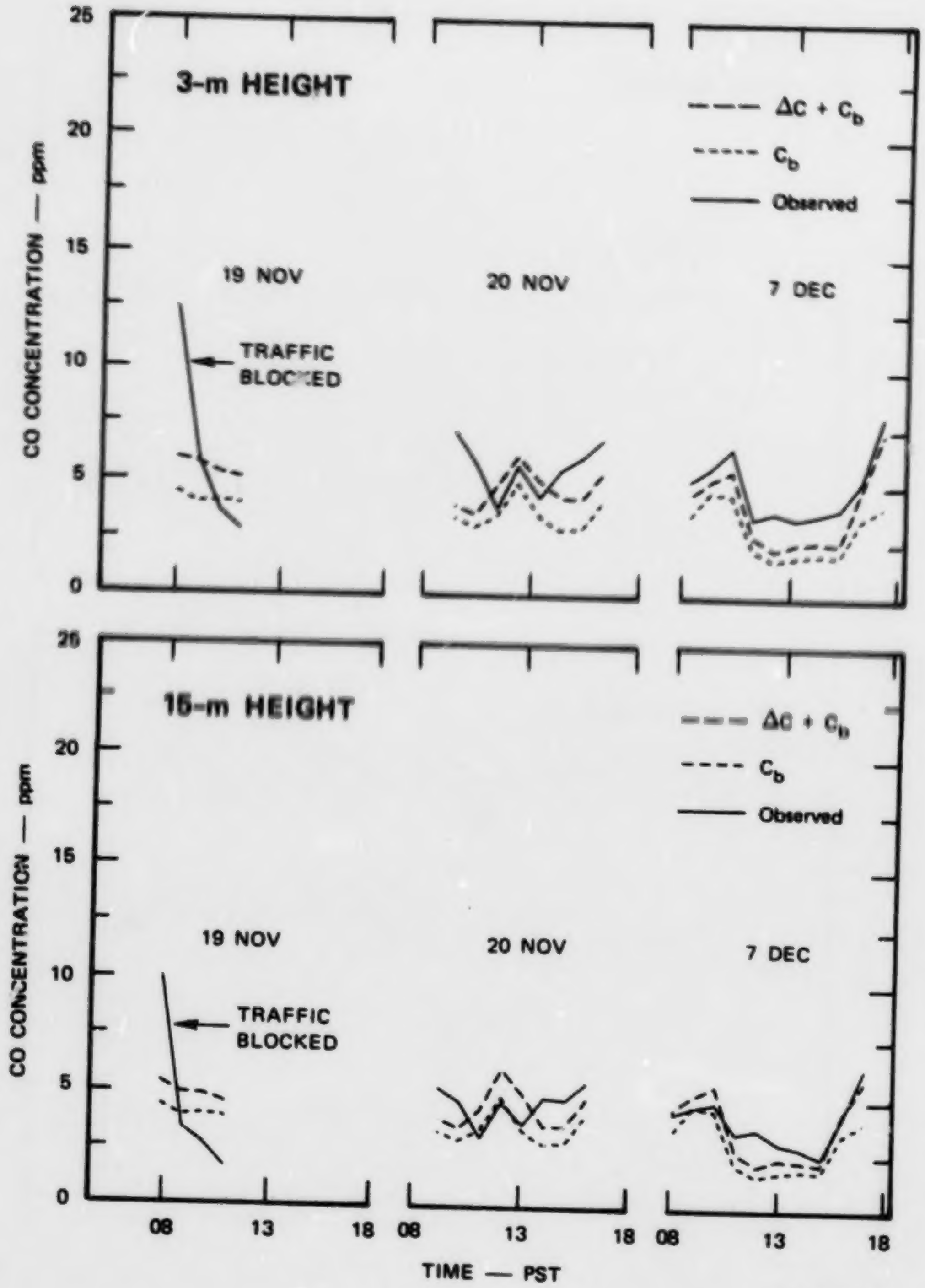

TA-8563-80

FIGURE 48 CALCULATED AND OBSERVED CO CONCENTRATIONS FOR STATION 4 AT TWO HEIGHTS FOR 19 AND 20 NOVEMBER AND 7 DECEMBER 1970

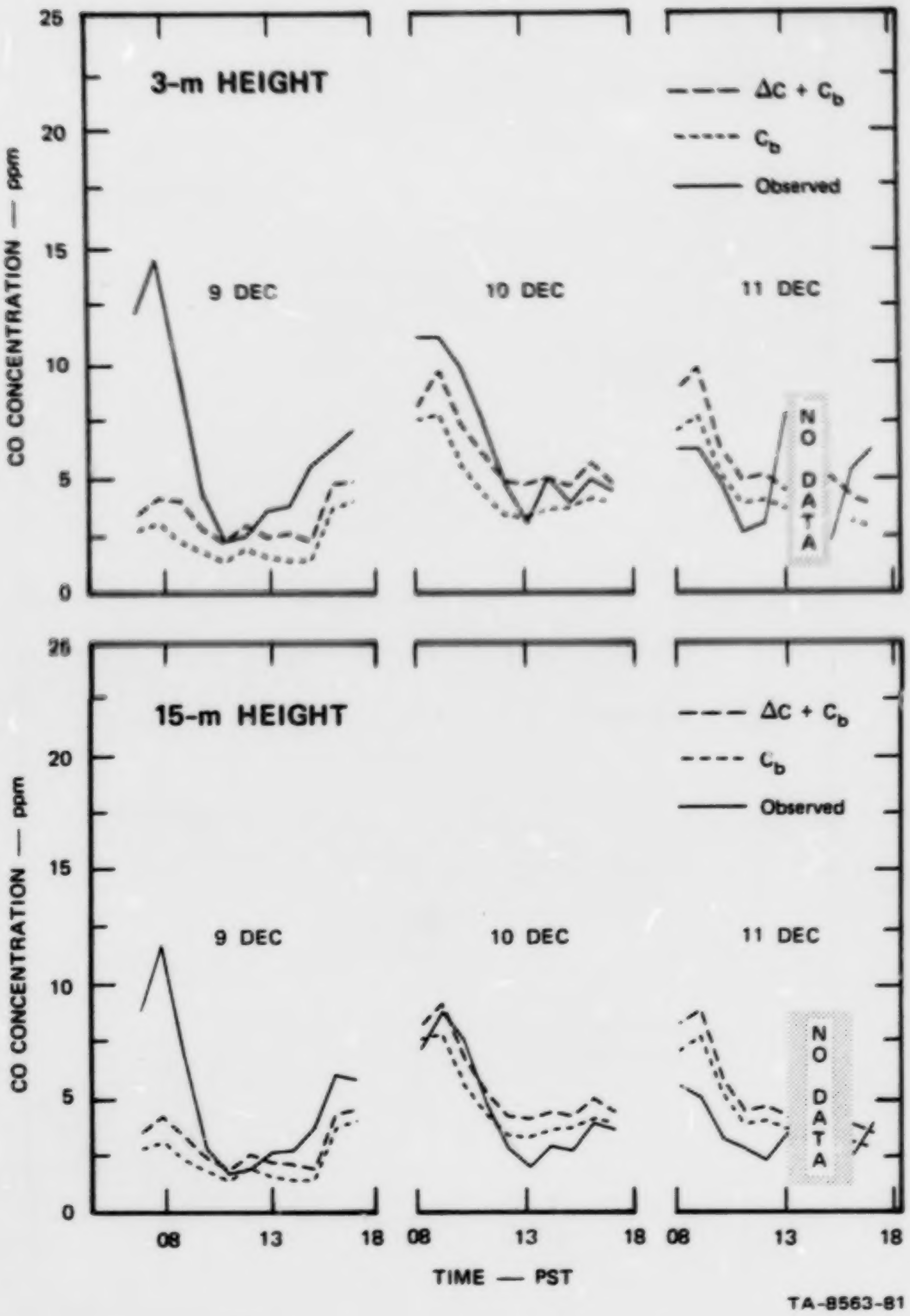

FIGURE 49 CALCULATED AND OBSERVED CO CONCENTRATIONS FOR STATION 4 AT TWO HEIGHTS FOR 9, 10, AND 11 DECEMBER 1970

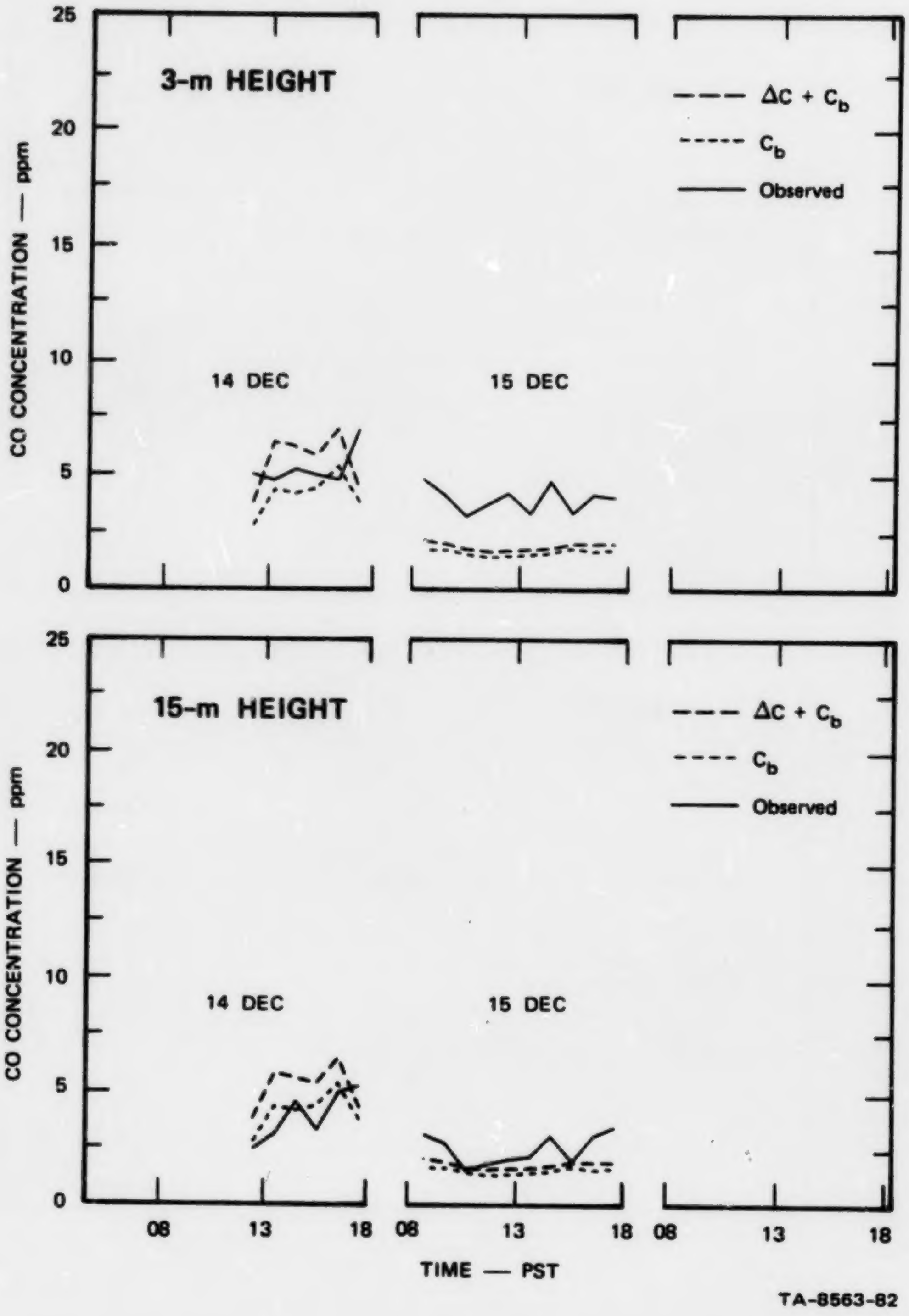

FIGURE 50 CALCULATED AND OBSERVED CO CONCENTRATIONS FOR STATION 4 AT TWO HEIGHTS FOR 14 AND 15 DECEMBER 1970

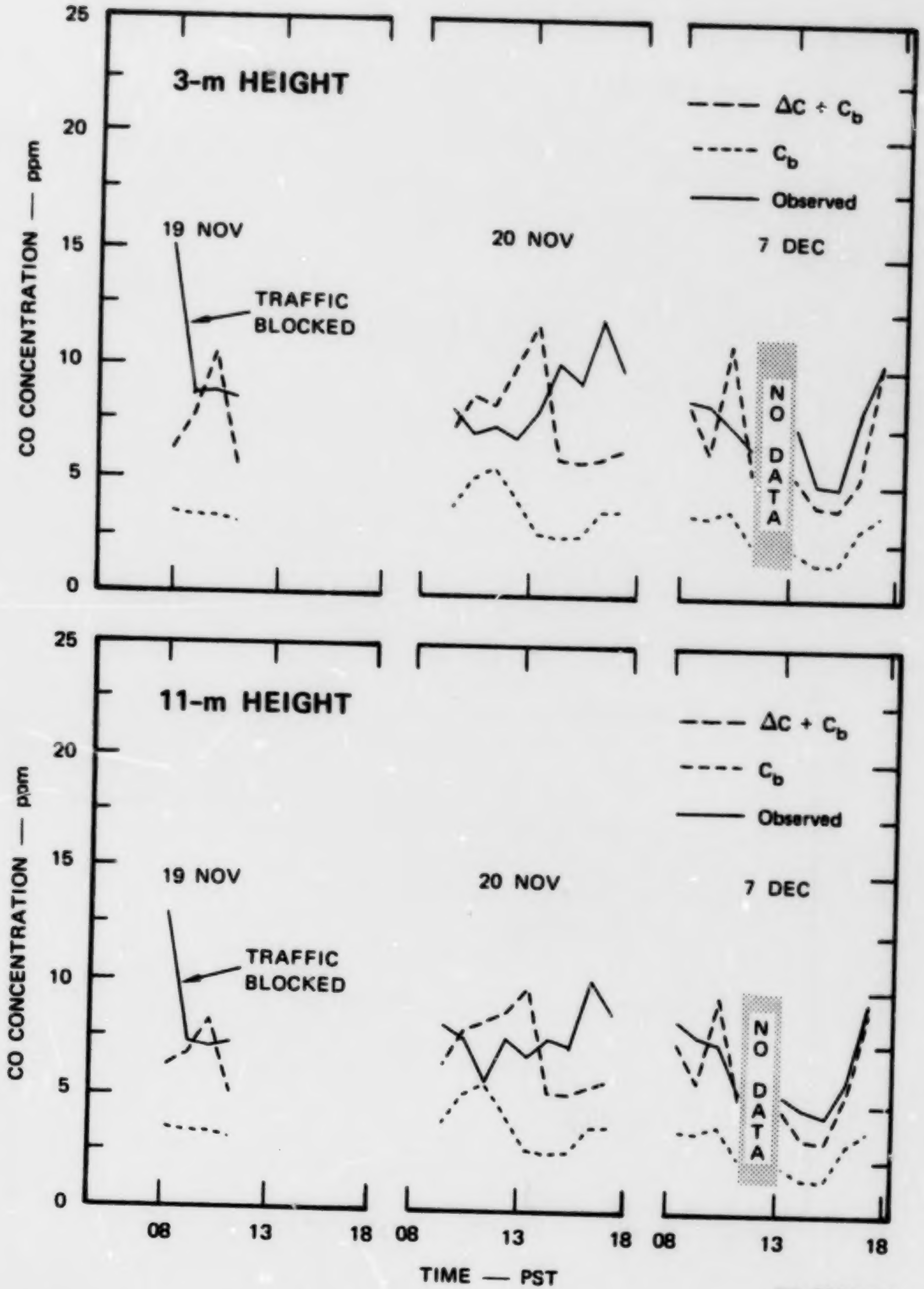

FIGURE 51 CALCULATED AND OBSERVED CO CONCENTRATIONS FOR STATION 5 AT TWO HEIGHTS FOR 19 AND 20 NOVEMBER AND 7 DECEMBER 1970

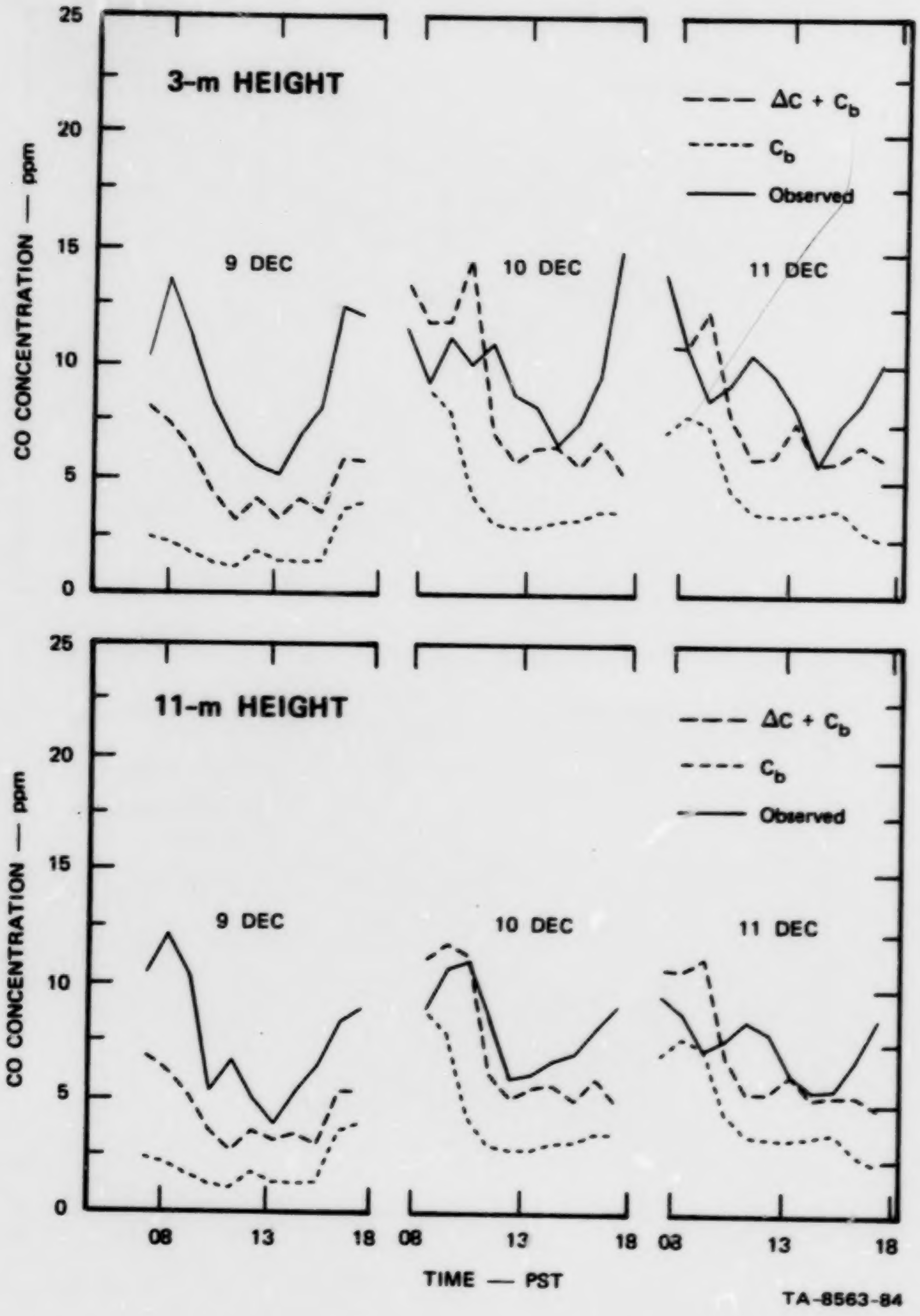

FIGURE 52 CALCULATED AND OBSERVED CO CONCENTRATIONS FOR STATION 5 AT TWO HEIGHTS FOR 9, 10, AND 11 DECEMBER 1970

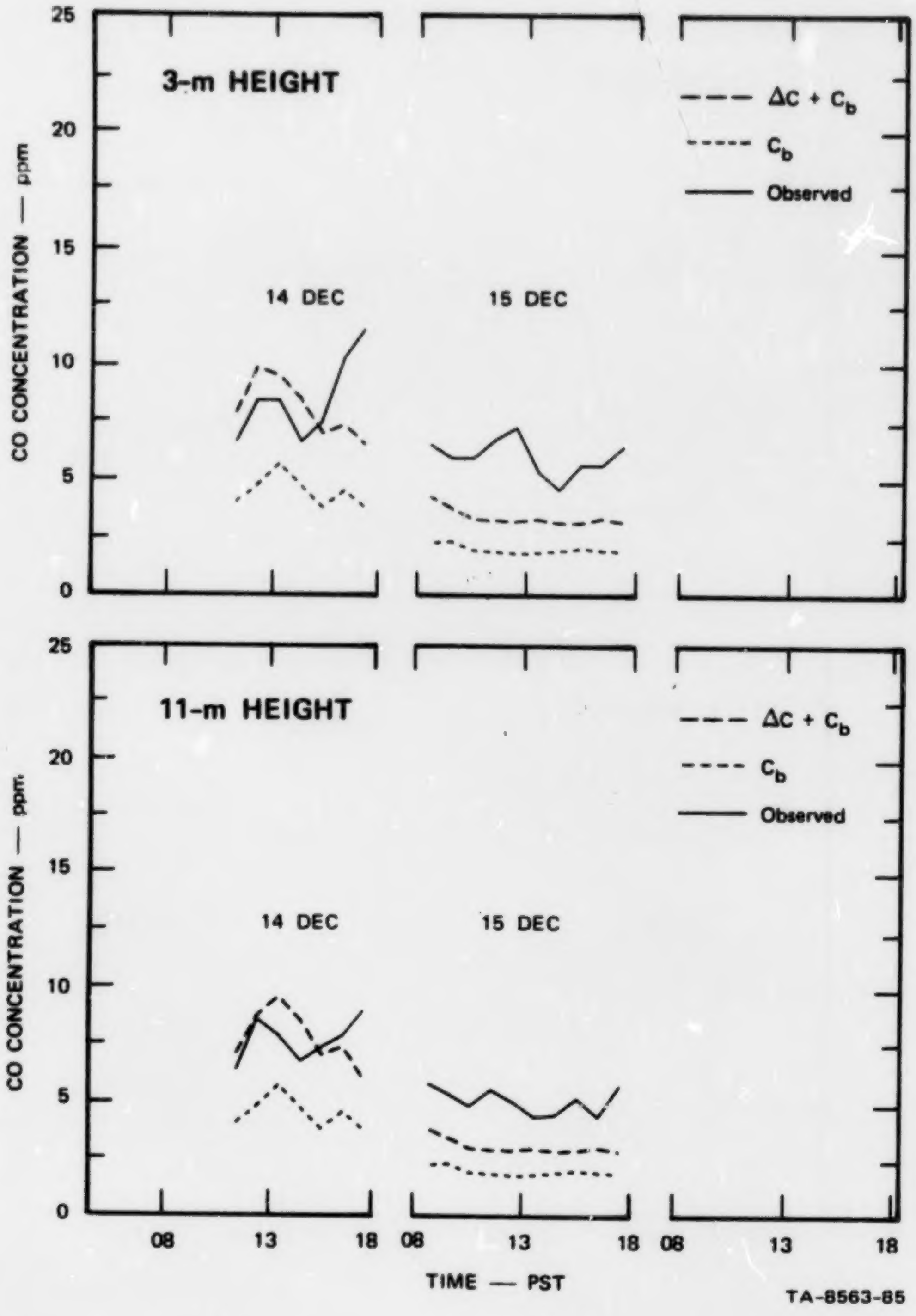

FIGURE 53 CALCULATED AND OBSERVED CO CONCENTRATIONS FOR STATION 5 AT TWO HEIGHTS FOR 14 AND 15 DECEMBER 1970

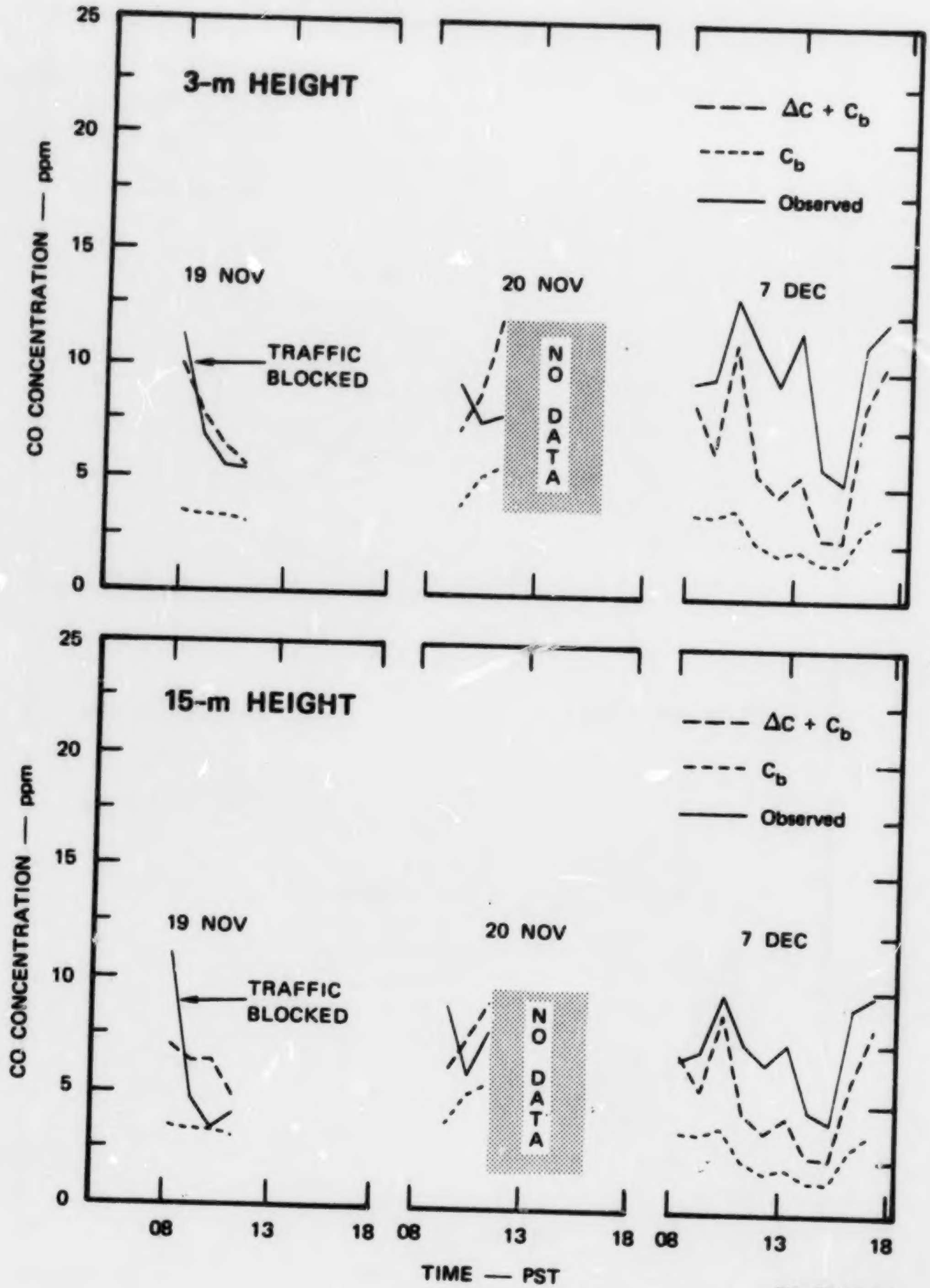

TA-8563-86

FIGURE 54 CALCULATED AND OBSERVED CO CONCENTRATIONS FOR STATION 6 AT TWO HEIGHTS FOR 19 AND 20 NOVEMBER AND 7 DECEMBER 1970

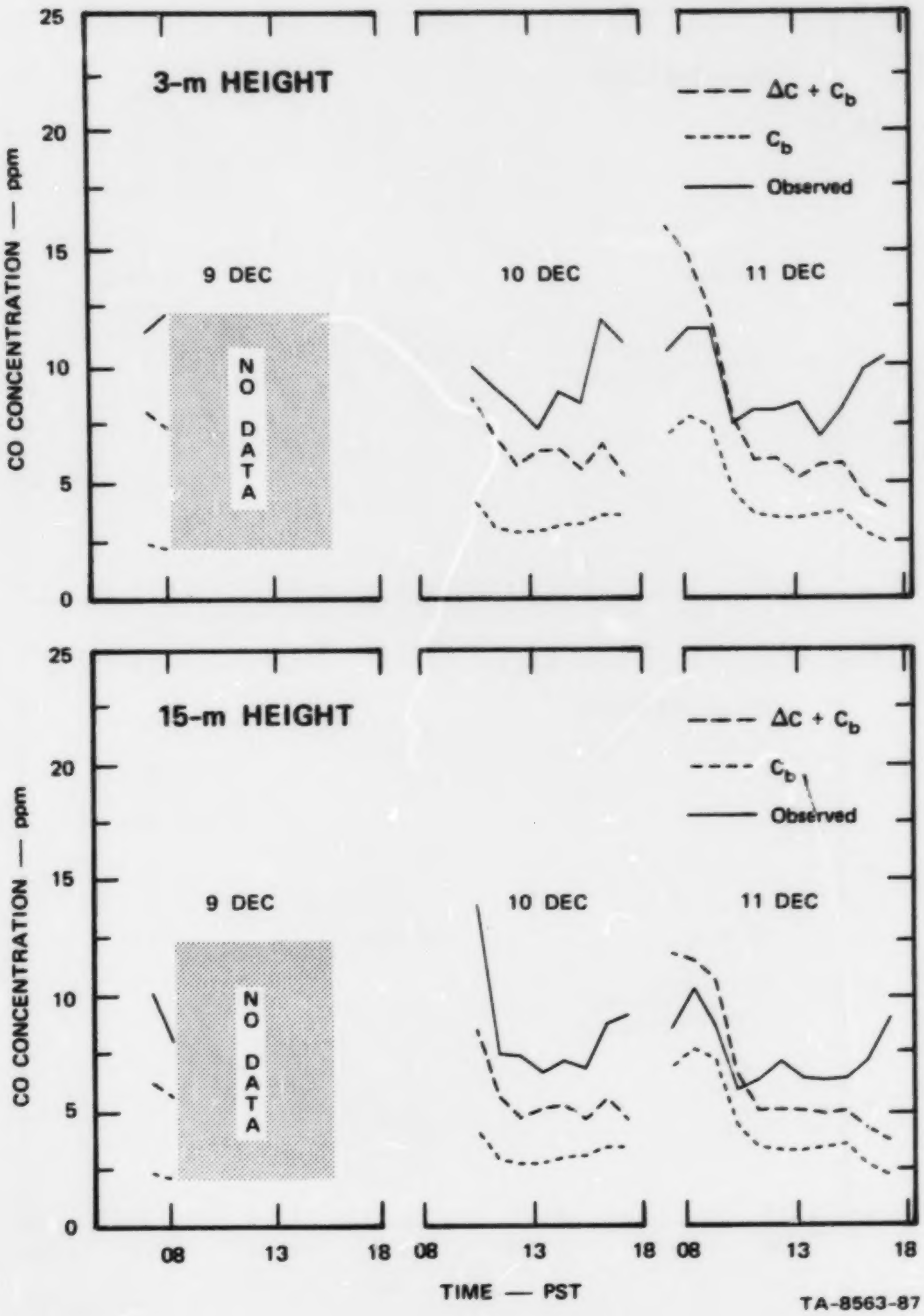

FIGURE 55 CALCULATED AND OBSERVED CO CONCENTRATIONS FOR STATION 6 AT TWO HEIGHTS FOR 9, 10, AND 11 DECEMBER 1970

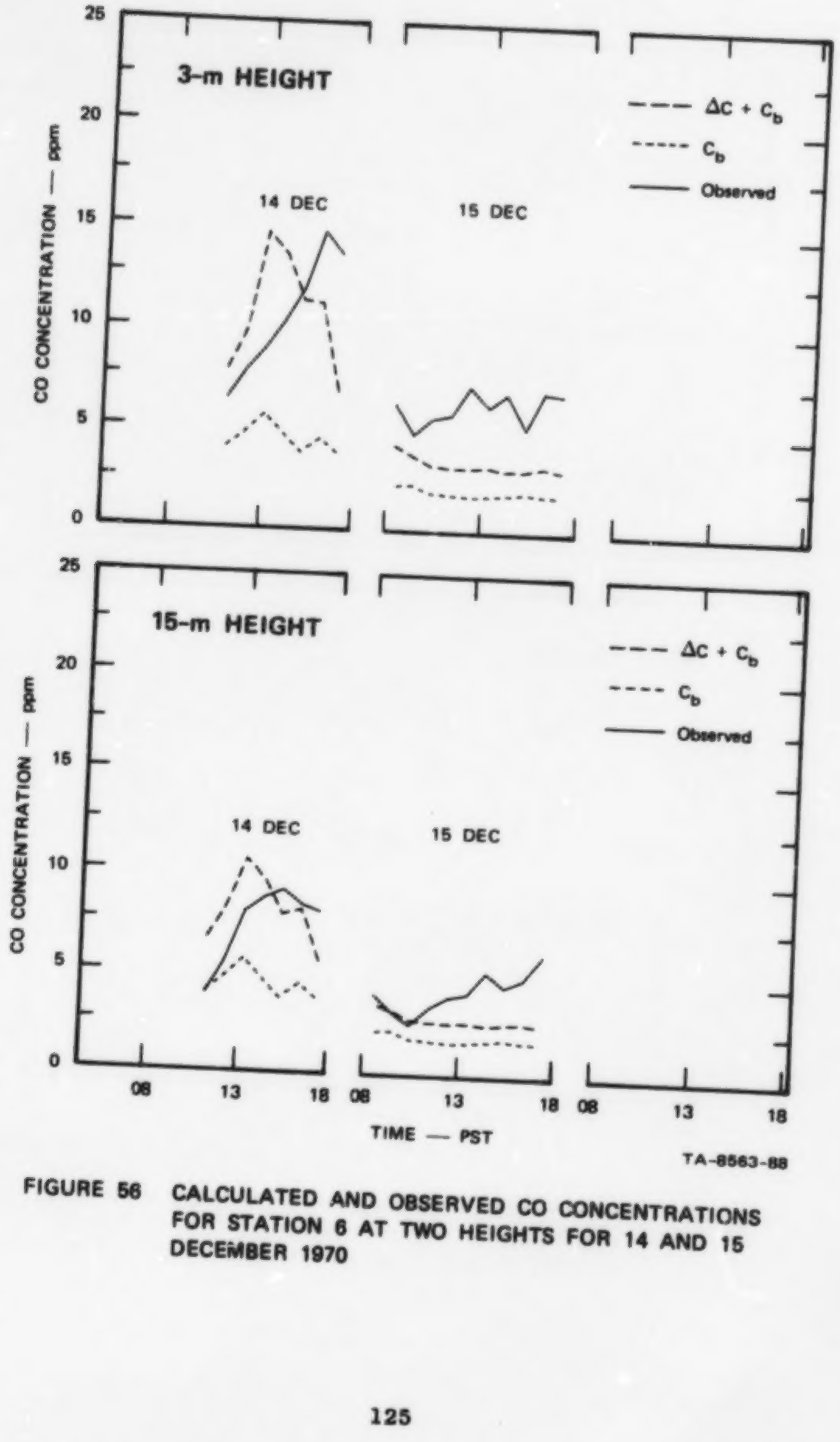

FIGURE 56 CALCULATED AND OBSERVED CO CONCENTRATIONS FOR STATION 6 AT TWO HEIGHTS FOR 14 AND 15 DECEMBER 1970

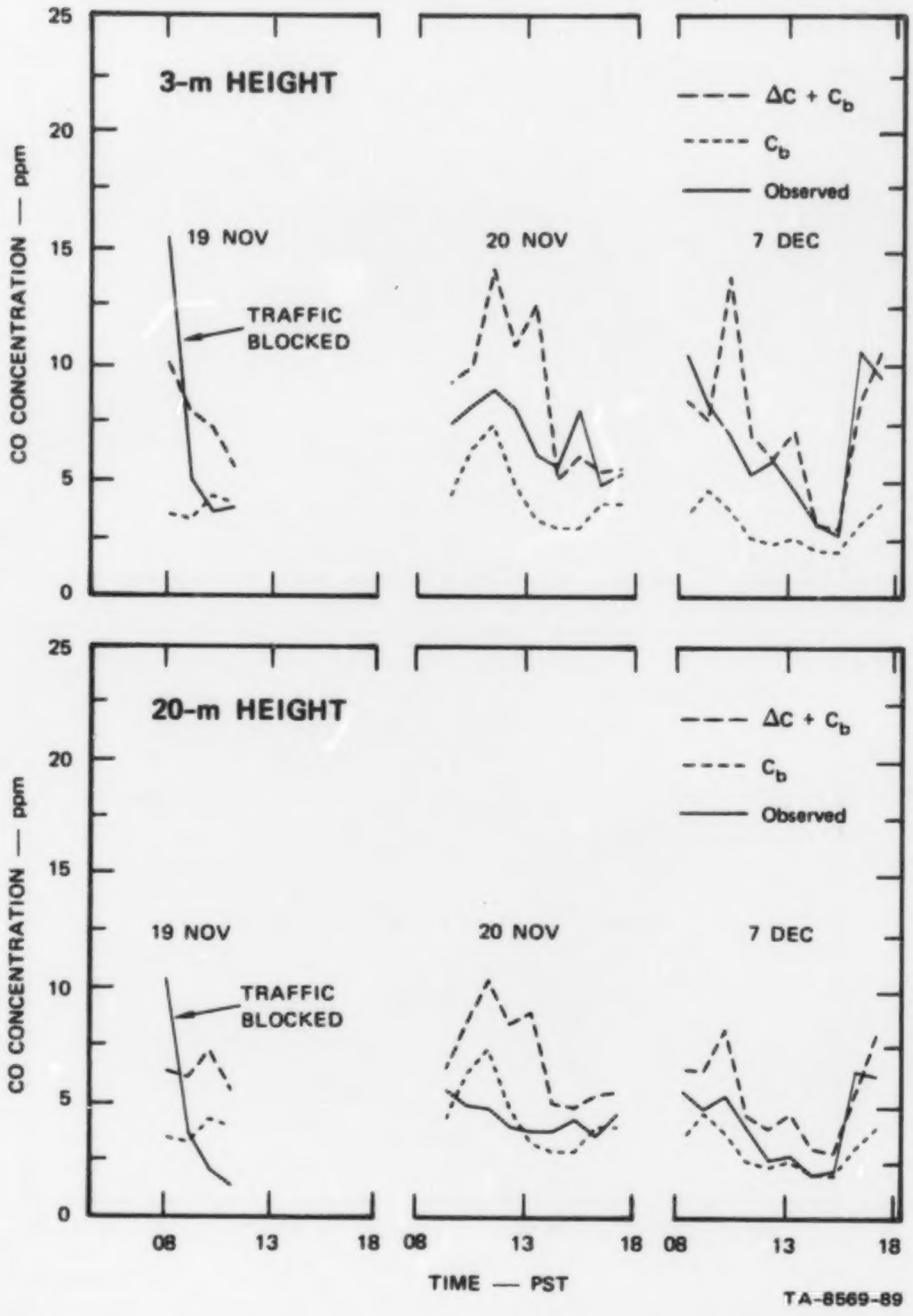

FIGURE 57 CALCULATED AND OBSERVED CO CONCENTRATIONS FOR STATION 7 AT TWO HEIGHTS FOR 19 AND 20 NOVEMBER AND 7 DECEMBER 1970

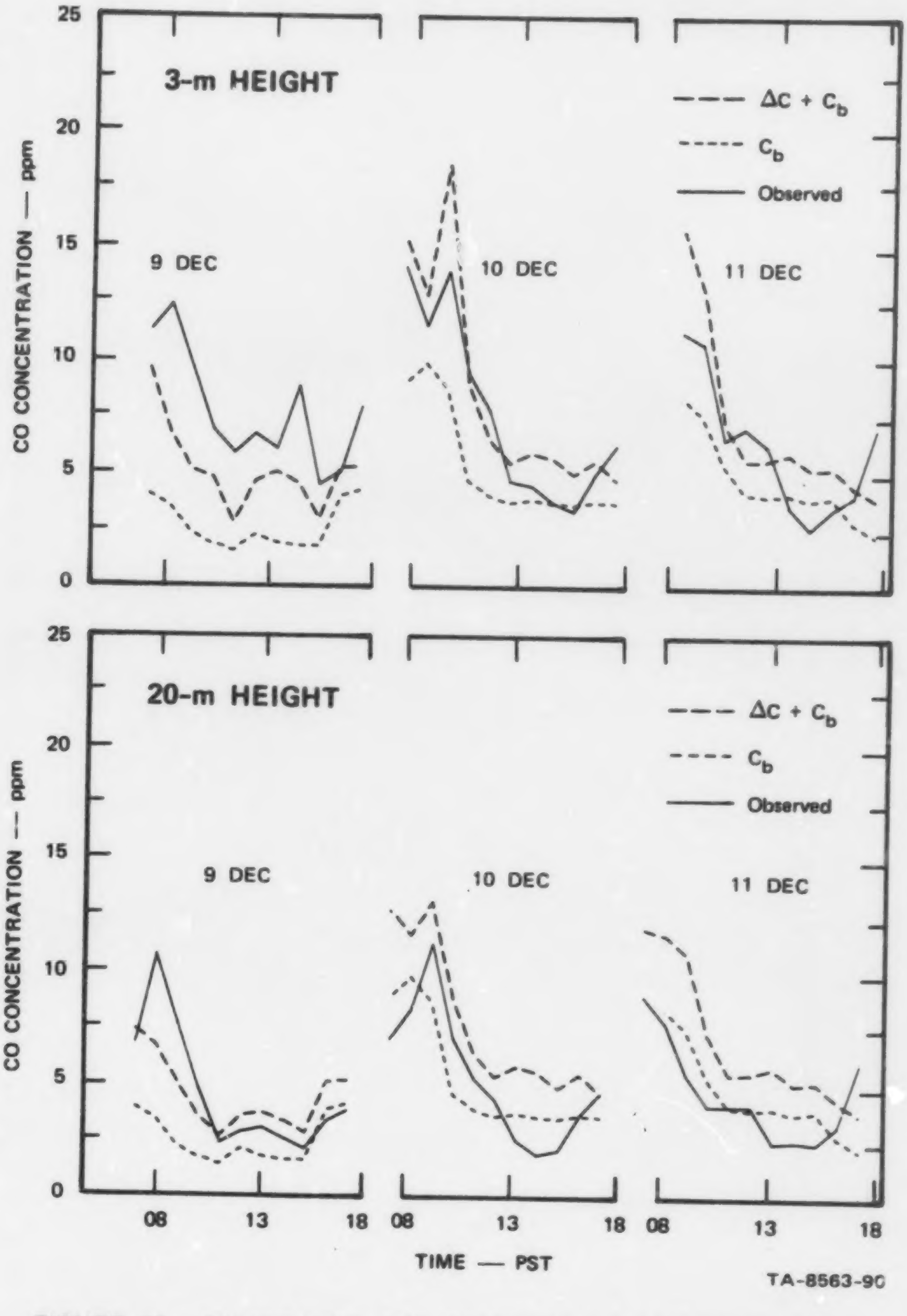

FIGURE 58 CALCULATED AND OBSERVED CO CONCENTRATIONS FOR STATION 7 AT TWO HEIGHTS FOR 9, 10, AND 11 DECEMBER 1970

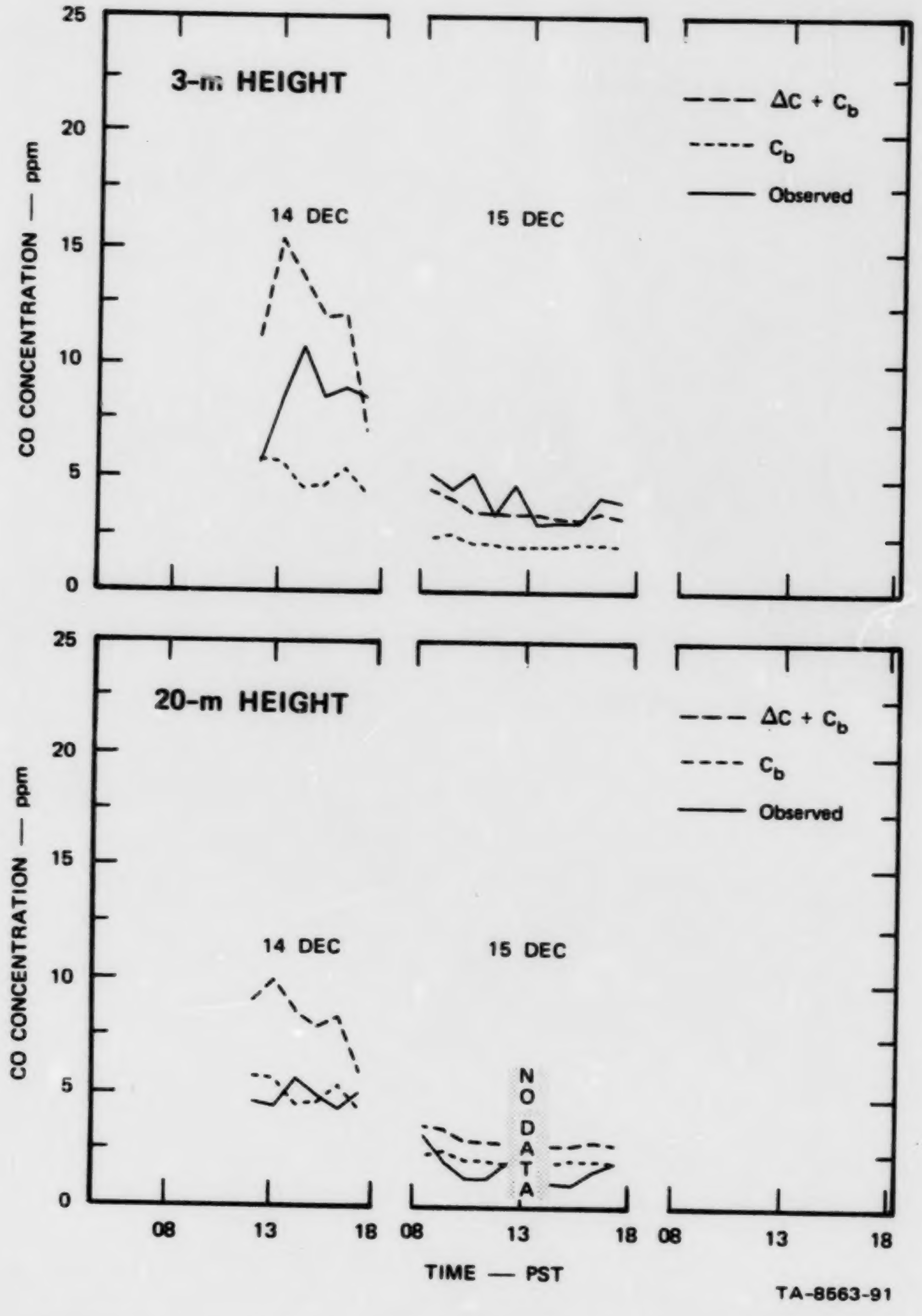

FIGURE 59 CALCULATED AND OBSERVED CO CONCENTRATIONS FOR STATION 7 AT TWO HEIGHTS FOR 14 AND 15 DECEMBER 1970

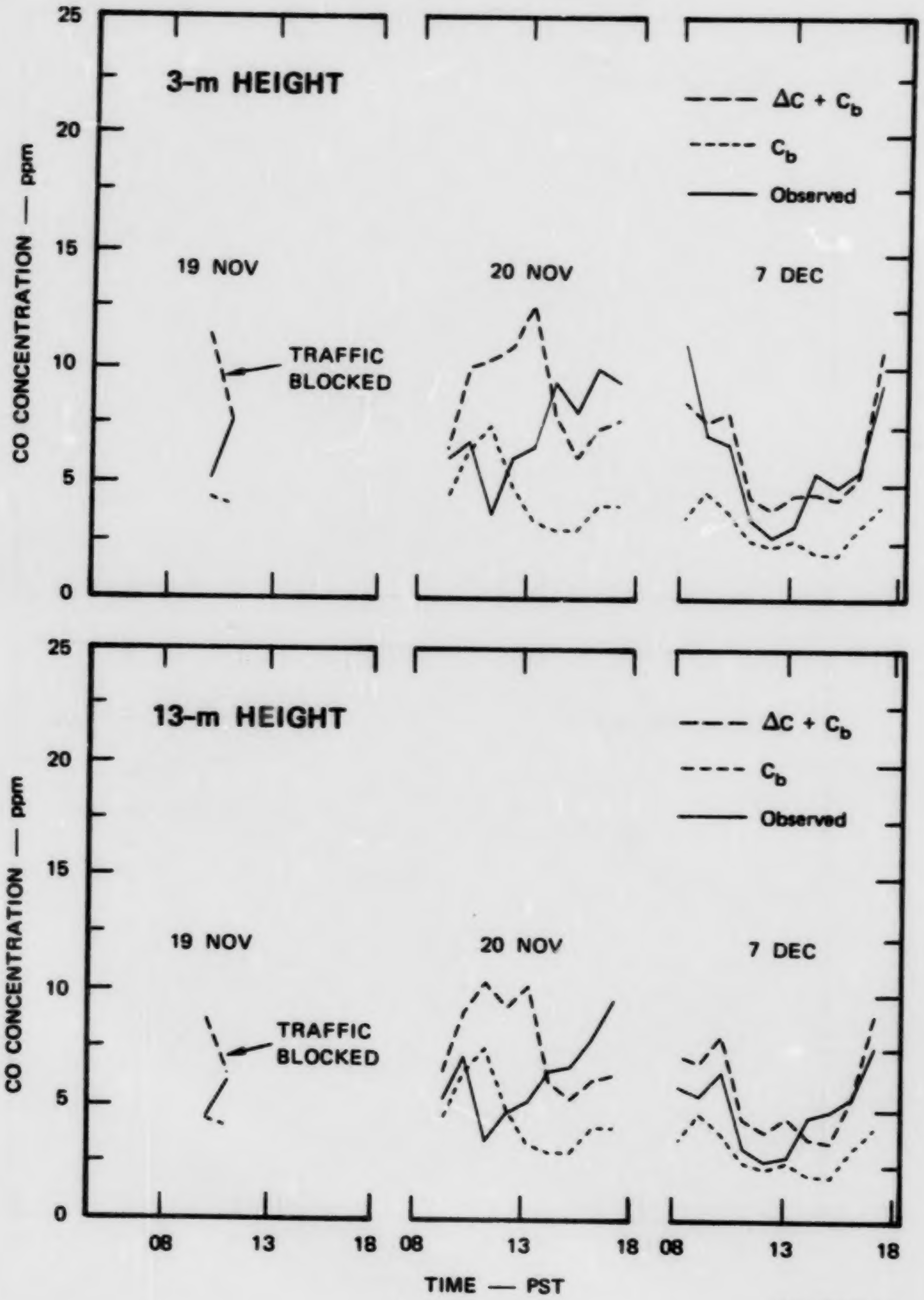

TA-8563-92

FIGURE 60 CALCULATED AND OBSERVED CO CONCENTRATIONS FOR STATION 8 AT TWO HEIGHTS FOR 19 AND 20 NOVEMBER AND 7 DECEMBER 1970

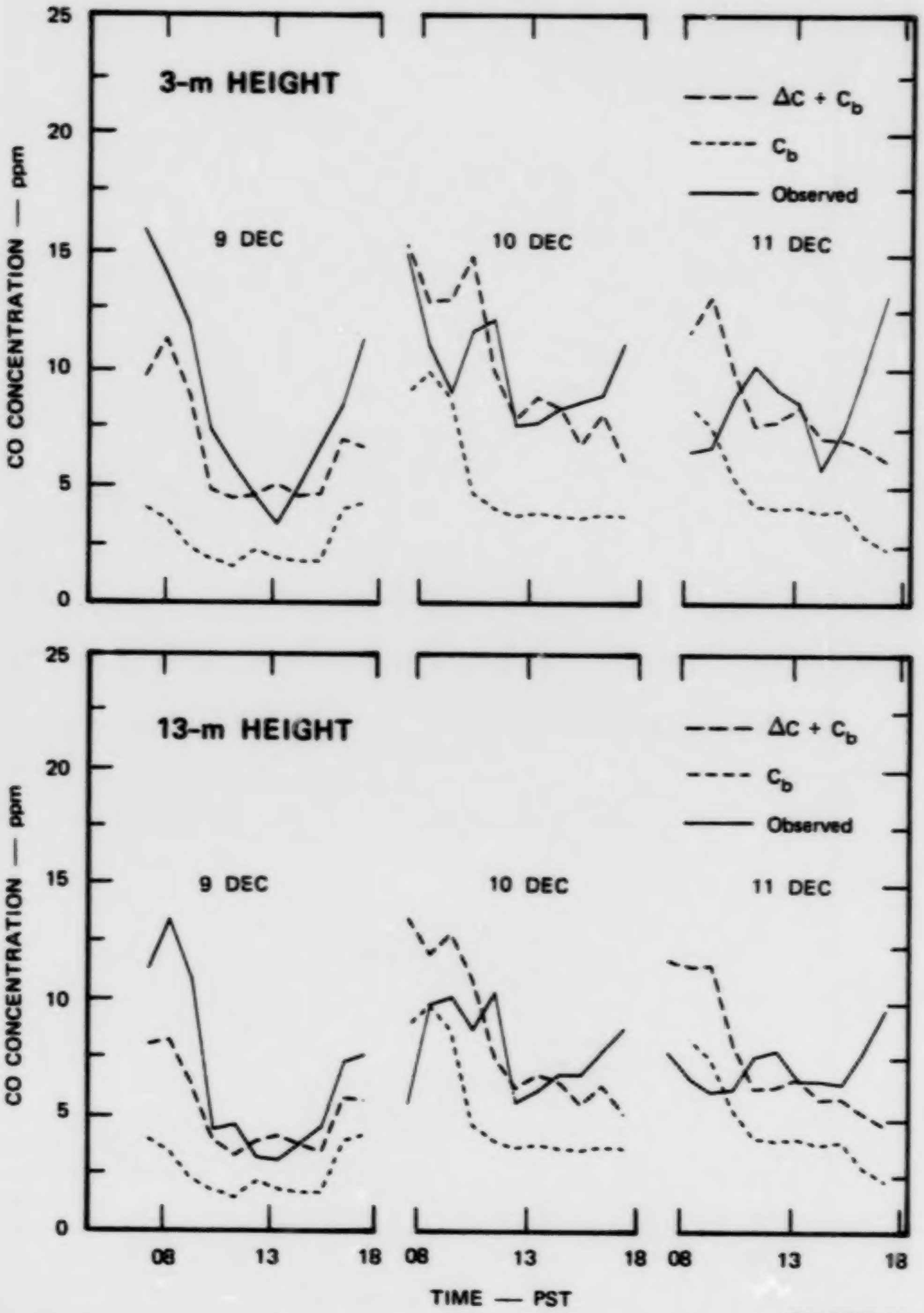

TA-8563-93

FIGURE 61 CALCULATED AND OBSERVED CO CONCENTRATIONS FOR STATION 8 AT TWO HEIGHTS FOR 9, 10, AND 11 DECEMBER 1970

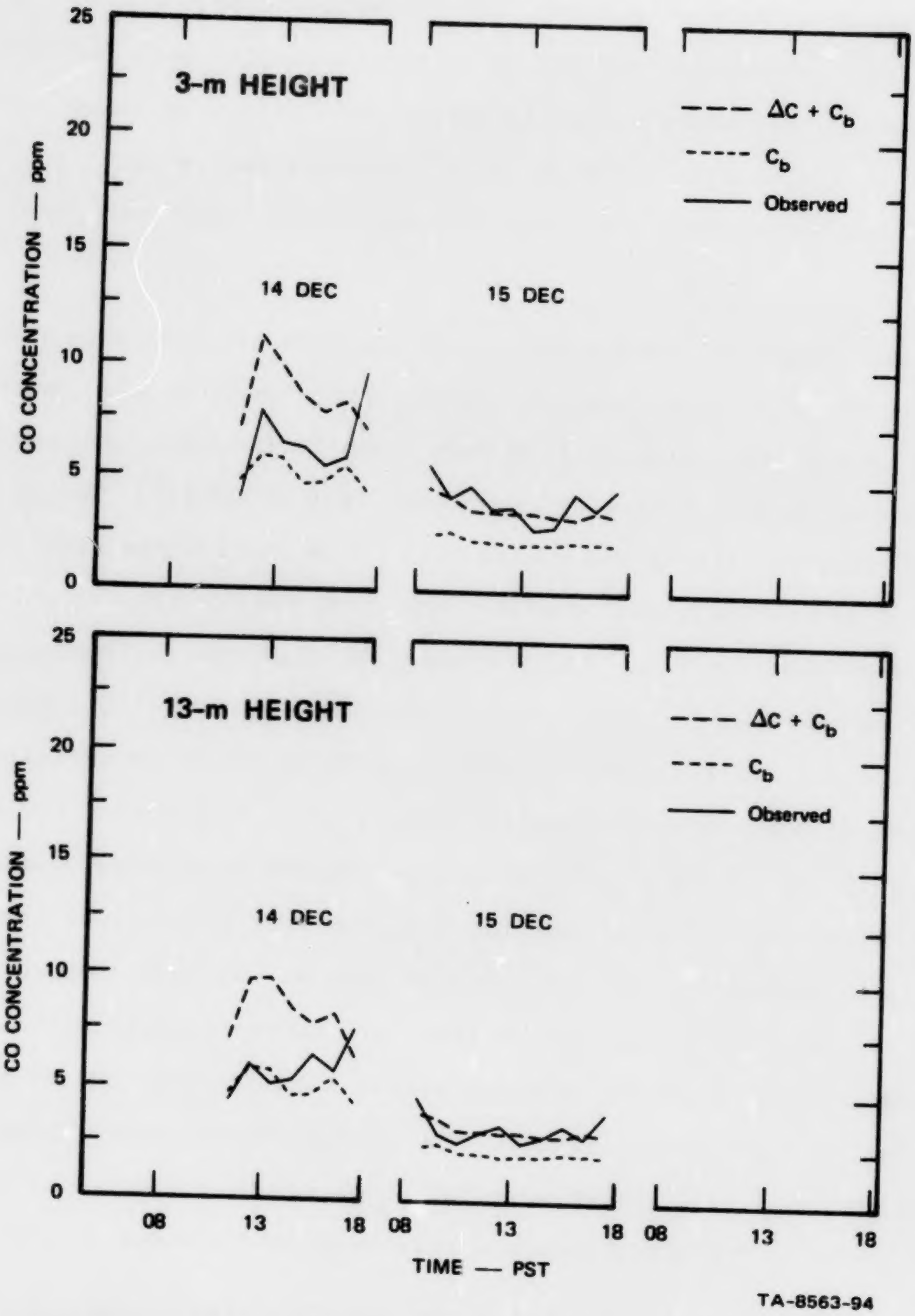

FIGURE 62 CALCULATED AND OBSERVED CO CONCENTRATIONS FOR STATION 8 AT TWO HEIGHTS FOR 14 AND 15 DECEMBER 1970

sum of (1) "street background" values determined from the basic, receptor-oriented Gaussian diffusion model, and (2) values computed with the street effects submodel. Evaluation of the composite model indicates that the predicted values generally agree quite well with the observations. The figures depict the observed concentrations as well as both the predicted values from the composite and street background (basic) models.

Street background concentrations at the five stations were computed from the vehicular emissions in the local downtown area immediately adjacent to the monitoring stations and added to the mean, ambient urban CO background representative of conditions farther upwind. The basic model was used to compute the contribution from the sources within about 2 km of the stations. Traffic data from the downtown monitoring network were used for these computations. Because the traffic network is oriented asymmetrically about the monitoring stations, it is augmented with historical traffic data (Turturici, 1970) to avoid an unrealistic dependence of the computed concentrations on wind direction. The enlarged grid is a circle of 1.9 km radius centered on the monitoring stations. The historical traffic data give the fraction that each street contributes to the total mean daily downtown traffic volume. We have assumed that this fraction is constant throughout the day; the hourly traffic volumes for these streets were computed from the hourly total traffic volume measured in the traffic monitoring network. The diurnal patterns for three different street types (major arterial, high volume collector, and collector) given by Turturici indicate only minor differences in the patterns.

It was not possible to compute the ambient urban background concentration entering the augmented grid area because we lacked detailed traffic data for the greater San Jose area; the magnitude of CO sources farther upwind are also uncertain. Background concentrations at the upwind edge of the circular grid were derived from the helicopter observations when available. It was assumed that the mean concentration along the upwind leg at the lowest level (60 m) was a representative value. During those days when helicopter measurements were not available, subjective estimates were based on the existing meteorological conditions and the CO concentration at the 30-m level of Station 9. A majority of the helicopter flights were made with northwesterly winds. The high correlation found to exist during these periods between the helicopter background values and the concentration at the uppermost level of Station 9 allowed us to "compute" the background in the absence of helicopter measurements for days with northwesterly winds. Ambient urban background concentrations of CO are given in Table 15. Because only three or fewer helicopter flights were made on any given day, background values were taken to remain constant during the following periods: 0700-1100, 1100-1600, and 1600-1800 PST.

On 19 November, data were collected during the morning hours only (see Figures 48, 51, 54, 57 and 60); traffic was blocked on two lanes of First Street south of San Antonio Street commencing at approximately 0830 PST and continuing throughout the rest of the data collection period on that day. The effect of this disruption in the traffic flow is reflected in the generally poor agreement between model and observations.

The performance of the model on the other seven days (20 November, and 7, 9, 10, 11, 14, and 15 December) is quite good. In general, both the trend and the magnitude of the predicted concentrations agree very well with the observations. During those cases when the composite model exhibited poor agreement with the observations, we assessed the relative performance of the basic model and the street effects submodel in order to identify those areas where additional refinements might be necessary. We found that both components contributed to poor results approximately

Table 15

AMBIENT URBAN CARBON MONOXIDE BACKGROUND CONCENTRATIONS (ppm)

Date (1970)	Time Period*	Background (ppm)	Source
19 November	I	2.7	Measured
	II	2.7	
20 November	I	2.0	Estimated
	II	2.0	Estimated
	III	2.5	Computed
7 December	I	2.0	Estimated
	II	1.0	Measured
	III	1.9	Measured
9 December	I	0.9	Measured
	II	0.7	
	III	2.6	
10 December	I	5.8	Measured
	II	2.4	
	III	2.4	
11 December	I	5.5	Measured
	II	3.0	
	III	1.5	
14 December	I	2.0	Estimated
	II	2.0	
	III	2.0	
15 December	I	1.0	Estimated
	II	1.0	
	III	1.0	

* I - 0700 to 1100 PST
II - 1100 to 1600 PST
III - 1600 to 1800 PST

the same number of times, indicating that refinements in both may be necessary. We have identified some of the problem areas and the changes necessary to rectify them.

Determination of the CO concentration in the air entering the circular grid is one of the most difficult problems in the computation of the street background at the receptor. As noted above, we have assumed that the upwind, 60-m helicopter measurement is a representative value; this seems to provide a reasonable estimate in the absence of reliable near-surface observations or detailed traffic data for the greater metropolitan area. In this manner we have obtained good qualitative estimates of the changes in the upwind background. The absolute value of the changes is subject to some uncertainty. The basic limitation in this procedure, however, is the small number (three or less) of such measurements that are available during the day. Because of this we have had to assume that the upwind background remains constant for a period of several hours and then changes abruptly to the value appropriate to the subsequent period. This can introduce serious errors in the computed street background, especially when meteorological conditions are changing rapidly in the interim between background observations.

A limitation in the street effects submodel is associated with the specification of the windward, leeward, and intermediate wind direction sectors (Table 3). Wind tunnel research (Hoydysh, 1971) indicates that the arcs of the various sectors may not be constant, but rather are dependent on the intensity of atmospheric turbulence. Hence, they will be a function of atmospheric stability, wind speed, and the aerodynamic roughness of the site. This effect will obviously be most significant at the outer limits of the wind direction sectors where the flow regime changes abruptly (i.e., from a lateral, cross-street circulation to longitudinal flow, or vice versa).

The street effects submodel is designed for application in the street canyon away from the influences of intersections. Stations 7 and 8 are most representative of this situation, while Stations 5 and 6 are less representative because of their proximity to San Antonio Street. Station 4, on the other hand, is quite poor because it is in a short block with irregular building heights. The effect of location is illustrated in Table 16, which lists the correlation between observed and predicted concentrations at each station for all eight days. As one would expect, the correlation coefficient (r) is highest for Station 7 (r = 0.68) and lowest for Station 4 (r = 0.47). Because of the highly uncertain conditions that existed on 19 November, the correlation coefficient for Station 7, as an example, was recomputed for the other seven days and increased to 0.71. Figure 63 is included to illustrate the degree of scatter represented by these correlations. It has the calculated CO values plotted versus the observed values at Stations 7 and 8 for all five levels and the same days illustrated in Figures 57 through 62.

Table 16

CORRELATION COEFFICIENTS (r) BETWEEN OBSERVED AND PREDICTED CARBON MONOXIDE CONCENTRATIONS

Station	r
4	0.47
5	0.51
6	0.58
7	0.68
8	0.55

Although encouraging, the correlations are not as large as we would desire. Aside from the problems already cited, one additional point should be mentioned. The model, in essence, presumes that changes in the concentration occur simultaneously with changes in the input parameters, e.g., wind speed, stability, and traffic. In reality, the response of the concentration function will lag changes in the inputs. This may especially be important during stable conditions with low wind speeds.

In summary, the composite model predicts CO concentrations that agree quite well with values measured in downtown San Jose. Additional refinements to the model have been proposed which we hope to evaluate during the next phase of the program and incorporate in the final version of the composite model.

D. Frequency Distribution of Concentrations

The model can also be used to calculate the frequency distributions of concentration from the hour-by-hour values. This is a somewhat less demanding use of the model than hour-by-hour prediction, and therefore better performance might be expected.

For those sites for which it is most applicable, we get good agreement between the calculated and observed frequency distributions of 3-m CO concentration. Figure 64 shows these results for Stations 4, 7, and 8. The concentration values represented by these figures are for the same days used for the calculations described in the preceding section. As before there is good agreement between calculations and observations at the midblock Stations, 7 and 8. Station 4 gives poorer results, as do the stations not shown, 5 and 6. As noted above, the model's results, when street effects are included, are best for those stations that best fit the assumptions of the street effects submodel.

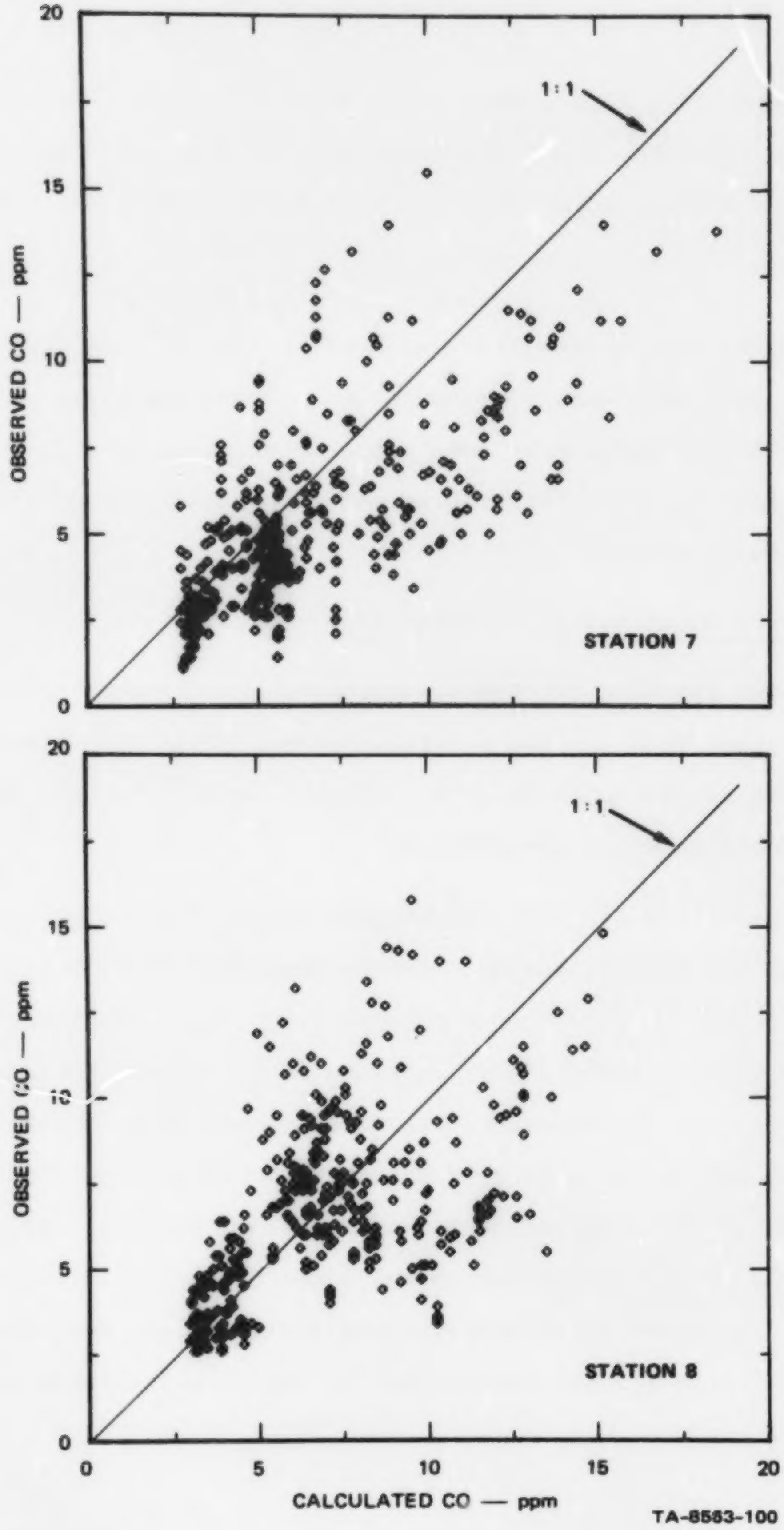

FIGURE 63 SCATTER DIAGRAM OF CALCULATED VERSUS OBSERVED CO CONCENTRATIONS FOR ALL FIVE LEVELS AT STATIONS 7 AND 8

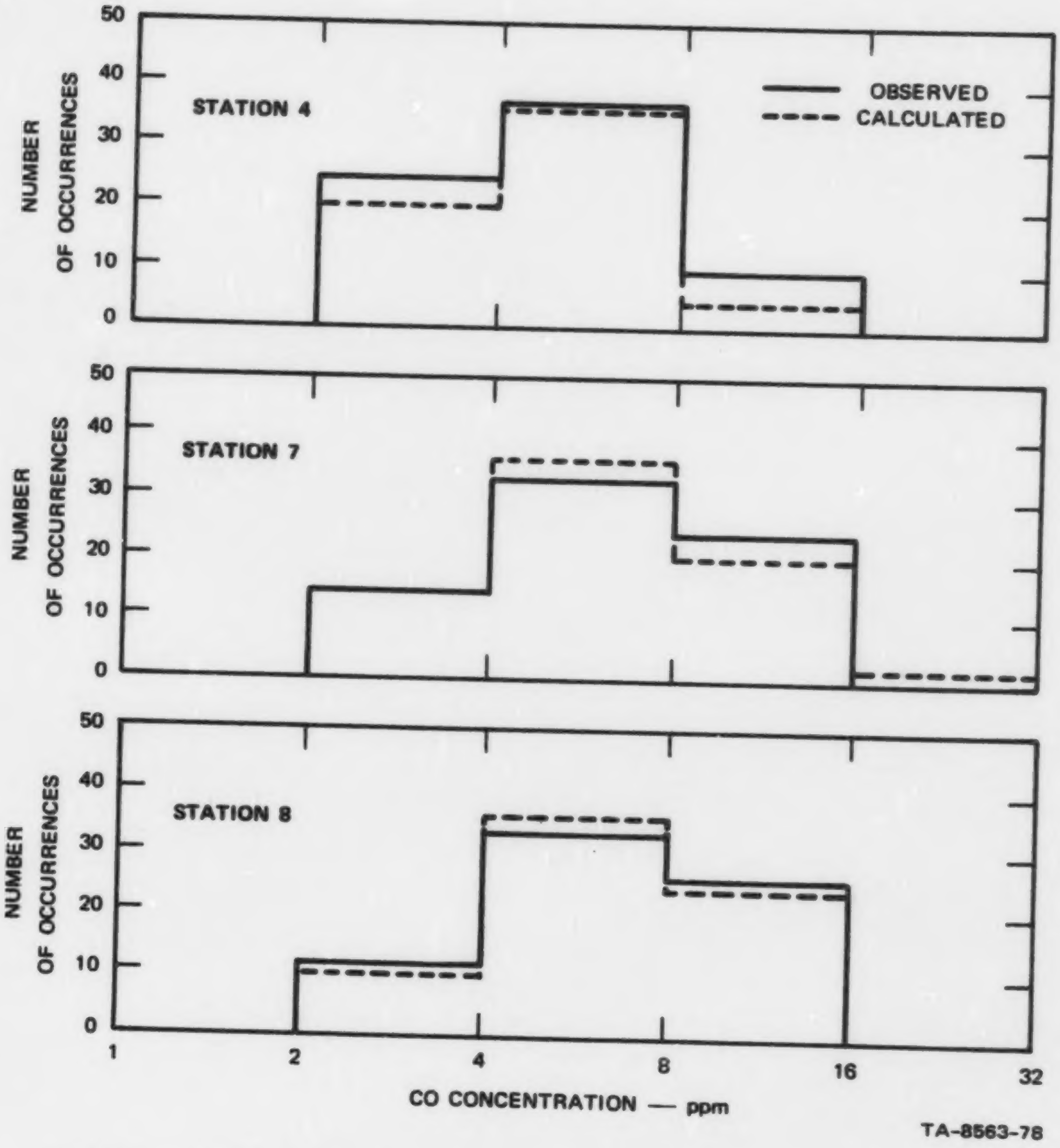

FIGURE 64 CALCULATED AND OBSERVED FREQUENCIES OF ONE-HOUR AVERAGE CO CONCENTRATIONS

BLANK PAGE

VII RECOMMENDATIONS

Our results indicate that the revised model gives very good results for midblock, street-canyon locations. However, some additional research is desirable, and the San Jose program has provided valuable information to define the best directions for future research. It would be very worthwhile to extend our evaluations of the stability, mixing depth, and traffic emissions submodels. We would like to examine the wind fields in urban areas to determine the representativeness of airport wind data. Finally, it is imperative that the model be tested further under substantially different "canyon" conditions, i.e., with a ratio of building height to street width larger than those in the San Jose experiment.

Analysis of the San Jose data has shown that the instrumentation could be more profitably used in the future for the detailed study of the canyon situation alone. The next phase of the program should be confined to the study of these effects. We can make good use of the background from our own San Jose studies and from several laboratory wind tunnel studies (Roshko, 1955; Maull and East, 1963; Fox, 1964 and 1965; Burggraf, 1966; and Hoydysh, 1971).

Study of the extremely complex flow patterns at an intersection should be deferred and should be first studied in a wind tunnel to provide qualitative background information for field efforts. It should be emphasized that wind tunnel simulations are often limited by difficulties in scaling atmospheric turbulence and stability, and the results need to be confirmed by field measurements.

PRECEDING PAGE BLANK

A user's manual per se is not included in this report; a separate manual should be prepared upon completion of the recommended additional research, incorporating further refinements that may result. The manual should provide potential users with the appropriate computer programs, and input and output formats and specifications. Additionally, it should specify the types of problems for which it will serve as a useful diagnostic and/or prognostic tool, as well as an account of conditions which may limit its applicability in certain problem areas.

ACKNOWLEDGMENTS

We are appreciative of the support provided by the Coordinating Research Council and the Air Pollution Control Office (EPA), and of the assistance furnished by their representatives on the CAPA-3 monitoring committee: J. F. Black (Chairman), A. P. Altshuller, J. M. Colucci, R. P. Doelling, C. R. Hosler, R. G. Larson, J. J. Mitchell, J. S. Seward, and A. E. Zengel.

We are grateful to a number of SRI personnel for their assistance. E. L. Younker, F. H. Burch, and W. B. Guthoerl were responsible for the design, building, and installation of the remote coupling units; B. Wheeler did the programming for the mini-computer. Equipment was installed in San Jose by A. H. Smith, L. Salas, W. Ward, W. Crossen, W. Fulcher, and D. Mouton. G. L. Williams, R. Mancuso, H. Shigeishi, R. Trudeau, J. Kealoha, and B. Ripple assisted in various aspects of data reduction and analysis. V. Klein, M. Kucinski, E. Cox, S. Hanson, D. Orr, M. Taylor, P. Monti, and T. Davis all aided in the preparation of this and other project reports.

The City of San Jose was most cooperative; particular thanks are deserved by G. Mahoney and B. Todd of the Traffic Engineering Research Group. The San Jose Redevelopment Agency was very helpful in arranging for suitable equipment sites.

Professors A. Miller, K. MacKay, and D. Mage of San Jose State College provided the project with access to data collected at the college, and arranged pilot balloon ascents. Professor Miller also made the arrangements necessary for the lidar van to be parked and operated on College property.

During some of our operations in San Jose, W. Ott of Stanford University was making special measurements of CO concentration in conjunction with the Bay Area Air Pollution Control District (BAAPCD). Much of their data was made available to us, for which we are grateful. The BAAPCD also provided us with their routinely collected data.

G. Young piloted our chartered helicopter in the heavy air traffic over downtown San Jose. He also made helpful suggestions concerning the installation of equipment in the aircraft.

Appendix A

FIXED-STATION INSTRUMENTATION SYSTEM

BLANK PAGE

Appendix A

FIXED-STATION INSTRUMENTATION SYSTEM

1. Brief System Description

The San Jose fixed-station instrumentation system consisted of a central station and seven satellite remote data-gathering terminals located in a two city block area. Figure 14 of the text shows the location of these sites. Figure A-1 of this appendix is a schematic representation of the system. There are two different types of terminals designed to gather data as follows:

Type A Terminal-- (two total)	Carbon monoxide (CO) concentrations are measured at five equally spaced heights to produce a vertical profile from 3 meters to the top of the building where installed. Temperature differences are measured between adjacent levels to obtain a vertical profile corresponding to the CO profile. Absolute temperature is monitored at either the top or bottom level (manually selected). Three-axis orthogonal (UVW) wind speed is sensed at the top of the building and near the 3-m level.
Type B Terminal-- (five total)	CO concentrations are measured at five equally spaced heights as at the Type A terminals. Horizontal wind speed and directions are measured at the 3-m level.

PRECEDING PAGE BLANK

Both the Type A and Type B terminals contain Model 1 remote line couplers; in addition, the A terminals contain a second remote line coupler called the Model 2. Both model couplers contain an address decoder, analog and digital multiplexers, an analog-to-digital converter, and associated modules. The Model 2 couplers also contain circuitry for controlling a low-level multiplexer used for selecting the various temperature sensor inputs. All remote couplers received commands and transmitted data via teletype lines leased from the phone company. Spare channels are available, so additional sensors can be added if needed.

"Mode code" generators were included so that "fixed" data such as the selected "range" for wind measurements could be supplied to the central station; this allowed the correct scale factor to be selected by the computer during data processing.

The two types of terminals also had differences in the support systems used to suspend the sensors from the buildings. These differences arose from the differences in the set of parameters measured at the two types of terminals. The Type A terminals required a more complicated suspension system than the Type B, because of the greater numbers of parameters to be measured.

The central station contained a small minicomputer/controller, a teletype unit, and magnetic tape storage. The purposes of this central station are (1) to interrogate the sensors at the various terminals; (2) to select the heights at which CO was to be monitored; (3) to store the gathered data returned by the seven satellite terminals; (4) to perform certain computations with part of the data; (5) to generate and place a "time elapsed" tag with each group of data collected; (6) to log the information digitally on magnetic tape; and (7) to print summaries of processed data periodically for monitoring purposes.

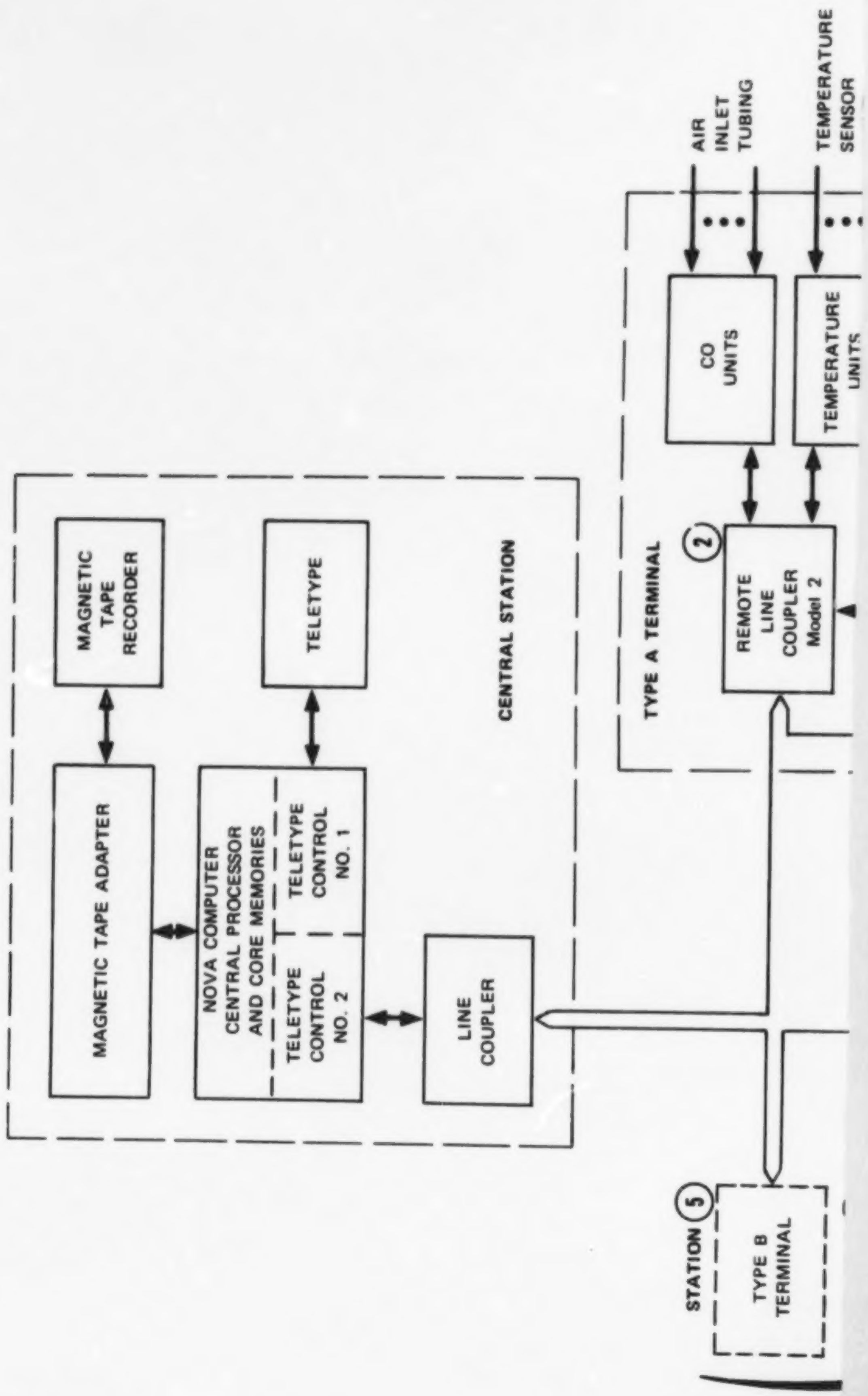
CENTRAL STATION
MAGNETIC TAPE RECORDER
TELETYPE
MAGNETIC TAPE ADAPTER
NOVA COMPUTER CENTRAL PROCESSOR AND CORE MEMORIES
TELETYPE CONTROL NO. 1
TELETYPE CONTROL NO. 2
LINE COUPLER
TYPE A TERMINAL
②
REMOTE LINE COUPLER Model 2
CO UNITS
TEMPERATURE UNITS
AIR INLET TUBING
TEMPERATURE SENSOR
STATION ⑤
TYPE B TERMINAL

A

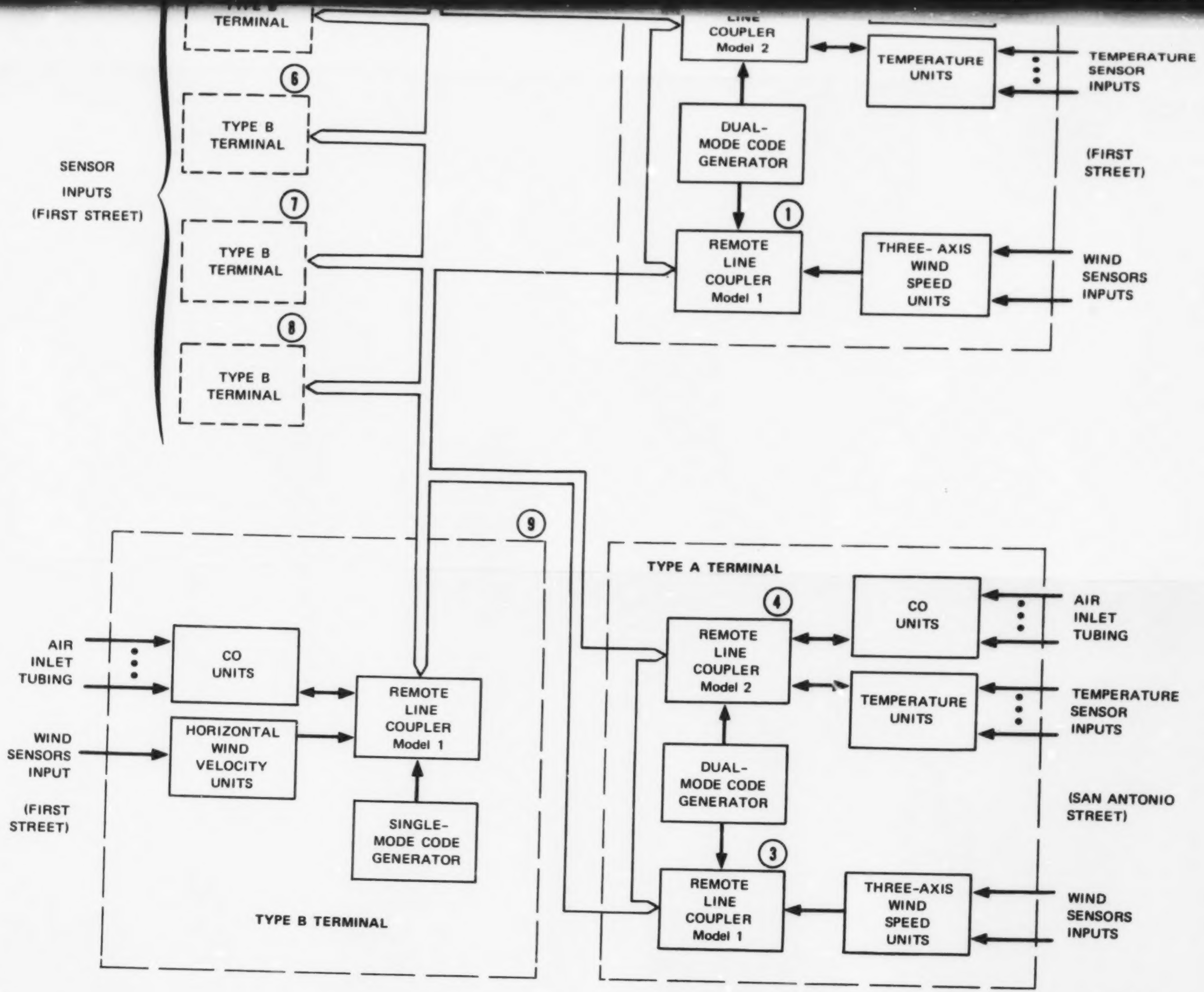
TYPE B
TERMINAL
LINE
COUPLER
Model 2
TEMPERATURE
UNITS
TEMPERATURE
SENSOR
INPUTS
⑥
TYPE B
TERMINAL
DUAL-
MODE CODE
GENERATOR
(FIRST
STREET)
SENSOR
INPUTS
(FIRST STREET)
⑦
TYPE B
TERMINAL
①
REMOTE
LINE
COUPLER
Model 1
THREE- AXIS
WIND
SPEED
UNITS
WIND
SENSORS
INPUTS
⑧
TYPE B
TERMINAL
⑨
TYPE A TERMINAL
④
CO
UNITS
AIR
INLET
TUBING
AIR
INLET
TUBING
CO
UNITS
REMOTE
LINE
COUPLER
Model 2
REMOTE
LINE
COUPLER
Model 1
TEMPERATURE
UNITS
TEMPERATURE
SENSOR
INPUTS
WIND
SENSORS
INPUT
HORIZONTAL
WIND
VELOCITY
UNITS
DUAL-
MODE CODE
GENERATOR
(FIRST
STREET)
SINGLE-
MODE CODE
GENERATOR
(SAN ANTONIO
STREET)
③
REMOTE
LINE
COUPLER
Model 1
THREE-AXIS
WIND
SPEED
UNITS
WIND
SENSORS
INPUTS
TYPE B TERMINAL
TYPE A TERMINAL

B

TB-8563-23

FIGURE A-1 BLOCK DIAGRAM OF FIXED-STATION INSTRUMENTATION SYSTEM

In the following section the two types of terminals are described, starting with the sensor supports and proceeding through the instrumentation system in the direction of the data flow. The final section in this appendix contains a description of the central station.

2. Description of Terminals

a. Sensor Support System

The prime requirements in the design of the two different types of sensor support systems were that they: (1) provide for the sensors to be suspended above the sidewalk and clear of the building; (2) be capable of supporting the weights involved without hazard to pedestrians; (3) not damage the roof or building; (4) be transportable and easy to install even on sloped roofs; and (5) not allow the suspended sensors to move about substantially. The sensor support systems shown in Figures A-2 and A-3 accomplished these goals with only two minor problems evolving from incorrect installations.* As can be noted, the complete sensor support system consists of a roof-located boom and counter-weighted support, rope(s) holding the air (CO) inlets and temperature aspirators, and the lower support boom installed 3 meters above the sidewalk.

Standard commercial 1-inch galvanized water pipes and fittings were used to support the single upper booms used at Type B terminals. At the Type A terminals, 1-1/4-inch pipes were used to support the dual upper boom. A 1.5- by 4-ft plywood pallet was used for mounting four front pipe floor flanges, and a 2.5- by 4-ft pallet for mounting four

---

*A truck hit one lower boom after it was moved from over a wide sidewalk on First Street to a narrower one on San Antonio Street. High winds bent a single roof boom that was improperly secured to an existing roof structure.

PRECEDING PAGE BLANK

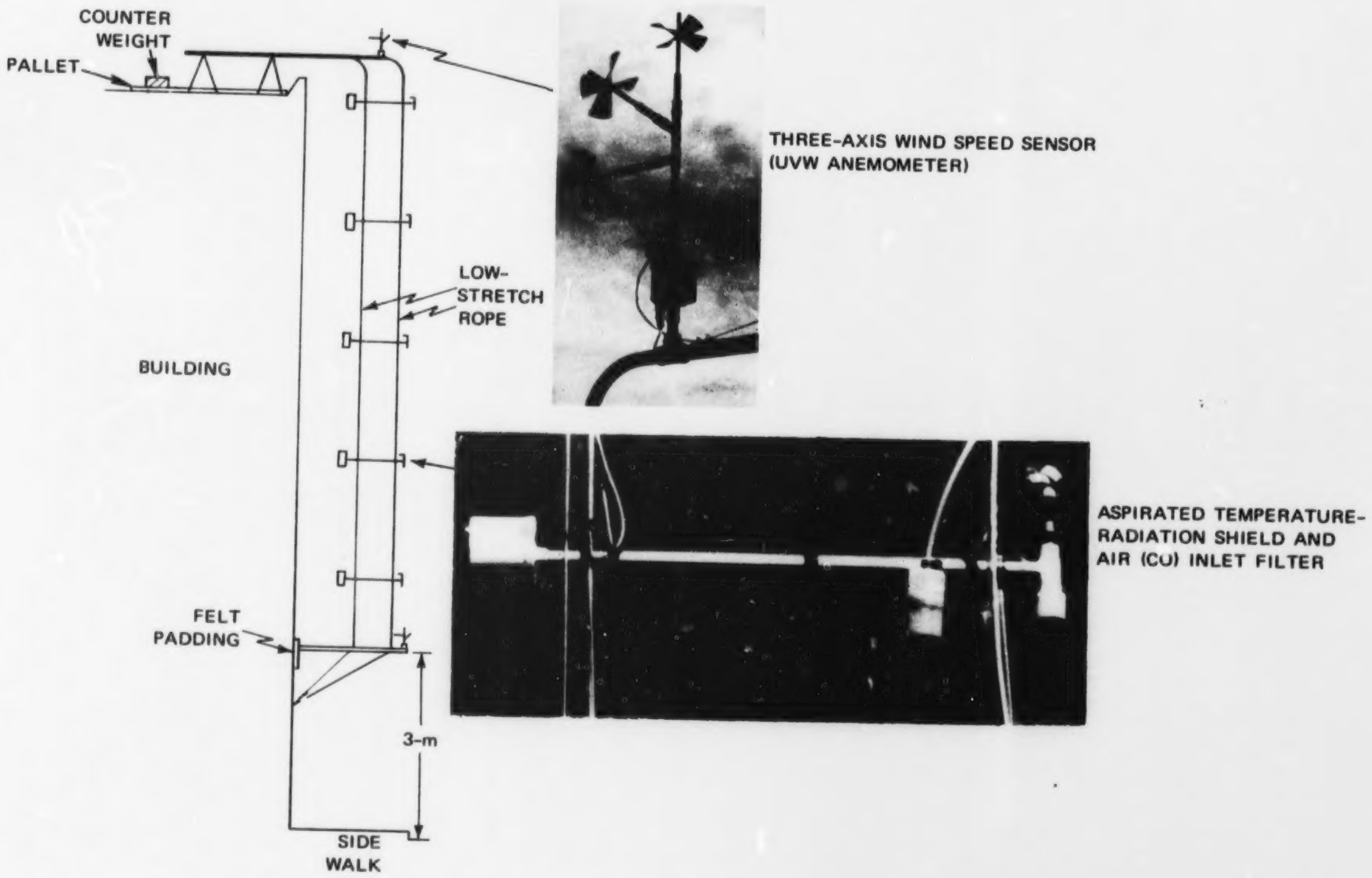
COUNTER WEIGHT
PALLET
BUILDING
LOW-STRETCH ROPE
FELT PADDING
3-m
SIDE WALK
THREE-AXIS WIND SPEED SENSOR (UVW ANEMOMETER)
ASPIRATED TEMPERATURE-RADIATION SHIELD AND AIR (CO) INLET FILTER
TA-8563-24R

FIGURE A-2 TYPE A TERMINAL SENSORS AND SUPPORT SYSTEM

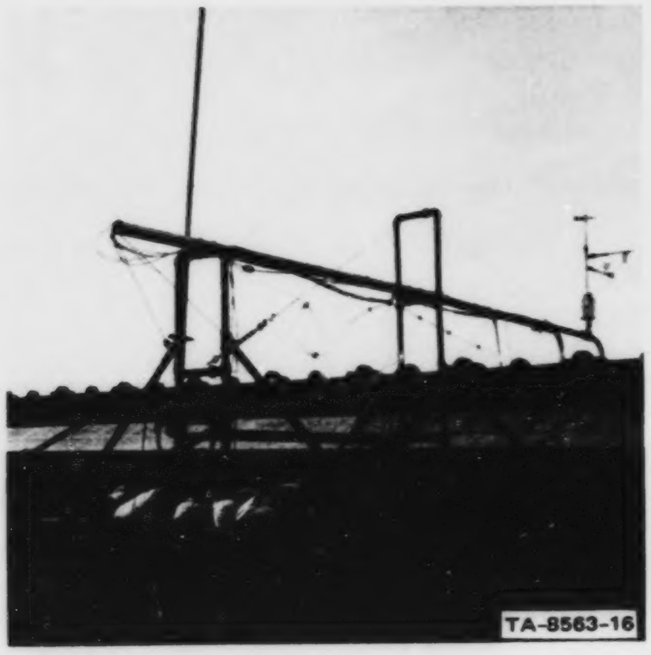

FIGURE A-3 DUAL ROOF BOOM—PART OF SENSOR SUPPORT SYSTEM

rear flanges plus providing an area for the concrete block and/or sandbag counter weights.

The upper booms were 1-1/2-inch rigid electrical aluminum conduit and fittings instead of steel as used in the support. The longest boom was assembled from two 10-ft sections and extended approximately 12 ft beyond the front steel pipe support. This front support extended 2 ft above the aluminum boom and supported an aircraft control type cable used to back-guy the far end of the boom overhang, as indicated in Figure A-3. Turn buckles and thimbles were used to adjust the tension on the guy wire. Four mercury leveling type switches were installed parallel to the two horizontal axes of the UVW sensor at the tip of the boom. Four lights installed in a remote readout box indicated when the wind sensor was properly oriented. One axis was leveled by rotating the booms, the other by adjusting guy-wire tension.

The lower support boom was constructed of a 1-inch rigid conduit and installed at a height of about 3 meters. A 1-ft-square, felt-backed piece of marine plywood was mounted on the end of a 10-ft section of conduit that fit against the building. Fittings as shown in Figure 16 were used to support the wind sensors and to provide means for fastening for the guy ropes on this lower boom. Mercury leveling switches were also used on this boom.

For the Type A terminals, two low-stretch 1650-lb test ropes were used to support the aspirated temperature sensor assembly, and the air inlet filter and associated tubing. These units are pictured in Figures 16 and 18 of the text. For the Type B terminal, a single low-stretch rope supported the air inlet filters and tubing as shown in Figure 16.

During installation these ropes were measured and laid along the sidewalk. The aspirator assemblies, the wiring, the air inlet filters, and the tubing were attached to the ropes so that the sensors would be properly located. The wire, tubing, and ropes were then pulled through the upper boom support until all sensors were suspended in their correct positions. The lower ends of the rope were secured to the lower boom to prevent sway. Cabling and tubing were routed from the roof, over the edge of the building, and through a window into the room containing the instrumentation units.

b. Carbon Monoxide (CO) System

The CO measuring system was the same at both types of terminals. It consisted of five rain-proof inlet filters, each attached to 200 ft of 1/4-inch-ID low outgassing polyethylene tubing, a five-inlet selector unit, and a Beckman model 315-AL CO analyzer (see Figure

A-4). A block diagram of the system is shown in Figure A-5; specifications are listed in Table A-1.

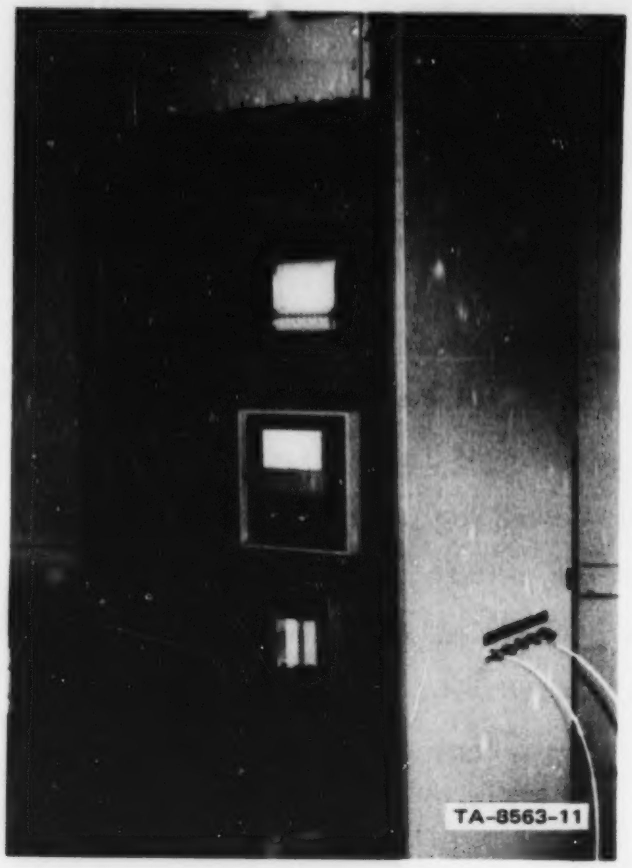

FIGURE A-4 BECKMAN CARBON MONOXIDE ANALYZER WITH REMOTE LINE COUPLER

Upon receiving a command from the remote coupling unit, one of five solenoid valves was energized; it opened so that air from a selected level could be pumped through the CO analyzer. The remaining four inlet lines were continuously purged by a pump located within the selector unit. Sampled air passed through a diaphragm pump in the CO analyzer; then excess air was bled off through a 2-psi relief valve. A needle valve was used to adjust the flow rate to 2 liters min^{-1}, as monitored with a rotameter. This flow flushed the cell every 8.2 seconds.

The analyzer section uses a double-beam optical system to measure differential absorption of infrared energy. Two infrared sources

Table A-1

MANUFACTURER'S STATED PERFORMANCE SPECIFICATIONS FOR THE NONDISPERSIVE, INFRARED CO ANALYZER

Operating Specifications:	
Range	0 to 50 ppm by volume
Flow rate	2 ℓpm
Output	0 to 1.0 V
Linearity	(curve provided)
Zero drift (maximum)*	±1 percent of full scale per 8 hours
Span drift (maximum)*	±1 percent of full scale per 24 hours
Response speed (amplifier)	0.5 second (90 percent)
Response speed (analyzer)	(not reported)
Sensitivity	0.5 percent of full scale
Repeatability	±3.0 percent of full scale
Interference	H_2O (3 percent equivalent to 1 ppm response)
Environmental Specifications:	
Ambient temperature range	-20 to 120° F
Physical Specifications:	
Weight	110 lb
Power	410 watts, 115 ± 15 V ac, 60 ± 0.5 Hz

*Span and zero drift specifications are based on ambient temperature shifts of less than 40° F at a maximum rate of 20° F per hour.

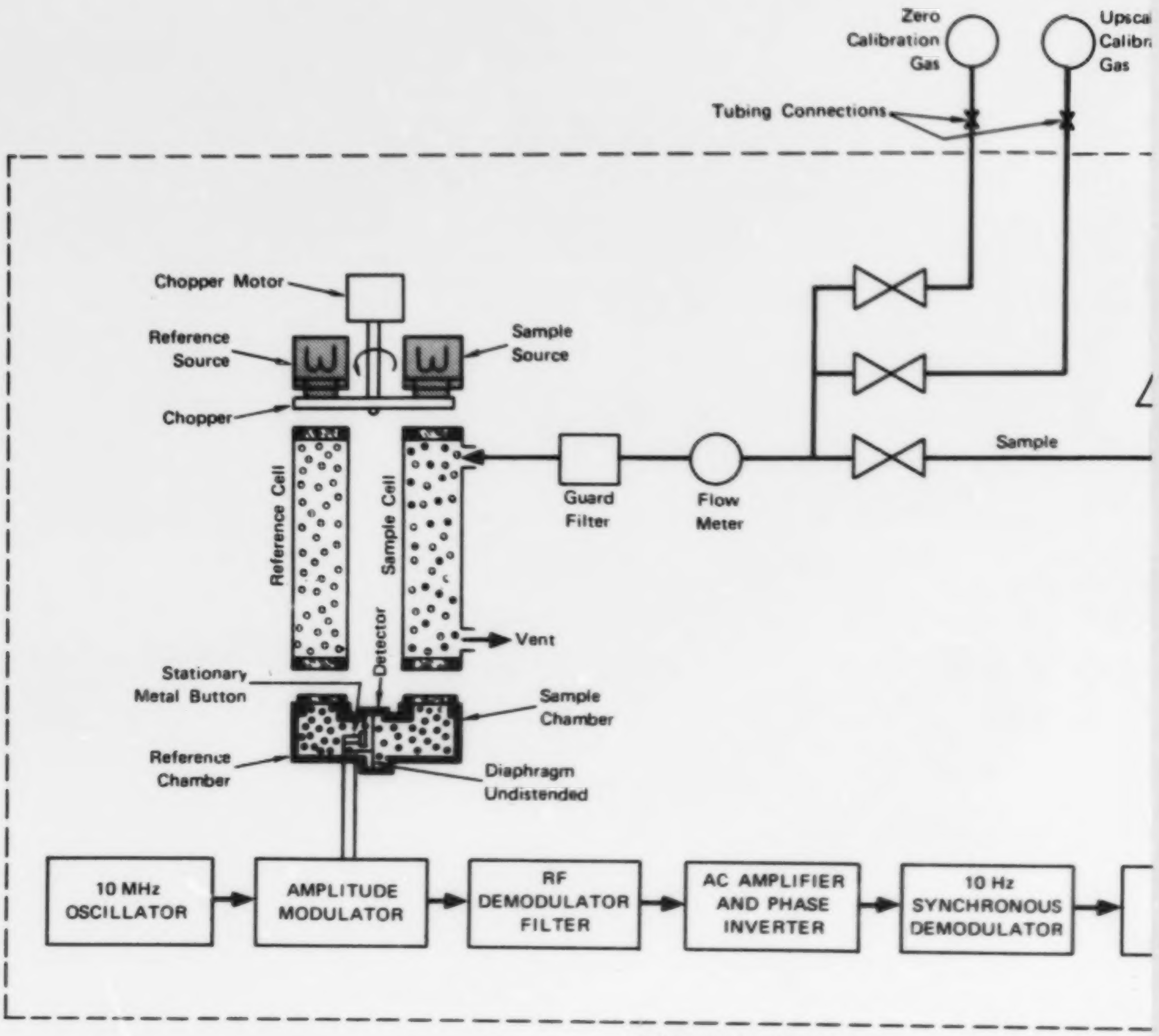
Zero
Calibration
Gas
Upsca
Calibr
Gas
Tubing Connections
Chopper Motor
Reference
Source
Sample
Source
Chopper
Sample
Reference Cell
Sample Cell
Guard
Filter
Flow
Meter
Vent
Detector
Stationary
Metal Button
Sample
Chamber
Reference
Chamber
Diaphragm
Undistended
10 MHz
OSCILLATOR
AMPLITUDE
MODULATOR
RF
DEMODULATOR
FILTER
AC AMPLIFIER
AND PHASE
INVERTER
10 Hz
SYNCHRONOUS
DEMODULATOR

BECKMAN CO ANALYZER

▨ Non-Absorbing Molecules

▨ Infrared Absorbing CO

a

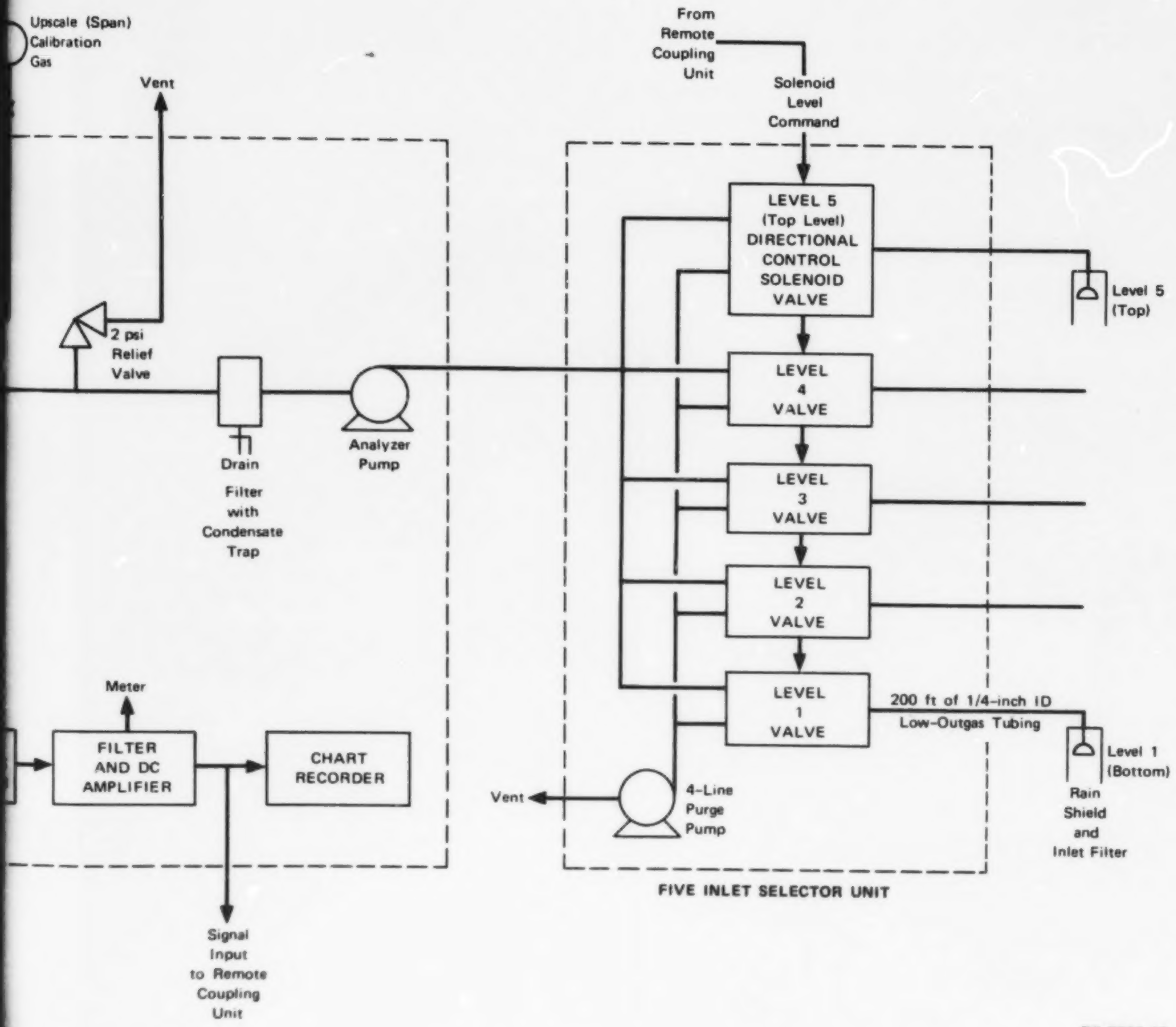
Upscale (Span)
Calibration
Gas
Vent
2 psi
Relief
Valve
Drain
Filter
with
Condensate
Trap
Analyzer
Pump
Meter
FILTER
AND DC
AMPLIFIER
CHART
RECORDER
Signal
Input
to Remote
Coupling
Unit
From
Remote
Coupling
Unit
Solenoid
Level
Command
LEVEL 5
(Top Level)
DIRECTIONAL
CONTROL
SOLENOID
VALVE
Level 5
(Top)
LEVEL
4
VALVE
LEVEL
3
VALVE
LEVEL
2
VALVE
LEVEL
1
VALVE
200 ft of 1/4-inch ID
Low-Outgas Tubing
Level 1
(Bottom)
Rain
Shield
and
Inlet Filter
Vent
4-Line
Purge
Pump
FIVE INLET SELECTOR UNIT

TB-8563-28

FIGURE A-5 BLOCK DIAGRAM OF CO MEASURING SYSTEM USING BECKMAN ANALYZER are used, one for the sample energy beam, the other for the reference energy beam. The beams are blocked simultaneously ten times per second by the chopper, a two-segmented blade rotating at 5 revolutions per second. In the unblocked condition, each beam passes through the associated cell and into the detector.

The sample cell is a flow-through tube that receives a continuous stream of sampled air. The reference cell is a sealed tube filled with a reference gas. This gas is selected for minimal absorption of infrared energy in the wavelengths absorbed by CO.

The detector consists of two sealed compartments separated by a flexible metal diaphragm. Each compartment has an infrared-transmitting window, and is filled to the same sub-atmospheric pressure with CO. This detector responds only to the net difference in transmitted IR energy resulting from absorption by CO in the sample cell. Inside the detector, gas in the reference chamber is heated more than in the other chamber because less energy has been absorbed from the reference beam. The higher temperature of the gas in the reference chamber raises the pressure in this compartment above that in the sample chamber and distends the diaphragm toward the sample chamber. The diaphragm and an adjacent stationary metal button constitute a two-plate variable capacitor. Distention of the diaphragm away from the button decreases the capacitance.

When the chopper blocks the beams, pressures in the two chambers equalize, and the diaphragm returns to the undistended condition. As the chopper alternately blocks and unblocks the beams, the diaphragm pulses, thus changing detector capacitance cyclically. The detector is part of an amplitude modulation circuit that impresses the 10-Hz information signal on a 10-MHz carrier wave provided by a crystal-controlled radio-frequency oscillator. Additional electronic circuitry demodulates and filters the resultant signal, yielding a 10-Hz signal that is amplified,

PRECEDING PAGE BLANK

phase inverted, and synchronously rectified. The resulting fullwave-rectified signal is filtered and the dc voltage is amplified to drive the meter and recorder and to provide a signal to the remote line coupler unit. The signal is proportional to the CO concentration in the sample cell.

c. Temperature System

The temperature system was required to provide one absolute temperature in the range from -25° C to +50° C and four differential temperatures with a resolution of 0.01° C. Originally it was planned to have electronics capable of operating on the roof in an environment that could have ranged from -25° C to +50° C. The sensors had to operate in the electrical noise environment of the city, and at distances of 200 ft from the electronics unit. To simplify signal processing, we wanted sensors with a linear signal output over their operating range. Their response to temperature had to be stable for periods of at least 3 months. The temperature system shown in the block diagram of Figure A-6 generally accomplished these goals.*

The complete temperature system consisted of: (1) the aspirated-radiation shielded sensor; (2) 200 ft of AWG #28 eight-conductor cable with an overall shield and jacket; (3) four differential and one absolute temperature bridge networks with a common 10-V dc power supply installed on one chassis; and (4) on a second chassis, a gold-plated low-level stepping switch and associated control circuitry, low-noise/low-drift differential amplifiers with automatic gain changing, meters

---

*The absolute temperature measurement was eliminated during the San Jose experiments because of ground-loop problems among the absolute and differential bridges, their common 10-V power supply, and the lead-wire shielding. This problem has subsequently been corrected.

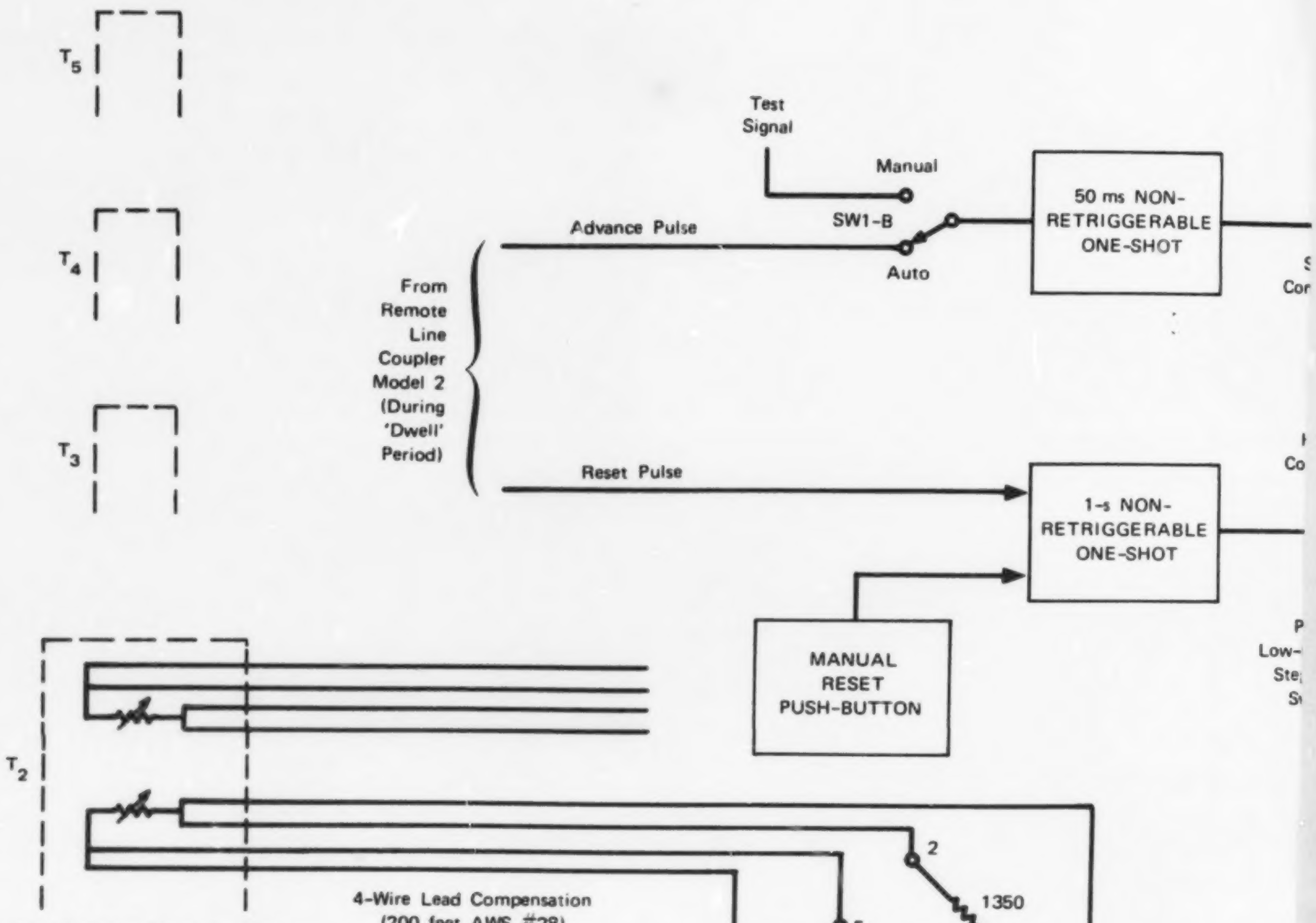
T5
T4
T3
Test Signal
Manual
SW1-B
Advance Pulse
Auto
50 ms NON-RETRIGGERABLE ONE-SHOT
From Remote Line Coupler Model 2 (During 'Dwell' Period)
Reset Pulse
1-s NON-RETRIGGERABLE ONE-SHOT
MANUAL RESET PUSH-BUTTON
T2
Dual Platinum Resistance Wire Temperature Sensors and Aspirated Radiation Shield
4-Wire Lead Compensation (200 feet AWS #28)
2
1350
5
200
10
200
4
+
Span
5
ZERO
1350
3
T2 - T1
T1
T5
MANUAL SELECT T1 OR T5
7
ZERO
5
20k
1k
87.54
+
10V
Span
1k
8
20k
T1 OR T5
Bottom Level (3-m Above Sidewalk)

a

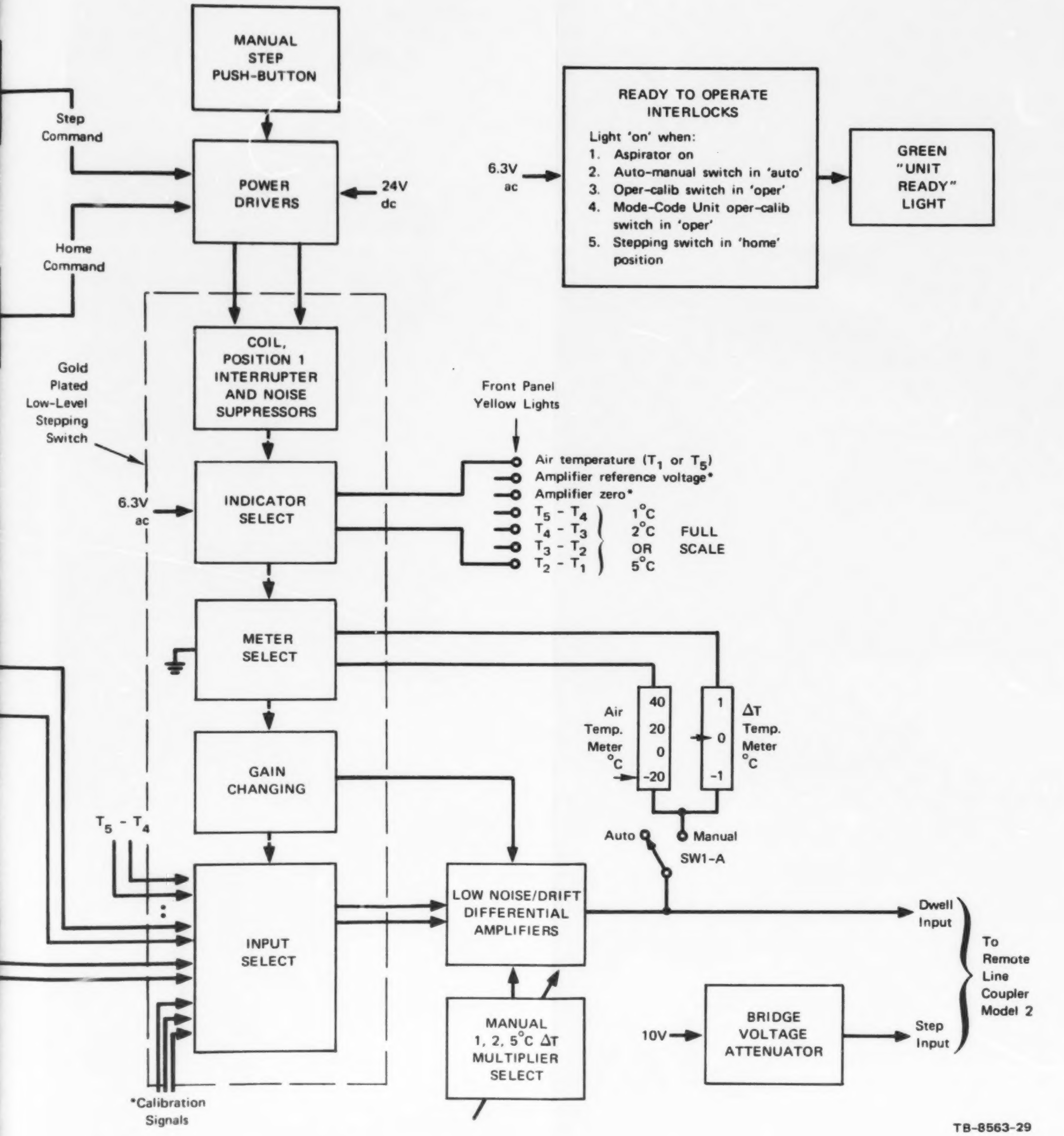
MANUAL STEP PUSH-BUTTON
Step Command
Home Command
POWER DRIVERS
24V dc
READY TO OPERATE INTERLOCKS
Light 'on' when:
1. Aspirator on
2. Auto-manual switch in 'auto'
3. Oper-calib switch in 'oper'
4. Mode-Code Unit oper-calib switch in 'oper'
5. Stepping switch in 'home' position
6.3V ac
GREEN "UNIT READY" LIGHT
Gold Plated Low-Level Stepping Switch
COIL, POSITION 1 INTERRUPTER AND NOISE SUPPRESSORS
Front Panel Yellow Lights
6.3V ac
INDICATOR SELECT
Air temperature (T_1 or T_5)
Amplifier reference voltage*
Amplifier zero*
$T_5 - T_4$
$T_4 - T_3$
$T_3 - T_2$
$T_2 - T_1$
1°C 2°C OR 5°C
FULL SCALE
METER SELECT
Air Temp. Meter °C
40
20
0
-20
1
0
-1
ΔT Temp. Meter °C
GAIN CHANGING
Auto
Manual
SW1-A
$T_5 - T_4$
INPUT SELECT
LOW NOISE/DRIFT DIFFERENTIAL AMPLIFIERS
Dwell Input
Step Input
To Remote Line Coupler Model 2
MANUAL 1, 2, 5°C ΔT MULTIPLIER SELECT
10V
BRIDGE VOLTAGE ATTENUATOR
*Calibration Signals

TB-8563-29

FIGURE A-6 BLOCK DIAGRAM OF TEMPERATURE SYSTEM for visually reading the absolute and differential temperatures at individual levels, and interlocking circuitry to ensure that the various switches are in the proper position during operation.

Dual platinum resistance-wire-type temperature sensors[*] were installed at each level. The small additional cost was paid for this type of sensor because of its inherent linearity (as opposed to thermistors), its long-term stability, and its relatively high signal output (as opposed to thermocouples). The dual resistance wire sensors were installed within a 1/4-inch-OD stainless steel housing. Their calculated time constant is about 40 seconds for the 15-ft s^{-1} ventilation used. A commercial low thermal-conduction teflon bushing was purchased and the stainless steel housings were installed within a silvered, double-walled glass cylinder open at both ends, but otherwise similar to a Dewar flask. The silvered cylinder provides a radiation shield for the temperature sensor. An aspirator assembly[†] draws air upward through the end of the cylinder, and past the stainless steel housing containing the dual sensors. A small blower located at the other end of the aspirator-radiation shield assembly provides the ventilation. The entire assembly is pictured in Figure 18 of the text.

The cabling was connected to the sensor leads with crimped, uncoated copper connectors to minimize thermocouple errors. This cable was shielded and supported by a different rope than the 110-V ac aspirator power cable. This minimized 60-Hz pickup. Four-wire lead compensation was used to minimize the effect of the differences in resistances of the lead wire and changes in the lead wire resistance due to temperature effects.

---

[*] Model 104MK-57-BB-CC, Rosemount Engineering.

[†] No. 43404, R. W. Young Company.

PRECEDING PAGE BLANK

A separate chassis with a 3.5-inch panel for rack mounting contained four plug-in hermetically sealed differential bridge networks, one plug-in type absolute bridge network, and a 10-V dc regulated floating power supply. These bridge networks contained both span and zero adjustments for calibration purposes. Variations in the supply voltage, if any, were monitored each time data were read by supplying an attenuated voltage just under 1 V dc to the remote line coupler. A further attenuated bridge voltage is also used as one of the inputs to the differential amplifiers, thereby providing a means for checking amplifier gain and determining long-term drift. These networks for attenuating the bridge voltage where assembled within plug-in modules similar to those used for the bridge networks and plugged into spare sockets on this bridge chassis.

Wires carrying the absolute temperature signal, the four differential temperature signals, and the calibration signals were routed to another chassis with a 5.25-inch rack-mounting front panel. The calibration signals consisted of the previously mentioned attenuated bridge voltage used as an amplifier reference (span) voltage and a 100-ohm "short circuit" which is used as a differential amplifier zero. These two signals, when compared to the 1-V dc attenuated bridge voltage, allow any amplifier drift and/or bridge voltage fluctuations occurring while gathering the experimental data to be determined during off-line data processing.

Upon receiving an "advance pulse," a gold-plated low-level stepping switch sequentially selects inputs and routes the individual signals to low-noise/low-drift differential amplifiers. Additional contacts on this stepping switch are used to select various combinations of feed-back/input resistors that control the amplifier gains.[*] Since a separate, center-zero type meter was required for visual readout of the differential temperatures, one of the stepping switch levels was used to select the correct meter. The meters are disconnected from the circuit during automatic stepping to minimize noise during the ten-step-per-second cycling run.

The fourth level of the stepping switch selects the indicator lights installed on the front panel of the multiplexer unit. The lights indicate the channel selected and are particularly useful when the channels are selected by manual stepping.

To ensure that the stepping switch always starts with the same selected input, a reset pulse is supplied from the Model 2 remote line coupler following the completion of the advanced pulse stepping sequence. Also a manual reset push button is provided to return the stepping switch to its "home" or "rest" position after completing some manual readout or calibration processes. To check that the stepping switch is in the "home" position prior to automatic operation, a "ready to operate" interlock has been included. This interlock as well as the four others indicated in Figure A-6 provide power to a green "unit ready" indicator light when all switches are in their correct position for system operation under control by the central station. The rack containing the temperature system electronics is shown in Figure A-7.

---

[*] The gains of the differential amplifiers are 100 when measuring the absolute temperature; they are 500, 250, and 100 when measuring differential temperatures on the 1°, 2°, and 5° C ranges, respectively.

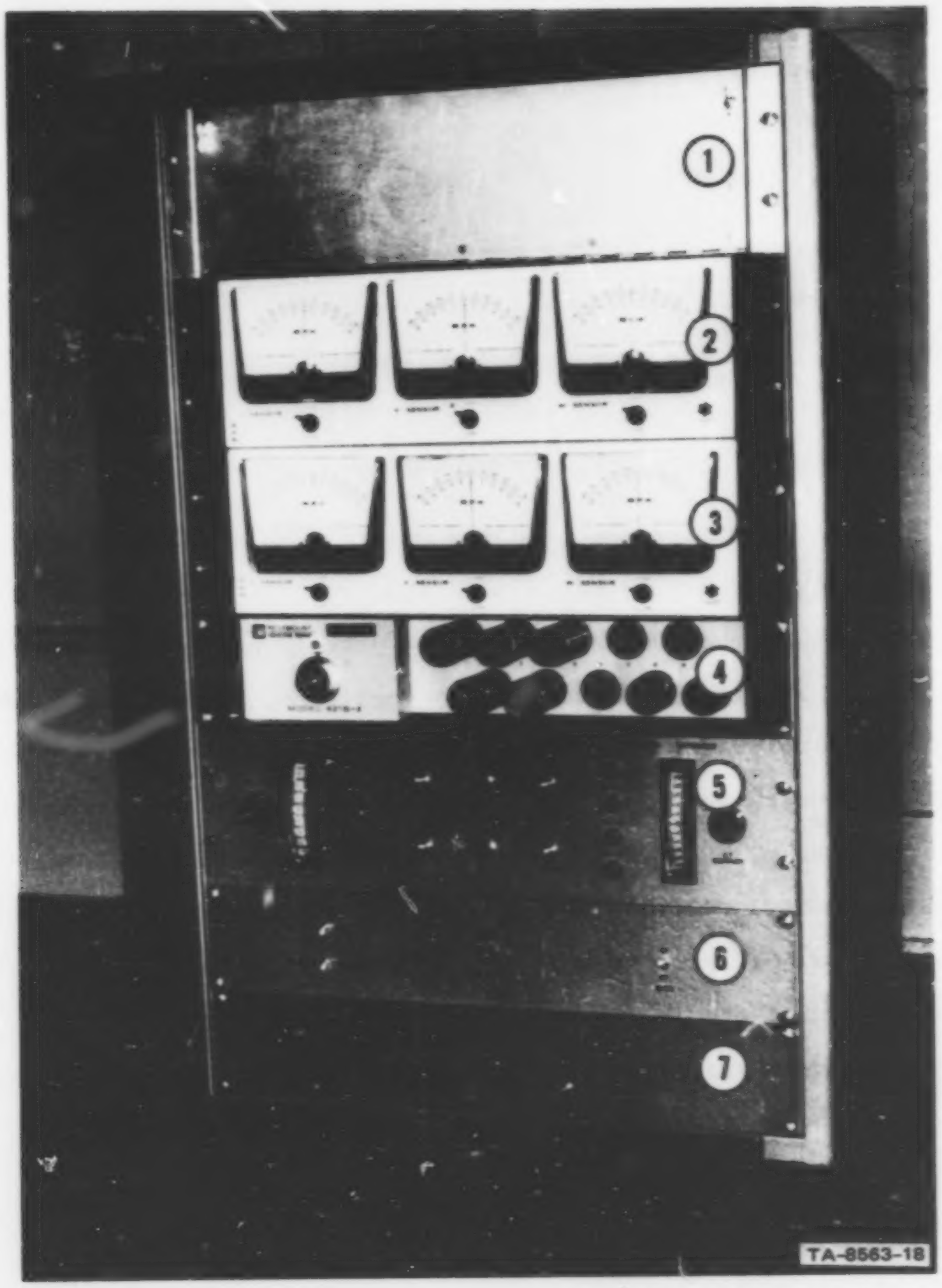

1. Remote Line Coupler
2,3. UVW Wind Component Indicators
4. Temperature Bridge
5. Temperature Multiplexer Amplifier
6. Mode Code Generator
7. Line Coupler Power Supply

FIGURE A-7 TEMPERATURE AND UVW ELECTRONICS

d. Wind System

1) Three-Axis (UVW) Orthogonal Anemometer

The Gill UVW anomometer[*] is a wind instrument designed for direct measurement of three orthogonal vectors of the wind. Three helicoid propeller sensors are mounted at right angles to each other on a common mast with sufficient separation between propellers so that there is no significant effect of one on the others for normal wind measurements. The two propellers sensing horizontal components of wind are designated U and V, and the third sensing the vertical component of wind is designated W. This instrument is shown in Figure 17 of the text. The foamed polystyrene propellers respond only to that component of the wind parallel to the axis of rotation. Both forward and reverse air flow are measured. The propeller stops rotating when the wind is perpendicular to the axis. The propeller response very closely approximates the cosine law, making the instrument especially suited for vertical wind component measurements.

The propeller rotates 0.96 revolutions per foot of wind for all wind speeds above 4 ft s^{-1} (2.7 mi h^{-1}). Slippage increases down to the threshold speed of 0.8 ft s^{-1} (0.5 mi h^{-1}). It has a distance constant[†] of 94 cm. The propeller drives a miniature dc tachometer generator providing an analog voltage output that is proportional to wind speed. The design allows for an optimum dynamic response in winds ranging from threshold to 50 mi h^{-1}.

---

[*] Model 27002/27302, R. M. Young Company.

[†] The distance constant is the wind passage required for the sensor to reach 63 percent of a stepwise change in wind speed.

The two propellers in the horizontal plane were aligned parallel and perpendicular to the street. The horizontal sensors provide a positive signal for wind flow from the front of the sensor; this causes counterclockwise propeller rotation. With wind flow from the rear of the sensor, propeller rotation and signal polarity reverse. The "W" or vertical sensor receptacle is wired for opposite signal polarity, so wind flow from the front of the sensor (a down draft) provides a negative signal for the meter and remote line coupler.

The lower housing of the UVW anemometer contains a small continuous-duty air blower with a polyurethane foam intake filter. This blower keeps the internal section of the instrument under a slight positive pressure. Filtered air moves continuously up the mast and out through each of the three sensors to the propeller hubs, where it is expelled to the atmosphere, preventing moisture and dust from entering the precision ball bearings and other internal parts.

The UVW anemometer signals are transmitted through a multiconductor cable to the "indicator-translator" unit. This unit, shown in Figure A-7, has three 4.5-inch meters that indicate the speed of each wind component in miles per hour. Two ranges are available: -25 to +25 mi h^{-1} and -50 to +50 mi h^{-1}. A switch on the front panel selects the desired range, which can be calibrated independently. A separate adjustment is provided for the output to the remote coupler, allowing the scale factor to be preadjusted. The instrument is calibrated with a small motor (Young Company model 27230 calibrator) that is connected to the propeller axle through a flexible shaft. This calibrator rotates at a constant 1800 rpm (using 60-Hz power). This corresponds to 21.3 mi h^{-1} and meter readings and output voltages are adjusted accordingly.

2) Horizontal Wind Velocity Sets

Two different types of measuring sets were used to determine horizontal wind speed and direction. Climet model CI-3 units were used at four sites and a military type AN/GMQ-12 was used at one site. The Climet wind speed sensor is a three-cup anemometer with a threshold less than 1 mi h^{-1} and a 5-foot distance constant. The wind speed transmitter produces a frequency signal that is proportional to the wind speed from threshold to full range (60 mi h^{-1}).

The Climet wind direction sensor has a threshold less than 1 mi h^{-1}. It uses a potentiometer to produce a voltage proportional to wind direction over a range of 354°. There is a "dead" region around 0°/360°.

Adjustable dc output voltages from the Climet were routed to the remote coupler and to local meters. The accuracy of the voltages in representing the wind is ±1.3 percent or ±0.15 mi h^{-1}, whichever is greater, and ±4° in azimuth. Three ranges are manually selectable: 15, 30, and 60 mi h^{-1} The computer was informed of which range had been selected by also manually adjusting a similar appearing rotary switch on the mode code unit discussed in the next section.

Wind speed and direction indicators were calibrated by removing sensor cables from the translators and inserting those from a special calibrator. Calibration points were provided for 0, 6, 15, and 30 mi h^{-1}, and for 0°, 180°, and 360°. The indicated wind direction was also checked by manually holding the wind vane at known angles.

The AN/GMQ-12 wind measuring set is similar to the Climet. It also uses a three-cup anemometer. It has four wind speed ranges: 6, 12, 30, and 60 mi h^{-1}. The wind direction covered a range of 354° with accuracy of ±3 percent at full scale. The wind speed accuracy was ±4 percent of full scale, with a threshold less than 1 mi h^{-1}. Provisions are incorporated within the electronics circuitry for a cursory check of the full-scale and zero outputs of the wind direction channel, but no easy method is available for wind speed calibration in the field. Direction output was checked by manually holding the vane at known angles, as with the Climet instruments.

e. Mode Code Generator

The mode code units were designed to provide the computer with a signal that indicates "fixed" data. These fixed data include the selected ranges of the wind and temperature measuring units, and whether each unit is being calibrated. Provisions have also been included to inform the computer which of two possible orientations of the wind direction sensor is being used. This latter provision was incorporated since the horizontal wind direction sensors have a gap near their 360° point and could require a change of orientation dictated by prevailing winds. The actual voltages for various switch combinations and their corresponding acceptable octal ranges, as indicated by the remote coupler unit, are shown in Table A-2.

The mode code generator has a dc power supply, a resistor-ladder network, and a series of switches similar to a digital-to-analog converter. The generator used to supply the code for the two remote couplers located at Type A terminals has a second ladder, but only the one dc power supply. Since the range of analog voltages for a given set of switch positions was ±10 mV, an expensive matched-resistor ladder network was not required.

Table A-2

MODE CODES FOR INDICATED REMOTE COUPLING UNITS

Mode Code Generator Output (mV ± 10)	Acceptable Octal Range for Wind Direction Orientation		Remote Coupler Units 1 and 3		Remote Coupler Units 2 and 4						Remote Couplers 5, 6, 7, and 9						Remote Coupler 8						
			Calib. (0) Oper. (1)		Delta T Multiplier			T_1 (1) T_5 (0)	Calib. (0) Oper. (1)		Wind Speed (mi h^{-1})			Calib. (0) Oper. (1)			Wind Speed Range (mi h^{-1})				Calib. (0) Oper. (1)		
	Number 1	Number 2	low UVW	high UVW	1	2	5	T_a	ΔT, T_a	CO	15	30	60	WS	CO	WD	6	12	30	60	WS	CO	WD
15.6	0-3	374-377					1	0	0	0			1	0	0	0				1	0	0	0
46.9	4-7	370-373	0	0			1	0	0	1			1	0	0	1				1	0	0	1
78.1	10-13	364-367					1	0	1	0			1	0	1	0				1	0	1	0
109.4	14-17	360-363	0	1			1	0	1	1			1	0	1	1				1	0	1	1
140.6	20-23	354-357					1	1	0	0			1	1	0	0				1	1	0	0
171.9	24-27	350-353	1	0			1	1	0	1			1	1	0	1				1	1	0	1
203.1	30-33	344-347						1	1	0			1	1	1	0				1	1	1	0
234.4	34-37	340-343	1	1			1	1	1	1			1	1	1	1				1	1	1	1
265.6	40-43	334-337				1		0	0	0		1		0	0	0			1		0	0	0
296.9	44-47	330-333				1		0	0	1		1		0	0	1			1		0	0	1
328.1	50-53	324-327				1		0	1	0		1		0	1	0			1		0	1	0
359.4	54-57	320-323				1		0	1	1		1		0	1	1			1		0	1	1
390.6	60-63	314-317				1		1	0	0		1		1	0	0			1		1	0	0
421.9	64-67	310-313				1		1	0	1		1		1	0	1			1		1	0	1
453.1	70-73	304-307				1		1	1	0		1		1	1	0			1		1	1	0
484.4	74-77	300-303				1		1	1	1		1		1	1	1			1		1	1	1
515.6	100-103	274-277			1			0	0	0	1			0	0	0		1			0	0	0
546.9	104-107	270-273			1			0	0	1	1			0	0	1		1			0	0	1
578.1	110-113	264-267			1			0	1	0	1			0	1	0		1			0	1	0
609.4	114-117	260-263			1			0	1	1	1			0	1	1		1			0	1	1
640.6	120-123	254-257			1			1	0	0	1			1	0	0		1			1	0	0
671.9	124-127	250-253			1			1	0	1	1			1	0	1		1			1	0	1
703.1	130-133	244-247			1			1	1	0	1			1	1	0		1			1	1	0
734.4	134-137	240-243			1			1	1	1	1			1	1	1		1			1	1	1
765.6	140-143	234-237															1				0	0	0
796.9	144-147	230-233															1				0	0	1
828.0	150-153	224-227															1				0	1	0
859.4	154-157	220-223															1				0	1	1
890.6	160-163	214-217															1				1	0	0
921.9	164-167	210-213															1				1	0	1
953.0	170-173	204-207															1				1	1	0
984.4	174-177	200-203															1				1	1	1

f. Remote Line Couplers

The block diagram (Figure A-8) shows the main functional elements of the remote line coupler unit. The inputs from the previously discussed signal-processing units are connected to the high-level analog multiplexer that acts as a single-pole selector switch. This module connects one input at a time, at 0.1-second intervals, to the input of the analog-to-digital converter in the sequence shown in Table A-3. The multiplexer controls are the "reset," which returns the switch to a rest (home) position, and the "advance," which steps it along to the next input. The rest position always corresponds to the mode code signal.

The analog-to-digital (AD) converter, when commanded by a "convert" signal, determines a binary number corresponding to the value of the input voltage within a range of 0 to ±1 volt. The conversion process takes about one millisecond, after which an "end-of-conversion" signal is generated that informs the control circuitry that the AD conversion outputs are ready for use. The end-of-conversion signal also steps the multiplexer to the next input.

The output of the AD converter, the contents of the register indicating the CO sampling level, and the output of the address code switch are selected by the digital multiplexer to make up the output message. This is done one character at a time by setting up a shift register in the parallel-to-serial converter, under control of signals generated by the output control section.

The remote coupler unit is in a quiescent condition most of the time. The busy signal is off (forcing the analog multiplexer reset), and the AD converter is set to an internal trigger mode, so that it will continually measure the mode code output and display this on the unit's binary indicator lights.

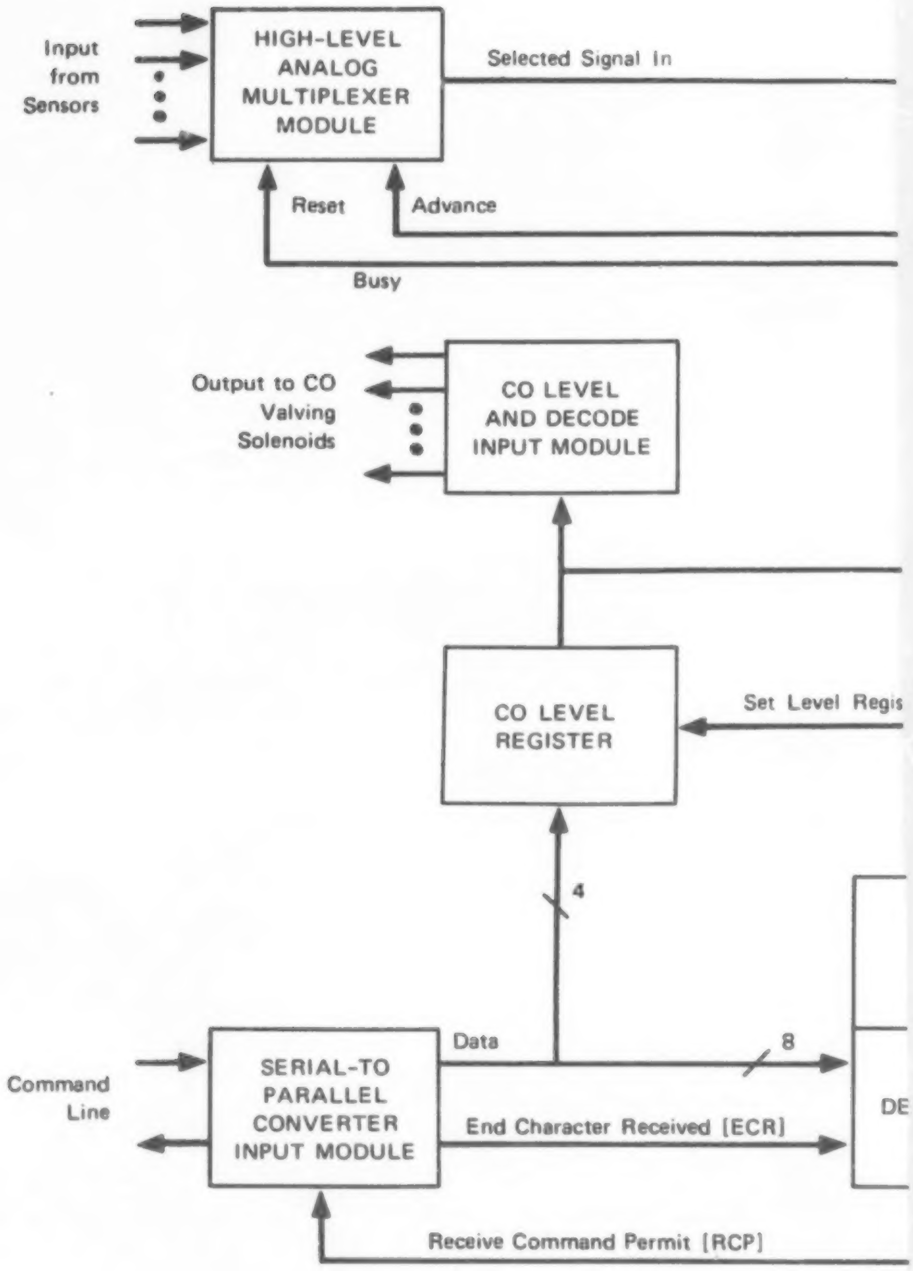
Input from Sensors
HIGH-LEVEL ANALOG MULTIPLEXER MODULE
Selected Signal In
Reset
Advance
Busy
Output to CO Valving Solenoids
CO LEVEL AND DECODE INPUT MODULE
CO LEVEL REGISTER
Set Level Regis
4
Command Line
SERIAL-TO PARALLEL CONVERTER INPUT MODULE
Data
8
DE
End Character Received [ECR]
Receive Command Permit [RCP]

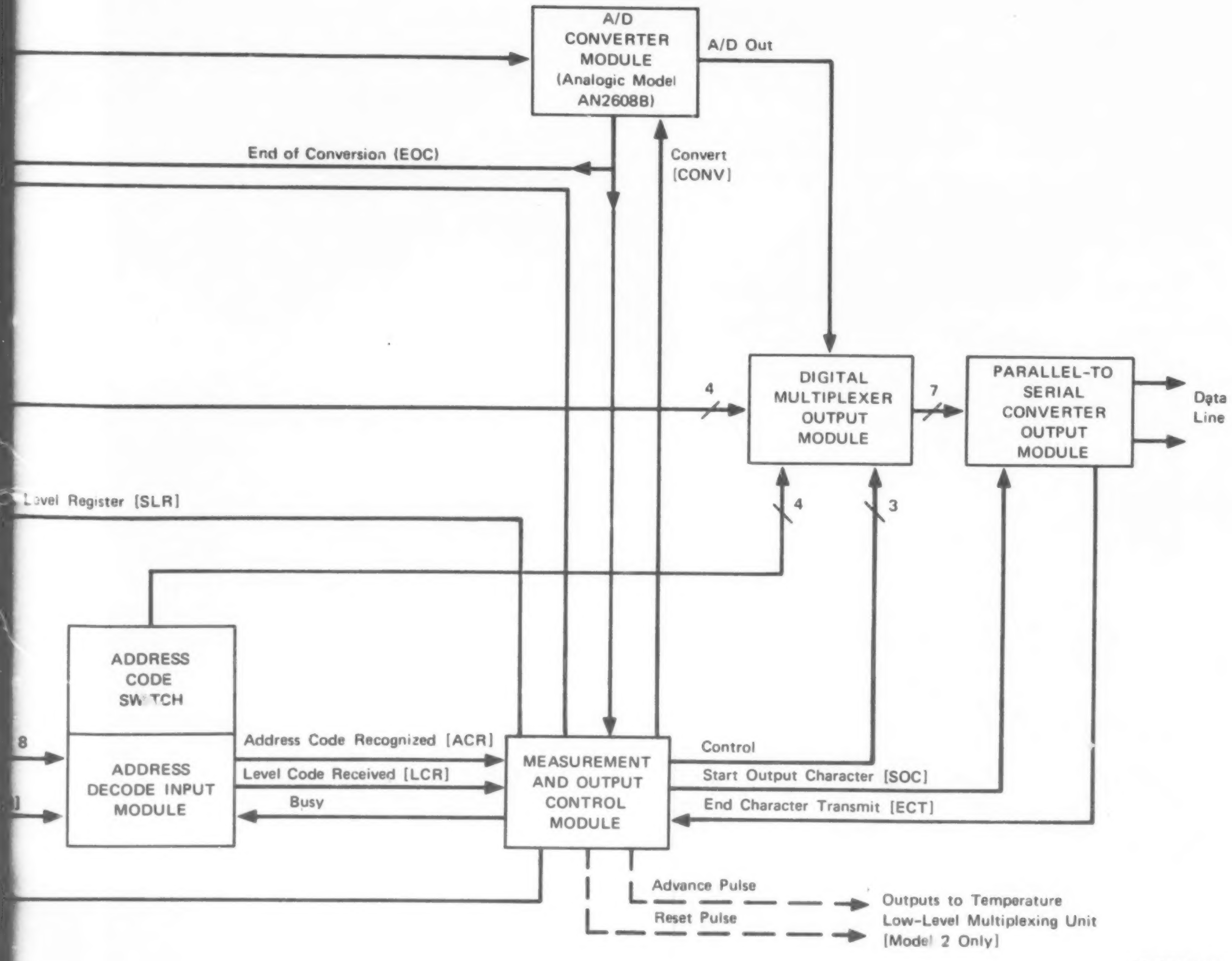
A/D CONVERTER MODULE (Analogic Model AN2608B)
A/D Out
End of Conversion (EOC)
Convert [CONV]
4
DIGITAL MULTIPLEXER OUTPUT MODULE
7
PARALLEL-TO SERIAL CONVERTER OUTPUT MODULE
Data Line
Level Register [SLR]
4
3
ADDRESS CODE SWITCH
8
ADDRESS DECODE INPUT MODULE
Address Code Recognized [ACR]
Level Code Received [LCR]
Busy
MEASUREMENT AND OUTPUT CONTROL MODULE
Control
Start Output Character [SOC]
End Character Transmit [ECT]
Advance Pulse
Reset Pulse
Outputs to Temperature Low-Level Multiplexing Unit [Model 2 Only]

TB-8563-30

FIGURE A-8 BLOCK DIAGRAM OF REMOTE LINE COUPLERS

Table A-3

REMOTE LINE COUPLER ASSIGNED SCANNING SEQUENCE

Model 1 Remote Line Coupler		
Input Jack	Measurement (Type A Terminal)	Measurement (Type B Terminal)
J 11 (Rest)	Mode Code	Mode Code
J 12	U_1 (Lower level wind component)	CO
J 13	V_1 (Lower level wind component)	V (Wind speed, lower level)
J 14	W_1 (Lower level wind component)	θ (Wind direction, lower level)
J 15	U_2 (Upper level wind component)	(Spare)*
J 16	V_2 (Upper level wind component)	(Spare)
J 17	W_2 (Upper level wind component)	(Spare)
J 18	(Spare)*	(Spare)
J 19	(Spare)	(Spare)
J 20	(Spare)	(Spare)
J 21	(Spare)	(Spare)
J 22	(Spare)	(Spare)

Model 2 Remote Line Coupler	
Input Jack	Measurement (Type A Terminal)
J 11 (Rest)	Mode Code
J 12	CO
J 13	(Spare)
J 14	(Spare)
J 15	Ground (Remote unit zero calibration)
J 16	Bridge voltage
J 17 (Dwell)	Absolute (air) temperature
	Amplifier reference voltage
	$T_2 - T_1$
	$T_3 - T_2$
	$T_4 - T_3$
	$T_5 - T_4$
	Amplifier zero

---

*Subsequent inputs without data were not scanned. Last input jack scanned is controlled by changing a jumper wire.

BLANK PAGE

Two of the nine remote line couplers have been modified slightly* for use with the temperature system. These Model 2 couplers provide an advance pulse at a 10-pps rate for stepping the low-level temperature multiplex unit. These signals are provided only after the remote unit has reached its "dwell" input, which is the J 17 input (Table A-3) of its high-level analog multiplexer. After a sufficient number of advance pulses have been sent to the temperature multiplexer unit, the Model 2 remote unit sends a "reset" pulse that returns the temperature multiplexer to its "rest" position, completing the cycle. All the other functions of the Model 2 remote unit are the same as that of the Model 1.

3. Description of Central Station

As indicated in Figure A-1, the fixed-station instrumentation system consists of seven remote terminals, described in the preceding section, and the central station, described in this section. The central station pictured in Figure A-9 was at the location marked "1,2" in Figure 14 of the text. It consisted of the NOVA computer, magnetic tape adapter, digital magnetic tape recorder, teletype unit (including a paper tape punch and reader), and a line coupler.

a. Line and Line Coupler

The nine remote line couplers located within the seven terminals were all connected in series with each other and to the computer through two dc (20 mA) teletype loops installed by the telephone company. One loop, the command line, was a series connection of the computer

---

*See dashed lines in Figure A-8.

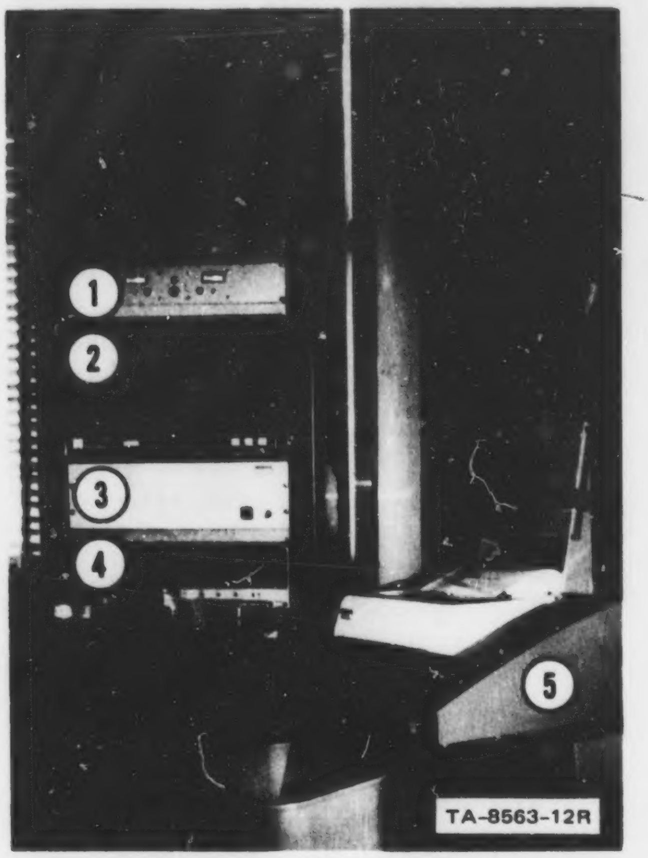

1. Line Coupler
2. Digital Magnetic Tape Recorder
3. Magnetic Tape Adapter
4. NOVA Computer
5. Teletype

FIGURE A-9 MINI-COMPUTER AND PERIPHERAL DEVICES AT CENTRAL STATION

transmitter contacts and the nine remote unit receiver terminals. The other loop, the data line, was a series connection of all the remote transmitter contacts and the computer receiver terminals. Thus, the computer transmits to all remote units simultaneously, but only one remote unit at a time transmits to the computer.

The computer terminals were the output of a line coupler unit that converts the low-voltage (approximately 20 V) operation of the computer's Teletype Control No. 2 interface to the high voltage (approximately 100 V) needed to drive the lines. This coupler provides dc isolation, through an optically coupled light-emitting diode isolator, between the low-voltage computer loops and the high-voltage remote loops. At the same time, it permits data to flow straight through. The coupler also supplies the voltage necessary to establish the remote loop currents.

Separate isolators are used for each of the remote loops. Meters and a potentiometer allow the loop currents to be adjusted to 20 mA.

b. Computer

A general-purpose NOVA mini-computer[*] was used as the control and real-time data-processing unit for the fixed-station instrumentation system. As used in the San Jose operations, the computer interrogated and directed the changing of sampling heights at the seven CO measuring sites. This took about seven seconds of every minute. During the remaining 53 seconds of the minute, the readings of the U, V, W sensors were recorded. All the data, together with the time from the computer's real-time clock, were stored in the memory until the available space had been filled. It was then transferred to magnetic tape through the adapter described in the next section.

In addition to interrogating the remote units, and receiving and recording their data, the computer also did some preprocessing. After each of the five CO intake heights had been sampled at each of the stations, the computer prepared and printed, on its peripheral teletype, a summary of data from the preceding five-minute period. An example of this printout is given in Appendix D, Figure D-1.

The block diagram in Figure A-10 shows the organization of this computer and Table A-4 lists its important characteristics. The central processor is the control unit for the entire system: it governs all peripheral in-out equipment, performs all arithmetic, logical, and

---

[*] Model 4001, Data General Corporation, Southboro, Massachusetts.

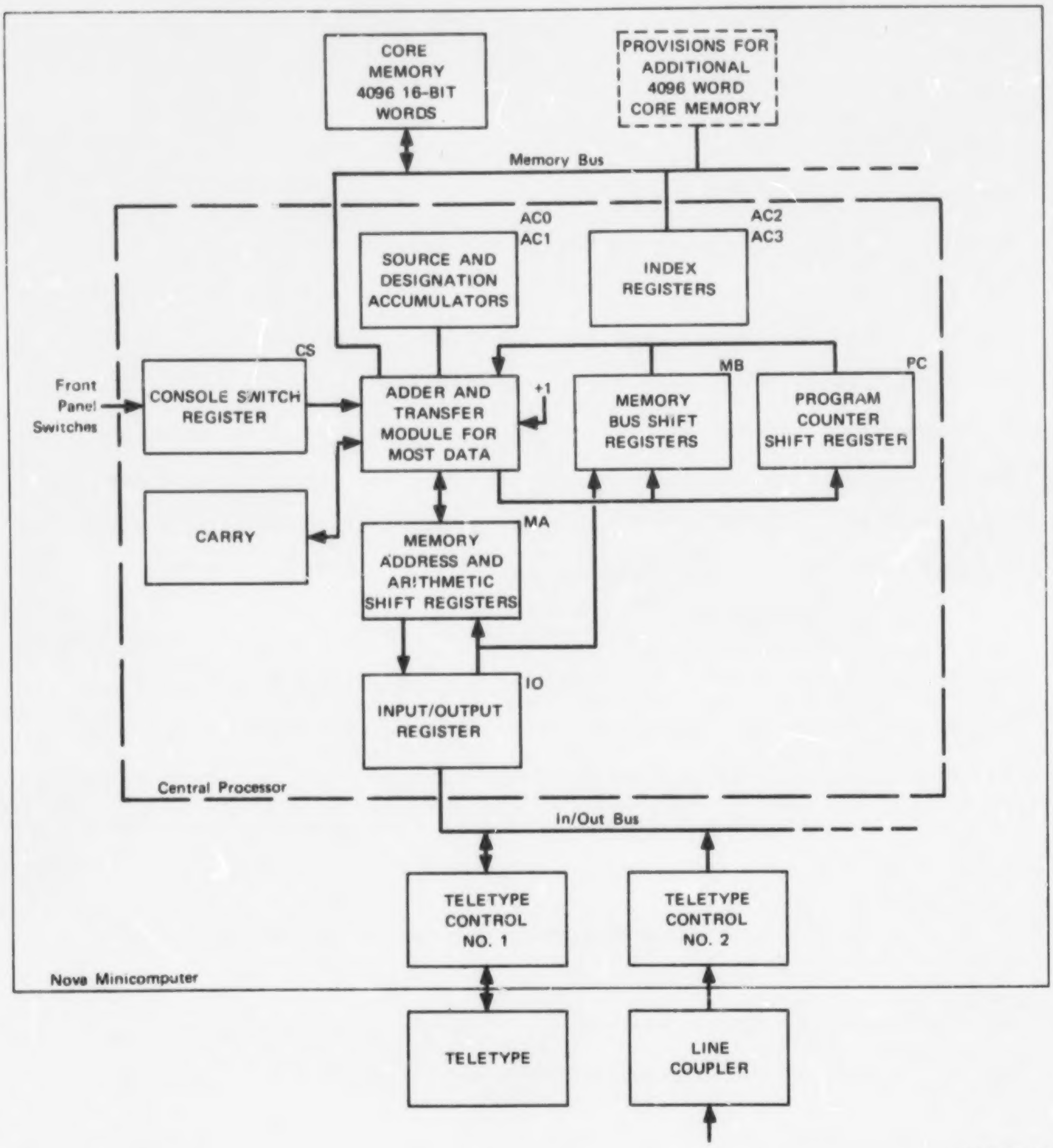
CORE MEMORY 4096 16-BIT WORDS
PROVISIONS FOR ADDITIONAL 4096 WORD CORE MEMORY
Memory Bus
AC0
AC1
SOURCE AND DESIGNATION ACCUMULATORS
AC2
AC3
INDEX REGISTERS
CS
Front Panel Switches
CONSOLE SWITCH REGISTER
ADDER AND TRANSFER MODULE FOR MOST DATA
+1
MB
MEMORY BUS SHIFT REGISTERS
PC
PROGRAM COUNTER SHIFT REGISTER
CARRY
MA
MEMORY ADDRESS AND ARITHMETIC SHIFT REGISTERS
IO
INPUT/OUTPUT REGISTER
Central Processor
In/Out Bus
TELETYPE CONTROL NO. 1
TELETYPE CONTROL NO. 2
Nova Minicomputer
TELETYPE
LINE COUPLER

TA-8563-31

FIGURE A-10 BLOCK DIAGRAM OF NOVA COMPUTER

Table A-4

CHARACTERISTICS OF NOVA COMPUTER

Operational:	
Word Size	16 bits
Memory Size	4096 words (expandable)
Cycle Time	2.6 μs
Number of Accumulators	4
Arithmetic	2's complement
Addressing	8-bit displacement, may be in page zero, or relative to either of two accumulators, or program counter
Physical:	
Dimensions	5-1/4-inch high, mounted in standard 19-inch rack
Power	115 V, 60 Hz, 6 A (with teletype)

data handling operations, and sequences the program. It is connected to the memory by a memory bus and to the peripheral equipment by an in-out bus. It is organized around four accumulators (AC0-AC3), two of which can be used as index registers. The arithmetic instructions operate on fixed-point binary numbers, either unsigned or equivalent signed numbers, using two's complement conventions.

Diagnostic programs are provided by the manufacturer to test various logic areas of the computer and I/O. The manufacturer also supplies special programs to help the user edit, assemble, load, and debug his programs. In addition, arithmetic subroutines are available with the computer.

c. Magnetic Tape Adapter

The magnetic tape adapter* provides the interfacing between the NOVA computer and the Kennedy digital magnetic tape recorder. An internal switch provides selection of either 556 or 800 BPI recording densities with a transport speed of 15 ips.

The "Write Data Lines" are active on the tape bus as "low-level" (true state) signals. Each of these "Write Data Lines" can be delayed, as needed. The read data lines from the tape transport carry high-level (true state) signals amplified by switching transistor circuitry.

Inter-Record Gap is produced by an internal clock. There is a 20-ms delay between the command "move" and Tape Unit Ready, which is triggered at the end of the RUN signal to allow the tape drive to stabilize.

d. Magnetic Tape Recorder

The tape recorder† is a seven-track synchronous digital magnetic tape recorder with dual gap read-after-write operation. A tape speed of 15 ips allows a read or write data transfer rate of 8.34 kHz at 556 BPI, or 12 kHz at 800 BPI. The lower density recording was used on this project. Selection of the recording densities can be accomplished either locally or remotely. The data were recorded on magnetic tape when the data storage block in the computer was filled, or when a data-collecting cycle was completed. Magnetic tapes were created to be compatible with the Control Data 6400 computer.

---

*Model 4035, Data General Corporation.

†Model 2812, Kennedy Co., Altadena, California.

This unit has the electronics necessary to control tape motion and the reading and writing. Available tape motion commands include the usual forward/reverse, run/stop, rewind, and so on. The formatting, parity generation, gap control, and the like, are provided from the Magnetic Tape Adapter.

Tape is controlled by a single capstan drive. When commanded to run, the capstan drive velocity servo responds to a linear ramp input, starting the tape with a constant acceleration. Since the capstan servo conforms almost identically to the ramp, start/stop times and distances are highly consistent and accurate. They are inversely proportional to rated tape speed (15 ips). In Rewind, start is a ramp of approximately 1/2-second duration to the rewind speed of 150 ips. Stop is an equivalent ramp to zero speed.

Write electronics produce NRZ1 (nonreturn to zero) recording. Data presented to the machine are recorded upon application of the "Write Data" strobe signal. NRZ1 recording continuously saturates the tape in either the positive or negative direction. The direction of current flow is altered to record a logic 1 and allowed to flow unaltered for a zero. This is the commonly used method of digital recording.

e. Teletype

A model 33-YZ teletypewriter* with a tape punch and tape reader provided a means of communicating with the NOVA computer. Entries into the computer are made either on the keyboard or by prepunched paper tape. Keyboard entries were usually used to prepare and debug programs or to start sampling. Prepunched paper tape was used to load computer programs.

---

*Teletype Corporation, Skokie, Illinois.

The five-minute summaries were always listed (see Figure D-1, Appendix D), and often punched on paper tape. The paper tape output was used as a backup for the magnetic tape records.

Appendix B

VAN INSTRUMENTATION SYSTEM

BLANK PAGE

Appendix B

VAN INSTRUMENTATION SYSTEM

1. Brief System Description

Two vans were used during the San Jose experiments. They were instrumented (Figures B-1 and B-2) for measuring carbon monoxide (CO) concentrations, temperature, and wind from a parked location, or CO concentrations and temperature while driving around selected city routes. All data plus voice comments were recorded on magnetic tape, and CO and temperature with superimposed event markers were recorded on a two-pen chart recorder. All equipment could be operated for an 8-hour period using wet batteries in the vans. The van engine was not run during stationary operation, so no CO was produced to bias the measurements. The effect of van-produced CO was minimized during driving by locating the sampling inlet at a height of about 3.5 m at the front of the van. Other equipment in the van included a battery charger, 115-V ac extension cord, a short ladder, and miscellaneous tools needed to be completely self-sufficient.

The CO analyzer air inlet and the wind sensors were mounted on vertical extendable antenna masts (Figure 19 in the text) modified for the purpose. It was possible to sample air from any height between 3 and 10 m. The wind sensor (which was stowed in the van during driving) was adjustable in height from about 3 to 5 m; however, it was usually operated at its maximum height when the van was stationary.

PRECEDING PAGE BLANK

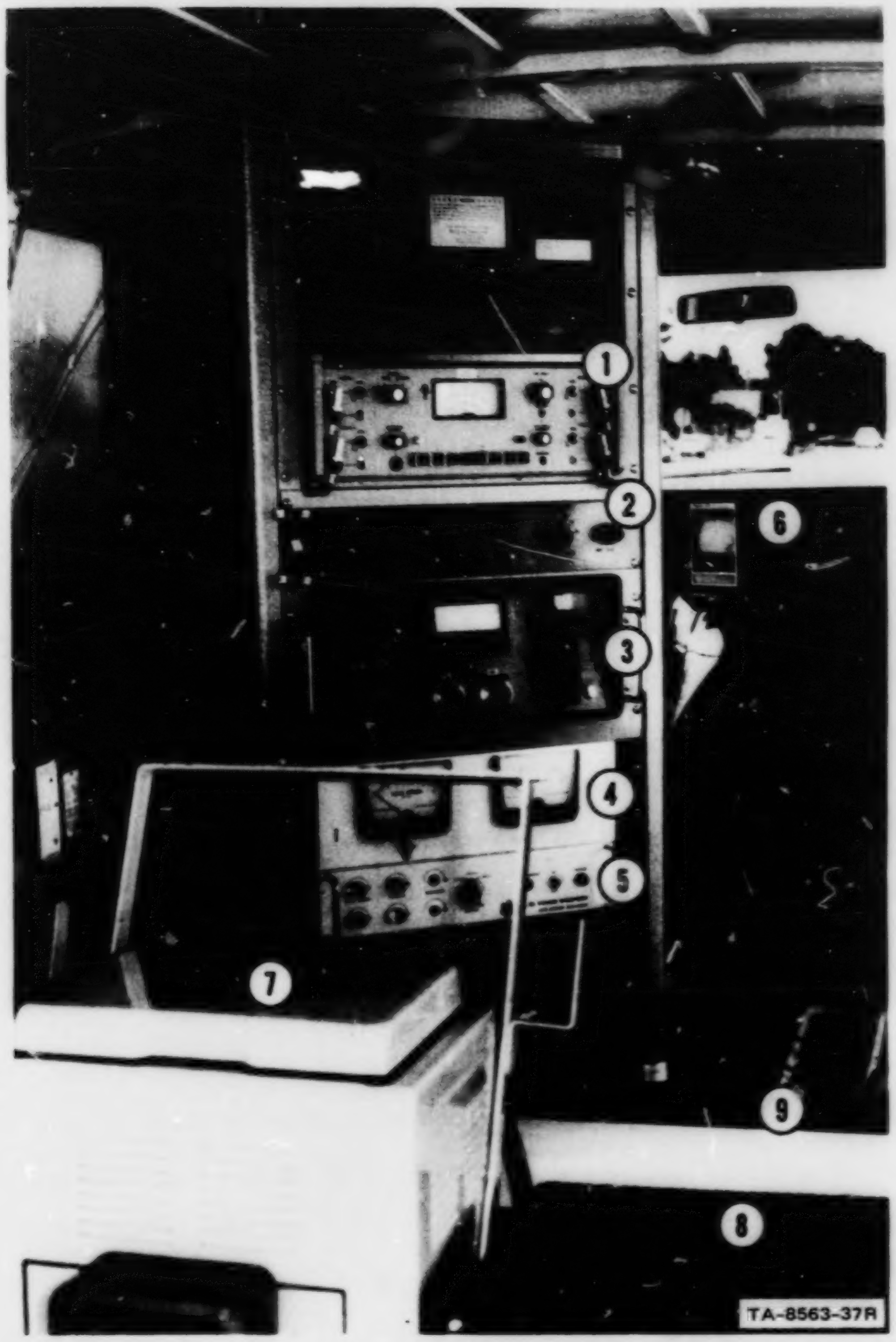

1. Magnetic Tape Recorder
2. Temperature/CO Signal Conditioner
3. CO Analyzer
4. Wind Indicator Panel
5. Power Supply Translator for Wind System
6. Dual Channel Chart Recorder
7. Battery Charger
8. 24 V dc to 115 V ac Inverter
9. Storage Batteries

FIGURE B-1 ELECTRONIC CONSOLE IN VAN

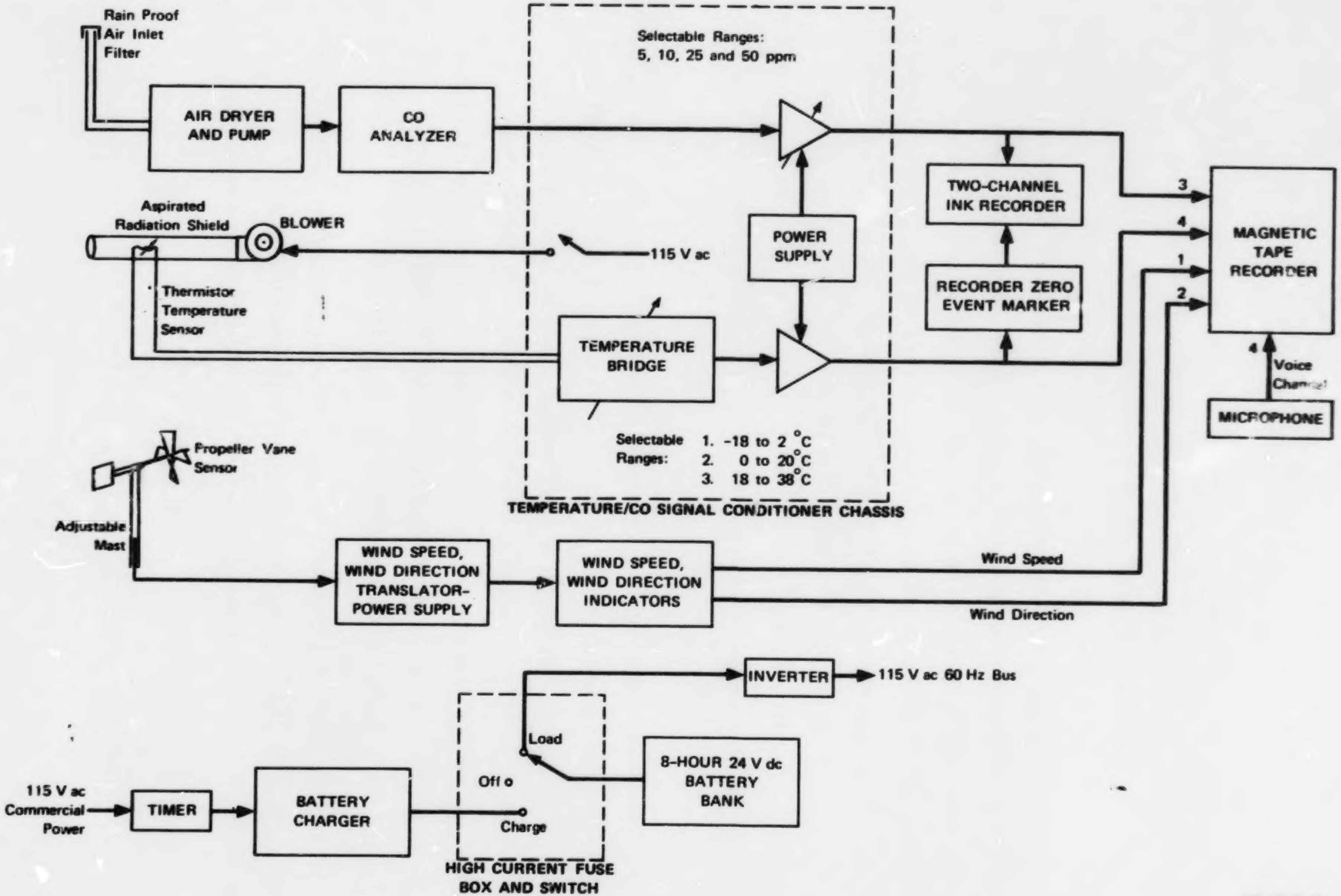
Rain Proof Air Inlet Filter
AIR DRYER AND PUMP
CO ANALYZER
Selectable Ranges: 5, 10, 25 and 50 ppm
Aspirated Radiation Shield
BLOWER
115 V ac
Thermistor Temperature Sensor
POWER SUPPLY
TEMPERATURE BRIDGE
Selectable Ranges: 1. −18 to 2 °C 2. 0 to 20°C 3. 18 to 38°C
TEMPERATURE/CO SIGNAL CONDITIONER CHASSIS
TWO-CHANNEL INK RECORDER
RECORDER ZERO EVENT MARKER
3
4
1
2
MAGNETIC TAPE RECORDER
4
Voice Channel
MICROPHONE
Propeller Vane Sensor
Adjustable Mast
WIND SPEED, WIND DIRECTION TRANSLATOR-POWER SUPPLY
WIND SPEED, WIND DIRECTION INDICATORS
Wind Speed
Wind Direction
INVERTER
115 V ac 60 Hz Bus
Load
Off o
Charge
8-HOUR 24 V dc BATTERY BANK
115 V ac Commercial Power
TIMER
BATTERY CHARGER
HIGH CURRENT FUSE BOX AND SWITCH

TB-8563-38

FIGURE B-2 BLOCK DIAGRAM OF VAN INSTRUMENTATION SYSTEM

2. Carbon Monoxide (CO) System

The Bacharach* CO analyzers used in the two vans and the helicopter are considerably smaller in size than the Beckman analyzers used with the fixed-station instrumentation system (Appendix A). The Bacharach analyzer combines a chemical and an optical technique for the automatic measurement of ambient carbon monoxide. The heterogeneous reaction between carbon monoxide and mercuric oxide is used to generate mercury vapor in the sample gas stream at a concentration proportional to the CO concentration. Optical absorption at the strong mercury absorption band, 2537 Å, in the near-ultraviolet is used to measure the resultant mercury vapor with high sensitivity. This combination of techniques provides a method for determining very low CO concentrations with a portable instrument, as has been demonstrated in the work of Robbins, Borg, and Robinson (1968).

The CO measurement system is shown schematically in Figure B-3, and its performance specifications are listed in Table B-1. Air is sampled through a filter installed in a rain shield outside the van on an adjustable mast. The air is passed through 1/4-inch-ID teflon tubing and into one of two silica-gel cartridges. Operation of the instrument requires that the air be dried, and silica-gel was used rather than the standard heatless air dryers in order to conserve power.

After drying, interfering hydrocarbons are removed by absorption in an activated charcoal filter. A diaphragm pump is used to avoid contamination from lubricants. Next, the sampled air is passed through

---

*Bacharach Instrument Company, 2300 Leghorn Avenue, Mountain View, California 94040.

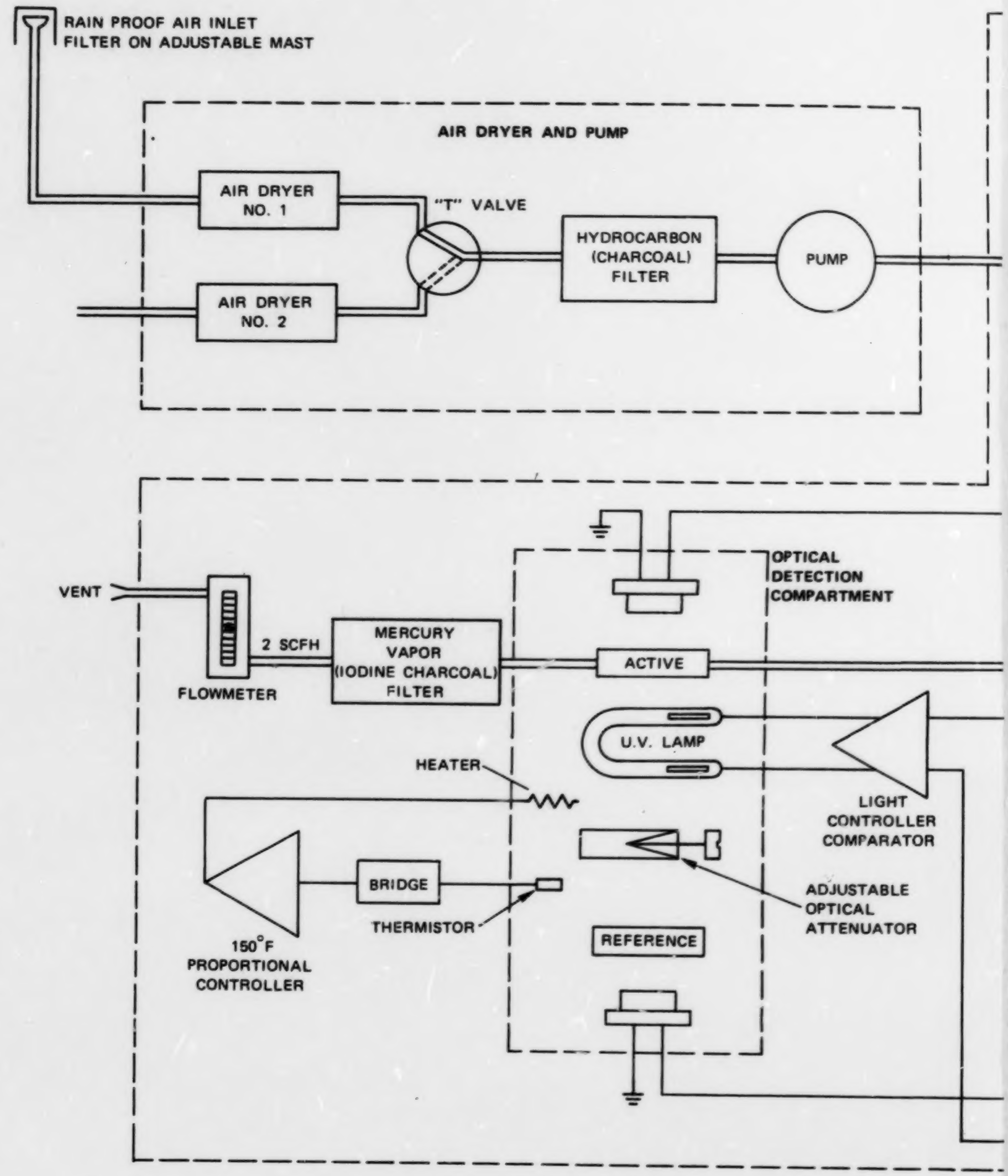
RAIN PROOF AIR INLET
FILTER ON ADJUSTABLE MAST
AIR DRYER AND PUMP
AIR DRYER NO. 1
AIR DRYER NO. 2
"T" VALVE
HYDROCARBON (CHARCOAL) FILTER
PUMP
OPTICAL DETECTION COMPARTMENT
VENT
2 SCFH
FLOWMETER
MERCURY VAPOR (IODINE CHARCOAL) FILTER
ACTIVE
U.V. LAMP
HEATER
LIGHT CONTROLLER COMPARATOR
BRIDGE
THERMISTOR
ADJUSTABLE OPTICAL ATTENUATOR
REFERENCE
150°F PROPORTIONAL CONTROLLER

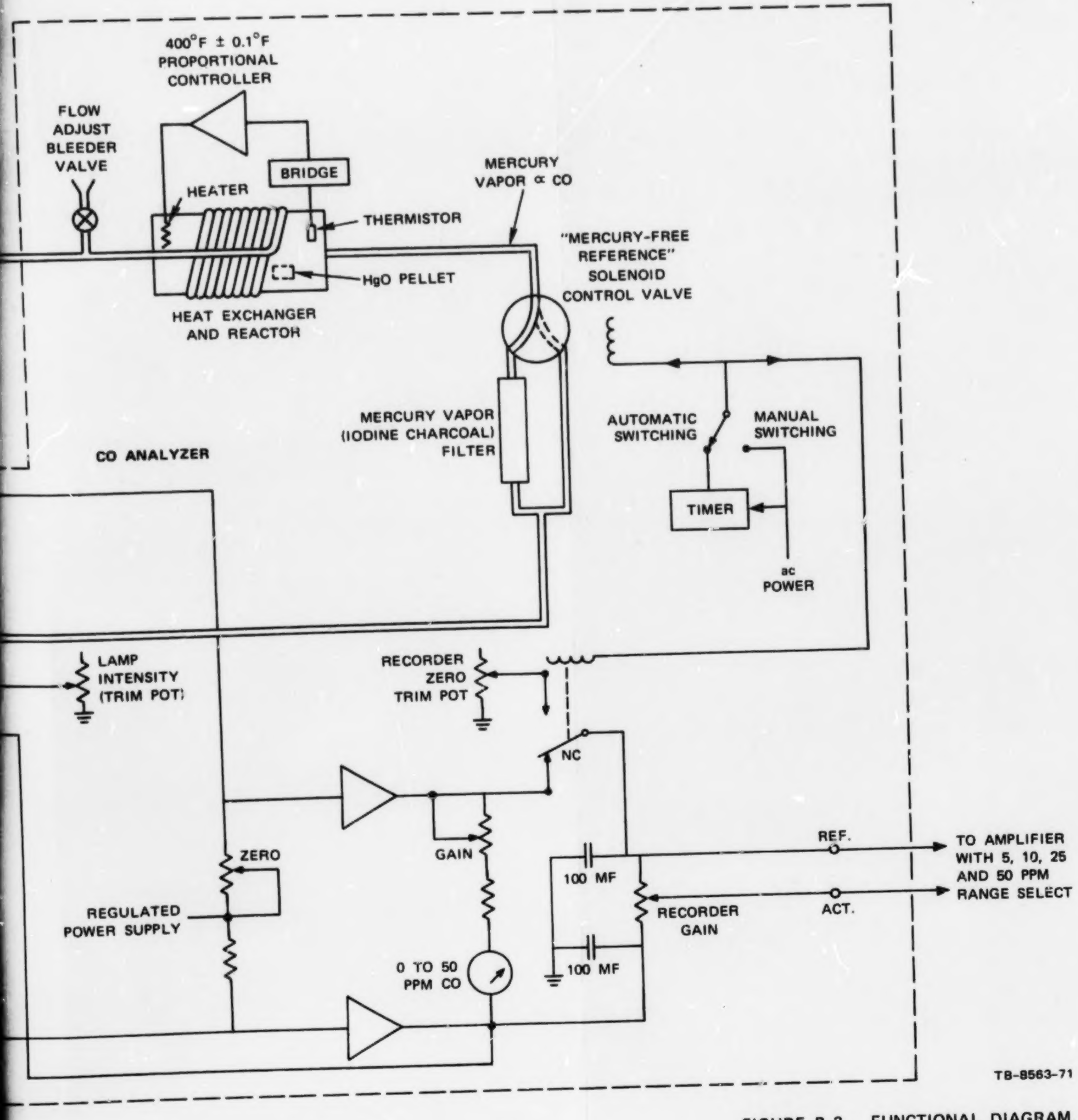
400°F ± 0.1°F
PROPORTIONAL
CONTROLLER
FLOW
ADJUST
BLEEDER
VALVE
BRIDGE
HEATER
MERCURY
VAPOR ∝ CO
THERMISTOR
"MERCURY-FREE
REFERENCE"
SOLENOID
CONTROL VALVE
HgO PELLET
HEAT EXCHANGER
AND REACTOR
MERCURY VAPOR
(IODINE CHARCOAL)
FILTER
AUTOMATIC
SWITCHING
MANUAL
SWITCHING
CO ANALYZER
TIMER
ac
POWER
LAMP
INTENSITY
(TRIM POT)
RECORDER
ZERO
TRIM POT
NC
ZERO
GAIN
REF.
TO AMPLIFIER
WITH 5, 10, 25
AND 50 PPM
RANGE SELECT
100 MF
ACT.
RECORDER
GAIN
REGULATED
POWER SUPPLY
0 TO 50
PPM CO
100 MF
TB-8563-71

FIGURE B-3 FUNCTIONAL DIAGRAM, VAN AND HELICOPTER CARBON MONOXIDE MEASURING SYSTEM

B

Table B-1

MANUFACTURER'S STATED PERFORMANCE SPECIFICATIONS FOR THE MERCURIC OXIDE REDUCTION CO ANALYZER

Operating Specifications:		
Range	0 to 50 ppm	
Flow rate	$2\ ft^3\ h^{-1}$	
Output	0 to 0.5 V	
Linearity:		
0-20 ppm	good	
>20 ppm	nonlinear (curve provided)	
Zero drift (average)	1.5 ppm in 12 h	can be greater with large ambient temperature fluctuations
Span drift (positive)	3 percent in 24 h	
Response		
lag	10 s	
rise time	15 s	
fall time	18 s	
Minimum detectable CO concentration	0.1 ppm	
Reproducibility	±2 percent	
Warm-up time	30 minutes	
Environmental Specifications:		
Ambient temperature range	0 to 125° F	
Shock and vibration	can operate in normal mobile uses	
Physical Specifications:		
Weight	20 lb	
Power	60 to 80 watts, 115 V ac ±10 percent 60 Hz	

1/4-inch-ID teflon tubing to the CO analyzer chassis. Flow is adjusted to 2 ft^3 h^{-1} using a bleeder valve and an end-of-line flowmeter. The purified, dried, regulated air next flows to a heat exchanger/reactor module, where it is preheated to the reactor temperature. The reactor is maintained at 400 ±0.1° F by a thermistor-bridge, proportionally controlled heater. At this operating temperature, the mercuric oxide produces a mercury vapor background by thermal decomposition. In the reactor the air contacts a mercuric oxide pellet and the CO produces mercury vapor by the reaction:

$$CO + HgO \xrightarrow{400^\circ\ F} CO_2 + Hg_v \quad .$$

The output of interest from this reactor is the sum of the thermally produced and the CO-generated mercury vapor.

When CO concentrations are monitored, the hot, mercury-laden gas is routed through a two-way solenoid valve to an "active" absorption cell in the optical detection compartment. When activated, this solenoid valve passes the mercury-laden gas through an iodine charcoal filter to remove mercury vapor. This provides a mercury-free "reference" to the active absorption cell. This signal can be used to correct for drift in the optical detection compartment and its associated circuitry. The solenoid can be switched either manually or automatically at regular intervals to provide this reference signal.

The mercury-free gas produces an arbitrary reference base line on the recorder, but the actual zero CO level is obtained by calibrating with a reference zero gas. Helium was used as the zero gas since it has been shown to be essentially CO free. The "true" zero signal includes the contribution from the thermally produced mercury vapor.

In the automatic switching mode, the mercury-free air reference signal was produced for 45 seconds, once every 5 minutes. This signal was summed with an offset voltage whose amplitude was adjusted by means of a trim pot. The polarity of this offset voltage provided up-scale recording of mercury-free air reference signals, allowing use of the full chart width for recording the atmospheric CO concentration.

When the hot, mercury-laden gas passes through the absorption cell in the optical detection compartment, ultraviolet light from a mercury lamp is passed through the gas and detected by a photocell that serves as one leg of a bridge. A second photocell with a separate optical cell provides a compensating reference in a second leg of the measuring bridge circuit. Close control of the UV lamp intensity was obtained by a UV source oscillator/controller tied into the "reference" leg of the photocell bridge circuit. A trim pot was provided for adjustment of the lamp intensity. Temperature of the compartment was maintained at 150° F by use of a second proportional controller and associated circuitry.

The active and reference photocell bridge circuitry included a zero control to provide fine zero adjustment for zero gas calibration. The bridge output circuit has two "gain" pots to adjust the calibration of the instrument, using a span gas of known CO concentration. One pot is used to adjust the meter reading on the front panel to the correct value. The second control is used to set the up-scale (span) reading of the chart and magnetic tape recorders. Electronic filtering reduces noise to the recorders.

An iodine filter at the exhaust of the instrument removes mercury vapor before venting.

The electronic CO concentration signal from the CO analyzer chassis goes to a separate differential amplifier on the air temperature/CO analyzer signal conditioner chassis (Figure B-3). This amplifier has selectable ranges for full-scale recorder readings of 5, 10, 25, and 50 ppm of CO (see Figure B-2). The switch can also short the input of the recorders electrically for recorder zeroing; a low-impedance short between the differential amplifier inputs is also available for adjusting the amplifier zero.

3. Temperature Instrumentation

The van temperature sensor was a thermistor* installed in an aspirated radiation shield mounted on top of the van as shown in Figure 19. The thermistor served as one leg of a bridge network. The bridge output was amplified and input to a chart and a magnetic tape recorder.

The thermistor was suspended in a 6-inch-long, 1-inch-OD polystyrene tube. This tube was glossy white outside and flat black inside. It was located concentric with and near the front of a larger outer tube. This larger tube was 1-5/8 inches ID, aluminum, 5 ft long. The aluminum tube was also black inside and white outside. The aspirator motor was at the opposite end of the tube from the thermistor, toward the rear of the van. The aspirator power was controlled inside the van from the same chassis that contains the temperature bridge and amplifier. This unit is pictured in Figure B-1.

The aspirated radiation shield minimizes errors from self-heating of the sensor. The self-heating error at a ventilation rate of 10 mi h^{-1} is less than 0.1° C, and was neglected. The time constant of the aspirated thermistor is 8 seconds.

---

*Veco 34D1.

A Wheatstone bridge was used with the thermistor as one leg. Any of three ranges could be selected: -18 to 2° C, 0 to 20° C, or 18 to 38° C. Values of bridge resistors were chosen for optimum linearity. Low-temperature-coefficient trim potentiometers were incorporated for zero and span adjustments during calibration.

Mercury batteries provided a stable bridge voltage source. Battery drift was checked with a reference potentiometer (with locking provisions), which was adjusted immediately after calibration to give full-scale output on the middle range. The reference can be switched into the circuit to check whether the supply voltage has changed.

The bridge output served as input to a differential amplifier on the same chassis. Switches were provided for zeroing the recorder and amplifier during calibration.

4. Wind Instrumentation

A Gill propeller vane* was used on the van for wind measurements. It has a 9-inch, four-blade helicoid propeller coupled to a miniature dc tachometer generator. The voltage output is directly proportional to rpm from 2.7 mi h^{-1} to 100 mi h^{-1}. Below 2.7 mi h^{-1}, slippage increases down to the threshold speed (approximately 0.5 mi h^{-1}). The voltage to the magnetic tape recorder is unipolar and adjustable from 0 to approximately 5.5 V dc for full scale on the 50-mi h^{-1} range.

A low-density foamed polystyrene vane, which is coupled to a precision linear conductive plastic type potentiometer, was used for wind direction measurements. A regulated power supply provides a constant voltage to this potentiometer to produce voltage output directly proportional to the azimuth angle of the vane, over 342 degrees of azimuth. The output voltage is unipolar and is adjustable from 0 to approximately ±8 volts.

---

*Model 35002/35402/35602, R. M. Young Company.

The wind speed system was calibrated in the same way as the wind component (UVW) sensors at the fixed station (see Appendix A). Wind direction calibration uses circuitry in the translator unit. A calibration switch provides a signal that corresponds to either the zero-degree position or the full-scale vane position. The wind vane was oriented to give the proper wind direction reading when it was aligned with the street. The mast supporting the wind sensor could be adjusted to the vertical, as determined from a level mounted on it. The wind sensor was taken from the mast whenever the van was moved.

5. Recorders

Chart and magnetic-tape analog-signal recorders were used with the van instrumentation. We used a dual channel Beckman Model 2550 servo-balanced potentiometer type strip chart recorder.

An event marker can be superimposed on the temperature trace by pushing a button within reach of the van driver. This back-loaded the temperature amplifier with a resistor that simulated the recorder input impedance, presenting a low-impedance (100 ohm) short to the recorder. This causes the recorder to return to its zero voltage position, providing an event mark. The event marks were numbered on the chart paper and in the operator's log.

The magnetic tape recorder was a standard Hewlett-Packard model 3960-A four-channel FM-type recorder. Voice comments could be recorded on Channel 4 while the van was being driven. When the van was parked, this channel was used primarily for recording the temperature signal with occasional voice comments superimposed.

6. Primary Power System

Primary power for the van was provided by four, 12-volt, 210-ampere-hour batteries[*] connected in series-parallel to provide 420 ampere-hours of primary power at 24 volts dc. These batteries were diesel truck type that allowed "deep cycling," i.e., they can be completely discharged and recharged each day without damage, unlike most vehicle batteries. The same batteries were used during the entire experimental period.

A commercial 40-A battery charger,[†] a separate timer, and a heavy-duty extension cable were installed in the van to be used for recharging the batteries during the night when the van was not in experimental use. The battery condition was periodically monitored with a hydrometer. A 60-A house-type double-pole, double-throw pull box was installed to remove the electrical load from the batteries and to connect the charger.

A Topaz model 1000GW 24-V dc to 115-V ac inverter[‡] was mounted near the batteries and supplied power to the various instruments. This high-quality inverter produces a low-harmonic-content sine-wave output. It is well regulated to provide stabilized 60 ± 1.0 Hz power output.

---

[*] Prestolite 8908X.

[†] Exide EM-40.

[‡] Topaz Electronics, San Diego, California.

A wooden frame constructed of 2 x 10-inch lumber coated with acid-proof paint secured the batteries over the rear axle of the van. Solidly secured batteries and equipment were important for safety in case of an accident or sudden stop.

7. Equipment Installation

The electronic units were installed in a standard 19-inch panel mounting cabinet which was 24 inches deep and 4 ft tall. It was shock mounted to a 3/4-inch-thick circular plywood base that was center bolted to the van floor. This "lazy susan" allowed the cabinet to be rotated for easy access. A safety cable was attached to the top of the cabinet to prevent forward travel in an accident. The cabinet could be oriented to provide for operation from either the driver's or passenger's seat. There is enough space to allow passage from the seats to the rear of the van.

The pump and air dryer assembly for the CO analyzer was located on the floor of the cabinet. This allowed easy replacement of the silica-gel cartridges. The cartridges were removed in the evening and dried by baking in an oven until the silica-gel crystals turned bright blue. This usually took about 2 hours.

The two-channel ink recorder was installed in the van on the engine cover (Figure B-1). A felt-lined wooden box housed the recorder and allowed the driver to write identification numbers on the chart paper periodically for later correlation with experimental notes.

Appendix C

HELICOPTER INSTRUMENTATION SYSTEM

BLANK PAGE

Appendix C

HELICOPTER INSTRUMENTATION SYSTEM

1. Brief System Description

The helicopter instrumentation recorded CO concentration, air temperature, and altitude. The air inlet and the temperature sensor were mounted on the helicopter skids ahead of the cockpit so that the effects of rotor downwash could be avoided by maintaining the helicopter's forward speed. The pressure transducer for the altimeter was inside the unpressurized cockpit.

The recorder, CO analyzer chassis, and the temperature/pressure bridge chassis were separated by padding and stacked on the seat between the pilot and the observer as shown in Figure C-1. This equipment was secured with a safety strap. The pump and dryer package for the CO analyzer was placed on the floor beneath the experimenter's legs. A 12-V dc to 115-V, 60-Hz ac inverter was installed with rain protection on the outside cargo rack where the pilot could turn it off or on. All the equipment was designed to operate within the limitations of available power from the helicopter's electrical system.

The CO analyzer used on the helicopter was the Bacharach instrument described in Appendix B. It differed from the version used in the two vans only in that it was painted white to minimize solar heating in the "bubble" cockpit.

PRECEDING PAGE BLANK

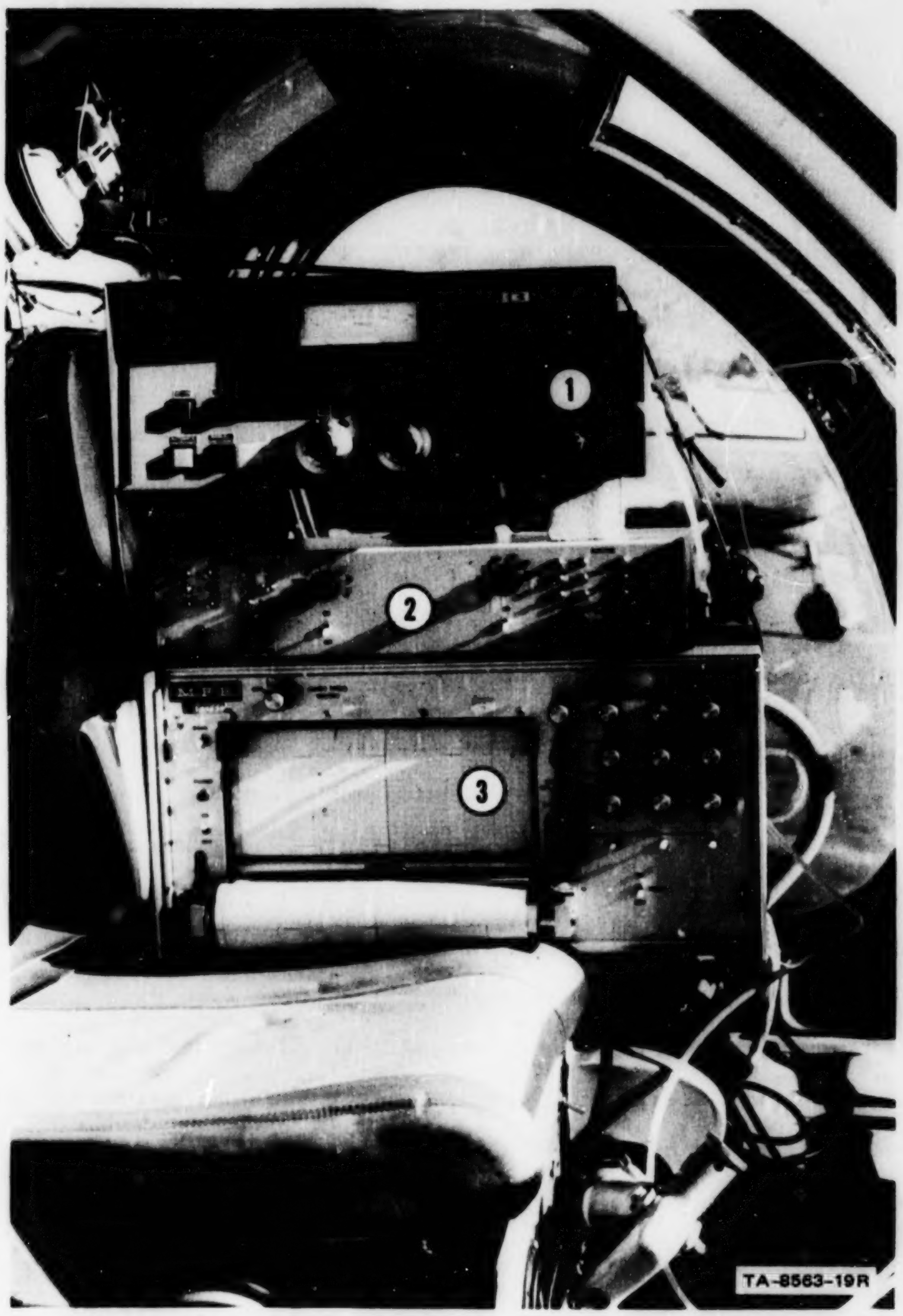
1
2
3
M.F.E.
TA-8563-19R

1. CO Analyzer
2. Temperature/Pressure Bridge Chassis
3. 4-Channel Chart Recorder

FIGURE C-1 HELICOPTER INSTRUMENTATION

2. Temperature System

The helicopter temperature instrumentation used a thermistor in a radiation shield on the helicopter skid, and bridge network. The bridge output was recorded by a chart recorder with a differential amplifier input.

The radiation shield has two 6-inch-long, concentric cylinders. The smaller was 1-inch-ID polystyrene, glossy white outside and flat black inside. Two VECO 33D12 thermistors were mounted at the center of this cylinder. The 1-11/16-inch-OD brass outer shield has a 1/32-inch wall that is chrome plated outside and flat black inside. The inner cylinder is centered and supported by machine screws in the outer cylinder. Ventilation is provided by the forward motion of the helicopter. With this ventilation the time constant is less than 2 seconds, and self-heating is negligible.

The two thermistors, connected in parallel to reduce self-heating errors, formed one leg of a Wheatstone bridge. A gang switch selects any of six ranges: -18 to -8, -9 to 1, 0 to 10, 9 to 19, 18 to 28, or 27 to 37° C. The many ranges were used to increase resolution, which was restricted by the recorder chart width. The bridge resistors were chosen for optimum recorder scale linearity. The maximum deviation from linearity on any range is 0.25° C. D-size mercury batteries provide a stable voltage for the bridge. Battery drift could be checked with a reference potentiometer as in the van's temperature measuring system (see Appendix B). The bridge circuitry and its batteries were mounted in a 3.5 x 17 x 14-inch chassis that also housed the pressure sensing system described in the next section.

The sensor was calibrated in a temperature control chamber at two temperatures for each range, one near the low end of the range and one near the upper end. Trim pots were available for each range for adjusting the circuitry to give correct readings. Adjustments were made first for the low-end temperature using a pot in the leg of the bridge opposite the thermistors. Adjustments at high-end temperatures were made using a potentiometer that controlled the voltage applied to the bridge. The adjustments were repeated to minimize errors that might arise because the two adjustments are not totally independent.

3. Altitude-Recording System

During the San Jose experiment, altitude was determined from the helicopter's altimeter and periodically marked on the chart records by the operator. A system was designed and built that had been planned to provide a primary record of altitude but was actually used only as a backup to the altimeter. Its resolution was less than originally planned because the desired transducer could not be delivered in time for the experiment.

One major problem in the design of an inexpensive pressure-sensing, altitude-recording system is that of altitude resolution. The atmospheric pressure might only go from 14.7 psi at sea level to approximately 12.3 psi at 5000 feet. A pressure transducer with a 3-psi full range containing a bellows with an internal reference pressure of 12 psia appears to be a logical choice. However, this 12-psia reference will vary as temperature and cannot be used without costly corrections. This temperature error becomes negligible as the reference pressure is reduced towards zero, but this also reduces resolution. A bellows with a near vacuum internally is relatively insensitive to temperature fluctuations, but has a smaller movement for a given pressure change.

The pressure transducer used in the helicopter system has a bellows-actuated potentiometer that serves as two legs of a bridge. Output voltage is measured at the movable contact. Any one of seven ranges can be selected: 0 to 1000 ft, 900 to 1900 ft, 1800 to 2800 ft, 2700 to 3700 ft, 3600 to 5600 ft, and 5400 to 7400 ft. A larger part of the chart width can be used by having a large number of available ranges. Nevertheless the nature of the transducer limited the resolution to about 88 feet.

Variations in atmospheric pressure from day to day would produce errors in recorded altitude if adjustments were not made. A dual ganged potentiometer in the bridge circuit was used to adjust the reading to the correct airport altitude before takeoff. The ganged potentiometers were wired as opposing rheostats in adjacent legs of the bridge and connected to the ends of the pressure transducer element. Adjustment caused an effect in opposition to that introduced by the atmospheric pressure variations at the time of adjustment.

The pressure transducer was calibrated in the laboratory in a partially evacuated bell jar. Trim potentiometers in the circuitry were adjusted to give the same readings as the pressure transducer at selected "altitudes." Once set, these potentiometers could be switched into the circuits later to provide field simulation of seven heights ranging from 50 to 7300 ft.

The output of the bridge was recorded on a chart recorder with a high-input-impedance differential amplifier. All the circuitry and the transducer were installed on the same chassis as the temperature measurement circuitry.

4. Chart Recorder

Power, space, weight, and cost were important factors in the recorder selection. The MFE Model 24C-AHA recorder* was used. It has three channels to record CO, temperature, and altitude and a fourth for possible future measurement of humidity. Amplification is provided internally by a high-gain, high-input-impedance differential amplifier, as required for the relatively low bridge output signals. It uses thermal writing, which is preferable to ink for use in a helicopter.

---

*Mechanics for Electronics, Inc., Wilmington, Massachusetts.

The recorder has a narrow chart. Each record is confined to a strip only 5 cm wide with 1-mm divisions. The four records are written side by side on the chart. There are four chart speeds, ranging from 1 to 50 mm s^{-1}, also with 1-mm divisions. One event marker and one timer marker were included. Calibration is provided by an internal 20-mV signal.

Appendix D

DATA PROCESSING

BLANK PAGE

Appendix D

DATA PROCESSING

1. Streetside Data

The San Jose Streetside data were obtained with a data-acquisition system under the control of a Data General NOVA mini-computer* and recorded on a Kennedy magnetic tape recorder (Model 2812).† These data consisted of a station identifier, CO level number, CO concentration, instrument status code, wind speed and direction, temperature, date, time and other measurements. These were stored by groups in the computer memory whenever one of the various sensor units was activated upon command by the computer. The data were recorded on magnetic tape when the data storage block in the computer was filled, or when a data-collecting cycle was completed.

The data collection cycles were generally 5 minutes long. During a cycle, CO concentration was recorded for each of the five levels at each of the stations. Also recorded during a cycle were five values of wind speed and direction for each of the locations that used cup and vane sensors. Similarly, five sets of readings of temperature gradient information were recorded for each of the two stations at which these parameters were measured, as were approximately 125 values of each of the wind component values. Also, other recorded material included information on equipment operation, e.g., bridge voltages, range factors,

---

*Data General Corp., Southboro, Massachusetts.

†Kennedy Co., Altadena, California.

PRECEDING PAGE BLANK

and so on. At the end of each cycle, the data were averaged for the period. These averages were summarized on the tape and printed out on the teletype for real-time monitoring of system operation. Figure D-1 is a sample of this real-time summary printout.

The first word of each magnetic tape record was assigned either a 0 or 1 (0 identified a data record and 1, a summary record). Records were of variable length and each was made up of variable-length subunits, which we will refer to as "groups." Each group was preceded by two words containing the addresses of the first and last words. These addresses defined the number of words in that group. The last two words in a group were the date and time of the sample. The end of a record was signified by 7777 following the last data group. Either an "end of file" or a blank record signified the end of tape. The magnetic tape was created to be compatible with the Control Data 6400 computer. Ten NOVA computer-stored data words are contained in three CDC 6400 computer words (60 binary bits per word). Hence, a record of data could easily be buffered out, masked, and operated on. A density of 556 bits per inch, odd parity mode, and seven-track tapes were used.

A new tape was written by the large computer. This tape contained all the information on the original field data tapes. In creating this new tape, the data were converted to engineering units (from the originally recorded voltages). Some of the editing and data correction was also accomplished at this time. For instance, data from certain instruments were eliminated during periods when those instruments were known to be operating improperly. Where connections were incorrect, they were reassigned properly at this step. For instance, the inlets from two CO sampling levels had been reversed; the readings were attributed to the proper level in the rewritten tape. Similarly, there was some confusion

```
12/11/70 1838

U,V,W 1/100'S MPH
A +00108 -00036 -00072 +00252 +00072 +00000
  +00108 +00072 +00072 +00144 +00072 +00072
C +00072 +00072 +00108 +00072 -00144 +00000
  +00072 +00072 +00072 +00108 +00144 +00072

CO 1/100'S PPM
B +00780 +00741 +00507 +00702 +00546
D +00585 +00507 +00390 +00390 +00429
E +00702 +00819 +00897 +01014 +01014
F +01677 +01092 +01131 +01014 +00858
G +00936 +00819 +00741 +00741 +00663
H +01521 +01365 +01053 +01638 +01092
I +00663 +00663 +00702 +00624 +00585

   TABS    DT1    DT2    DT3    DT4
B -00255 -00005 -00014 +00000 -00017
D -00250 -00002 -00007 -00004 -00013

WIND VEL  WIND DIR
E +00083 +00118
F +00125 +00039
G +00200 +00000
I +00208 +00101
H +00196 +00104
```

*Parameters

Average Wind Components at Lower and Upper Levels
Standard Deviations of Wind Components
Average Wind Components
Standard Deviations

Observed CO Concentrations at Levels 1 Through 5

Temperature 1/10°C and ΔT's 1/100°C
(Temperature Sensor not Connected)

Average Wind Speeds (1/100 mi h^{-1}) and Wind Directions (degrees, relative to First Street)

*Letters used as station identifiers in this printout
A = 1, B = 2 . . . I = 9

TA-8563-20

FIGURE D-1 EXAMPLE OF REAL-TIME SUMMARY PRINTOUT among the various wind components. In translating the tape, the observations were converted to a single right-handed coordinate system for all sensors. An example of the information contained on the tape generated by the CDC 6400 processing is shown in Figure D-2. At this point in the data processing, the data had not been corrected to account for drift of calibration in the CO analyzers. In general, the instruments were calibrated sometime during the first 2 or 3 hours of operation each day. Usually they read within ± 0.5 ppm of the analyzed zero or span gas values when these gasses were introduced for calibration. If not, the error was recorded in a notebook. For those cases where there were calibration changes greater than 0.5 ppm, the following correction was applied to the recorded CO values:

$$C_c = \left(C_R - C_o\right) \cdot \frac{19}{C_{19}} \quad ,$$

where C_c is the corrected value, C_R is the recorded value, and C_o and C_{19} are the readings when the zero gas and the 19 ppm span gas were introduced. The zero gas was introduced first, and the instrument was adjusted to read zero; then the span gas was introduced and that adjustment made. The correction was usually applied to those data collected between the time the instrument was put on line and the time it was calibrated. In a few special cases where the instrument was recalibrated during the day, the correction was applied for a period of an hour or two before the recalibration.

To this point the complete data set was still on tape and there had been no attempt to digest or simplify the records. We learned that it was difficult to obtain statistical summaries of the data from the unconsolidated tapes. For this reason we decided to produce a new tape where each record corresponds to one of the cyclical 5-minute data

1.0	701123.0	105449.2	30.0	-0.0	.3	-0.0	-.6	-.3	-0.0
3.0	701123.0	105450.4	15.0	-1.2	-.7	-1.9	1.3	0.0	.2
1.0	701123.0	105451.4	30.0	-0.0	.2	-.2	-.5	-.2	-.2
3.0	701123.0	105452.4	40.0	1.8	1.5	-.4	.3	-.2	4.3
1.0	701123.0	105453.4	30.0	-0.0	0.0	-.2	-.5	-.2	-0.0
3.0	701123.0	105454.4	35.0	1.5	.2	-0.0	-2.0	0.0	-1.7
1.0	701123.0	105455.4	30.0	-.2	0.0	-.2	-.5	-0.0	-0.0
3.0	701123.0	105456.4	40.0	2.0	1.7	-0.0	.3	-.2	3.7
1.0	701123.0	105457.4	30.0	-0.0	0.0	-.2	-.5	-0.0	-0.0
3.0	701123.0	105458.4	34.0	1.0	.3	-.2	-3.3	1.2	-1.7
1.0	701123.0	105459.3	30.0	-0.0	0.0	-.4	-.5	-0.0	-0.0
3.0	701123.0	105500.3	40.0	2.2	1.7	-.2	.3	-.2	3.1
10.0	701123.0	1050.0	1054.0	.2	163.6	.5	257.9	8.1	4.9
2.0	701123.0	105621.5	5.0	2.3	99.9	99.9	99.9	99.9	99.9
2.0	701123.0	105621.5	5.0	99.9	-1.0	-1.0	-128.0	1.0	29.0
4.0	701123.0	105623.1	5.0	1.2	99.9	99.9	99.9	99.9	99.9
4.0	701123.0	105623.1	5.0	99.9	0.0	67.0	-128.0	69.0	93.0
5.0	701123.0	105623.8	5.0	3.5	.3	188.3	-.3	.0	28.0
6.0	701123.0	105624.5	5.0	7.0	1.1	197.4	-1.1	.3	61.0
7.0	701123.0	105625.2	5.0	4.3	.5	320.3	.4	.3	62.0
8.0	701123.0	105625.9	5.0	3.5	.0	39.3	.0	-.0	62.0
9.0	701123.0	105626.5	5.0	4.7	.7	999.9	99.9	99.9	-97.0
1.0	701123.0	105627.5	29.0	-.3	0.0	-.4	-.5	-.2	-0.0
3.0	701123.0	105628.5	11.0	-3.3	1.7	-1.9	-.2	0.0	-.4
1.0	701123.0	105629.5	29.0	-.3	0.0	-.4	-.3	-.2	-.2
3.0	701123.0	105630.5	40.0	1.5	1.0	-0.0	-.2	-3.5	-1.7
1.0	701123.0	105631.5	30.0	-.3	.2	-.4	-.3	-.2	-.2
3.0	701123.0	105632.5	31.0	.3	.3	-0.0	-3.3	1.5	-2.5
1.0	701123.0	105633.5	30.0	-.3	.3	-0.0	-.3	-.2	-.2
3.0	701123.0	105634.5	29.0	0.0	-.2	1.4	1.3	1.0	-.4
1.0	701123.0	105635.4	30.0	-.2	.3	-0.0	-.3	-0.0	-.4
3.0	701123.0	105636.4	8.0	-3.7	1.7	-1.9	.3	0.0	-.4
1.0	701123.0	105637.4	30.0	-.2	.2	-0.0	-.3	-0.0	-.8
3.0	701123.0	105638.4	40.0	1.7	1.5	-0.0	0.0	-.2	3.1
1.0	701123.0	105639.4	30.0	-.2	.2	-0.0	-.3	-0.0	-.4
3.0	701123.0	105640.4	35.0	1.2	0.0	-0.0	-2.2	0.0	-2.3
1.0	701123.0	105641.4	29.0	-.2	.2	-0.0	-.3	-0.0	-.2
3.0	701123.0	105642.4	40.0	1.5	1.5	-0.0	-.2	0.0	3.5
1.0	701123.0	105643.4	30.0	-.3	0.0	-0.0	-.3	-0.0	-0.0
3.0	701123.0	105644.4	37.0	1.2	0.0	.2	-.5	-1.8	-1.9
1.0	701123.0	105645.3	30.0	-.3	-.2	-0.0	-.3	-0.0	-0.0
3.0	701123.0	105646.3	40.0	1.5	1.5	-.2	-.3	0.0	4.1
1.0	701123.0	105647.3	30.0	-.5	-.2	-0.0	-.3	-0.0	-.2
3.0	701123.0	105648.3	36.0	1.0	0.0	-0.0	-.5	-1.3	-2.1
1.0	701123.0	105649.3	30.0	-.5	0.0	-0.0	-.2	-0.0	-.4
3.0	701123.0	105650.6	29.0	0.0	0.0	4.3	1.3	1.5	-.6
1.0	701123.0	105651.5	30.0	-.5	-.2	-.2	-.2	-.2	-.2
3.0	701123.0	105652.5	21.0	0.0	-2.2	-1.9	1.0	0.0	-.4
1.0	701123.0	105653.5	29.0	-.3	-.2	-.6	-.2	-.2	-.2
3.0	701123.0	105654.5	40.0	1.5	1.7	-.4	0.0	-.2	3.9

<table>
<tr><td>If No. in 1st Column is:</td><td colspan="9">LEGEND</td></tr>
<tr><td rowspan="2">Station No. 1 or 3</td><td rowspan="2">Date (11/23/70) in this case)</td><td rowspan="2">Time (nearest 1/10 sec)</td><td rowspan="2">Instrument Status Indicator</td><td>u_1</td><td>v_1</td><td>w_1</td><td>u_2</td><td>v_2</td><td>w_2</td></tr>
<tr><td colspan="6">← Wind Components, 3m and Roof Levels ($msec^{-1}$) →</td></tr>
<tr><td rowspan="2">Station No. 2 or 4, 1st Line</td><td rowspan="2">Date</td><td rowspan="2">Time</td><td rowspan="2">Level of CO obs.</td><td rowspan="2">CO Concentration (ppm)</td><td>ΔT_1</td><td>ΔT_2</td><td>ΔT_3</td><td>ΔT_4</td><td rowspan="2">Temp., at 3m</td></tr>
<tr><td colspan="4">Temp. at Level 2-Level 1, Level 3-Level 2, etc. (°C)</td></tr>
<tr><td>Station No. 2 or 4, 2nd Line</td><td>Date</td><td>Time</td><td>Level of CO obs.</td><td colspan="6">← Information Concerning Instrument Status and Operational Parameters →</td></tr>
<tr><td>Station No. 5,6,7,8, or 9</td><td>Date</td><td>Time</td><td>Level of CO obs.</td><td>CO Concentration (ppm)</td><td>Wind Speed ($msec^{-1}$)</td><td>Wind Direction (deg.)</td><td colspan="2">u, v Wind Components (Calculated from Recorded Speed and Direction)</td><td>Instrument Status Indicator</td></tr>
<tr><td rowspan="2">10, Summary Record</td><td rowspan="2">Date</td><td rowspan="2">Time of 1st CO obs. (hr. min.)</td><td rowspan="2">Time of Last CO obs. (hr. min.)</td><td colspan="2">Average Roof Level Winds, Sta. 1</td><td colspan="2">Average Roof Level Winds, Sta. 3</td><td rowspan="2">Average CO for all Sta. at 3m</td><td rowspan="2">Average CO for all Sta. Roof Lev.</td></tr>
<tr><td colspan="4">Calculated from Components
Speed, Direction, Speed, Direction</td></tr>
</table>

99.9 or 999.9 indicate missing data.

TA-8563-22

FIGURE D-2 EXAMPLE OF PARTIALLY CORRECTED DATA CONTAINED IN ONE RECORD OF THE TAPE GENERATED BY INITIAL CDC 6400 PROCESSING collection periods. On this consolidated tape, each record contains all the wind, temperature, and CO concentration information from the stations where CO was measured and summaries of the data from the wind-component stations. A group of derived data was introduced for purposes of stratifying the data for statistical summaries.

On this basic summary tape, each record has 420 words. An annotated example of the recorded information is shown in Figure D-3. The first ten words include the date and times covered by the record, the average rooftop winds at Stations 1 and 3, and the CO concentration at 3 m and rooftop, averaged over all the stations.

The next 30 words on the basic summary tape contain date and time information, and the sums of all the Station 1 wind component observations during the 5-minute periods and the sums, their squares, and the numbers of observations. The following 30 words have the same information for Station 3. These sums, and sums of squares, are easily combined with the same items from other records to obtain means and standard deviations of the wind components.

The rest of the record contains the data from Stations 2, 4, 5, ..., 9, in ten-word groups. The data in these groups are the same as on the earlier unconsolidated tape, except that the recorded information relating to instrument operation (bridge and amplifier voltages, etc.) is not retained.

The basic summary tape has been used to obtain averages for several different data stratifications. Many of these have been discussed in the body of this report. A simplified flow chart of the data averaging routine is shown in Figure D-4. A sample of the type of output obtained from this processing is shown in Figure D-5. In this example, the means and standard deviations are given for all those cases occurring between

10.00	701130.00	1210.00	1214.00	.97	337.92	1.50	297.65	3.77	3.51
1.00	701130.00	1210.00	1214.00	45.35	-111.71	146.37	86.58	342.39	34.47
1.00	701130.00	1210.00	1214.00	61.39	245.32	398.84	221.78	1033.98	74.86
1.00	701130.00	1210.00	1214.00	124.00	124.00	124.00	124.00	124.00	124.00
3.00	701130.00	1210.00	1214.00	164.84	-86.32	54.03	72.87	37.85	-67.90
3.00	701130.00	1210.00	1214.00	793.48	377.19	409.85	329.82	351.45	768.37
3.00	701130.00	1210.00	1214.00	124.00	124.00	124.00	124.00	124.00	124.00
2.00	701130.00	121022.50	5.00	1.56	.91	-.23	-.05	-.11	99.90
4.00	701130.00	121024.10	5.00	.39	.03	.03	.05	.06	99.90
5.00	701130.00	121024.80	5.00	8.97	1.56	140.50	-1.21	-.99	62.00
6.00	701130.00	121025.40	5.00	3.90	1.86	186.17	-1.85	.20	61.00
7.00	701130.00	121026.10	5.00	.78	.74	177.03	-.74	-.04	63.00
8.00	701130.00	121026.80	5.00	5.46	.04	87.11	.00	-.04	62.00
9.00	701130.00	121027.50	5.00	99.90	2.83	999.90	99.90	99.90	60.00
2.00	701130.00	121103.00	2.00	2.73	.89	-.28	-.02	-.14	99.90
4.00	701130.00	121104.60	1.00	.78	.02	0.00	0.00	.05	99.90
5.00	701130.00	121105.30	1.00	8.19	.89	151.74	-.79	-.42	62.00
6.00	701130.00	121106.00	1.00	4.29	3.72	160.88	-3.51	-1.22	61.00
7.00	701130.00	121106.70	1.00	.78	.82	171.41	-.81	-.12	63.00
8.00	701130.00	121107.30	1.00	6.24	.06	95.54	-.01	-.06	62.00
9.00	701130.00	121108.00	1.00	99.90	2.38	999.90	99.90	99.90	61.00
2.00	701130.00	121201.60	1.00	2.34	.91	-.30	-.05	-.08	99.90
4.00	701130.00	121203.20	2.00	-.39	.06	0.00	.02	.01	99.90
5.00	701130.00	121203.90	2.00	5.46	2.60	115.21	-1.11	-2.36	63.00
6.00	701130.00	121204.60	2.00	3.12	1.79	28.81	1.56	-.86	61.00
7.00	701130.00	121205.30	2.00	99.90	99.90	999.90	99.90	99.90	64.00
8.00	701130.00	121205.90	2.00	13.26	.06	250.09	-.02	.06	62.00
9.00	701130.00	121206.60	2.00	99.90	3.20	999.90	99.90	99.90	62.00
2.00	701130.00	121302.20	3.00	.78	.95	-.31	-.02	-.14	99.90
4.00	701130.00	121303.80	3.00	-.39	.07	-.02	.09	-.05	99.90
5.00	701130.00	121304.50	3.00	4.68	1.12	148.93	-.96	-.58	62.00
6.00	701130.00	121305.20	3.00	4.29	2.90	186.17	-2.88	.31	61.00
7.00	701130.00	121305.80	3.00	.78	1.19	177.03	-1.19	-.06	62.00
8.00	701130.00	121306.50	3.00	7.41	.06	140.50	-.05	-.04	62.00
9.00	701130.00	121307.20	3.00	99.90	4.91	999.90	99.90	99.90	61.00
2.00	701130.00	121402.80	4.00	1.56	.94	-.25	-.11	-.14	99.90
4.00	701130.00	121404.40	4.00	2.34	.04	-.02	.09	-.02	99.90
5.00	701130.00	121405.10	4.00	5.46	.97	191.08	-.95	.19	62.00
6.00	701130.00	121405.70	4.00	7.41	1.26	166.50	-1.23	-.30	61.00
7.00	701130.00	121406.40	4.00	.78	2.31	151.74	-2.03	-1.09	62.00
8.00	701130.00	121407.10	4.00	2.34	.04	115.21	-.02	-.04	62.00
9.00	701130.00	121407.80	4.00	99.90	3.57	999.90	99.90	99.90	62.00

If No. in 1st Column is:	LEGEND									
10 (Summary)	Date (11/30/70 in this case)	Start Time of Period (hr. min.)	End Time of Period (hr. min.)	Average Rooftop Wind Speed Sta. 1	Average Rooftop Wind Direction Sta. 1	Average Rooftop Wind Speed Sta. 3	Average Rooftop Wind Direction Sta. 3	Average of all 3-m CO Concentrations	Average of all Rooftop CO Concentrations	
Station No. 1 or 3	Date	Start Time of Period	End Time of Period	Σu Σu^2 No. of obs.	Σv Σv^2 No. of obs.	Σw Σw^2 No. of obs.	Σu Σu^2 No. of obs.	Σv Σv^2 No. of obs.	Σw Σw^2 No. of obs.	1st Line 2nd Line 3rd Line
				← 3m Level →			← Rooftop Level →			
Station No. 2 or 4	Date	Time (hr., min., sec.)	Level of CO Reading	CO Concentration	ΔT Level 2-Level 1	ΔT Level 3-Level 2	ΔT Level 4-Level 3	ΔT Level 5-Level 4	3-m Temp.	
Station No 5,6,7,8,9	Date	Time	Level of CO Reading	CO Concentration	3-m Wind Speed	3-m Wind Direction	u Component	v Component	No. Indicating Instrument Status	

99.9 or 999.9 indicate missing data.

TA-8563-21

FIGURE D-3 EXAMPLE OF INFORMATION CONTAINED IN ONE RECORD OF THE BASIC DATA SUMMARY TAPE

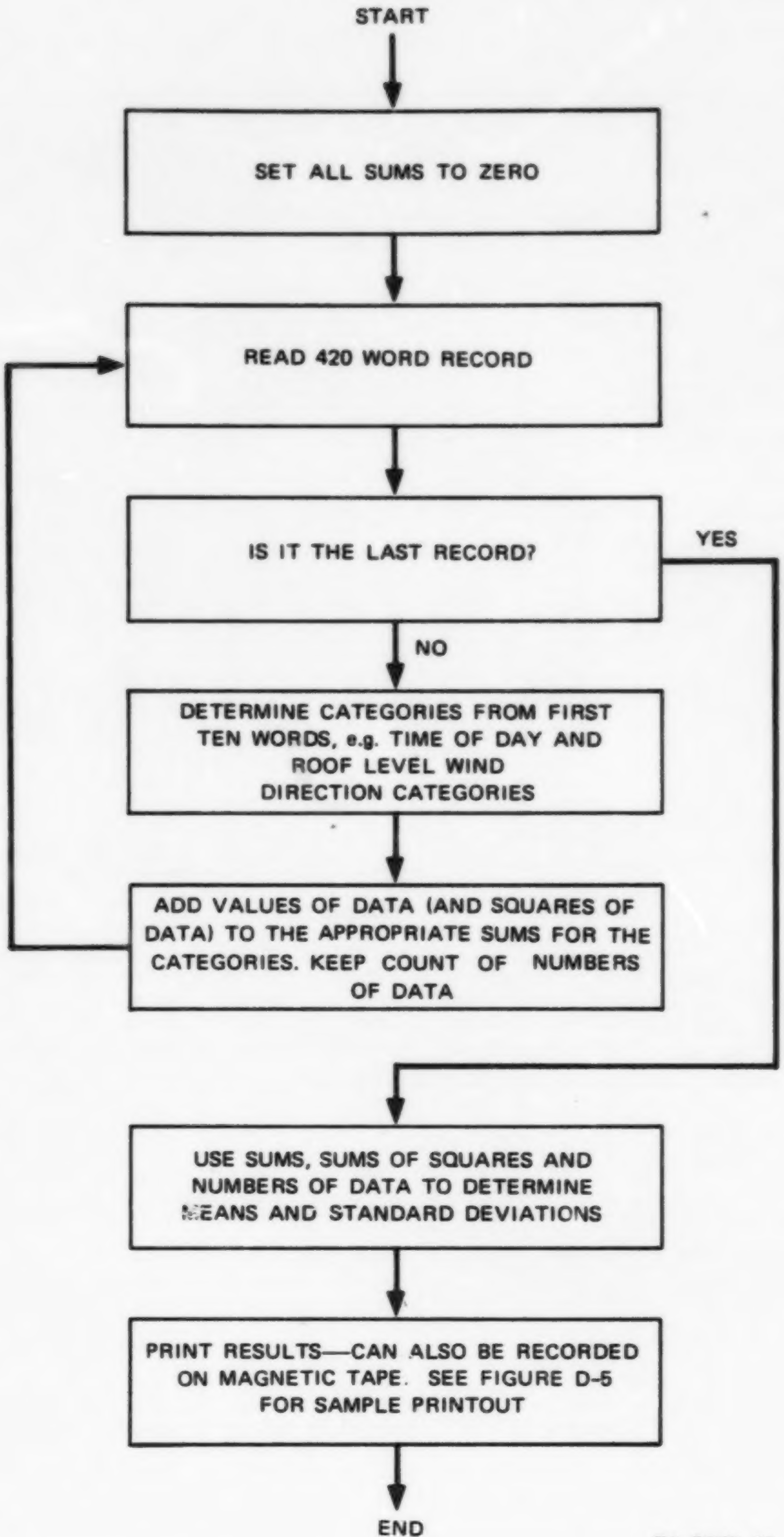
START
SET ALL SUMS TO ZERO
READ 420 WORD RECORD
IS IT THE LAST RECORD?
YES
NO
DETERMINE CATEGORIES FROM FIRST TEN WORDS, e.g. TIME OF DAY AND ROOF LEVEL WIND DIRECTION CATEGORIES
ADD VALUES OF DATA (AND SQUARES OF DATA) TO THE APPROPRIATE SUMS FOR THE CATEGORIES. KEEP COUNT OF NUMBERS OF DATA
USE SUMS, SUMS OF SQUARES AND NUMBERS OF DATA TO DETERMINE MEANS AND STANDARD DEVIATIONS
PRINT RESULTS—CAN ALSO BE RECORDED ON MAGNETIC TAPE. SEE FIGURE D-5 FOR SAMPLE PRINTOUT
END

TA-8563-17

FIGURE D-4 SIMPLIFIED FLOW CHART OF DATA-AVERAGING PROGRAM

ROOFTOP WIND
DIRECTION AT
STA. 2 = 180° ± 22.5°

INCLUDES DATA
FROM 1100–1200

```
W.D. =     180      HCUP = 1100

STA     WS1      WD1      W1     WS2      WD2       W2     TIU1    TIV1    TIW1    TIU2    TIV2    TIW2      N1      N2
  1     .57     1.57     .05    2.29   171.31      .16    30.43    1.61   15.92    2.66     .73    5.04    3318    3318
  3    1.25   280.70     .17     .37   287.66      .01     1.38    4.57    6.91    3.38    9.56  279.47    3071    3071

STA     CO1      CO2     CO3     CO4      CO5       WS       WD      S1      S2      S3      S4      S5      N1      N2
  2    2.85     3.12    2.57    2.78     2.64      .57     1.57    1.78    2.33    1.72    1.56    1.83      22    3318
  4    3.52     2.18    1.68    1.66     2.01     1.25   280.70    2.32    1.66    1.22    1.17    1.46      25    3071
  5    6.58     7.17    6.78    6.10     5.71      .68    69.91    2.89    3.12    2.81    1.44    2.27      24     117
  6    6.79     5.19    5.28    4.52     4.24     1.51    88.13    2.77    1.58    3.18    2.07    1.35      22     130
  7    4.07     3.79    3.39    2.75     1.98     1.54   100.20    3.07    3.10    2.57    1.92    1.83      22     111
  8    4.98     4.84    4.36    4.00     3.68     .08*    93.44    3.82    3.86    3.43    2.43    2.41      27     130
  9    5.58     5.01    3.80    3.21     2.43   -99.90  -999.00    2.48    3.55    2.28    2.29    1.50      20       0

STA     DT1      DT2     DT3     DT4        T       S1       S2      S3      S4      ST      N1      N2      N3      N4      NT
  2    .61*     -.11    -.04    -.14    15.70      .76      .31     .17     .06     .77  100.00  100.00  100.00  100.00   15.00
  4     .09     -.05     .01    -.02    16.02      .09      .05     .05     .07    1.44  100.00  100.00  100.00  100.00   15.00
```

Sta = Station number

WS1, WD1 = Wind speed (m s^{-1}) and direction at the 3-m level.

WS2, WD2 = Wind speed and direction at the rooftop level.

W1, W2 = Vertical velocity at 3-m and rooftop levels.

TIU1, TIV1, ..., TIW2 = Turbulence intensities defined as the ratio of standard deviations to their means for each component (U, V, W) and level (1 = 3m; 2 = rooftop); a NW wind parallel to First Street gives a positive U; an upward wind component gives a positive W.

CO1, CO2, CO3, CO4, CO5 = Average CO concentration at five evenly spaced levels from 3 m (1) to rooftop (5).

S1, S2, S3, S4, S5 = Standard deviations for the CO observations at the five levels.

DT1, DT2, DT3, DT4 = Average temperature differences between levels; e.g., DT1 = T2-T1.

T = Temperature at 3 m.

S1, S2, S3, S4, ST = Standard deviation of temperature differences (and 3-m temperature).

N1, N2, N3, N4, NT = Numbers of data points used to compile averages. For Stations 1 and 2, N1 and N2 are numbers used for levels 1 and 2 winds; for Stations 2, 4, 5,...9, N1 is average number of observations used for CO averages and N2 is number of observations used for wind averages. N1, ..., N4, NT are numbers of observations used for ΔT and T averages.

-99, -999 = Missing data indicators

*Faulty readings due to instrument malfunctions.

TA-8563-32

FIGURE D-5 EXAMPLE OF AVERAGED DATA

1100 and 1200 where the wind at roof level of Station 1 was from 180° ± 22.5° (relative to First Street). Similar summaries were obtained for data stratified by wind direction only and by wind direction, wind speed, and traffic amounts.

The basic summary tape can also be processed to give the data categories for each date and time interval. This information can be combined with the data from other sources, such as the vans, to provide additional stratified average concentrations.

2. Mobile Data

a. Van

The basic data from the instrumented vans were recorded on strip charts. The inlet to the carbon monoxide analyzer could be adjusted in height. Three different heights were used during the program, 3, 6, and 9 m for stationary measurements. While the van was traveling, the inlet was kept at about 3.6 m. When the van was stationed at a location near the intersection of First and San Antonio Streets, the height was generally changed at periodic intervals. The chart records were maked each time the inlet height was changed, and a log was kept of the van location and inlet heights. The inlet was generally kept at each height for 10 or 15 minutes.

The first step in reducing the stationary van data was to read the CO concentrations from the chart records at 1-minute intervals. These CO values, along with time and date information, were transferred to punched cards. Another deck of punched cards was prepared from the log information. These two decks were merged to yield a magnetic tape that contained all the data collected while the van was located in the vicinity of the intersection of First and San Antonio Streets. Each record on this tape contained 510 words, arranged in 85 groups of 6 words. Each group contained the van number, date, time, location, inlet height, and CO concentration.

In the preceding section, it was mentioned that lists of data categories versus time could be obtained. For example, it was possible to obtain, on punched cards, all those dates and time intervals during which the roof-level wind direction was 180° ± 22.5°. Then all the van measurements that were taken during these same time periods could be averaged and analyzed in combination with the stratified streetside averaged data. Thus, we were able to calculate average CO concentrations from the van data that were comparable to those obtained from the fixed station network, and we could thereby extend some of our analyses.

One van usually traveled a circuit around the downtown area while the helicopter was operating. This ground-level circuit was similar, but not identical, to the helicopter route, as can be seen in Figures 13 and 20 of the main text. As the van passed each of the numbered points shown in Figure 20, the chart record was marked and the time noted in a log.

In reducing the data, an average CO value was obtained visually from the chart record for each route segment between numbered points. The van generally made five or six complete circuits during each helicopter observation period. The five or six CO concentration averages for each route segment were averaged with a desk calculator to give a single value for each segment. These values were then used in combination with the corresponding helicopter data for further calculations. The considerable spatial and temporal averaging represented by the process described above is necessary to eliminate unrepresentative CO values arising from small-scale, short-period traffic variations.

b. Helicopter Data

Aerial CO and temperature measurements were made during the morning, noon, and evening peak downtown traffic periods with a chartered Hughes 300 helicopter. The data were recorded on a multichannel strip chart recorder.

Before each flight, recorder gains were checked with various known input voltages. The output voltage of the CO analyzer was first checked with a CO-free calibration ("zero") gas and adjusted to zero output, if necessary. Subsequently, a span gas (19 ppm CO from the same source used for all the analyzers) was fed into the instrument and the gain adjusted to a nominal value of 10 mV/ppm. This procedure was repeated to adjust for minor interactions between the zero and gain adjustments. The calibration procedure was occasionally repeated at the end of a flight.

Before taking data, the electronic reference signal of the analyzer was checked. This provided a reference for possible drift of the analyzer output. The electronic reference was frequently checked for drift in flight. This procedure was especially necessary for morning flights when ambient cockpit temperature changed as much as 15° C over a short period.

The helicopter measurements were of two types, vertical profiles and horizontal traverses. Two vertical profiles of CO and temperature to 1000-m altitude were made in the vicinity of Spartan Stadium (approximately 3 km SE of the San Jose central business district) at the beginning of each flight; a profile took approximately 6 minutes to complete. Horizontal traverses were made at various altitudes (62, 92, 152, 213, and 304 m) about a 1.03 × 1.45-km area encompassing the central business district, depicted in Figures 13 and 20 of the main text. The minimum traverse altitude was prescribed by the heights of nearby buildings and towers; the maximum was a function of several factors: (1) absolute value of CO concentration, (2) ceiling height, and (3) traffic control restrictions of the nearby San Jose Municipal Airport--the flight pattern intercepted the airport's localizer.

The vertical profiles of CO (mV) and temperature (°C) measurements were put onto cards from the strip chart at 15-m intervals from the surface to 150 m, and thereafter at intervals of 30 m to the top of the profile. The horizontal traverse data were reduced over 225-m increments, giving 19 values of each parameter for every height. Additionally, each profile and traverse was assigned a representative, mean electronic reference value as the result of frequent in-flight checks. The data were processed on the CDC 6400 computer with both printed and graphed output; the output format is illustrated in Figures D-6 and D-7.

3. Traffic Volumes

The raw 5-minute volume histories for selected sensors monitored by the traffic system were available from the traffic control computer on punched card output. Figure D-8 is an example of a card image listing for one trial (1109-1304 on 8 December 1970). Each line represents one card according to the following format:

Card Number	Columns		Contents
1	32-33	Month	Trial date
	35-36	Date	
	38-39	Year	
	43-44	Hour	Time of completion of initial 5-minute data collection interval
	46-47	Minute	
	49-50	Second	

```
                              ANALYSIS OF SAN JOSE CO DATA OBTAINED FROM A HELICOPTER.
DATE = 70/12/ 9/1645  N =   35                         2      8.10    46.50    46.90   171.50
                                                      IAT     Z25      EO       EOR      G*
NO.  HEIGHT      CO      TEMP
  1   15.24     3.40    12.20
  2   30.49     3.53    11.90
  3   45.73     3.63    12.00
  4   60.98     3.74    12.00
  5   76.22     3.51    11.40
  6   91.46     3.11    11.80
  7  106.71     2.91    11.60
  8  121.95     2.72    11.50
  9  137.20     2.83    11.30
 10  152.44     2.66    11.30
 11  182.93     1.82    11.20
 12  213.41     1.44    10.80
 13  243.90     1.29    10.70
 14  274.39     1.14    10.40
 15  304.88     1.12    10.10
 16  335.37     1.12     9.80
 17  365.85     1.12     9.60
 18  396.34     1.08     9.30
 19  426.83      .99     9.20
 20  457.32      .87     9.30
 21  487.80      .74     8.60
 22  518.29      .68     8.20
 23  548.78      .65     7.90
 24  579.27      .65     7.50
 25  609.76      .55     7.40
 26  640.24      .53     7.20
 27  670.73      .57     7.20
 28  701.22      .59     7.50
 29  731.71      .51     7.70
 30  762.20      .42     7.40
 31  792.68      .34     7.50
 32  823.17      .19     7.00
 33  853.66      .27     5.90
 34  884.15      .42     5.30
```

IAT = Recorder Attenuation (mV/mm)
Z25 = Reference Zero Gas Value (mm)
EO = In-flight Electronic Reference (mm)
EOR = Calibration Electronic Reference (mm)
G* = Gain of CO Analyzer (mV/19ppm)
HEIGHT = Altitude (m)
TEMP = Temperature (°C)
CO = Carbon Monoxide Concentration (ppm)

TA-8563-33

FIGURE D-6 COMPUTER OUTPUT FORMAT FOR HELICOPTER TEMPERATURE AND CARBON MONOXIDE PROFILE DATA

```
                    ANALYSIS OF SAN JOSE CO DATA OBTAINED FROM A HELICOPTER.
DATE = 70/11/10/1000  N =   19  HT = 200            IAT =  5  Z25 = 10.90  EO = 19.10  EOR = 18.50  G =  8.54

NO.  HEIGHT    TEMP      CO  AVG CO
  1  200.00   15.00    5.44
  2  200.00   15.00    5.50
  3  200.00   14.90    5.68
  4  200.00   14.80    5.56
  5  200.00   14.90    5.56    5.56
  6  200.00   14.90    5.27
  7  200.00   14.80    4.80
  8  200.00   15.00    4.74
  9  200.00   14.80    5.33
 10  200.00   14.90    5.68    5.15
 11  200.00   15.10    5.50
 12  200.00   15.00    5.39
 13  200.00   15.10    5.33
 14  200.00   15.00    5.09    5.40
 15  200.00   15.10    4.45
 16  200.00   15.00    4.16
 17  200.00   15.00    4.63
 18  200.00   15.10    4.57
 19  200.00   15.00    4.22    4.49
```

IAT = Recorder Attenuation (mV/mm)
Z25 = Reference Zero Gas Value (mm)
EO = In-flight Electronic References (mm)
EOR = Calibration Electronic Reference (mm)
G = Gain of CO Analyzer (mV/ppm)
HEIGHT = Altitude (ft)
TEMP = Temperature (°C)
CO = Carbon Monoxide Concentration (ppm)

TA-8563-34

FIGURE D-7 COMPUTER OUTPUT FORMAT FOR HELICOPTER TEMPERATURE AND CARBON MONOXIDE TRAVERSE DATA

```
                              12/08/70    11 08 52

TIME DET DET DET DET DET DET DET DET DET DET DET DET DET DET DET DET DET DET
     114 113 107 106 105 092 077 075 073 071 067 065 000 000 000 000 000 000

 001 021 042 024 006 016 009 011 016 012 024 000 007
 002 013 042 030 005 012 012 007 015 015 025 000 003
 003 014 028 023 007 015 009 010 014 015 035 000 006
 004 019 034 019 006 015 009 012 014 015 022 000 005
 005 022 041 022 007 013 003 008 013 017 019 000 003
 006 022 034 027 003 015 006 012 012 018 025 001 001
 007 010 035 025 007 014 015 009 018 016 030 000 004
 008 020 034 017 006 017 008 016 020 016 025 000 002
 009 015 033 023 005 019 003 018 013 015 020 000 002
 010 019 041 037 009 018 011 012 008 013 023 001 004
 011 016 040 018 005 018 011 008 021 017 036 000 003
 012 021 048 028 008 022 011 002 025 021 030 000 004
 013 016 044 025 007 023 013 014 015 021 029 001 006
 014 024 048 021 008 025 016 015 021 023 023 001 006
 015 021 048 031 010 022 017 009 023 029 033 001 002
 016 023 040 027 010 024 016 018 019 028 031 001 009
 017 019 052 028 009 019 006 020 027 025 043 001 007
 018 029 050 034 005 029 010 011 014 021 029 000 002
 019 016 038 019 010 029 011 024 019 024 033 000 003
 020 017 047 016 011 018 010 015 012 017 033 000 004
 021 024 034 020 007 028 008 007 020 024 023 000 006
 022 020 041 026 011 018 008 019 015 020 021 000 005
 023 018 049 021 002 011 009 011 023 015 027 000 003
```

TA-8563-35

FIGURE D-8 EXAMPLE OF RAW TRAFFIC DATA SUMMARY

Card Number	Columns	Contents
2	--	Ignore--Alpha heading material
3	6-9	Detector I.D. number
	10-13	Detector I.D. number
	.	
	.	
	.	
	74-77	Detector I.D. number
4--final	1-5	Sequence number for each 5-minute interval (Card 4 will contain "00001"; Card 5, "00002"; etc.)
	6-9	Traffic count for detector identified on Card 3, Columns 6-9
	10-13	Traffic count for detector identified on Card 3, Columns 10-13
	.	
	.	
	.	
	74-77	Traffic count for detector identified on Card 3, Columns 74-77.

Thus, each volume data card represents the total counts during a particular 5-minute interval for a maximum of 18 detectors. If less than 18 are of interest, Card 3 will contain only zeros in the final fields.

For more than 18 detectors, one or more additional decks, identical in format to the above, are appended, with two blank cards separating each deck.

Because of the large number of cards generated during the total data collection period, a preliminary processing step consisted of transferring the card data to magnetic tapes for more efficient processing. Three different tapes were generated, according to particular processing requirements. The first contains only data from the sensors adjacent to the San Antonio and First Street Test Site from 2 November to 11 December 1970. The format of this tape is depicted in Figure D-9.

TAPE I ("10 DETECTOR" DATA)

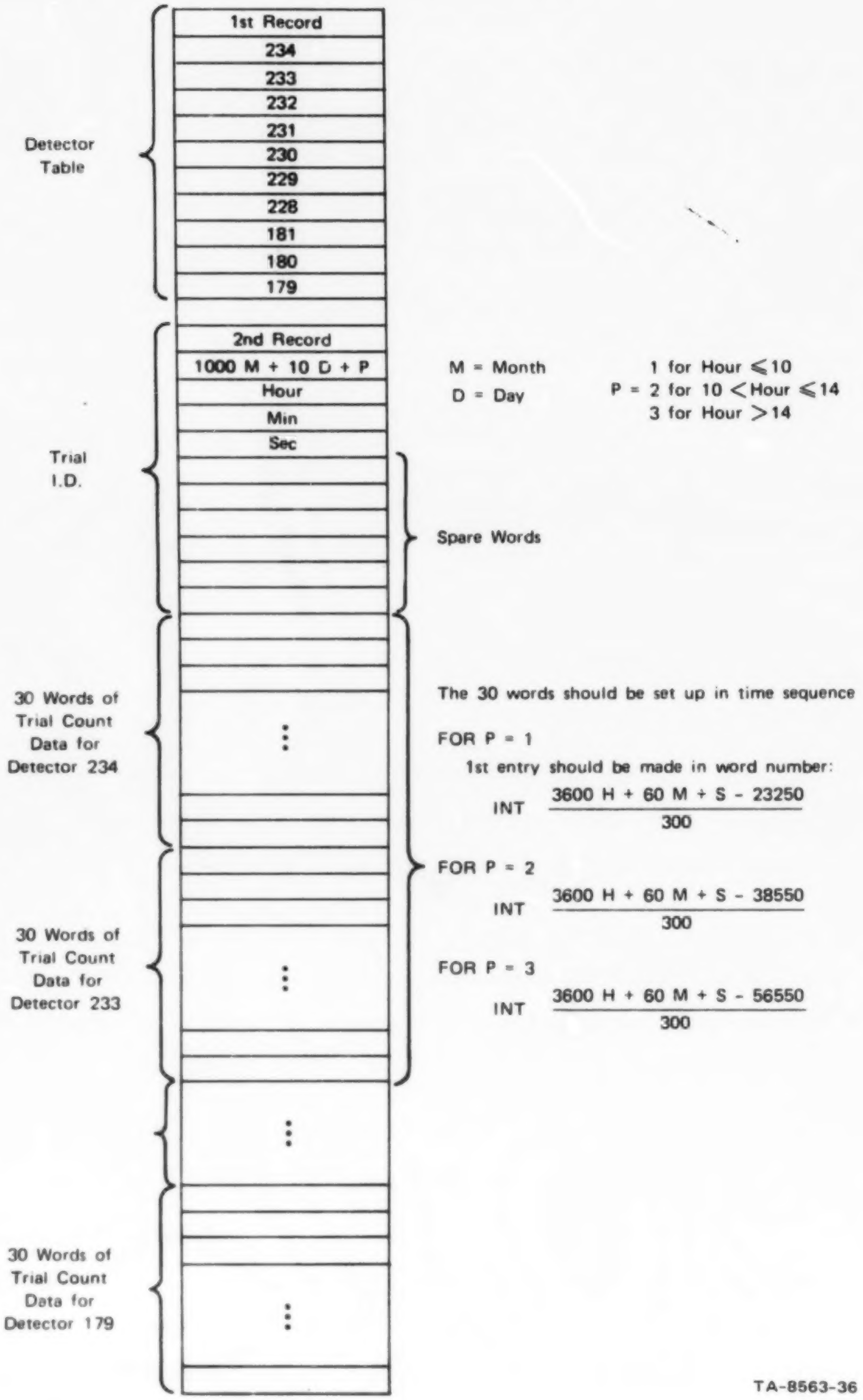
1st Record
234
233
232
231
230
229
228
181
180
179
Detector Table
2nd Record
1000 M + 10 D + P
Hour
Min
Sec
Trial I.D.
Spare Words
30 Words of Trial Count Data for Detector 234
30 Words of Trial Count Data for Detector 233
30 Words of Trial Count Data for Detector 179
TA-8563-36

M = Month

D = Day

$$P = \begin{cases} 1 \text{ for Hour} \leq 10 \\ 2 \text{ for } 10 < \text{Hour} \leq 14 \\ 3 \text{ for Hour} > 14 \end{cases}$$

The 30 words should be set up in time sequence

FOR P = 1

1st entry should be made in word number:

$$\text{INT} \frac{3600\ H + 60\ M + S - 23250}{300}$$

FOR P = 2

$$\text{INT} \frac{3600\ H + 60\ M + S - 38550}{300}$$

FOR P = 3

$$\text{INT} \frac{3600\ H + 60\ M + S - 56550}{300}$$

FIGURE D-9 MAGNETIC TAPE FORMAT FOR TRAFFIC DATA

The actual traffic volume data in the second and subsequent records are located in ten 30-word blocks, arranged chronologically for each sensor listed in the detector table, respectively. The time interval identification is implicit; for example, for morning trials, the first word in the block corresponds to data collected during a 5-minute interval that terminates between 0632.5 and 0637.5 PST, the second word is 5 minutes later, etc. If data collection had not yet begun or had been terminated during any particular interval, the corresponding word contains a "999."

The second tape contains data collected during the rush hour periods from 23 November to 15 December 1970 from all 291 sensors. The format is identical except that the detector table record contains 291 entries and the data records contain 291 blocks of 30 words.

The third tape contains only the all-day trials of 14 and 15 December. The format is the same as for Tape II, except that (1) the 30-word blocks were extended to 144 words; (2) maximum tape record size required the 291 sensors to be divided among four data records, the first three applying to 84 sensors each and the final record to 39 sensors; and (3) "p" in the identification number = 0.

The processing programs permitted flexibility with respect to the type of output. A basic summary of daily raw data, totaled for 15-minute intervals, was prepared for traffic at San Antonio and First Streets. A similar daily record was prepared for the total of all 291 detectors. Examples of these are shown in Tables D-1 and D-2, respectively.

Finally, mean traffic volumes and their standard deviations were computed for all streets and for all intersections within the grid. These means were based on data from the entire period of operation. Means were calculated as a function of time of day using 30-minute

Table D-1

TRAFFIC AT INTERSECTION OF FIRST AND SAN ANTONIO STREETS

FOR MONDAY, 2 NOVEMBER 1970

Time Interval	First St. In	San Antonio In	First St. Out*	San Antonio Out	Intersection In	Intersection Out*
0645-0700	130	22	138	15	152	153
0700-0715	177	32	172	26	209	198
0715-0730	207	45	225	27	252	252
0730-0745	304	67	307	49	371	356
0745-0800	287	105	288	104	392	392
0800-0815	220	87	220	65	307	285
0815-0830	196	87	198	67	283	265
1105-1120	214	68	247	59	282	306
1120-1135	235	65	244	68	300	312
1135-1150	210	84	184	76	294	260
1150-1205	221	83	211	74	304	285
1205-1220	212	86	189	71	298	260
1220-1235	207	71	195	65	278	260
1235-1250	251	70	264	72	321	336
1250-1305	258*	93*	274*	87*	351*	361*
1603-1618	178	65	169	57	243	226
1618-1633	198	70	163	72	268	235
1633-1648	190	84	192	75	274	267
1648-1703	180	59	163	57	239	220
1703-1718	156	76	141	69	232	210
1718-1733	159	52	142	51	211	193
1733-1748	177	55	177	48	232	225
1748-1803	168*	48*	171*	30*	216*	201*

*Estimate--only partial data available.

Table D-2

TOTAL TRAFFIC COUNTS FROM 291 SENSORS IN DOWNTOWN SAN JOSE FOR TUESDAY, 24 NOVEMBER 1970

Time Interval	Total Traffic
0648-0703	10,154
0703-0718	12,927
0718-0733	16,810
0733-0748	22,172
0748-0803	22,218
0803-0818	18,341
0818-0833	18,441*
1104-1119	19,293
1119-1134	19,229
1134-1149	19,946
1149-1204	21,409
1204-1219	20,866
1219-1234	20,742
1234-1249	20,359
1249-1304	20,153*
1603-1618	22,914
1618-1633	22,542
1633-1648	25,775
1648-1703	24,042
1703-1718	27,183
1718-1733	20,813
1733-1748	18,292
1748-1803	16,353*

*Estimate--only partial data available.

periods. Figure D-10 shows an example of this kind of summary plotted on a schematic representation of the downtown traffic grid. For any given time of day the traffic in the downtown area remains quite consistent from day to day. This can be seen from the relatively small deviations in Figure D-10. The relative variation of total traffic, on all links, is even less than on the individual links. Figure 47 of the text shows the total downtown traffic volume on two successive days in December 1970. It can be seen in that figure that the two curves nearly coincide.

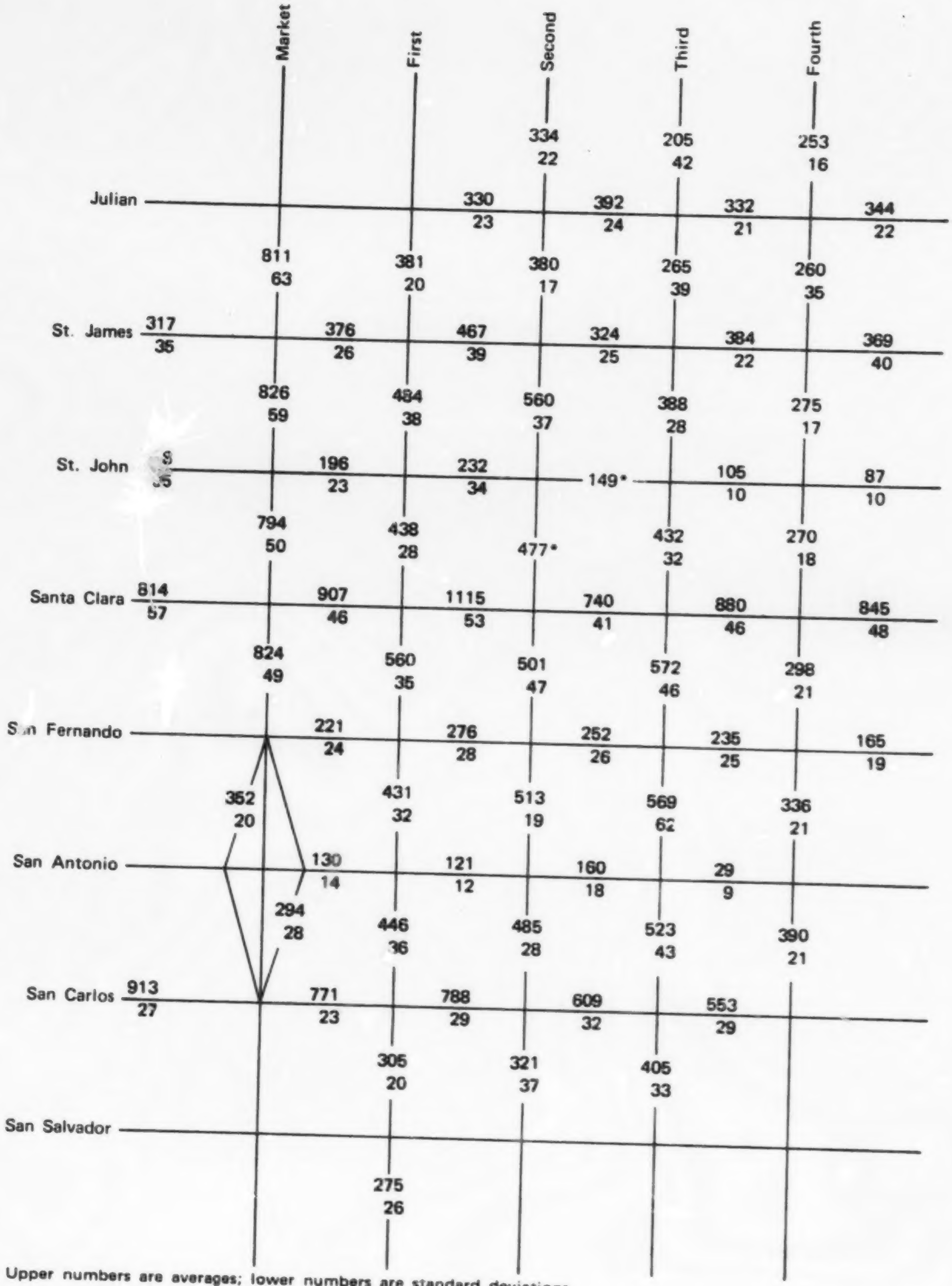
Market
First
Second
Third
Fourth
334
22
205
42
253
16
Julian
330
23
392
24
332
21
344
22
811
63
381
20
380
17
265
39
260
35
St. James
317
35
376
26
467
39
324
25
384
22
369
40
826
59
484
38
560
37
388
28
275
17
St. John
196
23
232
34
149*
105
10
87
10
794
50
438
28
477*
432
32
270
18
Santa Clara
814
57
907
46
1115
53
740
41
880
46
845
48
824
49
560
35
501
47
572
46
298
21
San Fernando
221
24
276
28
252
26
235
25
165
19
352
20
431
32
513
19
569
62
336
21
San Antonio
130
14
121
12
160
18
29
9
294
28
446
36
485
28
523
43
390
21
San Carlos
913
27
771
23
788
29
609
32
553
29
305
20
321
37
405
33
San Salvador
275
26

Upper numbers are averages; lower numbers are standard deviations based on 13 days' observations.

*Estimate—Insufficient data due to defective sensors.

TA-8563-39

FIGURE D-10 AVERAGE LINK VOLUMES, 1100-1130

Appendix E

PILOT BALLOON DATA SUMMARY

Appendix E

PILOT BALLOON DATA SUMMARY

Pilot balloon (pibal) soundings were made by the Meteorology Department at San Jose State College. The pibals were released at the College, which is located on the eastern leg of the helicopter and van traverses (see Figure 20), and were tracked by double theodolite. The soundings provide wind data for 11 periods with a maximum vertical resolution of 72 m. The winds are given in geographic coordinates in units of m s^{-1}.

PRECEDING PAGE BLANK

Table E-1

PILOT BALLOON DATA SUMMARY--SAN JOSE STATE COLLEGE (1970)

	2 November 0830 PST		2 November 1720 PST		3 November 0815 PST		3 November 1645 PST		4 November 1700 PST		5 November 0900 PST		5 November 1700 PST		10 December 1647 PST		11 December 0825 PST		11 December 1600 PST		15 December 1630 PST	
z	u	v	u	v	u	v	u	v	u	v	u	v	u	v	u	v	u	v	u	v	u	v
72	-1.4	0.0	3.1	-4.1	-0.3	0.7	-0.2	4.6	-4.7	4.8	-1.0	5.2	-0.1	-1.5	1.6	-1.5	-2.0	0.4	4.8	-1.2	-7.0	7.6
144	-1.2	0.2	2.6	-4.6	-0.5	1.9	-1.2	5.0	-5.0	6.5	-0.9	7.1	-0.7	-1.6	1.9	-1.5	-1.4	1.2	4.4	-2.2	-6.1	9.2
216	-1.4	0.6	2.4	-4.3	-1.3	3.7	-1.6	4.9	-5.3	7.8	-0.9	7.5	-1.0	-1.9	1.6	1.2	0.2	0.5	1.7	-4.2	-4.0	8.6
282	-0.9	0.2	2.4	-4.6	-2.7	5.6	-1.7	4.3	-6.1	9.6	-0.5	8.2	-0.9	1.7	1.3	-1.0	1.7	-0.4	0.4	-5.0	-2.2	8.4
348	-0.3	0.0	2.8	-3.9	-4.1	6.8	-1.8	4.0	-7.2	11.9	-0.1	8.7	-0.2	-1.5	0.9	-0.8	1.7	-0.3	0.4	-4.2	-2.2	10.8
414			2.7	-1.9	-4.2	5.6	-1.5	4.1	-7.4	13.1	0.3	8.3	0.2	-0.8	0.6	-0.5	1.2	0.5	-0.3	-4.2	-2.2	11.5
480			1.6	-0.8	-4.5	5.4	-0.9	4.1	-7.1	13.0	0.2	8.2	0.8	0.0	0.9	0.1	2.0	0.0	0.0	-4.6	-2.2	10.8
546			0.7	-0.9	-5.0	7.1	-0.5	4.1	-7.3	13.1	0.4	8.7	1.2	0.9	0.7	0.0	1.8	-2.9	-0.1	-5.1	-3.3	12.5
612			0.6	-0.9	-2.7	6.3	-0.2	4.3	-7.0	12.4	0.6	9.5	0.8	1.7	0.4	-0.5	0.0	-4.5	-0.8	-5.2	-3.0	14.6
675			0.6	-0.7	-1.3	5.6	-0.1	6.1	-5.8	11.0	0.6	9.1	0.7	1.9	0.1	-1.4	-1.3	-4.8	-1.3	-4.8	-1.9	17.3
738			0.4	0.4	-2.1	7.5	-0.2	7.8	-5.4	11.2	1.2	10.3	0.1	2.4	-0.6	-2.2	-2.0	-5.2	-2.0	-4.4	-2.0	20.0
801			0.4	2.4	-1.6	7.5	-0.1	8.8	-5.0	11.7	2.6	10.7	3.0	1.6	-0.3	-1.1			-2.6	-3.8	-2.1	19.7
864			1.4	2.7	-0.4	6.4	-0.4	10.4	-3.7	12.1	3.9	10.6	-0.7	1.7	-0.3	0.0			-2.0	-3.3	-1.2	21.6
927			1.1	2.0	0.6	6.3	-0.9	10.8	-2.4	12.2	4.2	13.0	0.4	5.3	-1.3	-0.9			-1.2	-2.8	0.5	21.4
990			-0.6	2.9	0.8	6.3	-1.4	10.3	-1.8	12.3	5.2	15.3	3.7	6.4	-2.3	-2.6			-0.2	-3.0	2.5	17.1

z = height (m).

u = east-west wind component (m s^{-1}).

v = north-south wind component (m s^{-1}).

REFERENCES

Burggraf, O. R., 1966: Analytical and numerical studies of the structure of steady separated flow, J. Fluid.Mech., 24 (1), pp. 113-151.

Fox, J., 1964: Surface pressure and turbulent airflow in transverse rectangular notches, NASA TN D-2501, 18 pp.

Fox, J., 1965: Heat transfer and air flow in a transverse rectangular notch, Int. J. Heat Mass Trans., 8, pp. 269-279.

Frost, R., 1947: The velocity profile in the lowest 400 ft, Meteorological Mag., 76, pp. 14-19.

Georgii, H. W., E. Busch, and E. Weber, 1967: Investigation of the temporal and spatial distribution of the emission concentration of carbon monoxide in Frankfurt/Main, Report No. 11 of the Institute for Meteorology and Geophysics of the University of Frankfurt/Main (Translation No. 0477, NAPCA).

Gifford, F. A., Jr., 1961: Use of routine meteorological observations for estimating atmospheric dispersion, Nuclear Safety, 2, 48.

Hoydysh, W., 1971: Personal communication, Env. Eng. Res. Labs., New York Univ., Bronx, New York 10453.

Johnson, W. B., Jr., F. L. Ludwig, and A. E. Moon, 1969: Development of a practical, multipurpose urban diffusion model for carbon monoxide, Proceedings of Symposium on Multiple-Source Urban Diffusion Models, Chapel Hill, North Carolina, 28-30 October 1969, pp. 5-1 to 5-38.

Leighton, P. A., and R. B.Dittmar, 1952: Behavior of aerosol clouds within cities, Joint Quarterly Report No. 2, October-December 1952, Contracts DA-18-064-cmc-1856 and DA-18-064-cml-2282, Stanford Univ. and Ralph M. Parsons Co., 100 pp., DDC No. AD 7261.

________ and ________, 1953a: ibid., Joint Quarterly Report No. 4, January-March 1953, 218 pp., DDC No. AD 31509.

REFERENCES (Continued)

Leighton, P. A., and R. B. Dittmar, 1953b: ibid., Joint Quarterly Report No. 4, April-June 1953, 196 pp., DDC No. AD 31508.

________ and ________, 1953c: ibid., Joint Quarterly Report No. 5, July-September, 238 pp., DDC No. AD 31507.

________ and ________, 1953d: ibid., Joint Quarterly Report No. 6, Vol. I, October-December 1953, 246 pp., DDC No. AD 31510.

________ and ________, 1953e: ibid., Joint Quarterly Report No. 6, Vol. II, October-December 1953, 187 pp., DDC No. AD 31511.

Ludwig, F. L., W. B. Johnson, A. E. Moon, and R. L. Mancuso, 1970: A practical multipurpose urban diffusion model for carbon monoxide, Final Report, Coordinating Research Council Contract CAPA-3-68, National Air Pollution Control Administration Contract CPA 22-69-64, Stanford Research Institute, Menlo Park, California, 184 pp., National Technical Information Service No. PB 196003.

Maull, D. J., and L. F. East, 1963: Three-dimensional flow in cavities, J. Fluid Mech., 16, pp. 620-632.

McCormick, R. A., and C. Xintaras, 1962: Variation of carbon monoxide concentrations as related to sampling interval, traffic, and meteorological factors, J. Appl. Meteor., 1, pp. 237-243.

McElroy, J. L., and F. Pooler, Jr., 1968: St. Louis dispersion study, Vol. II--Analysis, 51 pp., National Air Pollution Control Administration Publication No. AP-53, 51 pp.

Ott, W., J. F. Clarke, and G. Ozolins, 1967: Calculating future carbon monoxide emissions and concentrations from urban traffic data, PHS Publ. No. 999-AP-41, National Center for Air Pollution Control, Cincinnati, Ohio.

Pasquill, F., 1961: The estimation of the dispersion of windborne material, Meteorological Mag. (London), 90, pp. 33-49.

Pooler, F., 1966: A tracer study of dispersion over a city, J. Air Poll. Contr. Assoc., 11, pp. 677-681.

REFERENCES (Concluded)

Rand McNally, 1970: Commercial Atlas and Marketing Guide, 101 ed., Rand McNally Co., Chicago, 657 pp.

Robbins, R. C., K. M. Borg, and E. Robinson, 1968: Carbon monoxide in the atmosphere, J. Air Poll. Cont. Assoc., 18, pp. 106-110.

Rose, A. H., R. Smith, W. F. McMichael, and R. E. Kouse, 1964: Comparison of auto exhaust emissions from two major cities, U.S. Public Health Service, Cincinnati, Ohio.

Roshko, A., 1955: Some measurements of flow in a rectangular cutout, NACA TN 3488, 21 pp.

Rouse, H., 1951: Air tunnel studies of diffusion in urban areas, Meteor. Mono., 1, pp. 39-41.

Schnelle, K. B., F. G. Ziegler, and P. A. Krenkel, 1969: A study of the vertical distribution of carbon monoxide and temperature above an urban intersection, APCA Paper No. 69-152.

Turturici, A. R., 1970: 1969 Traffic Volumes, Metropolitan San Jose, California, Dept. Pub. Works, City of San Jose, California, 39 pp.